Cuspidal robots : theoretical study, classification, and application to commercial robots

Durgesh Haribhau Salunkhe

COLLEGE SCIENCES
DOCTORAL DE L'INGENIERIE
PAYS DE LA LOIRE ET DES SYSTEMES

CENTRALE NANTES

MEMOIRE DE DOCTORAT DE

L'ÉCOLE CENTRALE DE NANTES

ÉCOLE DOCTORALE N° 602
Sciences de l'Ingénierie et des Systémes
Spécialité : *Robotique*

Par

Durgesh Haribhau SALUNKHE

Robots cuspidaux : étude théorique, classification et applications aux robots commerciaux

Projet de recherche doctoral présenté et soutenu à l'École Centrale de Nantes, le 27/11/2023
Unité de recherche : UMR 6004 Laboratoire des Sciences du Numérique de Nantes (LS2N)

Rapporteurs avant soutenance :

Federico THOMAS	Full Professor, Universitat Politécnica de Catalunya, Espagne
Med Amine LARIBI	Maître de Conférences HDR , Université de Poitiers

Composition du Jury :

Président :	Mohab SAFEY EL DIN	Professeur des universités, Sorbonne Université
Examinateurs :	Federico THOMAS	Full Professor, Universitat Politécnica de Catalunya, Espagne
	Med Amine LARIBI	Maître de Conférences HDR , Université de Poitiers
	Solen CORVEZ-FERTE	Professeure agrégée, Académie de Lyon
	Michel COSTE	Professeur des universités émérite, Université de Rennes 1
	Adolfo SUAREZ ROOS	Dr, Expert Robotique, IRT Jules Verne, Bouguenais
Directeur de recherches doctorales :	Philippe WENGER	Directeur de recherche CNRS, École Centrale de Nantes
Co-dir de recherches doctorales :	Damien CHABLAT	Directeur de recherche CNRS, École Centrale de Nantes

ACKNOWLEDGEMENT

The past three years have been full of good memories, and I heartily thank each person that crossed my path. Many people have played an important role during my journey of completing the presented work and I am indebted to each and everyone of them.

My foremost gratitude goes towards my family (*Aai, Baba and Didi*). They have stood by me through thick and thin, and their constant support and abundant love has helped me get through tough times.

I am deeply grateful to *Prof. Philippe Wenger* who have been a constant guide and a companion during my doctoral journey. The knowledge gained from him is profound and the experience of working under his guidance was inspiring. I extend the same intensity of gratitude towards *Prof. Damien Chablat* who has always motivated my work, and added humor in the conversation whenever it was most needed. The results achieved in the thesis are a direct reflection of their persistent support and encouragement towards my work. I am thankful to *Prof. Federico Thomas*, and *Prof. Med Amine Laribi* for reviewing my thesis. I also thank the jury members (*Prof. Michel Coste, Prof. Mohab Safey El Din, Dr. Solen Corvez-Ferte*, and *Dr. Adolofo Suarez Roos*) for their supervision over my thesis defense. I am deeply grateful to the early works of *Prof. Federico, Prof. Michel, Dr. Solen and Prof. Mohab* on cuspidal robots. The results achieved in the presented thesis is possible because of the strong foundation laid by them.

I thank *Dr. Jose Capco*, for his strong support and friendly attitude because of which it was quite easy for me to collaborate with him on topics ranging from chess games to mathematical proofs. Thanks for all the free tutorials on maths, I have greatly benefited from those. I thank *Prof. Andreas Mueller* for his compassionate guidance on various subjects. His kind gesture helped me get a great head start in the field of kinematics. I also thank *Dr. Shivesh Kumar* for his mentorship during all these years. He has been a great encouragement adding different perspective on the topics related to research as well as politics. He is someone I always am eager to meet at the conferences. I also thank

my friends from the project, *Christoforos, Tobias, and Rémi*. It was sheer joy to work with you guys, and I am deeply thankful for your cheerful company. Chris's meticulous attitude towards proofs, and Tobias's ever positive energy of pushing through problems have encouraged me to push the boundaries myself.

I wish to express my special thanks to *Sanket* who is like a brother to me. We have shared conversations of great depth, and the trust developed between us is my great treasure. Thanks to my good old friends, *Vipul* and *Ankit*, whom none can replace. I'll be there for you like I've been there before. Thanks to *Ankit* for being a friendly guide on the journey of doctorate together. Your grit and perseverance has no match. Thanks to *Vimalesh*, for all the conversations we had over the past three years. They have provided great insights to my understanding. Thanks *Isabel*, for being a supportive friend and being a part of many cherishable moments in Nantes. Thanks to *Quan, Hyeryeong, Ivan*, and *Abhilash* for many joyous memories in Nantes. Thanks to *Francesco, Nicola, Alessandra, and Angelica* for your friendship. It is unbelievable to think that 5 years have passed since I first met you guys. I thank my cousin *Om*, who has always brought very thoughtful perspective on myriads of topics.

To *Aai* and *Baba*,
My first teachers who taught me to love and live

Table of Contents

List of Figures

List of Tables

NOTATIONS

$\mathcal{J}$ joint space

$\mathcal{W}$ workspace

IKM inverse kinematic model

IKS inverse kinematic solutions

INTRODUCTION

Cuspidal robots are robots with at least one singularity free connected region, *aspect*, with multiple inverse kinematic solutions (IKS). This allows cuspidal robots to change solutions without crossing singularities. This doctoral thesis discusses upon the theoretical study, classification, and application of cuspidal robots. The following sections detail the scope of the thesis as well as summarizes the architecture and contributions presented in the thesis.

Scope of the doctoral thesis

Before 1988, it was widely accepted fact in the kinematics community that all the IKS of a robot lie in distinct connected regions. The belief was founded due to the initial analysis of simpler robots that provided geometrical insights into different inverse kinematic solutions. For example, a 2R robot has two types of IKS commonly called as the "elbow up" and "elbow down" configurations. A similar separation of IKS is possible for anthropomorphic architectures with wrist partition at the end. The well known classification of the IKS of such robots is wrist(flip/No-flip)-shoulder(Right/left)-elbow(Up/down) and is often reported as the NRU configuration. The belief was further corroborated by a proof presented in 1986 [BL86] which went unchallenged as it provided a mathematical assertion to an already known (rather accepted) fact.

In 1988, Innocenti and Parenti-Castelli presented a numerical analysis of two 6R robots that broke the accepted norms in the community [PCI88]. These robots followed a solution changing path and the plot for the determinant of the Jacobian matrix never changed signs. Since then, robots with similar properties have been analyzed by researchers from different countries. A detailed analysis on 3R orthogonal robots was presented in 1992 [Wen92], and the term *cuspidal* was coined in 1995 [EOW95] due to the existence of cusp in the workspace of the robots exhibiting this "special" property. Algebraic tools were used to provide a complete analysis of 3R orthogonal robots establishing different classifications and criterias for cuspidality [BWC04; Wen04]. The algebraic analysis though global and complete, is computationally expensive and thus is cumbersome to extend to generic 3R

robots.

There did not exist an algorithm to decide upon cuspidality of a given generic 6R robot. An identification methodology can help designers decide upon the design parameters of robot in order to choose a noncuspidal robot. One of the most important limiting factor to the analysis of 6R cuspidal robots till early 2000's was the availability of a generic algorithm to resolve the inverse kinematic solutions of the robots. The wrist partitioned anthropomorphic architecture has a simplified geometry and thus provides an analytical solution [Ben91]. The inverse kinematics of generic 6R serial robots on other side was once termed as the 'Mount Everest of kinematics' [Fre73]. Several algorithms with varying approaches have been proposed since then, and we have algorithms that provide algebraic solutions for inverse kinematics of generic 6R robots [HPS07].

With the rise of application of robotics in daily life, robots have started moving out from strictly controlled industrial environment to a collaborative setup. In order to adapt to these requirements, the industry has implemented unconventional designs exploring architectures without a wrist partition. The limitation on a deciding methodology combined with low awareness on cuspidality have resulted into several existing robots to be cuspidal. The multiple regions with varying number of IKS in cuspidal robots leads to interesting properties that can be taken advantage of in certain cases while in other cases proves to be perilous. As we move towards more physical human-robot interaction, it is important to study cuspidality, and its implications on trajectory planning of cuspidal robots. Any accidents caused due to lack of awareness on cuspidality may result in a setback to the trust in collaboration with robots.

This doctoral thesis first presents theoretical study on cuspidality in generic 3R robots. Geometric interpretation of the inverse kinematic model (IKM) presented in [Pie68; Tho15] is revisited to elucidate important observations on the nature of IKS. A comparative study of nonsingular change of solutions in the joint space, workspace, and its geometric interpretation allows to prove the necessary and sufficient condition for a generic 3R robot to be cuspidal. In this process, the existence of reduced aspects (sub-regions of aspects with unique IKS) in generic 3R robots is proved too. The geometric analysis of 3R robots shed light on a new perspective to classify 3R robots that depends on the conic related to the kinematic polynomial. In [Pag08], the homotopy analysis presented a direction for counting the number of aspects in a generic 3R robot. Two of the presented homotopy classes namely 3(0, 0) and 4(0, 0) were suspected to exist which meant that the maximum number of aspects for a generic 3R serial robot would be five. A compar-

ative analysis of singularities in the joint space and conic interpretation confirms that these classes do not exist for 3R serial robot, thus allowing to close the topic of maximum number of aspects for a generic 3R robot.

The cuspidality analysis of simplified geometry is important from the point of view of applications. Almost all industrial robots have simplified geometry, and the analysis of constrained architectures allow us to analyze the determinant of the Jacobian matrix. The presented work shows that even though some simplified geometries lead to noncuspidal behavior, there exists others whose analysis remains challenging. A classification of robots with either orthogonal or parallel axes is presented to allow designers to choose from variety of designs that are noncuspidal. Later, a detailed framework for deciding cuspidality is presented that can analyze robots with collision constraints and joint limits. The thesis highlights a certified algorithm [Cha+22] as well as a numerical approach to deciding cuspidality. It is shown that almost all generic robots are cuspidal by nature.
Cuspidal robots lead to several issues in path planning. It is suspected that ABB IRB 6400C robot was recalled by the company after facing issues in path planning due to its cuspidal nature [WC22]. Recently, the issues in path planning of another cuspidal robot, MICO from Kinova robotics was identified in industry [Ver21]. Such reports of path planning issues in cuspidal robots have gone unnoticed, and the users generally blame the motion planning algorithms for a path failure.

The thesis details the issues in a commercial cuspidal robot, JACO Gen2 (non-spherical wrist), and discusses the implications of crossing multiple regions with varying IKS. It further points out issues in unique identification of 'configuration' of yet another cuspidal robot in industry, FANUC CRX-10ia/L. Most of the robots that are identified as cuspidal are sold in the market as cobots (fancy for collaborative robots) . Taking this point under consideration, the thesis further highlights why cuspidal robots should especially be avoided in collaborative applications. To utilise existing cuspidal robots in industrial setup, a detailed study for different types of paths and scenarios possible in path planning of cuspidal robots is discussed. A path planning framework is proposed that considers all the cases prior to the execution of the trajectory. An optimised trajectory planning is presented as an application of cuspidal robots to commercial robots.

Summary

This doctoral thesis is divided in four chapters and their main objectives are as follows:

1. State of the art and preliminaries

Chapter 1 presents the state of the art of all the topics related to cuspidal robots. It presents a literature review on the inverse kinematics of 6R robots, and later on the evolution of analysis of cuspidal robots. Later, the theoretical background for the cuspidality analysis is presented. It discusses the geometric interpretation of the IKM of a 3R robot as presented by Pieper [Pie68]. Later, certain terminologies developed for 3R robots in previous works [WEO96; Wen04; EOW95] is defined for ease of understanding of the proofs to follow. The chapter then presents concepts related to the cuspidal analysis of nR nonredundant robots. Singularities, and nonsingular change of solutions (its verification) with their representation in the joint space, workspace and the geometric interpretation are shown for comparative analysis.

2. Cuspidal analysis of 3R robots

The *orthogonal* 3R robots have been extensively analyzed in the past [Bur89; WEO96; Pag08; BWC04]. In [EOW95], it was stated that the cusp point in the workspace of a 3R *orthogonal* robot is necessary and sufficient condition for orthogonal 3R robots to be able to perform nonsingular change of solutions. Later, [Cor05] established that a cusp point was a sufficient condition for a *generic* 3R robot to be cuspidal. In chapter 2, a necessary and sufficient condition for a *generic* 3R robot to be cuspidal is presented. It utilises geometric interpretation of IKS, singularities and nonsingular change of solutions to present a proof by contradiction. As a result, the existence of reduced aspects in a generic 3R robot is proved by the same analysis too.

Geometric analysis of 3R robots is further extended to present classification of 3R robots based on the conic represented by the inverse kinematic polynomial. Each conic representation have interesting cases which allow a completely new perspective on the classification of 3R robots. Several sufficient criterias for a 3R robot to have maximum of two or four IKS are elucidated from the analysis. The geometric analysis combined with interpretation of IKS in the joint space is used to show nonexistence of a previously suspected homotopy classes $3(0,0)$ and $4(0,0)$. This allows to conclude upon the maximum

number of connected regions present in the joint space of a generic 3R robot.

3. Cuspidal analysis of 6R robots

The cuspidal analysis of a 6R robot is not well reported earlier. The only published work on cuspidality analysis of 6R robots is the anthropomorphic wrist-partitioned architecture, and UR5 from Universal robots [CSEDS20]. Both these examples are of noncuspidal robots with maximum eight IKS and the determinant of Jacobian matrix factoring into three distinct components. In Chapter 3, the cuspidality analysis of simplified geometries of 6R robots is presented initially. It discusses cases of robots with wrist located at the beginning, end, and in the middle of the chain. It further discusses 6R robots with three consecutive parallel axes present in the serial chain.

The detailed framework for deciding cuspidality of all 6R robots is presented in the later section. It discusses the building blocks of deciding cuspidality, and revisits the certified algorithm in [Cha+22] that uses tools from Real Algebraic Geometry and roadmap algorithms to decide cuspidal nature of the robot. The thesis presents a numerical approach for deciding cuspidality which is capable of considering collision constraints an joint limits of the robot. It uses Nelder Mead approach, time-optimal point-to-point trajectory planning to check connectivity of IKS in the joint space. Cuspidality analysis of 3240 robots including almost all the robots present in industry is presented as an application of the proposed framework. It is noted through this analysis that almost all generic robots are cuspidal by nature.

4. Path planning in cuspidal robots

Chapter 4 presents path planning issues in cuspidal robots. It presents two cases of existing commercial 6R robots that are cuspidal. A detailed kinematic analysis of both these robots is presented to motivate the reader about the interesting (a.k.a dangerous) properties of cuspidal robots. The FANUC CRX-10ia/L is used to highlight the issues of classifying sixteen solutions into eight categories. The misidentification of 'configurations' of this robot leads to a lot of confusion for the user. Later, JACO Gen2 (non-spherical wrist) is used to highlight the consequence of crossing multiple regions of varying IKS. This chapter discusses the dependence of feasibility as well as repeatability of the trajectory on the initial choice of IKS. It later motivates the reason to not implement cuspidal robots in collaborative applications where the trajectory is not pre-planned.

This chapter later presents a path planning framework for cuspidal robots that considers different types of trajectories possible in cuspidal robots. The different cases of scenarios arising in cupidal robots are discussed so that a future path planning optimisation algorithm can take cuspidality of a robot into account. Later a time optimised point-to-point trajectory planning for Jaco robot is presented as an application of the framework to commercial robots.

Chapter 1

State of the art, and theoretical background

This chapter sets a context of cuspidal robots and the evolution of research in this field. It provides a detailed history of cuspidal robots and the development of its theory to allow the reader get an overview as well as appreciate the presented work. The literature review is kept limited to cuspidal robots and inverse kinematics of 6R robots as they are closely related topics. Later, the theoretical context for the analysis of cuspidal robots presented in the thesis is put forth. Several definitions that are specific to cuspidality analysis are revisited and new definitions are put forth at the same time. The mathematical background utilised to implement different algorithms skipped from this chapter as it can be found in the initial research thus keeping the preliminaries focused on the contributions of the thesis. The algorithms wherever needed are mentioned in the Appendix of the thesis.

1.1 State of the art

Cuspidal robots are robots that have at least one singularity free connected region, *aspect* [BL86], with multiple inverse kinematic solutions (IKS). This implies that cuspidal robots can travel from one IKS to another without encountering a singularity. This property is applicable to parallel robots too [MD99], but it will not be discussed in the presented thesis (readers are directed to [WC22]). The following literature review details upon the work on serial cuspidal robots, and inverse kinematic solutions of nR non redundant robot.

1.1.1 Cuspidal robots: theoretical analysis

The possibility of changing IKS without crossing a 'special' configuration was never considered till the late 80s as it was strongly believed that the IKS always existed in distinct connected regions. The reason to believe the same was a quick analysis of 2R robots, and anthropomorphic robots with wrist partition. As these robots were widely used successfully across the industry, other designs were not analysed in depth. This made the analysis of nonsingular change of solutions a moot point. To bury the topic even deeper, a mathematical proof was presented to confirm that the IKS of a nR robot lie in distinct aspects [BL86].

This would change in 1988 when Innocenti and Parenti-Castelli produced two 6R robots who were able to travel from one IKS to another without crossing a singularity [PCI88]. Similar work was simultaneously reported by Burdick [Bur89] at CalTech where he presented an analysis of 3R regional manipulators. This result too went quite unnoticed, and was not given enough attention in the kinematics community. The research on 3R robots capable of changing IKS without crossing singularities was extended further by Wenger [Wen92]. The work presented the concept of characteristic surfaces after identifying that the number of IKS did not remain constant over an aspect for such robots. Later in 1995, Burdick presented a classification of 3R robots based on singularities, and put forth three conjectures. First two of them were related to the solvability as well as genericity of 3R robots and were refuted in [WE97].

In 1996, Wenger and El Omri [EOW95] noted that a cusp point in the workspace of 3R robots was a necessary and sufficient condition for a 3R *orthogonal* robot to be able to perform a nonsingular change of solutions. This paper coined the word 'cuspidal robots' due to the results on the analysis of *orthogonal* 3R robots. In 1998, Wenger presented a classification of 3R robots using homotopy classes [Wen98] which was extended in 2004 [CR04] that implemented computer algebra tools. Later in 2004, Baili [BWC04] presented an extensive and finer classification of 3R robots based on number of cusps based on algebraic analysis. A classification for a family of 3R robots was presented based on the topology of the workspace. It provided algebraic conditions for the bifurcation of the parameter space detailing domains for noncuspidal robots. In 2005, a D-H-parameter based condition for a 3R orthogonal robot to have maximum four IKS was presented [WCB05]. This provided a condition for designers to choose a robot with maximum two IKS which is always a noncuspidal case. In the same year, using Whitney's theorem [Whi55], Corvez [Cor05] noted that the existence of a cusp in the workspace of a 3R serial

robot is equivalent to a nonsingular change of solutions in a sufficiently small neighborhood of the cusp. This established the sufficient condition for a *generic* 3R robot to be cuspidal.

In 2006-07, Ottaviano presented workspace topologies [OCH07] of 3R robots and workspace analysis using level sets [OHC06] for 3R robots. An exhaustive study of workspace topologies for 3R robots with at least one parameter set to zero was presented by Zein [ZWC06] showing several examples whose workspace was well connected and had 4 IKS. In 2008, Paganelli presented complete homotopy classification of 3R robots. His work further presented two extra possible classes of homotopy namely 3(0, 0) and 4(0, 0). The later homotopy class if existent, would show that a generic 3R robot has a maximum of five aspects.

Several studies were presented for analysis of singularity loci of a 3R robot. The initial algebraic work of Kohli and Spanos [KS85] showed that relation of roots of the inverse kinematic polynomial with singularity. Later, Smith and Lipkin [SL90; SL93] presented a geometric interpretation for singularities, nodes and cusps in 3R robot workspace. Catastrophe theory was implemented for similar analysis by Thomas and Wenger [TW11]. Later, Thomas presented the analysis of singularity loci of 3R robots using the distance geometry approach reducing the IKM to analysis of two coplanar ellipses [Tho15]. Benoit [Ben17] presented a quantitative analysis of robots using topology and interval analysis. As cuspidality is a property dependent on the D-H parameters, it is important to study it in adaptable and reconfigurable robots. In 2016, Brandstötter [Bra16] presented cuspidality analysis in modular 6R serial robots. Recent studies on metamorphic 3R serial robots [KPMA19] further emphasize the importance of cuspidality analysis of robots with adjustable D-H parameters.

1.1.2 Cuspidal robots: industrial application

In industries, cuspidal robots are not well-known for a good reason. Before the introduction of non-redundant 'cobots', almost all the industrial arms consisted of a simplified geometry of anthropomorphic wrist-partitioned architecture. This meant that the IKM had analytical solutions and the IKS were separated by singularities. Not only were they separated by singularities but also provided a geometric intuition of the 'configurations' such as elbow up, shoulder right and wrist flip. Some of the robots known to deviate from the conventional designs were the ABB IRB 6400C, GMF150 and Fanuc P250iB [WC22] (refer to Figure 1.1). The ABB robot changed the permutation of first two axes that turned the anthropomorphic architecture to an orthogonal architecture. Due to the link

lengths chosen, this robot was cuspidal by nature. The robot was later recalled by ABB, and authors of [WC22] believe that the problems in path planning of cuspidal robots must have played a role in such decision. It has been noted that just tweaking the lengths of the robot would have rendered the robot noncuspidal [WC22]. GMF150 and Fanuc P250iB introduced an offset in the wrist, and were implemented for specific jobs such as painting jobs. The offset in the wrist alters the kinematic map and the number of IKS is not limited to eight anymore. Further analysis has shown that both these robots are cuspidal by nature. The joint limits play an important role limiting the workspace of the robot thus virtually avoiding the nonsingular change of solutions. The strong joint limits on GMF150 results into the operational space with maximum 2 IKS that are always separated by a singularity [WC22].

Another well known example of a robot with an offset in the wrist is the UR series from Universal Robots. The UR5 robot was analysed by Capco [CSEDS20] using computer algebra and it was shown that the robot has eight connected regions and the eight IKS of this robot are always separated by singularity. To the best of the author's knowledge, this is the only geometric architecture with an offset in the wrist implemented as an industrial robot and is a noncuspidal arrangement. Most of the cobots that exist in the market which have introduced the offset in the wrist by keeping the anthropomorphic architecture are cuspidal by nature (discussed in details in Chapter 3). Some of the analyzed robots include the widely used Jaco Gen 2 (non-spherical wrist), FANUC CRX-10ia/L, and Yaskawa HC10DTP. The Jaco robot and CRX series is discussed in details in Chapter 4. The path planning issues arising from existence of multiple kinematic regions with varying IKS are presented in [SCW23]. The cuspidality property can proved to be advantageous if the workspace is analysed completely, the trajectory is pre-planned considering the option for nonsingular change of solutions. Marauli [Mar+23] recently presented a time optimal point-to-point trajectories for cuspidal robots that included the consideration of nonsingular change of solutions for the first time.

1.1.3 Inverse kinematics

The evolution of the algorithms in inverse kinematics of 6R robots is important to have an idea of the strong correlation between the cuspidality analysis and generic algorithms for solving inverse kinematics. Kinematic analysis of 6R serial arms started more than half a century ago. The earliest kinematic analysis can be found in the work of [Pie68] in which the geometric interpretation of simplified geometries, *soluble robots*, was presented.

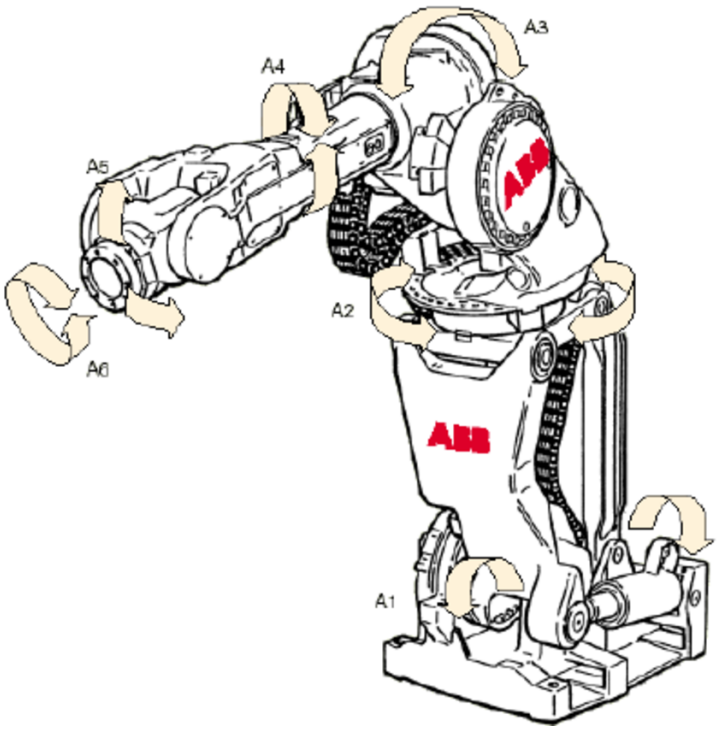

(a) ABB IRB 6400C robot

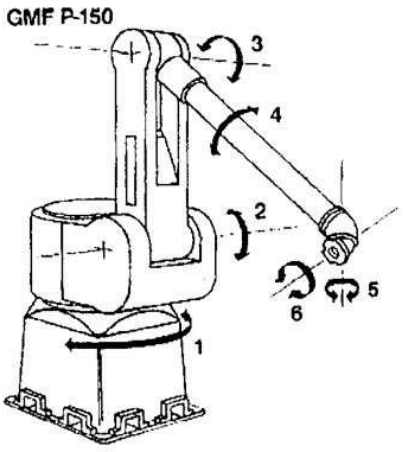

(b) GMF 150 robot

(c) FANUC 250ib robot

Figure 1.1 – Some of the first unconventional designs of industrial robots. Image credits: [WC22].

The work of Pieper,[Pie68], is well known to be the one of the first contributions towards 6R serial chains. He classified particular geometries of 6R serial chain, termed as soluble robots, that could be solved by decoupling the position analysis from the orientation. This work showed the inverse kinematic model (IKM) of a 3R serial chain as an intersection of a conic with a unit circle. This analysis has further helped in extending the cuspidality analysis for 3R serial chains [Sal+22b; Tho15; Sal+22a; SL90]. From 1973 to 1985, several proposals were made regarding the IKM for 6R serial chains [Rag+90; Fre73; Ang85]. In 1986, [Pri86] proved that the 6R serial arm have maximum 16 solutions over $\mathbb{C}$ using projective geometry. An analytical solution to an anthropomorphic architecture with an offset in the wrist was proposed by [Tri+15] using geometric methods. Inverse kinematics for similar architecture was proposed by [GL14; ZBSO21] with algebraic methods. One of the most recent advancement in the inverse kinematics of 6R serial chains was presented by [HPS07] where the geometric interpretation of the IKM was presented using dual quaternion representation and Study quadric (S_6^2), a six dimensional quadric in $\mathcal{P}^7$. [HPS07] showed that a generic 6R serial chain can be decomposed into two separate 3R serial chains whose workspace can be interpreted as the intersection of parameterized 3-space with Study quadric. The intersection of two 3-spaces, derived from four hyperplanes in $\mathcal{P}^7$ each, with the Study quadric gives the inverse kinematic polynomial required to solve the complete chain. The advantage of this method is that it uses equations linear in each joint value and thus is fast and accurate. It does not miss any IKS as we always get 16 solutions in $\mathbb{C}$. This method is extended for serial chains with prismatic joints too [CM19].

1.2 Preliminaries

1.2.1 Concepts related to 3R serial robot

This section covers the preliminaries necessary for the cuspidality analysis of a 3R serial robot. It begins by revisiting the geometric interpretation of the IKM proposed by Pieper [Pie68]. A presentation of several introductory concepts related to conics and their properties follows, as these hold significant relevance for the subsequent proofs. The section then introduces established definitions for cuspidal robots as mentioned in [Wen92; Wen04; BWC04], as well as conventions employed for the geometric description of the robot. An explanation of relevant definitions and their interpretations in different

spaces, such as joint space ($\mathcal{J}$), workspace, and the c_3s_3 plane (defined later), aims to provide the necessary background for the proof in Chapter 2. Finally, the section defines new terms specifically for the cuspidality analysis of generic 3R serial robots.

Concepts related to the inverse kinematics model

Kinematic analysis of 3R serial robots was first published seven decades ago. The earliest kinematic analysis can be found in the work of [Pie68] in which the geometric interpretation of simplified geometries, *soluble robots*, was presented. Later, algebraic tools were introduced to obtain the inverse kinematic polynomial and solve inverse kinematics for a generic 3R serial robots [KS85]. In this section, the preliminaries required for the analysis of IKS of a generic 3R serial robot. In this paper, original Denavit-Hartenberg parameters (D-H parameters) are used, as shown in Figure 1.2. The four parameters known as D-H parameters are linked to a specific convention used for connecting reference frames to the links of a robot manipulator or spatial kinematic robot [DH55]. These four transformation parameters used to denote the transformation of $(i+1)^{th}$ frame with respect to i^{th} frame are defined as:
d_i: offset along z_i to the common normal
θ_i: angle about z_i, from x_i to $x_{(i+1)}$
a_i: length of the common normal. This is the radius about z_i.
α_i: angle about $x_{(i+1)}$ from z_i to $z_{(i+1)}$

Generic 3R serial robot: A property that holds true for "almost all" of the functions is termed as a generic property of that class of functions. A general square matrix is invertible, and a generic polynomial does not have a root at zero. A generic property of a space is a property that holds at "almost all" points of the space (Sard's theorem). If we extend the same rationale, a robot qualifies to be a generic robot if there are no constraints on the geometric shape of the robot. But, the term *generic* for serial robots was defined in [PL92] which presented the relation of genericity with the nature of singularities of the robot. As per the work in [PL92], a generic 3R serial robot is defined as:

Definition 1. *A 3R serial robot is generic if there exists only rank-2 singularities, i.e., the locus of critical points in $\mathcal{J}$ has no self-intersection or does not include any isolated point singularity.*

This definition of *generic* robots is used in the kinematic community widely since its inception [Pag08; BWC04] and Figure 1.3 illustrates the singularities for generic and

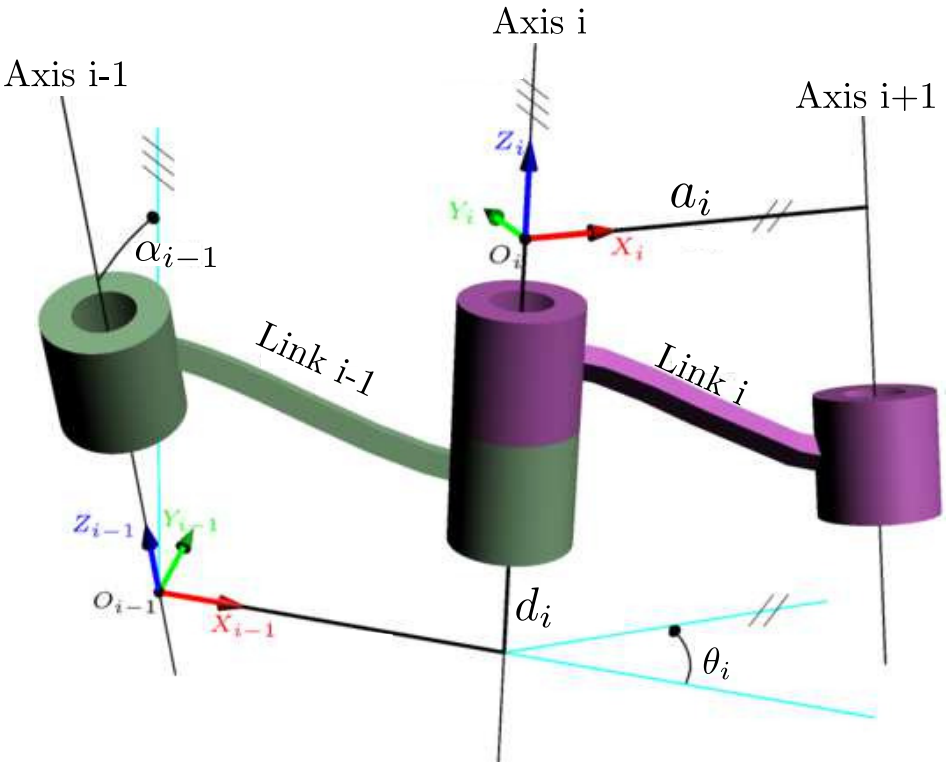

Figure 1.2 – The D-H parameter notations as presented in [DH55].

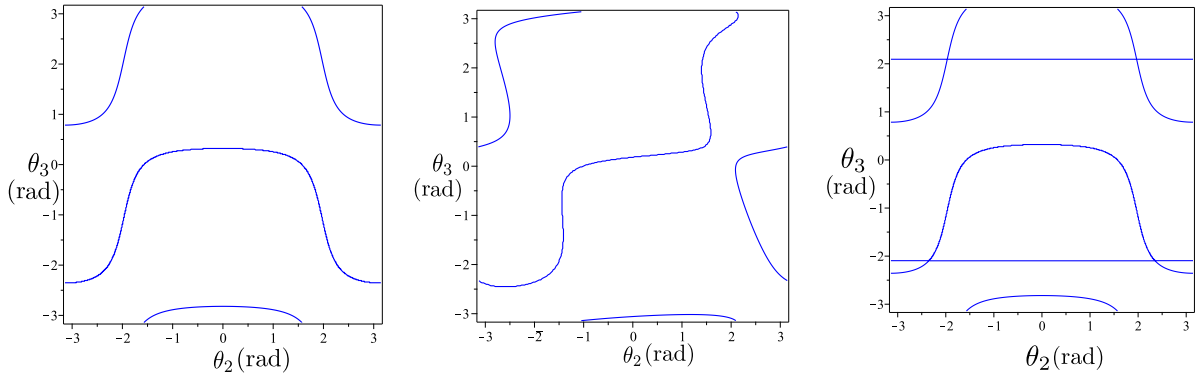

(a) Orthogonal generic robot (b) Generic robot (c) Non-generic robot

Figure 1.3 – Examples of generic and non-generic cases of a 3R serial robot
Robot parameters (1.3a): $\mathbf{d} = [0,\ 1,\ 0]$, $\mathbf{a} = [1,\ 2,\ \frac{3}{2}]$, $\alpha = [\frac{\pi}{2},\ \frac{\pi}{2},\ 0]$
Robot parameters (1.3b): $\mathbf{d} = [0,\ 1,\ 0]$, $\mathbf{a} = [1,\ 2,\ \frac{3}{2}]$, $\alpha = [\frac{\pi}{3},\ \frac{\pi}{6},\ 0]$
Robot parameters (1.3c): $\mathbf{d} = [0,\ 1,\ 0]$, $\mathbf{a} = [1,\ 2,\ 4]$, $\alpha = [\frac{\pi}{2},\frac{\pi}{2},0]$.

non generic robots. The issue with this definition is that the orthogonal 3R serial robots, robots with the constraint: α_1, α_2 equal to $\pm\frac{\pi}{2}$, are *generic* by the above definition. An example of the joint space of an orthogonal 3R serial robot with only rank-2 singularities is presented in Figure 1.3a.

In the presented work, the definition of a generic 3R serial robot is as defined by [PL92]. This definition allows us to classify robots with isolated singularities as non-generic which is helpful in the analysis discussed in coming chapters.

Inverse kinematic model of 3R serial robot

Solving the inverse kinematics of 3R serial robots was first reported in [Pie68] where it was noted that the solutions correspond to the intersection of a conic with a circle in $c_3 s_3$-plane, where c_3 and s_3 denote $\cos\theta_3$ and $\sin\theta_3$, respectively. The solution is presented briefly, as it has a key role in the proof to follow.
Let, $R = \rho^2 + z^2$, where $\rho^2 = x^2 + y^2 = g(\theta_2, \theta_3)$. The terms R and z can be written as

$$R = (F_1 \cos\theta_2 + F_2 \sin\theta_2)\, 2a_1 + F_3$$
$$z = (F_1 \sin\theta_2 - F_2 \cos\theta_2) \sin\alpha_1 + F_4$$

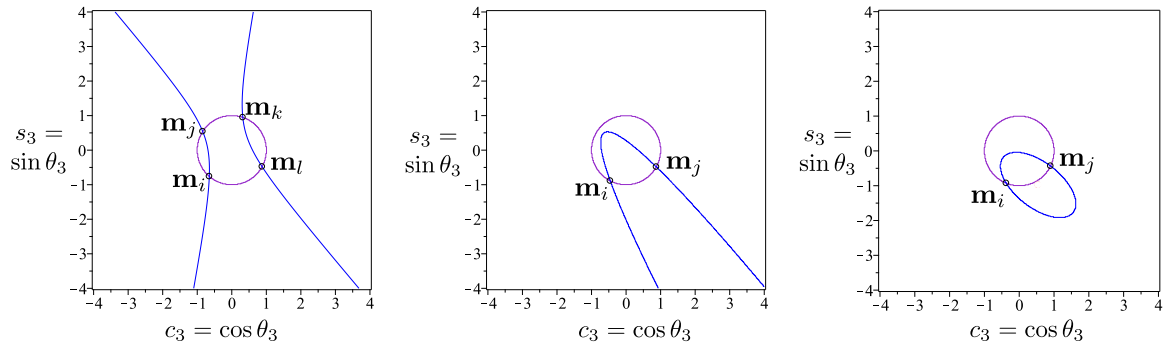

(a) Hyperbola case (b) Parabola case (c) Ellipse case

Figure 1.4 – Intersection of the conic and unit circle in c_3s_3-plane for robots with different D-H parameters. Every intersection is an IKS for the given pose.
Robot parameters (1.4a): $\mathbf{d} = [0,\ 1,\ 0]$, $\mathbf{a} = [1,\ 2,\ \frac{3}{2}]$, $\alpha = [\frac{\pi}{2},\ \frac{\pi}{6},\ 0]$, $(\rho, z) = (2.46, 0.15)$
Robot parameters (1.4b): $\mathbf{d} = [0,\ 1,\ 0]$, $\mathbf{a} = [1,\ 2,\ \frac{3}{2}]$, $\alpha = [\frac{\pi}{3},\ \frac{\pi}{2},\ 0]$, $(\rho, z) = (2.33, -0.26)$
Robot parameters (1.4c): $\mathbf{d} = [0,\ 1,\ 0]$, $\mathbf{a} = [1,\ 2,\ \frac{3}{2}]$, $\alpha = [\frac{\pi}{6},\frac{\pi}{2},0]$, $(\rho, z) = (2.4, 0.6)$.

where $F_i = g_i(\theta_3)$, for $i = 1, .., 4$. Upon rearrangement, we obtain the general equation of a conic in c_3s_3-plane as given in (1.1).

$$A_{xx}\, c_3^2 + 2A_{xy}\, c_3 s_3 + A_{yy}\, s_3^2 + 2B_x\, c_3 + 2B_y\, s_3 + C = 0 \tag{1.1}$$

The coefficients of the conic are skipped for brevity, but they are functions of the D-H parameters and of (R, z) as shown in (1.2),

$$\begin{aligned} A_{xx} &= h_1(a_1, a_2, a_3) \\ A_{xy} &= h_2(a_1, a_2, a_3, d_2, \alpha_2) \\ A_{yy} &= h_3(a_1, a_2, a_3, d_2, \alpha_1, \alpha_2) \\ B_x &= h_4(a_1, a_2, a_3, d_2, \alpha_2, R) \\ B_y &= h_5(a_1, a_2, a_3, d_2, d_3, \alpha_1, \alpha_2, R, z) \\ C &= h_6(a_1, a_2, a_3, d_2, d_3, \alpha_1, \alpha_2, R, z) \end{aligned} \tag{1.2}$$

The inverse kinematic solutions are defined by the intersection points between the conic (1.1) and the unit circle $c_3^2 + s_3^2 = 1$ in c_3s_3-plane. This conic can be a hyperbola, parabola or an ellipse depending on the D-H parameters and end-effector pose. An example of each one is shown in Figure 1.4. Performing the half tangent substitution, $t = \tan\frac{\theta_3}{2}$, we get a quartic inverse kinematic polynomial $M(t) = at^4 + bt^3 + ct^2 + dt + e$ similar to the one

mentioned in [KS85]. The coefficients of $M(t)$ are functions of the D-H parameters and of R and z. The solutions to the polynomial equation, $M(t) = 0$, are the intersection points between the conic and the circle and are labeled as $\mathbf{m}_\psi$, where $\psi \in \{i, j, k, l\}$ in the $c_3 s_3$-plane.

1.2.2 Singularities

The Jacobian of f at a certain configuration, denoted by $\mathbf{J}(\mathbf{q})$, is the Jacobian matrix of the robot at configuration $\mathbf{q}$:

$$\mathbf{J}(\mathbf{q}) = \frac{\partial f(\mathbf{q})}{\partial \mathbf{q}} \tag{1.3}$$

The singularities are the critical points of f in the $\mathcal{J}$ and correspond to the set of all configurations in the joint space where the Jacobian matrix loses rank, i.e. when the determinant of $\mathbf{J}$ is zero. The critical values are the images of the critical points in the workspace ($\mathcal{W}$). It is known that the roots of the inverse kinematic polynomial have multiplicity 2 or more at a singularity [KS85]. The algebraic expression of the singularity condition for an arbitrary 3R manipulator is recalled in Appendix A.1. The singularity in the workspace, the locus of critical values, is the image of the locus of critical points in the workspace and can be obtained from the inverse kinematic polynomial. The critical values in the workspace are those points where the following relation is satisfied:

$$\begin{aligned} M(t) &= 0 \\ \frac{\partial M(t)}{\partial t} &= 0 \end{aligned}$$

Where, $t = \tan\frac{\theta_3}{2}$ and $M(t)$ is the quartic inverse kinematic polynomial related to a 3R serial robot. The resulting algebraic expression is very large and is not reported here, see [KS85] and [TKA93] for more details.

With the conic representation, the geometric interpretation of a singularity associated with a double root is a point where the conic is tangent to the circle, as shown in Figure 1.5. The geometrical interpretation of a singularity associated with a root multiplicity higher than 2 is discussed in details in [SL90; SL93].

It is known that the singularities of 3R serial robots are independent of the first joint angle, θ_1 [PL92]. This allows us to reduce the 3-dimensional joint space to $\mathbb{T}^2$ parameterized by θ_2 and θ_3. In this part, the joint space, $\mathcal{J}$, will be used for the reduced joint space

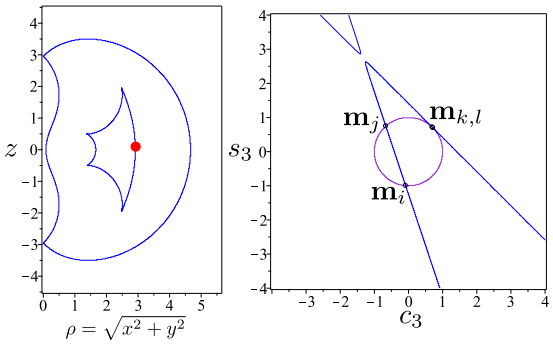

(a) Point in workspace with root multiplicity 2

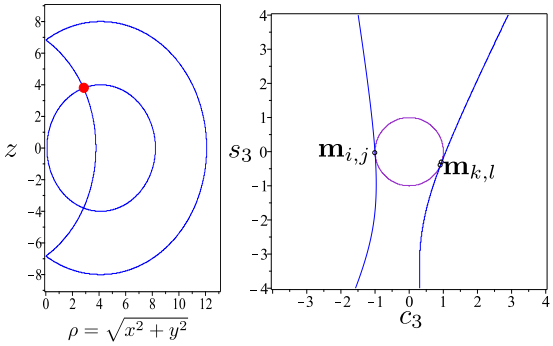

(b) Node point - pair of roots with root multiplicity 2

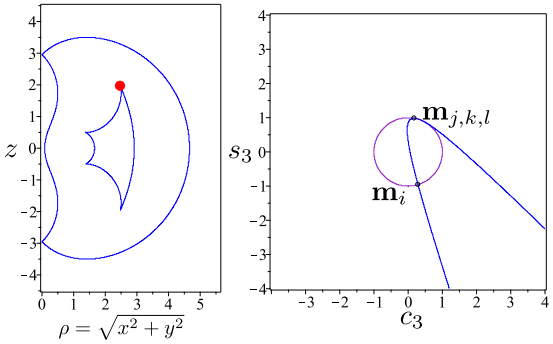

(c) Cusp point in workspace with root multiplicity 3

Figure 1.5 – Types of critical values in the workspace and corresponding tangency in $c_3 s_3$-plane.
Robot parameters (1.5a): $\mathbf{d} = [0,\ 1,\ 0]$, $\mathbf{a} = [1,\ 2,\ \frac{3}{2}]$, $\alpha = [-\frac{\pi}{2},\ \frac{\pi}{2},\ 0]$, $(\rho, z) = (2.913, 0.1)$.
Robot parameters (1.5b): $\mathbf{d} = [0,\ 1,\ 0]$, $\mathbf{a} = [4,\ 2,\ 6]$, $\alpha = [-\frac{\pi}{2},\ \frac{\pi}{2},\ 0]$, $(\rho, z) = (2.84, 3.79)$
Robot parameters (1.5c): $\mathbf{d} = [0,\ 1,\ 0]$, $\mathbf{a} = [1,\ 2,\ \frac{3}{2}]$, $\alpha = [-\frac{\pi}{2},\ \frac{\pi}{2},\ 0]$, $(\rho, z) = (2.48, 1.96)$.

in $\mathbb{T}^2$. Consequently, the workspace is symmetric about the first joint axis. Assuming unlimited joint travel, it can be described by a half cross-section in the plane ($\rho = \sqrt{x^2 + y^2}$, z).

Definition 2. *A node is a point in the workspace of a 3R serial robot where the inverse kinematic polynomial, $M(t)$, admits two distinct roots of multiplicity two.*

Definition 3. *A cusp is a point in the workspace of a serial robot that satisfies the following conditions:*

$$\begin{cases} M(t) = 0 \\ \frac{\partial M}{\partial t}(t) = 0 \\ \frac{\partial^2 M}{\partial t^2}(t) = 0 \end{cases} \tag{1.4}$$

where $M(t)$ is the inverse kinematic polynomial of degree four for a generic 3R serial robot.

In Figure 1.5c, the robot has four cusps located at the corners of the inner region of the workspace. The cusp has to satisfy:

$$\frac{\partial^3 M}{\partial t^3}(t) \neq 0 \tag{1.5}$$

in order to exclude quadruple roots. However, it was shown in [PL92] that quadruple roots cannot exist in generic 3R robots, and the condition in (1.5) is thus always satisfied here. So, in the context of a generic 3R serial robot, the cusp in the workspace relates only with satisfying condition in (1.4).

A n-solution region in the workspace is always bounded by the locus of critical values which, for a generic 3R serial robot, can include cusps and/or nodes.

Definition 4. *The components of critical values are the connected components of the locus of critical values, upon excluding all cusps and nodes.*

Figure 1.6 shows an example workspace of 3R serial robot with the components of the critical values formed by the presence of four cusps in the workspace.

Definition 5. *A binary robot is a 3R serial robot with maximum 2 inverse kinematic solutions for any feasible position.*

Definition 6. *A quaternary robot is a 3R serial robot with at least one reachable position with 4 inverse kinematic solutions.*

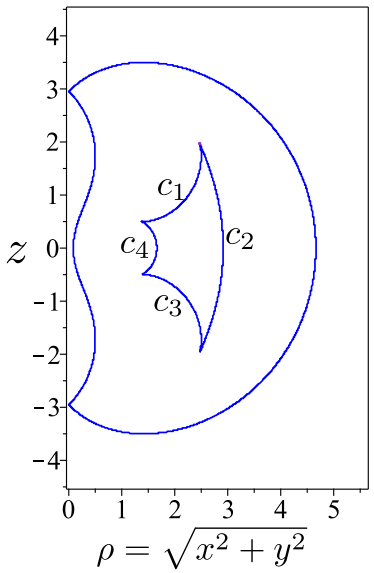

Figure 1.6 – An example showing the four components of a critical values in the workspace of a 3R serial robot. Robot parameters: $\mathbf{d} = [0,\ 1,\ 0]$, $\mathbf{a} = [1,\ 2,\ \frac{3}{2}]$, $\alpha = [-\frac{\pi}{2},\ \frac{\pi}{2},\ 0]$.

1.2.3 Concepts related to nR serial robots

In this section, the definitions related to a non redundant nR cuspidal robot are detailed. The previously known definitions of 'configuration' are revisited and redefined to make a distinction arising in cuspidal robots. Few known definitions are presented for clarity and new definitions relevant to Chapter 3 and Chapter 4 are introduced. The definition of cuspidal robots is presented at the end of the section. Some of the definitions in this section are explained with an example of 3R serial robot, but are applicable to any non redundant nR serial robot.

Definition 7. *An IKS that can be uniquely identified, either geometrically or analytically, is called a* configuration *of the robot.*

Commonly known examples of configurations in the 2R serial robots are the elbow up and elbow down configurations. These configurations are generally identified because of the factors of the determinant of the Jacobian. The conventional 6R serial robot such as KUKA KR5 is known to have maximum eight IKS and are separated into eight different configurations. If we denote the elbow position, shoulder position, and the wrist position in binary, then the eight configurations for such a robot are shown in Figure 1.7. The terms configuration and IKS have been used interchangeably in the past [Wen04; Bra16], but in this work we mark a distinction between them. Changing from one configuration

to another necessarily means that the two IKS are separated by a singularity such that the 'operation mode' does not change unless we cross the singularity. The main difference between a configuration and an IKS is that a configuration allows one to identify the operation mode of the robot without ambiguity. This can act as a type of classification when the configurations are identified by geometric differences, e.g. elbow up configuration. An IKS on the other side is simply a pre-image of the pose in the workspace. It is to be noted that a geometric interpretation may not be always possible for configurations. For example, in a quaternary noncuspidal 3R robot, the four solutions are separated by singularities but the four IKS do not necessarily hold a geometric meaning. In such case a given configuration can be checked for the aspect in which it belongs, and it can be assured that the robot will stay in this configuration unless we have crossed a singularity. An example of such a robot is shown in Figure 1.8a, where the four IKS are separated by the singularities allowing one to claim that there are four configurations of the robots. The Figure 1.8b on the other side is an example of a cuspidal robot with four IKS separated in 3 aspects. The IKS separated by singularities can be uniquely identified at any given time, and thus can be termed as configurations. The two IKS in the same aspect in this figure cannot be uniquely identified, and so do not qualify as a configuration.

Definition 8. *If S is the set of critical points in $\mathcal{J}$, the pre-image of the critical values excluding S is defined as the pseudosingularity curve, PS [TKA93; WEO96]:*

$$\begin{aligned} S &= \{\mathbf{q} \,|\mathbf{q} \in \mathcal{J}, \det \mathbf{J}(\mathbf{q}) = 0\} \\ PS &= f^{-1}(f(S)) \setminus S \end{aligned} \tag{1.6}$$

Definition 9. *The aspects are the largest singularity free connected regions in the joint space of a serial robot [BL86] (refer to Figure 1.9).*

Definition 10. *A reduced aspect is a region in the joint space that is bounded by the pseudosingularity curve and/or the locus of critical points and which has a one-to-one map to a bounded region in the workspace [Wen04].*

$$f_r : A_r \rightarrow W_r | A_r \in \mathcal{J}, W_r \in \mathcal{W} \tag{1.7}$$

then A_r is a reduced aspect if and only if f_r is a bijection. Figure 1.10 illustrates an example of a set of reduced aspects in an aspect of the joint space for an orthogonal 3R

(a) Configuration elbow(up)-shoulder(right)-wrist(unflip)

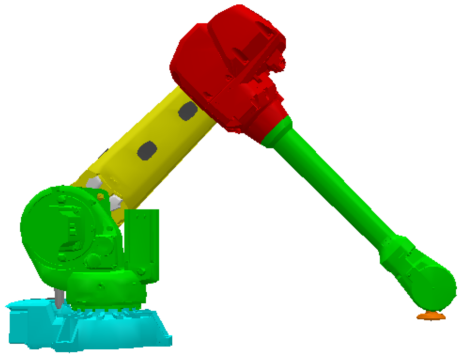

(b) Configuration elbow(up)-shoulder(left)-wrist(unflip)

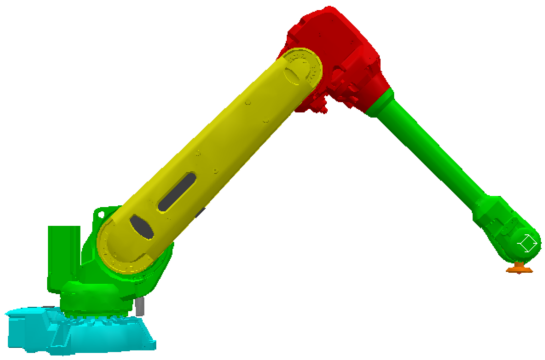

(c) Configuration elbow(up)-shoulder(right)-wrist(flip)

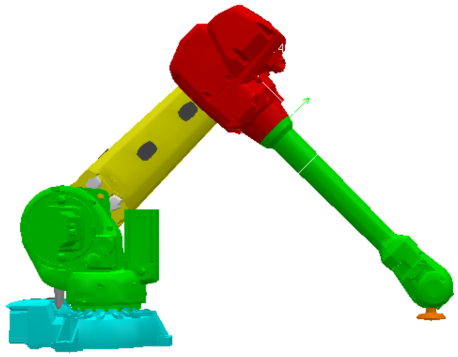

(d) Configuration elbow(up)-shoulder(left)-wrist(flip)

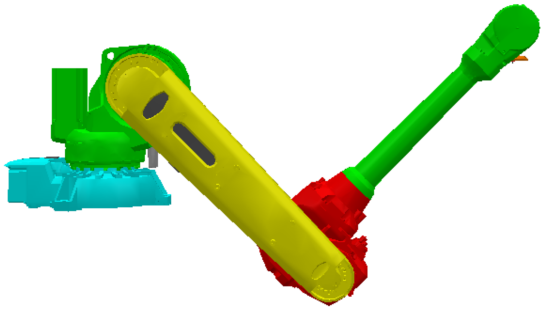

(e) Configuration elbow(down)-shoulder(right)-wrist(unflip)

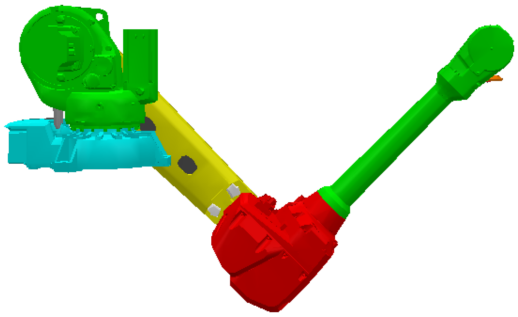

(f) Configuration elbow(down)-shoulder(left)-wrist(unflip)

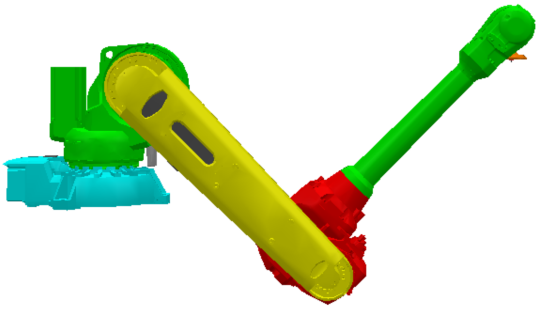

(g) Configuration elbow(down)-shoulder(right)-wrist(flip)

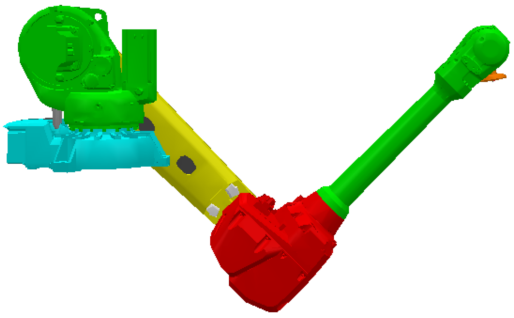

(h) Configuration elbow(down)-shoulder(left)-wrist(flip)

Figure 1.7 – The eight configurations of a wrist-partitioned arm enumerated in binary to denote the positions for elbow-shoulder-wrist.

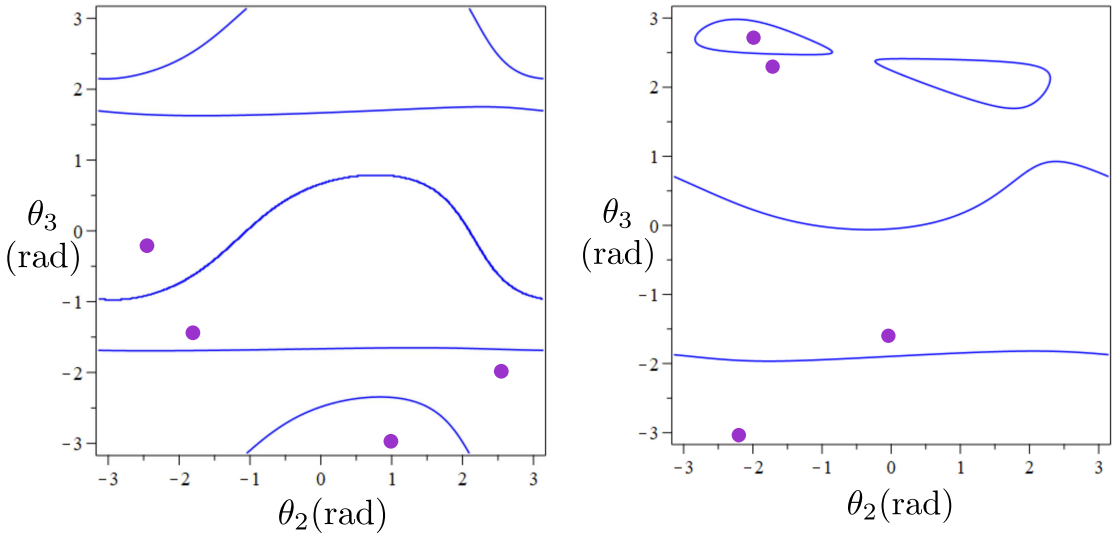

(a) Joint space of a noncuspidal robot with 4 IKS in 4 aspect

(b) Joint space of a cuspidal robot with 4 IKS in 3 aspect

Figure 1.8 – Joint space of a noncuspidal and cuspidal robot. On the left, we have 4 aspects and four IKS separated by singularities and thus a 'configuration' can be uniquely assigned. On the right a robot has 4 IKS distributed in 3 aspects and no unique classification is possible.

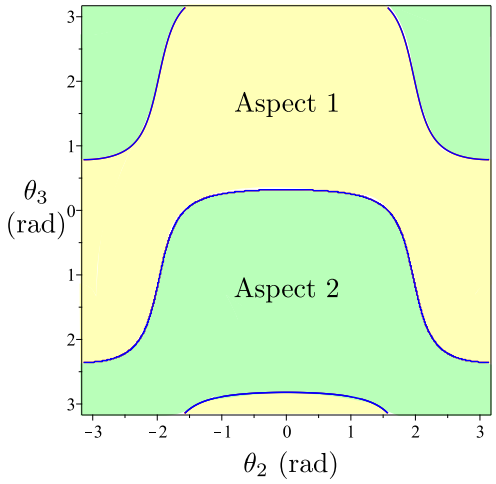

Figure 1.9 – The two singularity free connected regions, called aspects, in joint space for a 3R serial robot. Robot parameters: $\mathbf{d} = [0, 1, 0]$, $\mathbf{a} = [1, 2, \frac{3}{2}]$, $\alpha = [-\frac{\pi}{2}, \frac{\pi}{2}, 0]$

cuspidal robot. The blue lines are the locus of critical points and critical values in the joint space and the workspace, respectively, while the red lines are the pseudosingularities present in the joint space. Note that the pink and yellow regions in the joint space map to the same region in the workspace. This means that there are two IKS in an aspect.

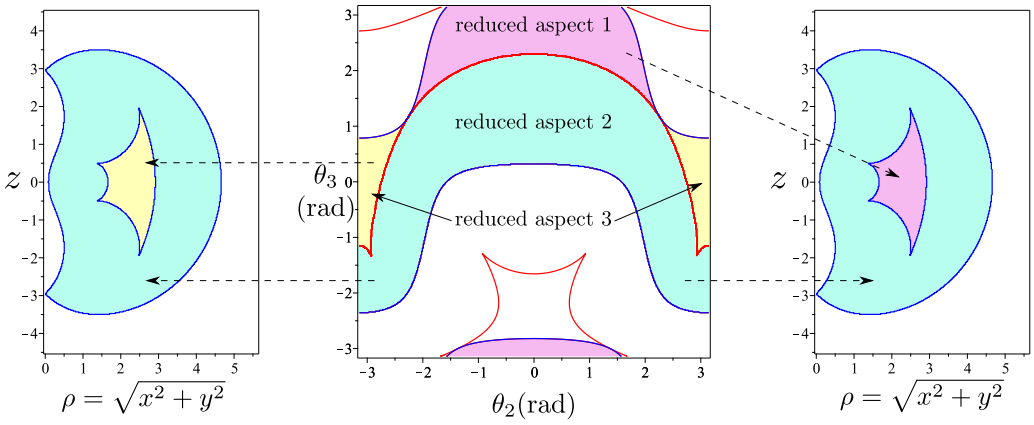

Figure 1.10 – An example showing a set of reduced aspects present in an aspect of the joint space.
Robot parameters: $\mathbf{d} = [0,\ 1,\ 0]$, $\mathbf{a} = [1,\ 2,\ \frac{3}{2}]$, $\alpha = [-\frac{\pi}{2},\ \frac{\pi}{2},\ 0]$.

Denote with

$$\mathcal{I}_{\mathbf{x}} = \{\mathbf{q} \in \mathbb{T}^n \,|\, \mathbf{x} = f(\mathbf{q})\} \tag{1.8}$$

the set of IKS for given EE-pose $\mathbf{x}$. For a non-redundant robot, i.e. $\dim W = \dim \operatorname{im} f \leq n$, the IKS set consists of a finite $n_{\mathbf{x}}$ number of IKS $\mathcal{I}_{\mathbf{x}} = \{\mathbf{q}_1, \ldots, \mathbf{q}_{n_{\mathbf{x}}}\}$.

Definition 11. *Let $\mathbf{q}_1$ and $\mathbf{q}_2$ be two points in $\mathcal{J}$ and $\sigma(\mathbf{q}_1, \mathbf{q}_2, t)$ where $t \in [0, 1]$ is a parameter such that $t = 0, \sigma = \mathbf{q}_1$ and $t = 1, \sigma = \mathbf{q}_2$, be a path between these two points, then, $\sigma(\mathbf{q}_1, \mathbf{q}_2, t)$ is defined as a nonsingular change of solutions if and only if:*

$$\sigma(\mathbf{q}_1, \mathbf{q}_2, t) \cap S = \varnothing \,|\, \mathbf{q}_1, \mathbf{q}_2 \in \mathcal{I}_{\mathbf{z}} \tag{1.9}$$

In the workspace, a nonsingular change of solutions defines a loop as we end up at the same position we started from. It has been noted in [Wen19] that the nonsingular trajectory in workspace always starts from a point in the workspace with four IKS. The nature of this trajectory in the workspace will be studied in details in the next chapter. In the $c_3 s_3$-plane, the nonsingular change of solutions has an interesting interpretation. If we have four intersection points, $\mathbf{m}_i$, $\mathbf{m}_j$, $\mathbf{m}_k$ and $\mathbf{m}_l$, between the conic and the unit circle in $c_3 s_3$-plane corresponding to the four IKS at a particular end-effector pose, then

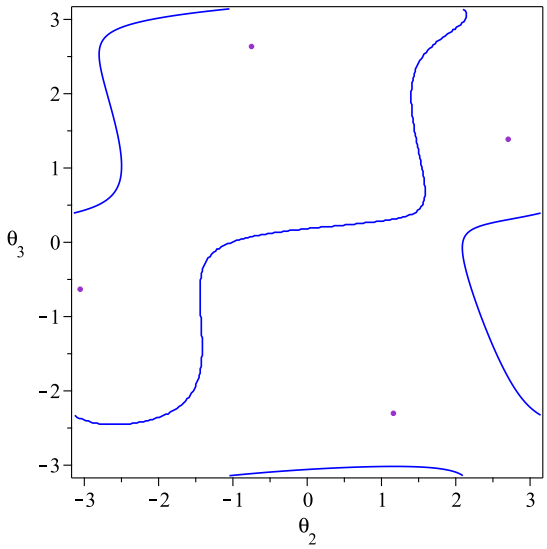

Figure 1.11 – Example of nonsingular change of solutions in the joint space and the progress of det(**J**) on the path.
Robot parameters: $\mathbf{d}$ = [0, 1, 0], $\mathbf{a}$ = [1, 2, $\frac{3}{2}$], α = [-$\frac{\pi}{2}$, $\frac{\pi}{2}$, 0], path = (-3, -0.5) to (-0.742, 2.628).

the nonsingular change of solutions between two IKS corresponding to $\mathbf{m}_j$ and $\mathbf{m}_l$ is such that $\mathbf{m}_j$ switches with $\mathbf{m}_l$ without vanishing as an intersection point of the conic and the unit circle. An example of a nonsingular change of solutions is illustrated in Figure 1.12.

The singularities of generic 6R robots depend on $\theta_i, i = 2, ..5$, and thus lie in a 4-dimensional space that cannot be visualized. It can be confirmed that a given change of solutions path is nonsingular if the determinant of the Jacobian matrix does not change sign along the path. Figure 1.11 shows an example of a nonsingular change of solutions in a 3R robot. It can be seen that the path in the joint space never crosses the locus of critical points (shown in blue lines) and, accordingly, the determinant value does not change signs throughout the path.

Definition 12. *Cuspidal robots without collision constraints or joint limits can be defined as robots that have at least one aspect with more than one IKS. Alternatively, it can be defined as a robot, R, for which there exists a nonsingular change of solutions.*

$$R : \exists\, \sigma(\mathbf{q}_1, \mathbf{q}_2, t) \cap S = \varnothing \,|\, \mathbf{q}_1, \mathbf{q}_2 \in \mathcal{I}_{\mathbf{x}} \tag{1.10}$$

Definition 13. *A closed path in the workspace is defined as a repeatable path if the path*

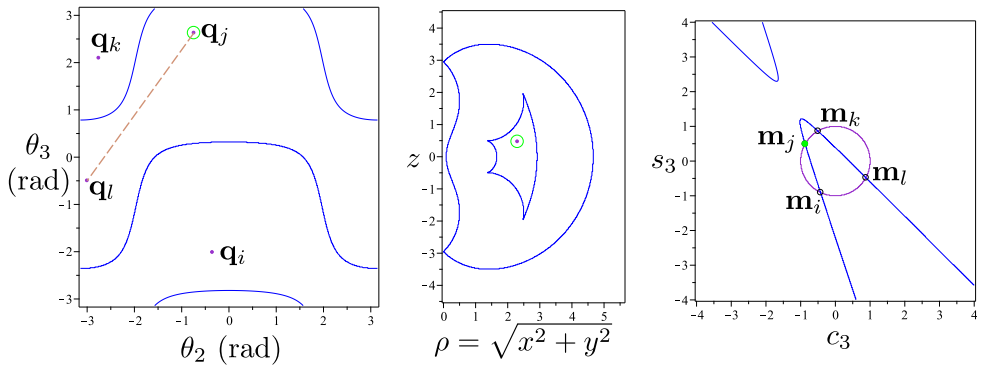

(a) Phase 1: Starting from a point in workspace with 4 IKS

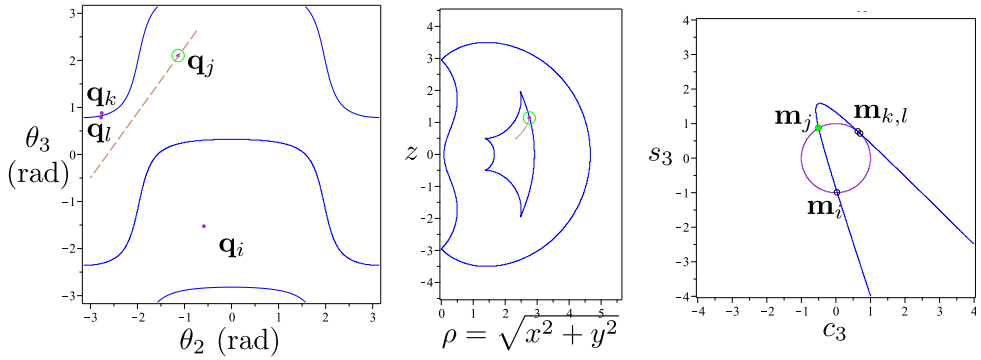

(b) Phase 2: Entering a 2 solution region in workspace

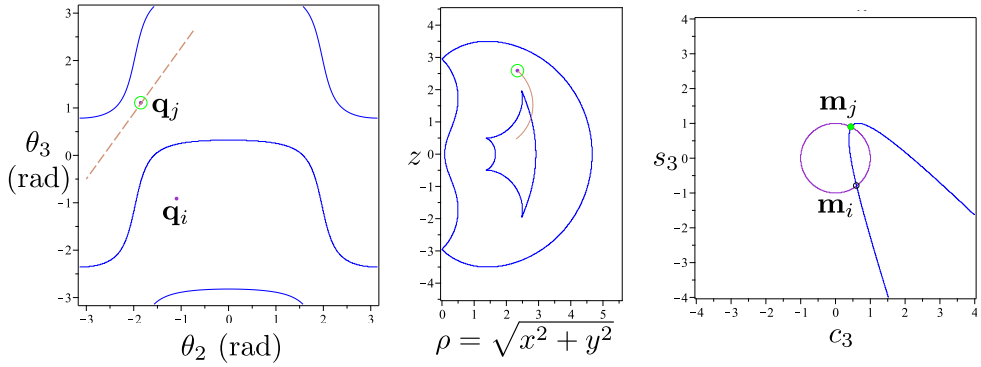

(c) Phase 3: intersection point crosses the vertex of the conic

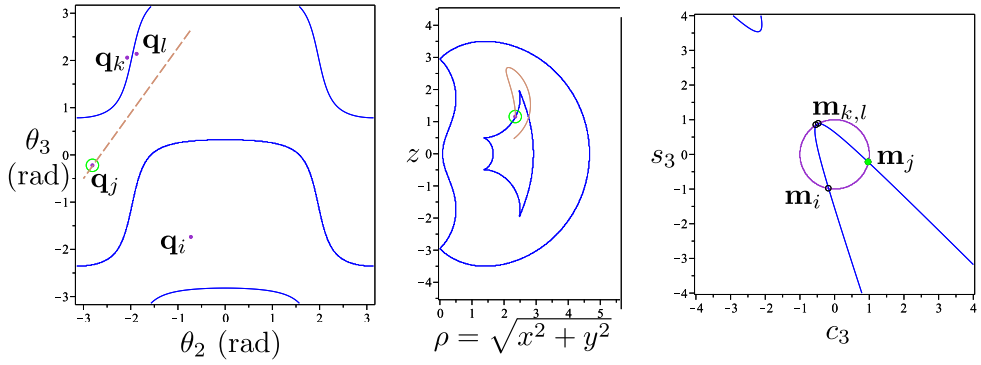

(d) Phase 4: Re-entering the 4-solution region in workspace

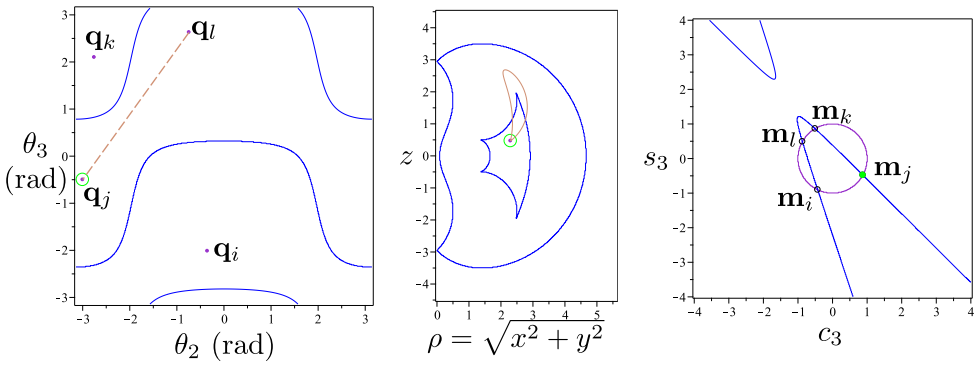

(e) Phase 5: Reaching the same position in workspace

Figure 1.12 – An example of a nonsingular change of solutions in the joint space and the workspace, and its corresponding geometrical interpretation in the c_3s_3-plane.
Robot parameters: $\mathbf{d} = [0, 1, 0]$, $\mathbf{a} = [1, 2, \frac{3}{2}]$, $\alpha = [-\frac{\pi}{2}, \frac{\pi}{2}, 0]$.
path in the joint space (θ_2, θ_3): from (-0.742, 2.628) to (-3, -0.5).

can be executed infinite times. A repeatable path can correspond to a nonsingular change of solutions.

Definition 14. *A closed path in the workspace is defined as non-repeatable path if the path can be executed strictly finite number of times. A non-repeatable path is compulsorily a nonsingular change of solutions and thus a property of cuspidal robots.*

Definition 15. *A regular closed path is a repeatable path such that the initial IKS is same as the final IKS. Such path is a closed loop in the workspace as well as the joint space.*

Definition 16. *The path defined in the workspace which cannot be traversed starting from a defined IKS is termed as an infeasible path.*

Definition 17. *The path defined in the workspace which can be traversed starting from a defined IKS without discontinuity is termed as a feasible path.*

Proposition 1. *A non-repeatable path can execute a closed loop for no more than seven times.*

Proof. It has been shown already that a 6R robot has 16 solutions in the complex field. As there exists a singularity for every robot, the number of aspects for a given a robot is at least 2. Each IKS has an access to a point on the locus of critical values, and the number of IKS decreases or increases upon crossing this locus. This suggests that every point on the locus of critical values is shared by at least two IKS and both of them have different

signs of det(**J**). Following this argument, it can be shown that the IKS in aspects with positive det(**J**) equal the IKS in aspects with negative det(**J**). If a given pose, $\mathbf{x} \in \mathcal{W}$, has $m(\leq 16)$ IKS, $\mathbf{q}_i, i \in i, .., m$, then

$$n(\mathbf{q}_{\det(\mathbf{J})>0}) = n(\mathbf{q}_{\det(\mathbf{J})<0}) = \frac{m}{2}$$

It follows that there exists maximum eight IKS in an aspect. In order to not be able to repeat the path continuously, the initial IKS should be different from the final IKS and there should be no path such that its final IKS corresponds to any of the previously reached IKS.

Alternatively, consider a graph, $G = (V, E, \varphi)$, such that the vertices, $v_i \in V, i \in \{1, 2, .., 8\}$, are the IKS of a pose in the workspace in an aspect. Each edge of this graph corresponds to a nonsingular change of solutions and in order for the given path to be a non-repeatable path, the graph should not have any closed robots. The longest simple robot of G with v vertices has $v - 1$ edges and thus the closed path in the workspace can be repeated maximum 7 times, as $(v \leq 8)$. □

Chapter 2

3R SERIAL ROBOTS

In this chapter, the kinematic analysis for 3R serial robot is presented. Section 2.1 presents a necessary and sufficient condition for a generic robot to be cuspidal. It utilizes the geometric interpretation of the IKM and compares the nonsingular change of solutions in the joint space, workspace and the $c_3 s_3$-plane. The existence of reduced aspects for a generic 3R serial robot is proved too. In section 2.2, the geometric analysis is extended to present special cases of 3R serial robots representing each type of possible conic. The bifurcation criteria is discussed and special properties related to the conics are presented in this section. This section further provides sufficient conditions for binary as well as quaternary 3R serial robots. In section 2.2.2, we prove that the two homotopy classes suspected in [Pag08] do not exist allowing us to claim that the maximum number of aspects for a generic 3R serial robot is four. The chapter concludes by summarizing the results obtained from the work on geometric analysis of generic 3R serial robots.

2.1 Generic 3R serial robots

In this section, we present the necessary and sufficient condition for a given generic 3R serial robot to be cuspidal. The proof discusses several lemmas and propositions, and utilizes the definitions in Chapter 1.2 to arrive at a conclusion. Figure 2.1 shows a flowchart of the step-wise organization of the proof. Figure 2.1 should be read as follows: Proposition 2 is the necessary condition for a 3R serial robot to be cuspidal, which along with the sufficient condition for the robot to be cuspidal, Theorem 1, makes it possible to establish the necessary and sufficient condition of cuspidality at the end of this section, Theorem 3. To prove Proposition 3, Lemmas 1, 2 and 3 are first established, leading to Theorem 2 which, along with Proposition 2, leads to Lemma 4. Lemmas 4 and Lemma 5 lead to Lemma 6, which makes it possible to prove Proposition 3.

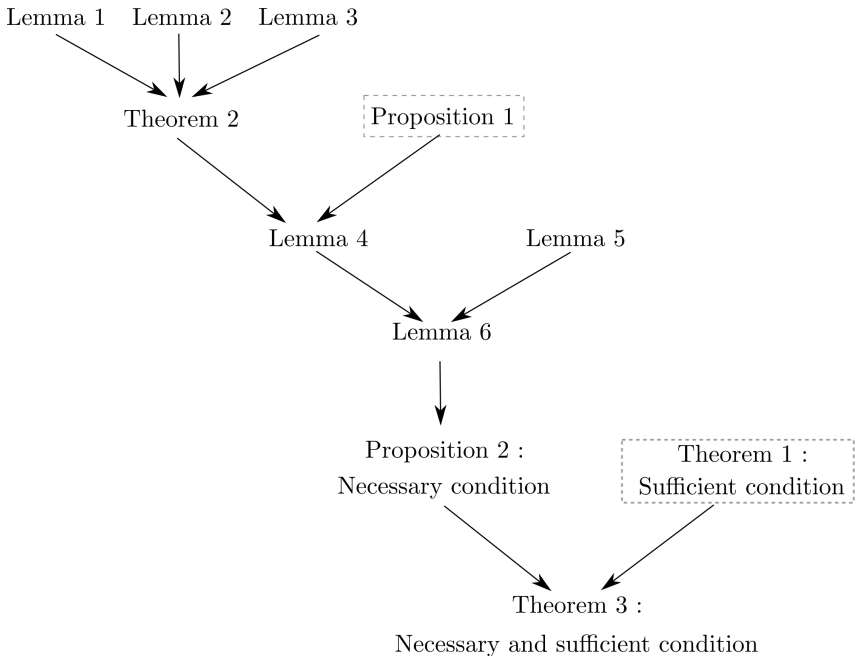

Figure 2.1 – The step-wise organization of the proof for the necessary and sufficient condition for a generic 3R serial robot to be cuspidal. The dotted box corresponds to Proposition 2 and Theorem 1 which are already proven statements.

2.1.1 Sufficient condition

Theorem 1. *In a 3R serial robot, the existence of a cusp in the workspace is a sufficient condition for the robot to be cuspidal.*

Proof. Using Whitney's theorem [Whi55], it has been noted in [Cor05], that the existence of a cusp in the workspace of a 3R serial robot is equivalent to a nonsingular change of solutions in a sufficiently small neighborhood of the cusp. □

It is important to note that the work in [Cor05] does not establish the necessary and sufficient cuspidality condition, as the existence of a cusp can be confirmed only if we have a nonsingular change of solutions in a *sufficiently small* neighborhood. In Figure 2.2, the nonsingular change of solutions from $\mathbf{q}_1$ to $\mathbf{q}_3$ for a point, $\mathbf{x}$, in the workspace is not local and thus the equivalence in [Cor05] cannot be used to prove that the statement in Theorem 1 is a necessary condition too.

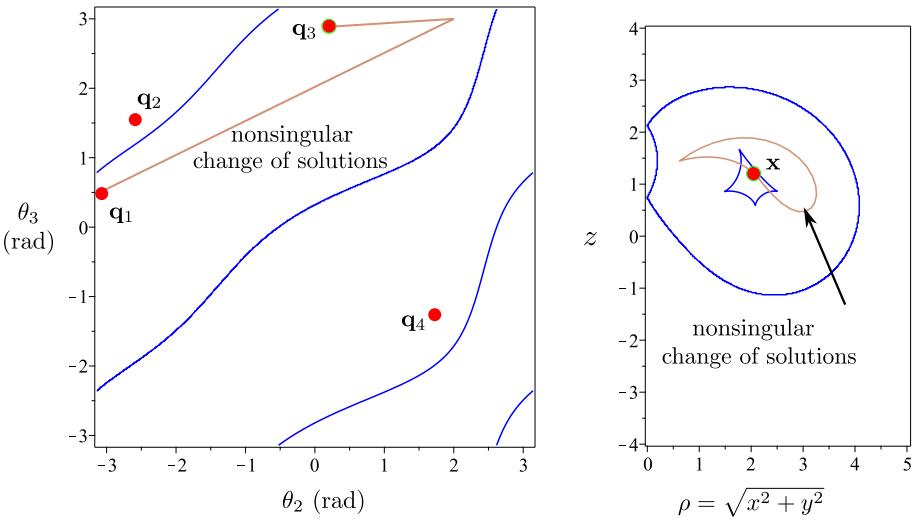

Figure 2.2 – Example showing a non-local nonsingular change of solutions in joint space and workspace.
Robot parameters: d = [0, 1, 0], a = [1, 2, 1], $\alpha = \left[\frac{\pi}{6}, \frac{\pi}{2}, 0\right]$.
Trajectory in joint space (θ_2, θ_3): (-3, 0.5) to (2, 3) to (0.2, 2.8).

2.1.2 Proof for reduced aspects in 3R serial robot

The existence of reduced aspects was investigated in the past for 3R orthogonal robots [Wen04; EOW95]. The existence of reduced aspects in a generic robot was not proven earlier and remained an open question. In this section we present lemmas related to the conic interpretation of the IKM of a generic 3R serial robot and later prove the existence of the reduced aspects in a generic 3R serial robot. This proof is a significant contribution of the thesis as it answers a long standing question and allows one to analyze the 3R serial robots with better clarity. The proof of existence of reduced aspects provides a foundation to establish the necessary and sufficient condition for a generic 3R serial robot to be cuspidal.

Proposition 2. *If $\mathcal{A}$ and $\mathcal{B}$ are two bounded regions in the same aspect sharing a common pseudosingularity curve $\mathcal{AB}^*$ and their image in the workspace belongs to regions $\mathcal{A}_w$ and $\mathcal{B}_w$ respectively, then the absolute difference between the number of IKS in the region $\mathcal{A}_w$ and region $\mathcal{B}_w$ is always two (refer to Figure 2.4). Moreover, the absolute difference between the number of IKS in region $\mathcal{A}_w$ or $\mathcal{B}_w$ and at any point on the boundary $\mathcal{AB}^*_w$ between them, is always one (Figure 2.3).*

This is a well-known property [KS85] and is commonly interpreted as two inverse

kinematic solutions merge at a singular configuration. It is important to note that for a generic 3R robot, the shared boundary does not include isolated finite points.

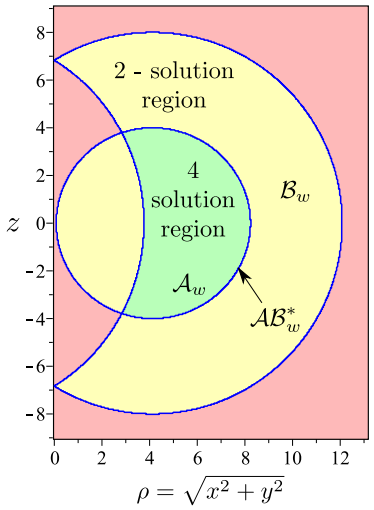

Figure 2.3 – Regions separated by the locus of the critical values in the workspace. There are 3 IKS on $\mathcal{AB}^*_w$.Robot parameters: d = [0, 1, 0], a = [4, 2, 6], α = [-$\frac{\pi}{2}$, $\frac{\pi}{2}$, 0].

If a pseudosingularity exists in the joint space of a 3R serial robot, then each point on the pseudosingularity curve has an image on the locus of critical values in the workspace. Therefore, crossing a pseudosingularity curve in the joint space is similar to crossing the locus of critical values in the workspace, and thus the images of the regions sharing the pseudosingularity curve should have absolute difference of two.

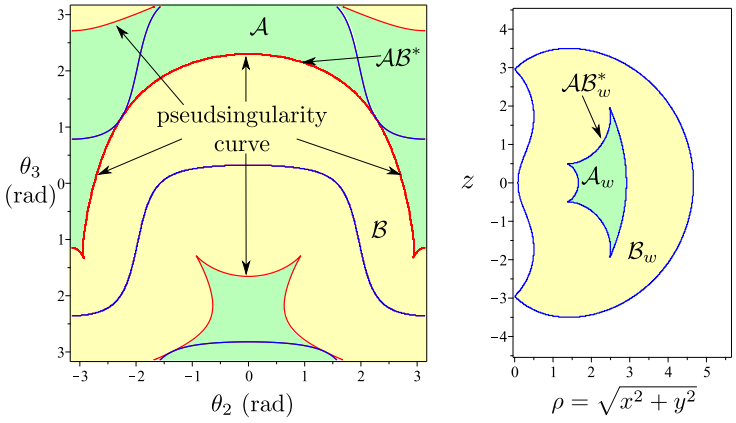

Figure 2.4 – An example of the regions separated by the pseudosingularity curve in joint space and the corresponding images in workspace.
Robot parameters: d = [0, 1, 0], a = [1, 2, $\frac{3}{2}$], α = [-$\frac{\pi}{2}$, $\frac{\pi}{2}$, 0], (ρ, z) = (2.5, 0.5).

Lemma 1. *The nature of the conic, i.e. ellipse, hyperbola or parabola, related to a particular set of D-H parameters of a generic 3R serial robot remains the same throughout the workspace of the robot.*

Proof. The determinant of matrix $\mathbf{N}$ displayed in (2.1) determines the nature of a given conic. Since A_{xx}, A_{xy} and A_{yy} are functions of D-H parameters only as shown in (1.2), the nature of conic remains same throughout the workspace.

$$\mathbf{N} = \begin{bmatrix} A_{xx} & A_{xy} \\ A_{xy} & A_{yy} \end{bmatrix} \tag{2.1}$$

□

Lemma 2. *The orientation of the principal axes of the conic related to a particular set of D-H parameters of a generic 3R serial robot is constant throughout the workspace of the robot.*

Proof. The eigenvectors of $\mathbf{N}$ determine the orientation of the principal axes and, as noted in the proof of Lemma 1, $\mathbf{N}$ is independent of R and z and the eigenvectors are thus constant for a given robot. □

For a given point $\mathbf{p}$ in the workspace of a generic 3R serial robot, let there be $n \in \{1, 2, 3, 4\}$ distinct pre images such that we have n intersection points between the conic and the circle in $c_3 s_3$-plane. We will say that an intersection point, $\mathbf{m}_j$, in $c_3 s_3$-plane is adjacent to another intersection point, $\mathbf{m}_i$, if it is the first intersection point encountered after traveling in either clockwise or counterclockwise direction starting from $\mathbf{m}_i$. It has been illustrated in Figure 1.5 that any path in the workspace starting from $\mathbf{p}$ to any point on the boundary, results in at least 2 intersection points coming together at the tangent point in the $c_3 s_3$-plane. Accordingly, the following Lemma is set:

Lemma 3. *In a generic 3R serial robot, two intersection points, $\mathbf{m}_i$ and $\mathbf{m}_j$, meet at a tangent point corresponding to roots of the inverse kinematic polynomial with multiplicity two, only if they are adjacent to each other in the cyclic ordering of the intersection points in the $c_3 s_3$ - plane.*

Proof. For two IKS $\mathbf{m}_i, \mathbf{m}_j$ to meet together, $\mathbf{m}_i$ should start traveling towards $\mathbf{m}_j$, or $\mathbf{m}_j$ should travel towards $\mathbf{m}_i$. If there exists an intersection point $\mathbf{m}_k$ between them, then $\mathbf{m}_i$ and $\mathbf{m}_j$ can meet at a tangent point only after either $\mathbf{m}_i$ or $\mathbf{m}_j$ meets $\mathbf{m}_k$ at a tangent

point. A graphical illustration of the tangency between the adjacent points is given in Figure 2.5. □

As the critical values represent tangent points in the c_3s_3-plane, a node in the locus of critical values is when we have two tangency points. A cusp occurs when three out of four intersection points merge together at a tangent point. All four solutions cannot meet together at a tangent point in a generic 3R serial robot [PL92]. Isolated finite points of critical values cannot exist in a generic 3R robot, and thus this particular case is not considered in the context of critical values.

Theorem 2. *In an arbitrary generic 3R serial robot, the inverse kinematic solutions lie always in distinct reduced aspects.*

Proof. As shown in Lemma 2, the orientation of the conic corresponding to a particular set of D-H parameters remains constant. Suppose that the inverse kinematic solutions do not belong to distinct reduced aspects. Then, there should exist a path between two inverse kinematic solutions without intersecting a pseudosingularity or the locus of critical points. The interpretation of such a path in the c_3s_3-plane is that two intersection points $\mathbf{m}_j$ and $\mathbf{m}_l$ switch places and neither $\mathbf{m}_j$ nor $\mathbf{m}_l$ becomes a tangent point in the c_3s_3-plane.
As the orientation of the principle axes of the conic does not change, the intersection points, $\mathbf{m}_j$ and $\mathbf{m}_l$, in the c_3s_3-plane cannot be adjacent in a cyclic ordering since it would imply $\mathbf{m}_j$ meeting $\mathbf{m}_l$ at a tangent point to switch with $\mathbf{m}_l$. Let $\mathbf{m}_k$ lie between $\mathbf{m}_j$ and $\mathbf{m}_l$ while traveling clockwise starting from $\mathbf{m}_j$ and let $\mathbf{m}_i$ lie between $\mathbf{m}_j$ and $\mathbf{m}_l$ while traveling counterclockwise starting from $\mathbf{m}_j$ as shown in Figure 2.5a. As we know that the conic is not rotating, the only way for $\mathbf{m}_j$ to switch to $\mathbf{m}_l$ is to meet either $\mathbf{m}_k$ or $\mathbf{m}_i$ at a tangent point. If not, then $\mathbf{m}_l$ meets $\mathbf{m}_k$ or $\mathbf{m}_i$ at a tangent point. This is a contradiction of the assumption that the inverse kinematic solutions associated with $\mathbf{m}_j$ and $\mathbf{m}_l$ do not lie in distinct reduced aspects. □

2.1.3 Necessary condition

In this section, we establish a proof that the existence of a cusp in the workspace is a necessary condition for a 3R generic robot to be cuspidal. By using the proof for existence of reduced aspects in a generic 3R serial robot (Theorem 2), we analyze the nature of nonsingular change of solutions to present the necessary condition for a 3R serial robot

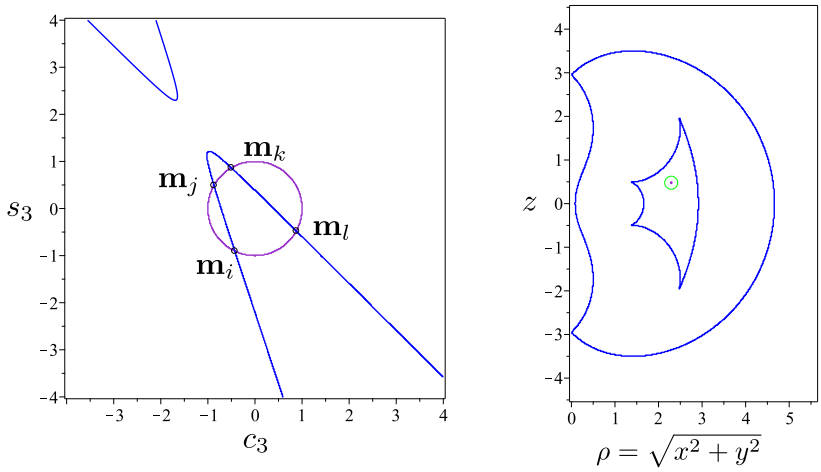

(a) Initial configuration with 4 intersections in $c_3 s_3$ - plane

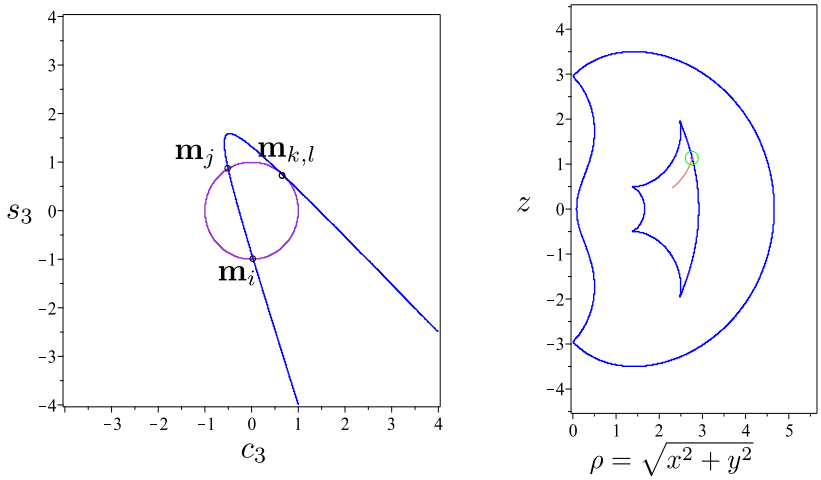

(b) Tangency between adjacent points on either side of the vertex

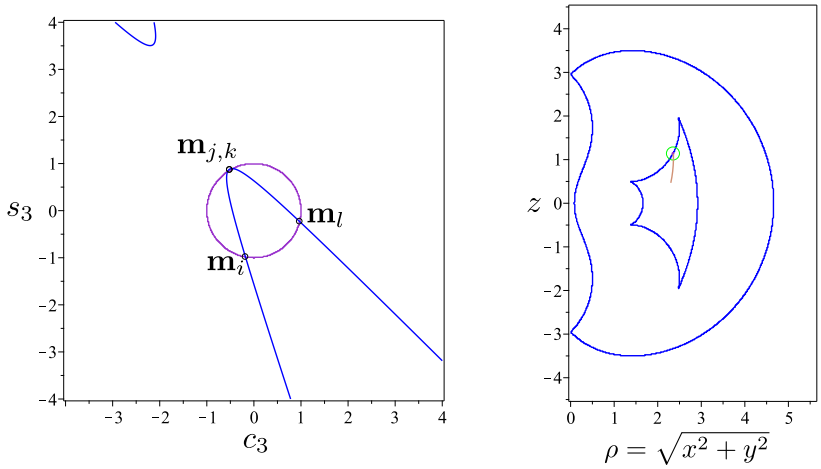

(c) Tangency between adjacent points on same side of the vertex

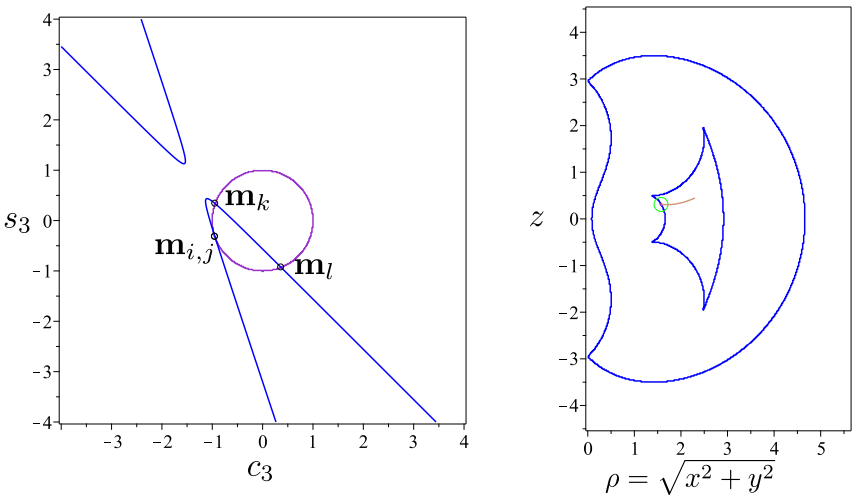

(d) Tangency between adjacent points on same side of the vertex

Figure 2.5 – The merging of two adjacent points in a conic at a tangent point and geometrical interpretation of the components of the locus of critical values.
Robot parameters: d = [0, 1, 0], a = [1, 2, 3/2], $\alpha = \left[-\frac{\pi}{2}, \frac{\pi}{2}, 0\right]$, $(\rho, z) = (2.5, 1)$ and $(3, 0)$.

to be cuspidal. Later, the established sufficient condition is combined with Theore 3, we present the necessary and sufficient condition for a generic robot to be cuspidal.

Proposition 3. *If a generic 3R serial robot is cuspidal, then there exists a cusp in the workspace of the given robot.*

We prove Proposition 3 by contradiction: we consider a hypothetical cuspidal robot that has no cusps in its workspace and show that this case cannot exist. In order to do so, we first need to set and prove a series of lemmas.

In a cuspidal robot, at least two inverse kinematic solutions lie in an aspect, let them be $\mathbf{q}_1$ and $\mathbf{q}_2$. By using Theorem 2, we know that $\mathbf{q}_1$ and $\mathbf{q}_2$ lie in two separate reduced aspects, and thus we cross pseudosingularities during the nonsingular change of solutions. As pseudosingularities separate the reduced aspects whose image in the workspace lie in distinct non-connected regions (from Proposition 2), we cross the pseudosingularities at least twice in a nonsingular change of solutions.

In order to discuss the path corresponding to the nonsingular change of solutions in the workspace, the concept of components of the locus of critical values is discussed. The geometrical interpretation of these components in the $c_3 s_3$-plane allows one to draw

important conclusions about certain constraints on the nature of nonsingular change of solutions.

Components of critical values

A n-solution region in the workspace is always bounded by the locus of critical values which, for a generic 3R serial robot, can include cusps and/or nodes. Upon the exclusion of the nodes/cusps, we get the components of critical values. In this section, we present the geometric interpretation of the components of critical values.
A point $\mathbf{p}$ in a region of the workspace with four preimages, corresponds to a situation where the conic intersects the unit circle at four points with in c_3s_3-plane (Figure 2.5a). Let the intersection points be $\mathbf{m}_i$, $\mathbf{m}_j$, $\mathbf{m}_k$ and $\mathbf{m}_l$. There are up to four different pairs in which the points can merge, viz. $\mathbf{m}_i\mathbf{m}_j$, $\mathbf{m}_j\mathbf{m}_k$, $\mathbf{m}_k\mathbf{m}_l$ and $\mathbf{m}_l\mathbf{m}_i$ (Figure 2.5). Thus, depending upon the type of robot, a 4-solution region in the workspace can be bounded by a maximum of four distinct components of singularities. A geometrical interpretation of the component of critical values is associated with the merging of a particular pair of intersection points in the c_3s_3 - plane, as shown in Figure 2.5.

Lemma 4. *Let $\mathbf{q}_1$ and $\mathbf{q}_2$ be two inverse kinematic solutions in the same aspect. Considering a generic nonsingular change of solutions from $\mathbf{q}_1$ to $\mathbf{q}_2$, the images of the pseudosingularities that the point $\mathbf{q}_1$ crosses to go to $\mathbf{q}_2$, belong to at least 2 different components of the critical values in the workspace.*

Proof. It is evident from the definition of pseudosingularity curve that if an IKS of a robot lies on the pseudosingularity curve, then there exists an IKS of the robot on the locus of critical points as well. An example of nonsingular change of solutions is shown in Figure 2.6 where the path crosses the pseudosingularity curve twice. $\mathbf{q}_j$ crosses the pseudosingularity curve twice at $\mathbf{ps}_1$ and $\mathbf{ps}_2$ in order to switch with $\mathbf{q}_l$ in a nonsingular way. From Theorem 2, we know that $\mathbf{q}_j$ and $\mathbf{q}_l$ lie in two reduced aspects $\mathcal{A}$ and, $\mathcal{B}$ respectively. The reduced aspect $\mathcal{A}$ is bounded by the locus of critical points and at least by the segment of the pseudosingularity curve including $\mathbf{ps}_1$. The reduced aspect $\mathcal{B}$ is bounded by the locus of critical points and at least by the segment of the pseudosingularity curve including $\mathbf{ps}_2$. By Proposition 2, we assert that in generic 3R serial robots, pseudosingularities always separate the reduced aspects whose image in the workspace belong to regions with different number of IKS. So, we know that when $\mathbf{q}_j$ crosses $\mathbf{ps}_1$, $\mathbf{q}_l$ disappears after meeting the locus of critical points bounding the reduced aspect $\mathcal{B}$. Clearly, $\mathbf{q}_j$ crosses

the pseudosingularity at $\mathbf{ps}_2$ in order to enter the reduced aspect $\mathcal{B}$. For each point in the reduced aspect $\mathcal{B}$, there should be a corresponding point in the reduced aspect, $\mathcal{A}$, as both of them map to the same bounded region in the workspace as shown in Figure 1.10. Thus, when $\mathbf{q}_j$ is on $\mathbf{ps}_2$, there appears a point corresponding to $\mathbf{q}_l$ on the locus of critical points bounding the reduced aspect $\mathcal{A}$.

Let $\mathbf{m}_i, \mathbf{m}_j, \mathbf{m}_k, \mathbf{m}_l$ be the four intersection points in c_3s_3-plane corresponding to the four IKS in the joint space, $\mathbf{q}_i, \mathbf{q}_j, \mathbf{q}_k, \mathbf{q}_l$ (refer to Figure 2.6). When $\mathbf{q}_j$ crosses the pseudosingularity curve at $\mathbf{ps}_1$, $\mathbf{q}_l$ meets either $\mathbf{q}_i$ or $\mathbf{q}_k$. In the c_3s_3-plane, the comparison of $\mathbf{q}_l$ meeting $\mathbf{q}_i$ or $\mathbf{q}_k$ is similar to $\mathbf{m}_l$ meeting either $\mathbf{m}_i$ or $\mathbf{m}_k$ at the tangent point. Now, when $\mathbf{q}_j$ crosses the pseudosingularity curve at $\mathbf{ps}_2$, $\mathbf{q}_l$ enters $\mathcal{A}$. The comparison of $\mathbf{q}_l$ emerging on the locus of critical point bounding $\mathcal{A}$ is similar to $\mathbf{m}_l$ merging with $\mathbf{m}_i$ or $\mathbf{m}_k$ in the initial setup. Thus, the images of the critical points bounding $\mathcal{A}$ and $\mathcal{B}$ belong to two separate components of critical values. This proves that the images corresponding to $\mathbf{ps}_1$ and $\mathbf{ps}_2$ lie on two distinct components of critical values in the workspace. □

So a nonsingular change of solutions in the workspace looks like a path that exits the 4-solution region by crossing a component of critical values and re-entering in the region by crossing another component of critical values. Figure 1.12 shows an example of a point crossing two components of critical values in a nonsingular way. The path does not necessarily enter and exit from the components of critical values that form a cusp (refer to Figure 2.2), but it is imperative to note that by proving Lemma 4, we know that the path has to exit and enter by crossing two distinct components of critical value.

Lemma 5. *If points $\mathbf{m}_j$, $\mathbf{m}_l$ in the c_3s_3-plane belong to the same aspect in the joint space, and there exists a cusp in the workspace, then there exists another intersection point, $\mathbf{m}_k$, in the middle of (in terms of circle ordering) $\mathbf{m}_j$ and $\mathbf{m}_l$ such that $\mathbf{m}_j$,$\mathbf{m}_k$ and $\mathbf{m}_k$,$\mathbf{m}_l$ correspond to the two components of critical values that form a cusp in the workspace (see Figure 2.7).*

Proof. As shown in Figure 1.5, the interpretation of a cusp in the c_3s_3-plane is such that 3 intersection points come together at a tangent point. A cusp is a merging point of two separate components of critical value. It has been shown that the components of critical values relate to merging of a particular pair of intersection points in the c_3s_3-plane. If two components are meeting at a cusp in workspace such that $\mathbf{m}_j, \mathbf{m}_k$ and $\mathbf{m}_l$ merge in the c_3s_3-plane with $\mathbf{m}_k$ being in between $\mathbf{m}_j$ and $\mathbf{m}_l$, then the two components of critical values must belong to the merging of $\mathbf{m}_j\mathbf{m}_k$ and $\mathbf{m}_k\mathbf{m}_l$. □

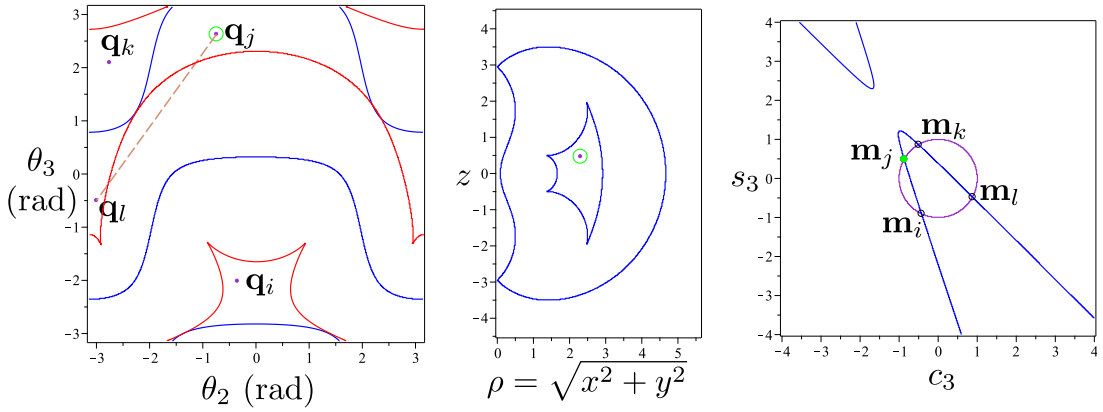

(a) Phase 1: Starting from a point in workspace with 4 IKS, $\mathbf{q}_j$ and $\mathbf{q}_l$ are in same aspect.

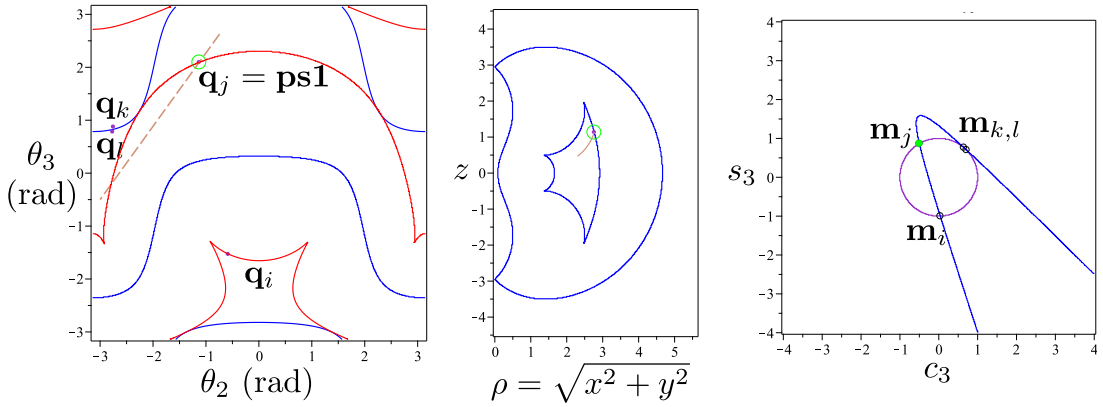

(b) Phase 2: $\mathbf{q}_j$ meets $\mathbf{ps}_1$ and $\mathbf{q}_l$ meets $\mathbf{q}_k$ at singularity curve.

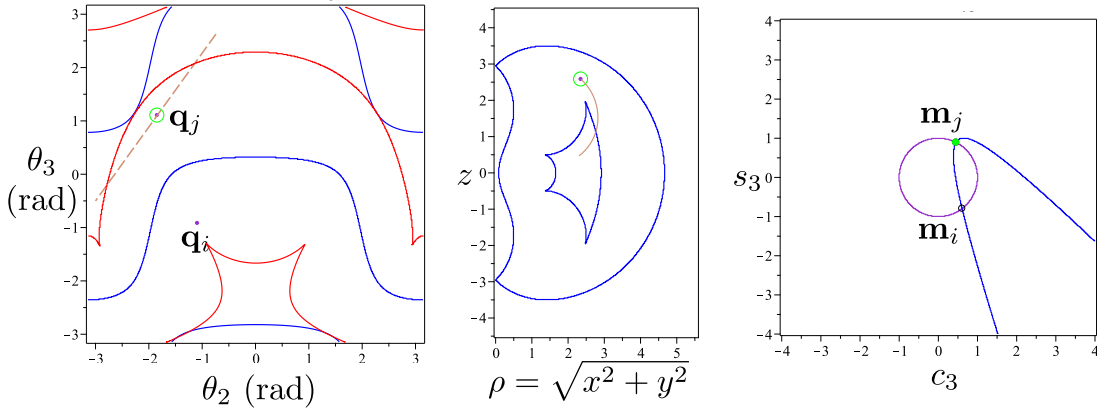

(c) Phase 3: $\mathbf{q}_j$ enters another reduced aspect and $\mathbf{q}_l$ disappears.

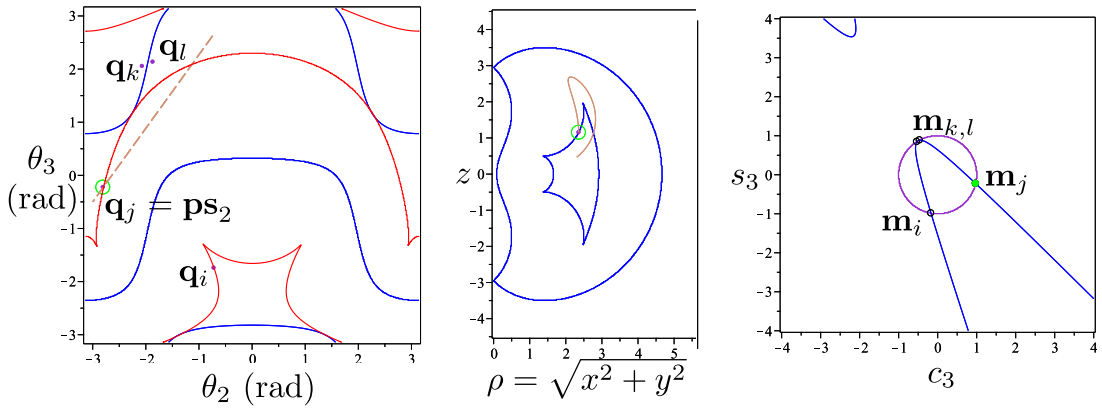

(d) Phase 4: $\mathbf{q}_j$ meets $\mathbf{ps}_2$ and $\mathbf{q}_l$, $\mathbf{q}_k$ reappear, but in different reduced aspects.

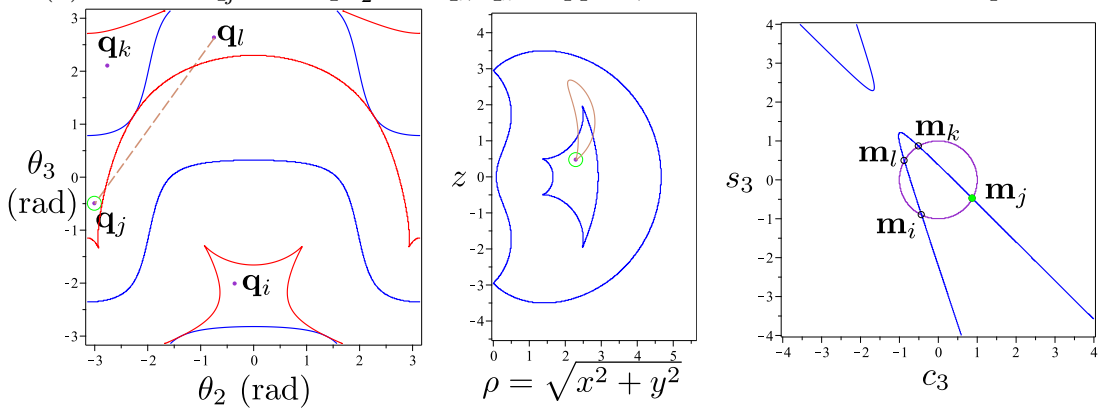

(e) Phase 5: $\mathbf{q}_j$ switches with $\mathbf{q}_l$ without disappearing.

Figure 2.6 – An example of nonsingular change of solutions crossing a pseudosingularity curve at 2 points.
Robot parameters: d = [0, 1, 0], a = [1, 2, 3/2], $\alpha = [-\frac{\pi}{2}, \frac{\pi}{2}, 0]$.
path in the joint space (θ_2, θ_3): from $(-0.742, 2.628)$ to $(-3, -0.5)$.

Lemma 6. *For a nonsingular change of solutions starting from a point in a bounded region $\mathcal{A}_w$ in the workspace: there exists a path in the workspace that does not meet any critical values not bounding region $\mathcal{A}_w$.*

Proof. If there exists a cusp, the Lemma is automatically true [WEO96]. We thus consider only the case in which there is no cusp in the boundary of region $\mathcal{A}_w$. The proof of the Lemma comes from the simultaneous analysis of the nonsingular change of solutions in the workspace as well as in the $c_3 s_3$-plane. Considering a point $\mathbf{p}$ in the 4-solution region in the workspace (refer to Figure 2.8), let the four intersection points corresponding to this position in $c_3 s_3$-plane be $\mathbf{m}_i$, $\mathbf{m}_j$, $\mathbf{m}_k$ and $\mathbf{m}_l$. Let, $\mathbf{m}_i$ and $\mathbf{m}_k$ be the solutions in the same aspects. We know from Lemma 4 that region $\mathcal{A}_w$ is bounded by at least 2 components of

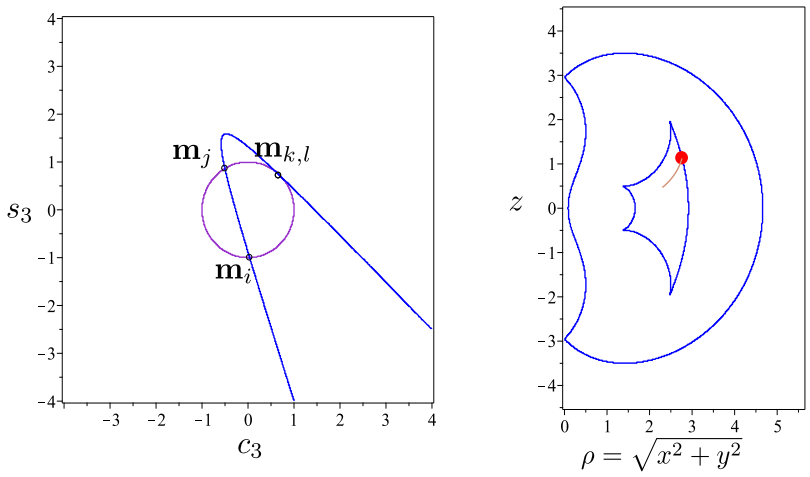

(a) Component of critical value adjacent to a cusp point

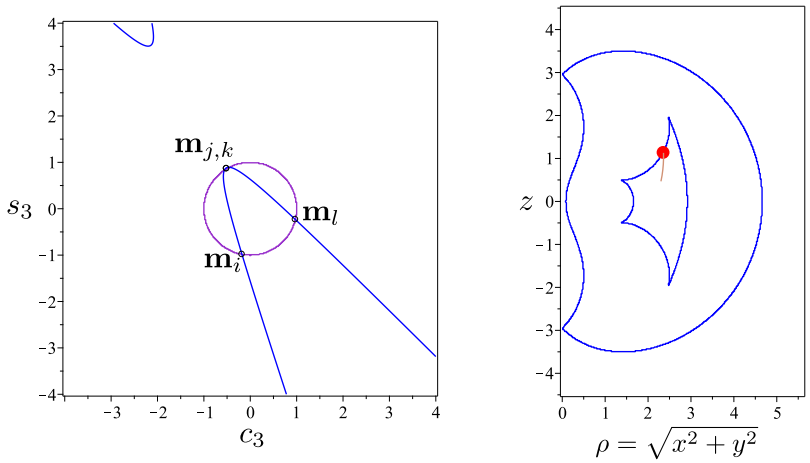

(b) Component of critical value adjacent to a cusp point

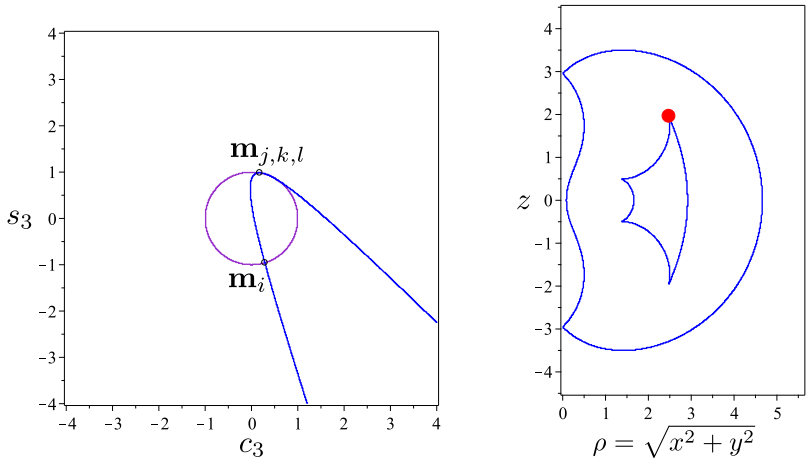

(c) Cusp point

Figure 2.7 – Geometrical interpretation of the cusp point and the adjacent components of critical values.
Robot parameters: d = [0, 1, 0], a = [1, 2, 3/2], α = [-$\frac{\pi}{2}$, $\frac{\pi}{2}$, 0].

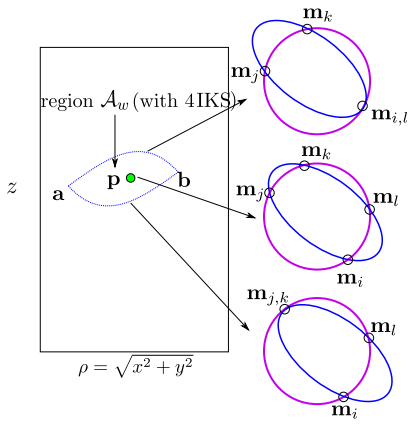

Figure 2.8 – Region $\mathcal{A}_w$ in the workspace with 4 IKS and its geometrical interpretation. Robot parameters are imagined to illustrate a particular case. The conic can be a hyperbola or an ellipse.

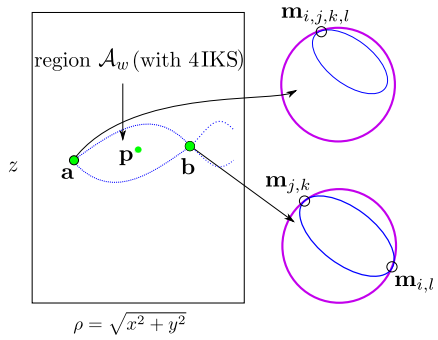

Figure 2.9 – The intersections of components of critical values bounding $\mathcal{A}_w$ in the workspace and its geometrical interpretation. Robot parameters are imagined to illustrate a particular case. The conic can be a hyperbola or an ellipse.

critical values. As the boundary of region $\mathcal{A}_w$ does not have a cusp, the components of critical values that bound region $\mathcal{A}_w$ in the workspace are related to two cases: merging of $\mathbf{m}_i$, $\mathbf{m}_l$ and $\mathbf{m}_j$, $\mathbf{m}_k$ (refer to Figure 2.8) or $\mathbf{m}_i$, $\mathbf{m}_j$ and $\mathbf{m}_k$, $\mathbf{m}_l$. Without loss of generality, we may assume the first case. As there are only two possible tangent points, $\mathcal{A}_w$ is bounded by only 2 components of critical values.

As region $\mathcal{A}_w$ is bounded and there exists no cusps, the two components of critical values bounding region $\mathcal{A}_w$ must intersect. In the $c_3 s_3$-plane, points ($\mathbf{m}_i$,$\mathbf{m}_l$) and ($\mathbf{m}_j$,$\mathbf{m}_k$) either meet simultaneously at two distinct points (bitangent case) or they meet at a single point of tangency between the conic and the circle as illustrated in Figure 2.9. Since we are considering generic robots, we cannot have four equal IKS and we can immediately conclude that the intersection of the components of critical values corresponds to the

bitangent case.

Let $\mathcal{B}_w$ be an arbitrary region in the workspace that is not $\mathcal{A}_w$. Proceeding by contradiction, it is sufficient to show that a path crossing two distinct components of the critical values bounding region $\mathcal{B}_w$ in order to enter and exit $\mathcal{B}_w$, does not correspond to a nonsingular change of solutions. An example of such a workspace is illustrated in Figure 2.10 and the interpretation of a closed loop path in the workspace is given in Figure 2.11, which shows that such a path cannot define a nonsingular change of solutions. From Lemma 4,

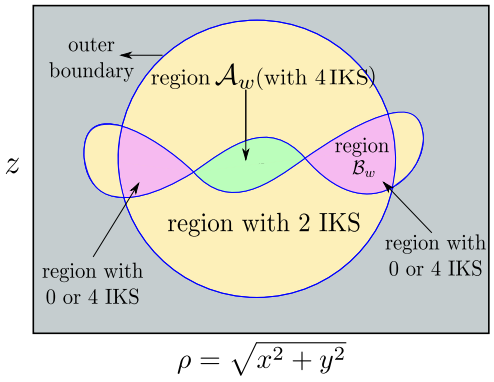

Figure 2.10 – An example of the shape of the workspace, where a closed loop path starting from a point in $\mathcal{A}_w$ must cross two distinct components of critical values bounding region $\mathcal{B}_w$.

we already know that the path in workspace corresponding to the nonsingular change of solutions crosses two different components of critical values of region $\mathcal{A}_w$. If the path exits $\mathcal{A}_w$ by crossing the component corresponding to the merging of $\mathbf{m}_i$ and $\mathbf{m}_l$, then it must cross the component belonging to the merging of $\mathbf{m}_j$ and $\mathbf{m}_k$ while entering the same region. Now, if the case shown in Figure 2.10 exists, then in order to enter $\mathcal{A}_w$, we will have to cross another 4-solution region, $\mathcal{B}_w$, bounded by at least 2 different components of critical value. As we are considering only the case without cusps in the workspace, $\mathcal{B}_w$ is bounded by two components of critical values having no point in common too, i.e. if one component corresponds to the merging of $\mathbf{m}_i$,$\mathbf{m}_l$ then the other component must correspond to the merging of $\mathbf{m}_j$,$\mathbf{m}_k$. While crossing $\mathcal{B}_w$, one needs to cross both components. This means that if one tracks the intersection point $\mathbf{m}_i$ from its initial position, then this point will have been a tangent point (in c_3s_3-plane) while crossing either of the two components of $\mathcal{B}_w$. This leads to a contradiction, as we have assumed that one of the points we are tracking will not be tangent to the unit circle to qualify as a valid nonsingular change of solutions. Figure 2.11 illustrates a path where two singularities of

another 4-solution region without any cusp are crossed. We start from an initial point $\mathbf{p}$ in the 4-solution region, $\mathcal{A}_w$, of the workspace that corresponds to State 1 in the c_3s_3-plane (refer to Figure 2.11). We assume that the robot corresponding to this case is cuspidal and the IKS corresponding to $\mathbf{m}_j$ and $\mathbf{m}_l$ lie in the same aspect. In State 2, we cross the component of critical values that belongs to the merging of $\mathbf{m}_i$ and $\mathbf{m}_l$. This already suggests that for a valid nonsingular change of solutions, $\mathbf{m}_j$ should switch places with $\mathbf{m}_l$ without being a tangent point in the c_3s_3-plane. The path going from State 3 to State 5 is the entry into another 4-solution region, $\mathcal{B}_w$. As we have entered region $\mathcal{B}_w$ by crossing the component of critical values corresponding to the merging of $\mathbf{m}_i$ and $\mathbf{m}_l$, we need to exit the region by crossing the component of critical values corresponding to the merging of $\mathbf{m}_j$ and, $\mathbf{m}_k$ as shown in State 6. This proves that such a path is an invalid nonsingular change of solutions, as we encountered a singular configuration while exiting $\mathcal{B}_w$. □

The "candy" case

Proof of Proposition 3. By Lemma 6, the curves corresponding to the critical values are enclosed by an outer boundary of the workspace and would have a shape as illustrated in Figure 2.12. We shall refer to this shape as the "candy" case. We arrive at this case by starting with a point, $\mathbf{p}$, in the workspace with four preimages. Let the points of intersection in the c_3s_3-plane corresponding to $\mathbf{p}$ be $\mathbf{m}_i$, $\mathbf{m}_j$, $\mathbf{m}_k$ and $\mathbf{m}_l$. The region, $\mathcal{A}_w$, in which $\mathbf{p}$ exists must be bounded by the locus of critical values. As we are assuming that there are no cusps, the region will have to be bounded by only two components corresponding to the merging of ($\mathbf{m}_i$,$\mathbf{m}_j$ and $\mathbf{m}_k$,$\mathbf{m}_l$) or ($\mathbf{m}_i$,$\mathbf{m}_l$ and $\mathbf{m}_j$,$\mathbf{m}_k$) as shown in Figure 2.8. These two components of the critical values intersect at two points, $\mathbf{a}$ and $\mathbf{b}$. The geometrical interpretation of the intersection of the components of critical values is that both $\mathbf{m}_i$,$\mathbf{m}_l$ and $\mathbf{m}_j$,$\mathbf{m}_k$ merge at tangent points simultaneously. This can happen in two cases, either all four intersection points merge together or $\mathbf{m}_i$,$\mathbf{m}_l$ and $\mathbf{m}_j$,$\mathbf{m}_k$ meet together at separate tangent points in the c_3s_3-plane forming a node point in the workspace as shown in Figure 2.9. As the case where all four points merge at a single tangent point belongs to a nongeneric case, we will consider only the case of $\mathbf{m}_i$,$\mathbf{m}_l$ and $\mathbf{m}_j$,$\mathbf{m}_k$ meeting together at separate tangent points. As at the ends of our candy shape, only two segments meet without forming a node (see $\mathbf{m}$ and $\mathbf{n}$ in Figure 2.12), it corresponds to a case of four solutions merging at a common point. This is a contradiction to the assumption of a generic 3R robot because points with multiplicity four correspond to a nongeneric 3R robot [PL92]. □

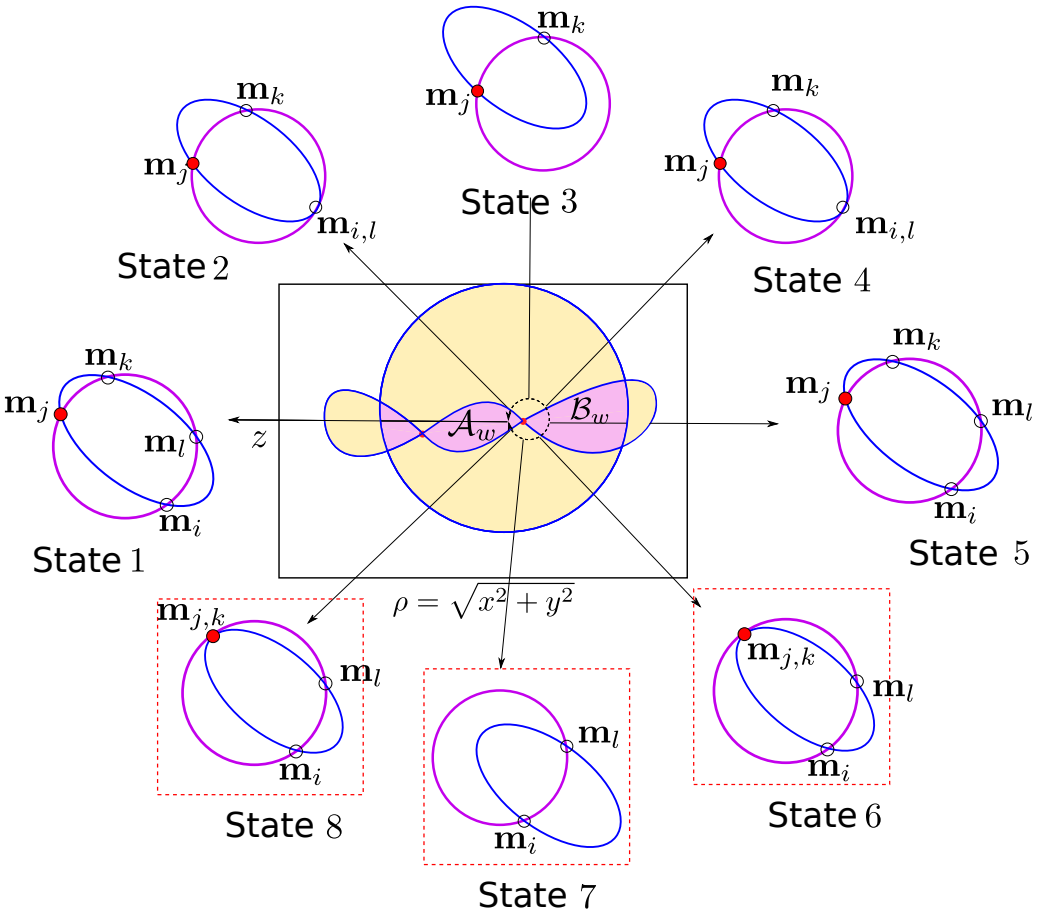

Figure 2.11 – The closed loop path in the workspace, where the path crosses another 4-solution region and its corresponding interpretation in $c_3 s_3$-plane. Robot parameters are imagined to illustrate a particular case to show that such a path does not correspond to a nonsingular change of solutions. The figures in red dotted boxes correspond to the steps in the shown path where the definition of nonsingular change of solutions is violated.

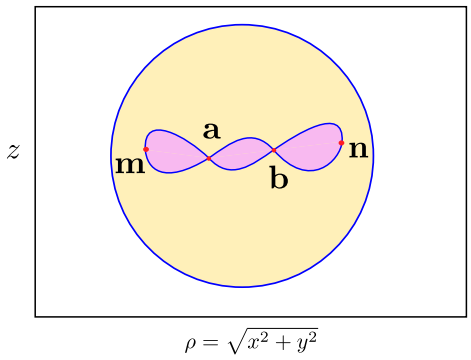

Figure 2.12 – The "candy" case.

By using the Theorem 1 and Proposition 3, a necessary and sufficient condition can be derived for a generic 3R cuspidal robot. Formally, the theorem is stated as:

Theorem 3. *For a generic 3R serial robot, the existence of a cusp point in the workspace is a necessary and sufficient condition for the robot to be cuspidal.*

Figure 2.13 illustrates an example of non-orthogonal cuspidal and non-cuspidal robots in the joint space, workspace and the $c_3 s_3$ - plane.

2.2 Further analysis of 3R serial robots

The cuspidal property can be analyzed by understanding the IKM as well as the singularities in the joint space and in the workspace. It is well-known that binary 3R robots (i.e. with at most two IKS) are noncuspidal. In this section, the geometric analysis is further extended to present classification of robots based on the type of conic in the $c_3 s_3$-plane. Algebraic conditions for 3R orthogonal robots to be a binary robot was previously presented through algebraic analysis. In this section, we revisit the geometrical interpretation of the IKM and present some important observations. The conditions of getting different conics and their implication on singularities are discussed in the chapter. Further, a sufficient condition for a 3R robot to be binary robot as well as quaternary (i.e. with up to 4 IKS) is put forth by analyzing the geometrical interpretation of the IKM. The possibility to extend this condition of binary and quaternary for generic 3R serial robots is presented too. Later, we use the geometric analysis to close a conjecture presented in [Pag08] regarding the maximum aspects present in a generic 3R serial robot.

This section is divided into three parts: Section 2.2.1 discusses the classification of 3R robots based on the geometry of the IKM as well as discusses its implication in the joint space and the workspace. Section 2.2.1 shows cases of binary and quaternary robots by analyzing the geometrical properties of the IKM. Section 2.2.2 discusses the results from Paganelli's homotopy analysis and answers the question on the maximum number of aspects present in a 3R serial robot. Section 2.3 concludes the results from the geometric analysis by discussing the implications of the contribution and addressing a few pointers to future work.

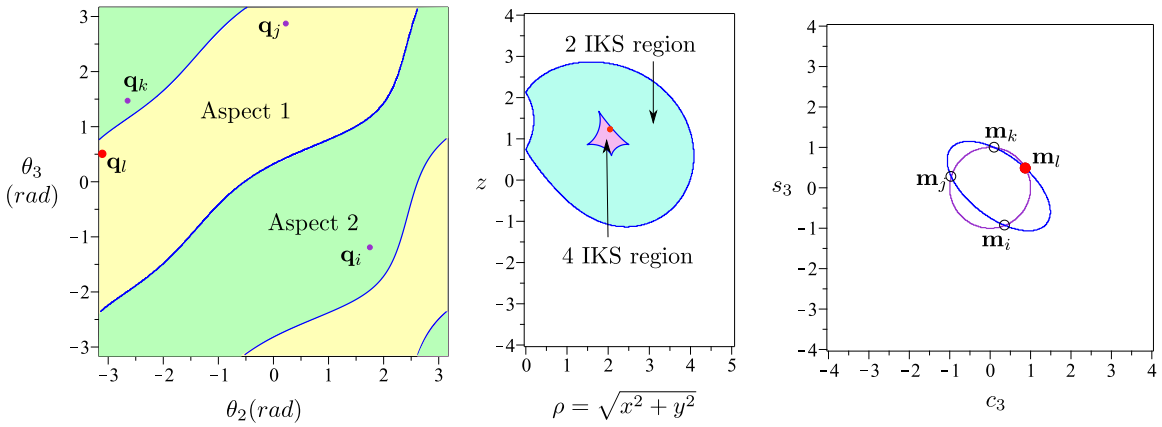

(a) An example of generic cuspidal case.
Robot parameters: Robot parameters: d = [0, 1, 0], a = [1, 2, 1], α = [-$\frac{\pi}{6}$, $\frac{\pi}{2}$, 0].

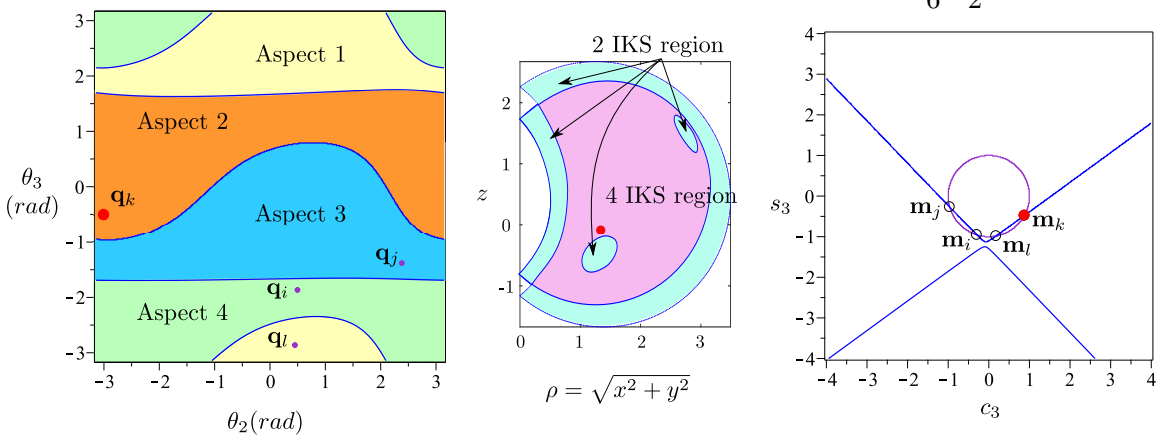

(b) An example of generic non-cuspidal case.
Robot parameters: Robot parameters: d = [0, 1, 0], a = [1, 0.2, 2], α = [-$\frac{\pi}{3}$, 1.745, 0].

Figure 2.13 – The aspects in the joint space, regions in the workspace and corresponding conics in the $c_3 s_3$ - plane for a cuspidal and non-cuspidal generic robot.

2.2.1 Geometric analysis of 3R serial robots

As cuspidal robots have multiple IKS in an aspect, unique identification of a 'configuration' is not possible [Wen92], which makes the task of trajectory planning more challenging [Wen04]. It is known that a 3R robot can have at most four IKS, and it is generally preferred to choose a robot geometry that maximizes the size of regions with four IKS. This allows an end-user to choose IKS from different regions to counter the collision issues in the workspace. Robots that have 4 IKS regions in their workspace are referred to as *quaternary* robots, while robots that have at most 2 IKS are referred to as *binary* robots [WCB05]. It is important to note that though quaternary robots have their advantages, they can be cuspidal too, while on the other hand binary robots cannot be cuspidal [Wen92]. *Orthogonal* 3R robots have been studied extensively in the past with a D-H parameter based condition for quaternary orthogonal 3R robots presented with algebraic analysis [WCB05]. An extension of such an algebraic analysis to generic 3R robots is more challenging, and no conditions for binary or quaternary generic robots have been studied prior to the presented thesis.

In Chapter 2.1, the cuspidality of *generic* 3R robots was analyzed by using a geometric interpretation of the IKM. We show the geometric interpretation of different concepts such as singularity, and nonsingular change of solutions by analyzing the interaction of the conic with the unit circle in the $c_3 s_3$-plane. This section details extended properties of the conic and its implication on the maximum number of IKS in the workspace. The classification presented provides a simple and intuitive geometric interpretation for the condition of binary and quaternary robots.

Classification of robots based on geometric conditions

We present an example of the geometry based classification of 3R serial robots. Figure 2.14 shows the classification in the parameter space of α_1 and α_2 for an example set of D-H parameters. The blue colored region corresponds to the D-H parameters with the IKM representing ellipse in the $c_3 s_3$-plane. The red colored represents the hyperbolas in $c_3 s_3$-plane while the separating curve which is a parabola in $c_3 s_3$-plane is shown in green. Figure 2.15 shows the classification of robots on similar criteria but parameterized in the lengths a_2 and d_2 while keeping other D-H parameters fixed. The rest of the D-H parameters are those corresponding to a generic robot.

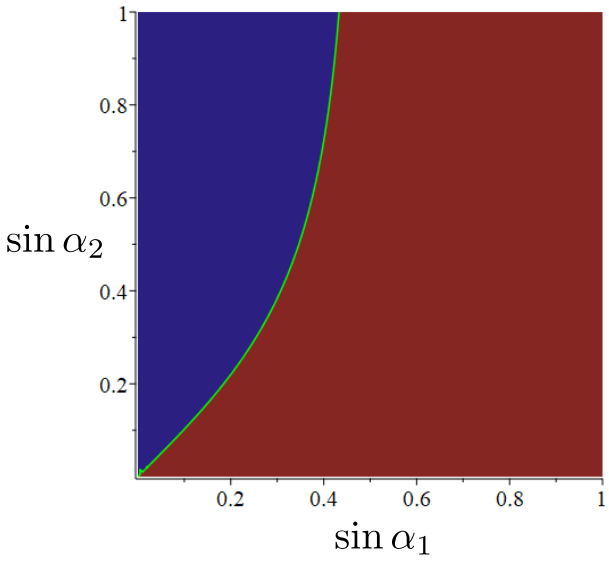

Figure 2.14 – The bifurcation curve parameterized in α_1 and α_2. The red part is a 3R serial robot corresponding to a hyperbola, the blue part to the ellipse, and the green curve corresponds to a parabola in the c_3s_3-plane. The rest of parameters are: $\mathbf{d} = [0,\ 1,\ 0]$, $\mathbf{a} = [1, 2, 3/2], \alpha_3 = 0$. The bifurcation is symmetrical about the x-axis and y-axis.

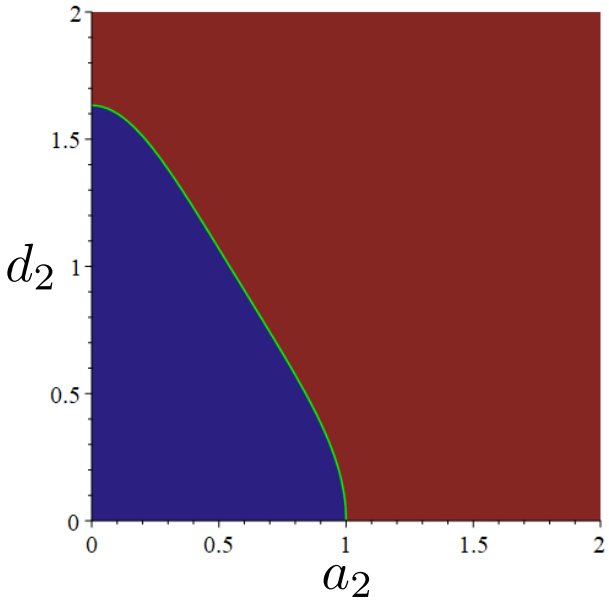

Figure 2.15 – The bifurcation curve parameterized in a_2 and d_2. The red part is a 3R serial robot corresponding to a hyperbola, the blue part to the ellipse, and the green curve corresponds to a parabola in the c_3s_3-plane. The rest of the parameters are $a_1 = a_3 = 1, d_1 = d_3 = \alpha_3 = 0, \alpha_1 = \pi/3, \alpha_2 = \pi/6$.

Degenerate conic

This section recalls the conic equation related to the IKM of 3R serial robot (1.2) and the lemmas related to the conic nature, Lemma 1 and Lemma 2. The nature of the conic depends on the sign of the determinant of $\mathbf{N}$, where $\mathbf{N}$ is the Hessian of the conic. The degeneracy of a conic is given by $\det(\mathbf{D}) = 0$, where $\mathbf{D}$ is the Hessian of the quadratic form and given as:

$$\mathbf{D} = \begin{bmatrix} A_{xx} & B_{xy} & D_x \\ B_{xy} & C_{yy} & E_y \\ D_x & E_y & F \end{bmatrix} \tag{2.2}$$

We know that the hyperbola ($\det(\mathbf{N}) < 0$) degenerates into two intersecting lines, while the ellipse ($\det(\mathbf{N}) > 0$) degenerates to a point. The degenerate case of a parabola ($\det(\mathbf{N}) = 0$) is of particular interest as it degenerates into two parallel lines, and they can be distinct or coincident. The work presented in this thesis related to the degeneration of the parabola discusses the case of two coincident lines, resulting in two multiple roots. This case is important to analyze as it is a special degeneracy case, and relates to a peculiar feature in the workspace. Following are the conditions for a parabola to degenerate into two coincident lines:

$$\begin{cases} \det(\mathbf{N}) = 0 \\ \det(\mathbf{D}) = 0 \\ B_x^2 + B_y^2 - (A_{xx} + A_{yy})\, C = 0 \end{cases} \tag{2.3}$$

$$\det(\mathbf{N}) = \frac{a_3^4 \left((-d_2^2\, sa_2^2 + a_1^2 - a_2^2)\, sa_1^2 + (-a_1^2 + a_2^2) * sa_2^2\right)}{(a_1^2\, sa_1^2)} \tag{2.4}$$

Solving $\det(\mathbf{N}) = 0$ for d_2 yields:

$$d_2 = \pm \frac{\sqrt{(a_1 + a_2)\,(a_1 - a_2)\,(sa_1 - sa_2)\,(sa_1 + sa_2)}}{sa_1\, sa_2} \tag{2.5}$$

We conclude from (2.4) that the parameters a_3 and d_3 do not play any role to define a parabola for a generic case ($a_3 \neq 0$). Upon substituting either value from (2.5) into $\det(\mathbf{D}) = 0$ and solving for R, we obtain the same solution. Solving the last equation in (2.3) for z, the solutions R and z take the following form, provided that $ca_2 \neq 0$ and

$sa_1 \neq sa_2$:

$$\begin{aligned} R &= \frac{f(z)}{sa_1^2 - sa_2^2} \\ z &= \frac{ca_1}{ca_2}\left(d_3\, sa_1\, sa_2 + d_2\, ca_2\right) \end{aligned} \tag{2.6}$$

The complete expression for $f(z)$ is presented in Appendix A.2. From (2.6), it is interesting to note that a robot such that ($ca_2 \neq 0$, $sa_1 \neq sa_2$) and corresponding to a parabola will always have a point in the workspace (R, z) such that its geometric interpretation is a parabola degenerating into a coincident line. When $ca_2 = 0$ (resp. $sa_1 = sa_2$), z (resp. R) is indeterminate.
A point satisfying (2.6) is a tangency point between two loci of critical values, as shown in Figure 2.16.

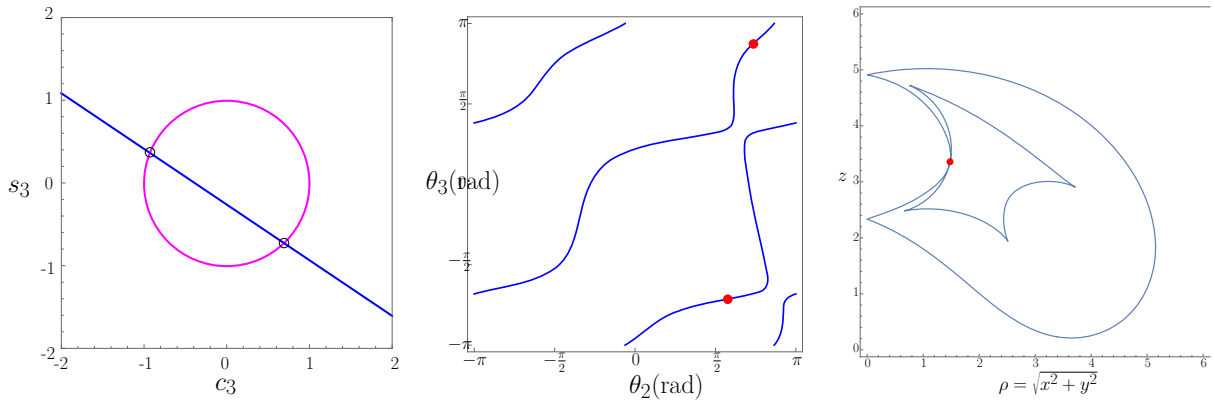

Figure 2.16 – Degenerate parabola case: joint space (center) and workspace (right). The point shown in red is associated with two coincident lines in the $c_3 s_3$-plane (left).
Robot parameters: $d = [0, 2.828, 0.5], a = [1, 2, \frac{3}{2}], \alpha = [\frac{\pi}{6}, \frac{\pi}{3}, 0], (\rho, z) = (1.471, 3.315)$.

Special classes of robots

In this section, we present a sufficient condition for a 3R robot to be binary and quaternary, respectively. The motivation for the search of binary robots comes from the well-known property that two circles have at most two distinct intersections. Section 2.2.1 discusses the neighborhood of such binary robots. We claim that the parameters corresponding to all the ellipses that are in a sufficiently small neighborhood of the parameters corresponding to a circle, result in binary robots too. Section 2.2.1 discusses a condition for a hyperbola to compulsorily have four intersections with the unit circle in the $c_3 s_3$-plane, thus resulting in a quaternary robot.

Binary robots

Trivial case: Circle

A trivial case of a binary robot is when the associated conic is a circle. The condition for a conic to be circle is:

$$\begin{cases} A_{xy} = 0 \\ A_{xx} = A_{yy} \\ \det(\mathbf{N}) > 0 \end{cases} \tag{2.7}$$

Here,

$$A_{xy} = \frac{2a_2\, a_3^2\, d_2\, sa_2}{a_1^2}$$
$$A_{xx} - A_{yy} = -a_3^2 + \frac{a_2^2\, a_3^2}{a_1^2} - \frac{a_3^2\, d_2^2\, sa_2^2}{a_1^2} - \frac{a_3^2\, ca_1^2\, sa_2^2}{sa_1^2} + a_3^2\, ca_2^2$$

Analyzing A_{xy}, (2.7) has 4 cases of solutions:

1. $a_2 = 0$
2. $a_3 = 0$
3. $\alpha_2 = 0$
4. $d_2 = 0$

Solving, $A_{xx} - A_{yy} = 0$ for $\sin\alpha_1$ gives two solutions:

$$\sin\alpha_1 = \pm\frac{\sin\alpha_2\, a_1}{\sqrt{-d_2^2\, \sin\alpha_2^2 + a_2^2}} \tag{2.8}$$

Out of these four cases presented, the first three do not lead to good solutions. The case of $a_2 = 0$ results in negative square root in (2.8), $a_3 = 0$ represents a circle centered at $(0, 0)$ and thus we have either zero or infinite solutions. If $\alpha_2 = 0$, then $\alpha_1 = 0$ is the only solution leading to three parallel axis resulting into a 3R planar robot which is a degenerate case. So, the only case leading to multiple solutions is $d_2 = 0$. Upon setting $d_2 = 0$, we have the following conditions:

$$\begin{cases} \sin\alpha_1 = \pm\dfrac{\sin\alpha_2\, a_1}{a_2} \\ (a_1 - a_2)\,(\sin\alpha_1 - \sin\alpha_2) > 0 \\ a_1 \neq 0, a_2 \neq 0, a_3 \neq 0, \alpha_2 \neq 0 \end{cases} \tag{2.9}$$

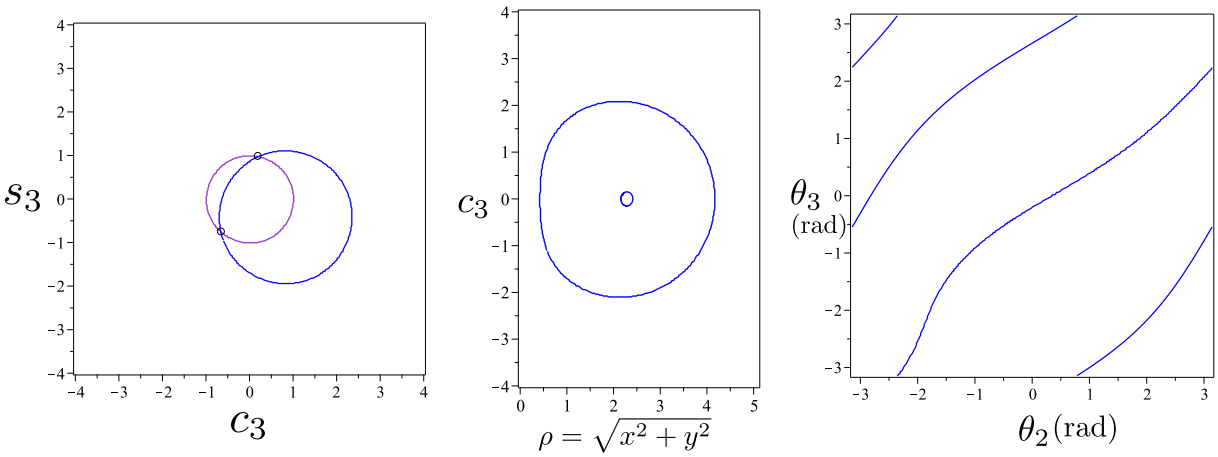

(a) c_3s_3-plane (b) workspace (c) joint space

Figure 2.16 – 3R serial robot corresponding to a circle in the c_3s_3-plane.
Robot parameters: d = [0, 0, 1], a = [1, 2, 1], $\alpha = [\frac{\pi}{6}, \frac{\pi}{2}, 0]$.

An example of a 3R serial robot with conic as circle is illustrated in Figure 2.16:

Non trivial case: binary ellipses

We now consider a robot such that its associated conic is an ellipse. We prove that it is possible to find a binary robot whose IKM corresponds to an ellipse in the c_3s_3 plane if the eccentricity of the conic is close to 0. We consider a Lemma in geometry:

Lemma 7. *Consider the unit circle S^1 and a number, $e \in (0, 1)$*

(i) There is an ellipse $\mathcal{C}$ with eccentricity e such that $\#\mathcal{C} \cap S^1 = 4$

(ii) As $e \to 0$ the ellipses with eccentricity e with property (i) will have centers that approach the origin (center of S^1) and have minor and major semi-axes that approach length 1.

Proof. (i) Given an ellipse with arbitrary eccentricity, we can place its center at the center of S^1 and scale it proportionally so that it lies entirely in S^1 and similarly so that it completely contains S^1. Eccentricity is invariant under scaling and scaling is continuous, so there is a scale for which the ellipse intersects S^1 transversally, at finite points (S^1 and the ellipse are different algebraic curves) and symmetrically.

(ii) Without loss of generality, we may assume that the principal axes of the ellipse are parallel with the coordinate axes. One can then look at the analytic equation of an ellipse in normal form and apply continuity argument on the aspect ratio (which is an easier invariant to work with than the eccentricity for this proof) to prove the result (note that

one can replace 'the circle and the ellipse has four intersection points' with 'the circle and ellipse are bitangent' and arrive to the origin as the limit).

□

Lemma 8. *The eccentricity of the conic corresponding to the IKM is strictly dependent on the D-H parameters only and is independent of the position in the workspace* (R, z).

Proof. The eccentricity is dependent on the entries of $\mathbf{N}$ (refer to Chapter 2.1), and these entries only depend on the D-H parameters of the robot and not on the position of the end-effector, as shown in (1.2). □

By combining Lemma 8 and Lemma 7, we can put forth the following theorem:

Theorem 4. *There are infinitely many binary robots whose associated conic is an ellipse (that is not a circle).*

Proof. We claim that it suffices to have one binary generic robot with this condition. The associated ellipse for such a robot will never degenerate, and so the minor and major axes must achieve their (non-zero) minimum values. By the previous Lemma, these lengths must lie in an interval $I \subset \mathbb{R}$ centered at 1 (radius of an ellipse) for the ellipse to intersect the unit circle four times and for a fixed sufficiently small eccentricity e. If a generic binary robot is given with an associated ellipse of eccentricity e, then the minimum major (or minor) axes (recall the axes' length now depends on the end-effector position) is outside I. This minimum value is not in the boundary of I and is continuously dependent on the D-H parameters. One parameter that does not affect the eccentricity but does affect the minimum major/minor axes' length is d_3. So the robot obtained upon perturbing the length corresponding to d_3 within a small interval of the given binary robot still corresponds to a binary robot.

To conclude the proof, we give an example of a binary robot (refer to Figure 2.17) whose associated conic is an ellipse.

□

Following this proof, we present a conjecture:

Conjecture 1. *As the eccentricity of the associated ellipse approaches* 0 *(the ellipse becomes more like a circle), we will get more such binary robots however we will always be able to find a robot that is quaternery for such an eccentricity (as long as it is not* 0*).*

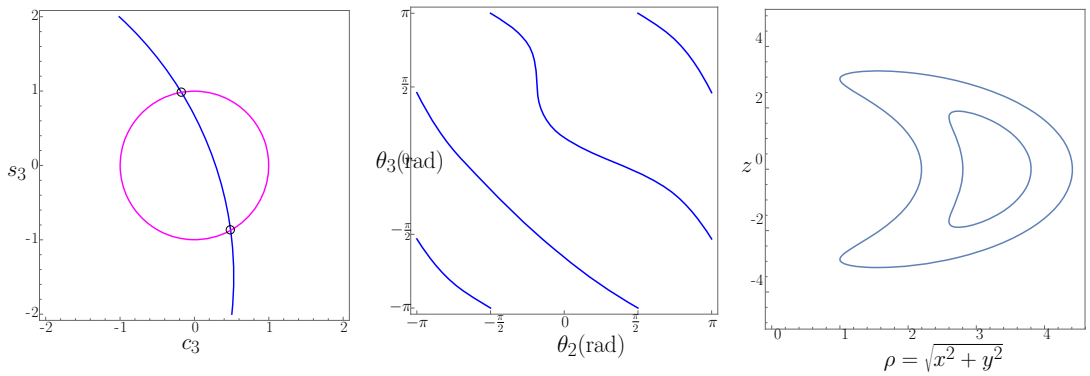

Figure 2.17 – An example of a binary robot's representation in $c_3 s_3 - plane$, the joint space and the workspace. Robot parameters: $d = [0, 0, 3], a = [-\frac{1503}{1879}, -1, -1], \alpha = [-2.21, \frac{-\pi}{2}, 0]$.

Quaternary robots

In this subsection, we discuss the case of a 3R robot such that the hyperbola degenerates and the center of the conic is inside the circle. It is straightforward to argue why such a robot is compulsorily quaternary. If the intersecting lines have their intersection point inside a circle, then each line will intersect the circle twice, thus yielding four intersection points in total. If c_x, c_y is the center of the conic in the $c_3 s_3$-plane, then the sufficient condition for a quaternary robot is:

$$\begin{cases} \det(\mathbf{N}) < 0 \\ \det(\mathbf{Q}) = 0 \\ \sqrt{c_x^2 + c_y^2} < 1 \end{cases} \tag{2.10}$$

To illustrate the simplicity of the derivation of the sufficient condition, we present a case of orthogonal 3R robots (see an example in 2.18).

$$\begin{aligned} \det(\mathbf{N}) &= -\frac{a_3^4\, d_2^2}{a_1^2} \\ \det(\mathbf{Q}) &= \frac{a_3^4\, d_2^2\, (d_3^2 - z^2)}{a_1^2} \\ c_x^2 + c_y^2 &= \frac{aR^2 + bR + c}{4\, d_2^2\, a_3^2} \end{aligned} \tag{2.11}$$

In (2.11), a and b are functions of the D-H parameters only and are not expressed fully for brevity. It is clear from (2.11) that an orthogonal 3R robot always corresponds to a hyperbola in the c_3s_3-plane, the condition for degeneracy depends only on d_3 and z while the condition for the center of the conic to lie inside the circle is a quadratic in R. It is important to note that the degeneracy depends only on z and not on R and thus, for $z = d_3$, the conic is always degenerate. This property further leads to some interesting observations about the hyperbolas corresponding to an orthogonal 3R serial robots but are not discussed here to limit the scope of the presented work.

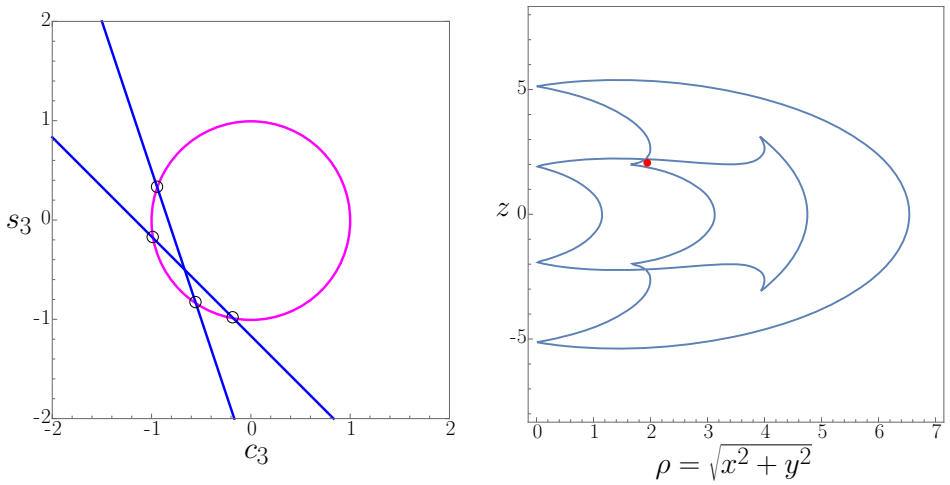

Figure 2.18 – An example of an orthogonal quaternary robot corresponding to an hyperbola.
Robot parameters : $d = [0, 1, 2], a = [1, 2, 3], \alpha = [\frac{-\pi}{2}, \frac{\pi}{2}, 0], (\rho, z) = (2, 2)$.

Quaternary 3R robots corresponding to ellipse in c_3s_3-plane

In this section, we present the working proof for a conjecture:

Conjecture 2. *For a quaternary 3R robot to be cuspidal, it is sufficient that the conic equation related to the inverse kinematic model corresponds to an ellipse.*

Proof. In order to prove the above theorem, we recall the properties discussed in section 1.2 and section 2.1. Given a quaternary 3R robot with $\mathbf{m}_i$, $\mathbf{m}_j$, $\mathbf{m}_k$ and $\mathbf{m}_l$ as the IKS for a pose in the 4 IKS region (refer to Figure 2.19), we know that a cusp in the workspace corresponds to the intersection of 3 intersection points in the c_3s_3-plane. Let the solutions be in circular order of $\mathbf{m}_i$, $\mathbf{m}_j$, $\mathbf{m}_k$ and $\mathbf{m}_l$. Let us consider $\mathbf{m}_k$ in the c_3s_3-plane. We know for certain that there exists a point such that the ellipse is tangential to the unit circle

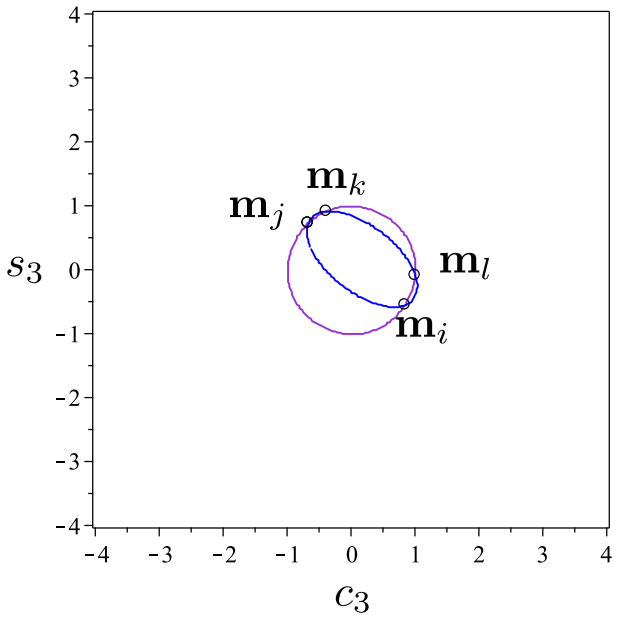

Figure 2.19 – An example of quaternary robot. Robot parameters: $\mathbf{a}$ = [1, 2, $\frac{3}{2}$], $\mathbf{d}$ = [0, 1, 0], $\alpha = [\frac{pi}{6}, \frac{pi}{2}, 0]$. Point in joint space (θ_2, θ_3) = [-0.97 rads, 2.32 rads].

and $\mathbf{m}_k$ is one of the points that merged at the tangent. This is attributed to the reason that every IKS in the joint space is bounded by the locus of critical points. We assume that $\mathbf{m}_k$ meets $\mathbf{m}_j$ without loss of generality as the case is similar to assuming $\mathbf{m}_k$ meets $\mathbf{m}_l$.

Starting from the given point in Figure 2.19, if we can shift the ellipse in horizontal direction without changing the size of the ellipse then we can claim that $\mathbf{m}_k$ meets $\mathbf{m}_l$ and thus there exists a cusp in the workspace such that $\mathbf{m}_k, \mathbf{m}_j, \mathbf{m}_l$ meet together at the tangent point between the ellipse and the circle. By lemma 8, we know that the eccentricity of the given ellipse is constant. We proceed by showing that the center and the minor axis of the ellipse is a function of R and z.

The center of the ellipse is given as $(\frac{f_1(R,z)}{\Delta}, \frac{f_2(R,z)}{\Delta})$.

$$\begin{aligned}
\Delta &= 2a_1^6\, sa_1^2\, a_3^4\, (a_1^2\, ca_1^2\, sa_2^2 - a_1^2\, ca_2^2\, sa_1^2 - a_2^2\, ca_1^2 sa_2^2 + a_2^2\, ca_2^2\, sa_1^2 + d_2^2\, sa_1^2\, sa_2^2) \\
f_1(R,z) &= -a_2\, a_3^3\, a_1^6\, (2\, ca_2^3\, d_2\, d_3\, sa_1^2 + 2\, ca_2\, d_2\, d_3\, sa_1^2\, sa_2^2 + a_1^2\, ca_1^2\, sa_2^2 - a_1^2\, ca_2^2\, sa_1^2 - \\
&\quad a_2^2\, ca_1^2\, sa_2^2 + a_2^2\, ca_2^2\, sa_1^2 - a_3^2\, ca_1^2\, sa_2^2 + a_3^2\, ca_2^2\, sa_1^2 + ca_1^2\, d_2^2\, sa_2^2 - ca_1^2\, d_3^2\, sa_2^2 + \\
&\quad ca_2^2\, d_2^2\, sa_1^2 + ca_2^2\, d_3^2\, sa_1^2 + 2\, d_2^2\, sa_1^2\, sa_2^2 + ca_1^2\, R\, sa_2^2 - 2\, ca_1\, d_2\, z\, sa_2^2 - ca_2^2\, R\, sa_1^2)\, sa_1^2 \\
f_2(R,z) &= a_3^3\, sa_2\, a_1^6\, (2\, a_1^2\, ca_1^2\, ca_2\, d_3 + 2\, a_1^2\, ca_2\, d_3\, sa_1^2 - 2\, a_2^2\, ca_1^2\, ca_2\, d_3 - 2\, a_2^2\, ca_2\, d_3\, sa_1^2 + \\
&\quad 2\, ca_2\, d_2^2\, d_3\, sa_1^2 + 2\, a_1^2\, ca_1^2\, d_2 + a_1^2\, d_2\, sa_1^2 - 2\, a_2^2\, ca_1^2\, d_2 - a_2^2\, d_2\, sa_1^2 + a_3^2\, d_2\, sa_1^2 + \\
&\quad d_2^3\, sa_1^2 + d_2\, d_3^2\, sa_1^2 - 2\, a_1^2\, ca_1\, z + 2\, a_2^2\, ca_1\, z - d_2\, R\, sa_1^2)\, sa_1^2
\end{aligned} \tag{2.12}$$

From (2.12), it can be concluded that the center of the ellipse can be controlled by R and z. Moving the center of the ellipse in a desired direction is not enough to prove that $\mathbf{m}_k$ meets $\mathbf{m}_l$ as the size of ellipse can shrink or enlarge while keeping the eccentricity constant. This means that the ellipse may shrink faster than the horizontal shift assuring $\mathbf{m}_k$ always meets $\mathbf{m}_j$ at a tangent point. As the eccentricity is constant, if the length of major or minor axis is a dependent on R or z, then we can shift the ellipse by keeping the size of the ellipse in check forcing $\mathbf{m}_k$ to meet $\mathbf{m}_l$ at a tangent point.
For an ellipse in standard form in $c_3 s_3$-plane centered at (h, k) given as:

$$\frac{(c_3 - h)^2}{a^2} + \frac{(s_3 - k)^2}{b^2} = 1$$

the length of the minor axis is $2a$ or $2b$, depending upon the orientation of the conic. A general equation of a conic is a transformation of the standard form (1.1), and can be written as:

$$A'_{xx}\, c_3^2 + A'_{yy}\, s_3^2 + 2B'_x\, c_3 + 2B'_y\, s_3 + C' = 0 \tag{2.13}$$

such that

$$
\begin{aligned}
A'_{xx} &= \frac{A_{xx}+A_{yy}}{2} + \frac{(A_{xx}-A_{yy})|A_{xx}-A_{yy}| \pm |B|B}{2\sqrt{(A_{xx}-A_{yy})^2+A_{xy}^2}} \\
A'_{yy} &= \frac{A_{xx}+A_{yy}}{2} - \frac{(A_{xx}-A_{yy})|A_{xx}-A_{yy}| \pm |B|B}{2\sqrt{(A_{xx}-A_{yy})^2+A_{xy}^2}} \\
B'_x &= B_x\sqrt{\frac{1}{2}+\frac{|A_{xx}-A_{yy}|}{2\sqrt{(A_{xx}-A_{yy})^2+A_{xy}^2}}} \pm B_y\sqrt{\frac{1}{2}-\frac{|A_{xx}-A_{yy}|}{2\sqrt{(A_{xx}-A_{yy})^2+A_{xy}^2}}} \\
B'_y &= B_y\sqrt{\frac{1}{2}+\frac{|A_{xx}-A_{yy}|}{2\sqrt{(A_{xx}-A_{yy})^2+A_{xy}^2}}} \mp B_x\sqrt{\frac{1}{2}-\frac{|A_{xx}-A_{yy}|}{2\sqrt{(A_{xx}-A_{yy})^2+A_{xy}^2}}} \\
C' &= C
\end{aligned}
\tag{2.14}
$$

We can split C into three parts C_1, C_2 and C_3 such that it is possible to write the equation as:

$$
\begin{aligned}
&\frac{(c_3^2+\frac{B'_x}{A'_{xx}}+\frac{C_1}{A'_{xx}})}{\frac{-C_3}{A'_{xx}}} + \frac{(s_3^2+\frac{B'_y}{A'_{yy}}+\frac{C_2}{A'_{yy}})}{\frac{-C_3}{A'_{yy}}} = 1 \\
&C_1+C_2+C_3 = C \\
&C_1 = \frac{B'^2_x}{4A'_{xx}} \\
&C_2 = \frac{B'^2_y}{4A'_{yy}}
\end{aligned}
\tag{2.15}
$$

From (2.15), it is seen that the length of major axis and minor axis is dependent on R and z. From this result it can be confirmed that any 2 of the four entities viz., the x coordinate, y coordinate of the center, the length of minor axis, and the length of the major axis of the ellipse can be defined by varying R and z. This allows us to fix the vertical position of the center of the ellipse and increase the length of the minor axis. As we increase the length of minor axis the intersection point $\mathbf{m}_k$ will meet $\mathbf{m}_l$, or $\mathbf{m}_j$ will meet $\mathbf{m}_i$. Both scenarios will lead to the conclusion of existence of cusp in the workspace as we will have either $\mathbf{m}_j, \mathbf{m}_k, \mathbf{m}_l$ meeting together or $\mathbf{m}_i, \mathbf{m}_j, \mathbf{m}_k$ meeting together at a tangent point.

This result combined with the Theorem 3 proves that a quaternary 3R serial robot whose IKM corresponds to an ellipse in the c_3s_3-plane is a cuspidal robot. □

2.2.2 Comments on maximum aspects in 3R robots

In this section, we discuss the existence of two homotopy classes presented by [Pag08] in his dissertation. In his work, he extends the homotopy classes presented for singularities of 3R robots in [Wen98]. As the singularities of a 3R robot are functions of θ_2 and θ_3 only, the joint space of 3R robot can be considered as $\mathbb{T}^2$ for singularity analysis. The homotopy classification of singularity curves is discussed in details in [Wen98; Pag08], and the following work uses the definition mentioned in previous articles. A homotopy class of a generic 3R robot can be characterized by a series of couples (l_1, l_2). l_1(resp. l_2) = 1 signifies a branch of the locus of critical points encircling the θ_2(resp. θ_3)-generator of $\mathbb{T}^2$. There exist four types of singularity curves (branches) in the joint space of a 3R robot viz., (1, 0), (0, 1), (1, 1), and (0, 0), depending upon the encirclement of the torus along the θ_2 generator only, θ_3 only, both θ_2, θ_3, and no encirclement [Wen98]. The homotopy analysis in [Pag08] showed that there might exist 3R robots belonging to the homotopy class of 3(0, 0) and 4(0, 0).

Conjecture 3. *There does not exist a 3R robot belonging to the homotopy class of n(0, 0), with n > 2.*

Proof. The above conjecture can be proved by contradiction. We consider the following proposition:

Proposition 4. *The 3R robot belonging to n(0, 0) homotopy class has to be a quarternary robot for n > 1.*

Proof. This statement can be easily proved by checking the case when the robot is binary. Let us consider a binary robot with 2(0, 0) homotopy class and let A and B be the two (0, 0) branches. By definition, a (0, 0) branch is a loop on $\mathbb{T}^2$. Let an IKS lie in the region defined by the (0, 0) branch, A, while the other outside the regions associated to the two (0, 0) branches. This implies that there can be no path in joint space starting from the IKS outside the (0, 0) branches to the (0, 0) branch, B. This cannot happen as there should always exist a path in joint space between any two points. □

As it is shown from the above proposition, the robots belonging to 3(0, 0) and 4(0, 0) must be necessarily quaternary. Now we consider a robot belonging to 3(0, 0) class, and start from a pose with four IKS. Let the aspects bounded by each (0, 0) branch be A, B and C, and the aspect exterior to A, B, C be D. As the number of IKS with $\det(\mathbf{J}) > 0$ must be equal to IKS with $\det(\mathbf{J}) < 0$, let solutions $\mathbf{m}_i, \mathbf{m}_j$ belong to D and $\mathbf{m}_k, \mathbf{m}_l$ belong

to A and B respectively. Now, we consider a path in joint space from $\mathbf{m}_i$ to the boundary of C. In order to meet a point on the boundary of C, we need to necessarily cross at least two pseudosingularities. When the first pseudosingularity is crossed, $\mathbf{m}_j$ meets $\mathbf{m}_k$ or $\mathbf{m}_l$ at the boundary of A or B respectively. The next pseudosingularity is crossed by $\mathbf{m}_i$, and at this point $\mathbf{m}_j$ and $\mathbf{m}_k$ or $\mathbf{m}_l$ must appear at either side of the boundary of C. In this case both $\mathbf{m}_i$ and $\mathbf{m}_j$ will exist in the same reduced aspect and this contradicts Theorem 2. If 3(0, 0) cannot exist, then by the same argument no robot can exist corresponding to n(0, 0) homotopy class with n $>$ 2. □

2.3 Conclusions

In this chapter, the proof for the necessary and sufficient condition for a generic 3R serial robot to be cuspidal was presented. The proof studied the geometric interpretation of the IKM of a 3R serial robot and presented observations about the constant nature and orientation of the conic corresponding to a given set of D-H parameters. It is for the first time that a mathematical proof has been presented for the necessary and sufficient condition for cuspidality of generic 3R serial robots. The existence of reduced aspects in a generic serial robot was proved by using geometric analysis of the IKM. These results mark the closure of the conjecture presented after noting the cusp in the workspace and its relation with nonsingular change of solutions. In the second part of the chapter, we have revisited the geometric interpretation of the inverse kinematic model of 3R robots to extend the geometric analysis of 3R robots. The special case of a parabola degenerating into two coincident lines was presented along with its interpretation in the workspace. The work presented a sufficient condition for a 3R serial robot to be binary (circle and ellipse case) and quaternary (hyperbola case) by using geometric observations. The advantages of the geometry based analysis is that the conditions for binary or quaternary robots can be extended to more generic cases of 3R robots without resorting to complex algebraic derivations. This advantage was motivated by presenting the conjecture that all quaternary robots associated with ellipse are cuspidal. In the future, we aim to present a necessary and sufficient condition for a generic 3R robot to be binary or quaternary. This will allow the designer to include the condition while optimizing for a workspace with 4 IKS. Later, using the geometric interpretation, the work commented upon a conjecture provided by Paganelli in his thesis [Pag08] regarding the maximum number of aspects in a 3R serial robot.

Chapter 3

6R SERIAL ROBOTS

In this chapter, the results on cuspidality analysis on 6R serial robots is presented. The first section details the simplified geometries and analyses the role of geometric architecture and the form of determinant in the number of aspects as well as the cuspidality of the robot. Later, the chapter discusses the generic architecture of 6R serial chain. In this section, the designs by Parenti-Castelli [IPC98] are discussed and the claim on generic 6R serial robots is reverified. A certified algorithm to decide upon the cuspidality of a generic nR non-redundant serial manipulator is further presented to allow a designer to choose a design as per requirements. Owing to the computational complexity of this algorithm, the section proposes a simplified methodology to check the cuspidality of the robots. Finally, the chapter concludes with a proposal of a framework for deciding the cuspidality of a generic 6R serial robot.

3.1 Simplified 6R geometry

In this section, we present simplified geometries of 6R serial chains. A simplified geometry is one where the inverse kinematics may simplify due to special arrangement of joints and links in the serial chain. Some of the examples are: 1. Existence of a three intersecting axes forming a wrist, 2. Three parallel joint axes forming a 3R sub chain in the 6R serial chain. Most of the industrial robots are simplified geometries due to the ease in conceptualizing and straightforward kinematic relations. This makes the analysis of such simplified geometries important from the industrial applications point of view.

3.1.1 Wrist at the end

The most widely known geometry of a 6R serial chain is an anthropomorphic architecture with the wrist at the end. The last three axes intersecting at a point forms a wrist which allows the decoupling of position analysis from the orientation analysis of

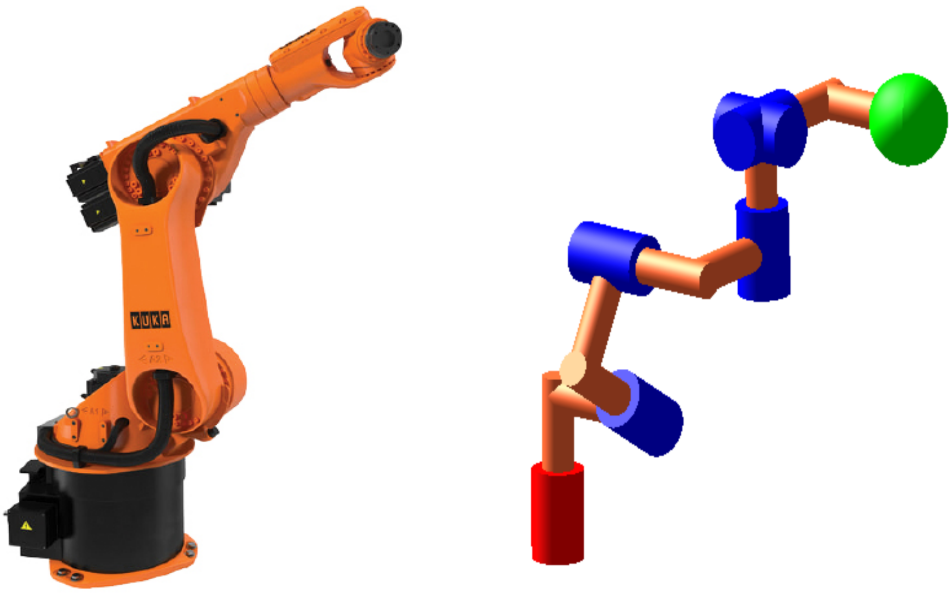

(a) Example of anthropomorphic robot with wrist at the end

(b) Schematic representation of a robot with wrist at the end

Figure 3.1 – Simplified geometry with wrist at the end

the robot. The orientation of the robot is strictly controlled by the last three axes only while the pose of the origin of the wrist (the intersection point of the last three axes) is a function of first three joints only. This decoupling in the 6R serial manipulators simplifies the kinematics to a great extent alleviating many complex calculations to a point that we have an analytical solutions to a specific architectures of 6R serial robot with the wrist at the end. These architectures have perpendicular and parallel arrangements between the joints and due to their resemblance with a human arm, are termed as anthropomorphic 6R serial robots. Figure 3.1 shows an example of the industrial 6R serial robot with anthropomorphic architecture and an example architecture of 6R serial robot with wrist at the end.

Theorem 5. *For a wrist-partitioned 6R serial chain, i.e, three intersecting consecutive axes, at the end of the chain, the existence of a cusp in the workspace of the 3R serial chain formed by first three axes is a necessary and sufficient condition for the robot to be cuspidal.*

Proof. As the inverse kinematics model of a robot with wrist at the end is decoupled, it is possible to decouple the cuspidality analysis too. This is attributed to the reason that any change of IKS can be studied as change of IKS in the 3R sub chain responsible for position

and change of IKS in the 3R sub chain responsible for the orientation (wrist). The IKM of the wrist is well known, and there exists two aspects in the joint space with two IKS for any given orientation. These IKS are always separated by the wrist singularity, a configuration where the first and last axes of the wrist coincide. This makes the wrist architecture a non-cuspidal sub chain. So if the sub chain responsible for position is cuspidal in nature, we can change the position without crossing a singularity and as there exists a solution for any orientation, the new orientation is guaranteed to be reached without encountering the wrist singularity. From this known result, it is clear that the cuspidality of a 6R serial chain with wrist at the end solely depends on the cuspidal nature of the positional 3R sub-chain as shown in table 3.1. This suggests that all the theorems proved for a generic 3R serial chain can be extended to wrist-partitioned 6R serial chains with wrist at the end as well. The presence of a cusp being a necessary and sufficient condition for a generic 3R serial chain has been proved [Sal+22b] (refer to section 2.1). The presented theorem is simply an extension of theorem 3. □

Position 3R chain	Wrist	6R serial chain
Cuspidal	Non-Cuspidal	Cuspidal
Non-Cuspidal	Non-Cuspidal	Non-Cuspidal

Table 3.1 – The relation for cuspidality in 6R serial robot with wrist at the end

3.1.2 Intersecting three axes at the beginning

Another interesting geometry of 6R serial robots is with the first three axes intersecting to form a wrist. The inverse kinematics of this robot is can be interpreted in similar fashion that of the 6R serial robot with wrist at the end. If we apply the transformation of frames and switch the end-effector frame as the base and the frame of first joint as the end-effector frame, the inverse kinematics for position and orientation is decoupled as discussed earlier. This allows one to extend the results obtained in section 3.1.1 to this class of robots. It has been verified that the analysis of conic in $c_3 s_3$-plane holds true for the 6R serial chains with first three axes forming a wrist. It can be readily shown that the analysis done in the $c_3 s_3$-plane in chapter 2.1 can be done in $c_4 s_4$-plane for the robots with wrist in the beginning where c_3, c_4 stands for $\cos\theta_3, \cos\theta_4$ and s_3, s_4 denote $\sin\theta_3, \sin\theta_4$. This allows us to put forth the following theorem:

Theorem 6. *For a wrist-partitioned 6R serial chain, i.e, three intersecting consecutive*

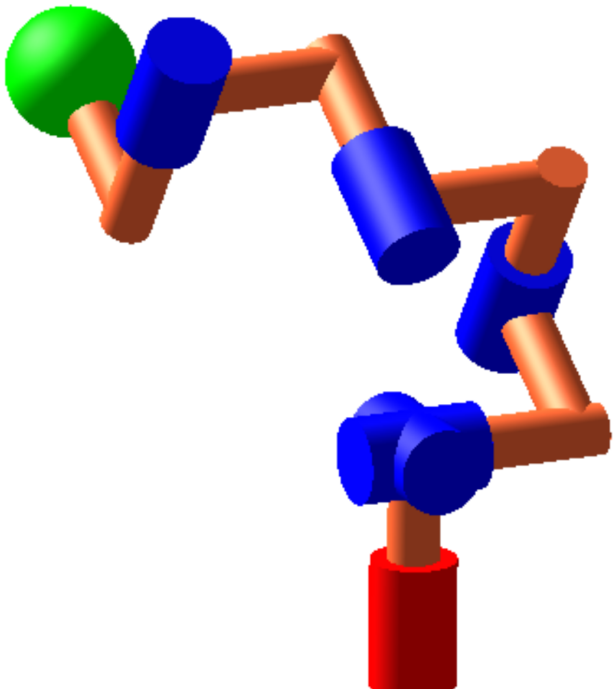

Figure 3.2 – Schematic of a 6R serial chain with wrist in the beginning

axes, at the beginning of the chain, the existence of a cusp in the workspace of the 3R serial chain formed by last three axes is a necessary and sufficient condition for the robot to be cuspidal.

Figure 3.2 shows a schematic of a generic 6R serial chain with first three axes intersecting forming a wrist and Figure 3.3 shows the conic representation of the IKM of such robot at a given instance.

In both the cases when the wrist is formed at the extreme of the 6R serial chain, the determinant factors in the form:

$$\det(\mathbf{J}) = C_1 \sin\theta_w \, f(\theta_{p1}, \theta_{p2}) \tag{3.1}$$

where, C_1 is a constant, θ_w is the second axis of the wrist, and θ_{p1}, θ_{p2} are the axes of the positional sub chain with $\theta_{p1}, \theta_{p2} \notin \theta_1, \theta_6$.

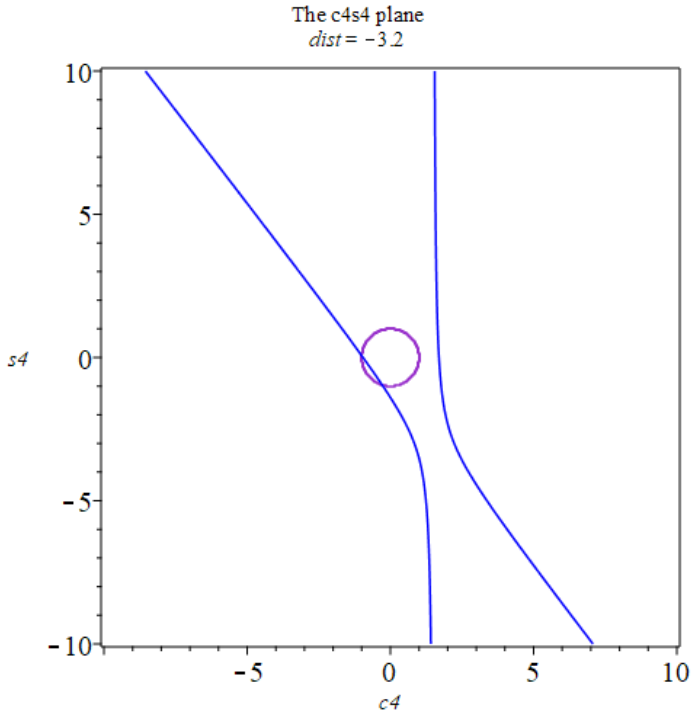

Figure 3.3 – conic representation of IKM for a 6R serial robot with wrist in the beginning. The DH parameters of the robot are:
$\theta = [0, 0, 0, \frac{\pi}{2}, \frac{\pi}{6}, \frac{\pi}{4}], \mathbf{d} = [1, 0, 1, 1, 0, 0], \mathbf{a} = [0, 0, 1, 1, 1, 0], \alpha = [\frac{\pi}{2}, -\frac{\pi}{2}, \frac{\pi}{9}, -\frac{\pi}{3}, \frac{\pi}{6}, 0]$.

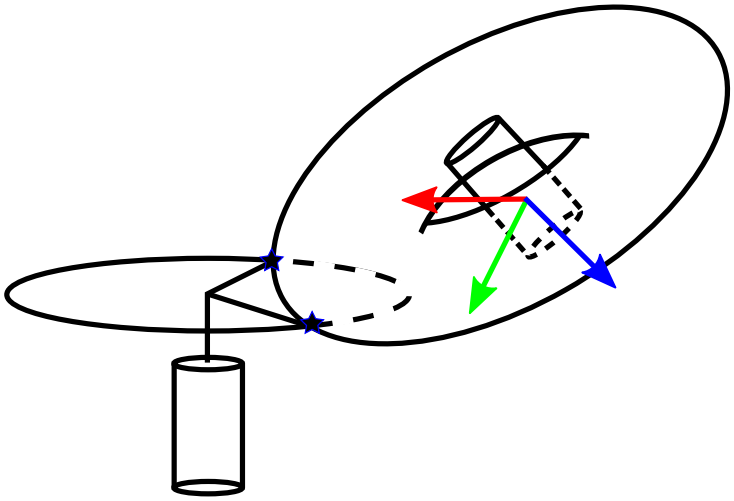

Figure 3.4 – Geometric explanation for the IKM with wrist in the middle

3.1.3 Wrist in the middle

The last subclass of 6R robots with wrist as a subchain is when the second, third, fourth or third, fourth, and fifth axes intersect to form a wrist. We note these cases as the wrist in middle case. This case is particularly interesting as even though it is a simplified geometry, nature of positional subchain is different from the previously discussed examples. The IKM of this robot was discussed by using analytic [Pie68] as well as algebraic tools [Ben91] in the past. We discuss a simple geometric interpretation of the IKM to provide a visual intuition for the IKS. As the wrist is in the middle, any orientation can be achieved for the frame with origin at the intersection point of the wrist. Assuming $d_3 = 0$ for simplifying analysis, the intersection point lies on a circle centered at $(0, 0, d_1)$ with radius $\sqrt{a_1^2 + d_2^2}$. If the end-effector frame is fixed, then the manifold generated by the 2R chain formed by the fifth and sixth axes is a torus with center of axis coinciding with the axes of the sixth joint. As the origin of the wrist is connected with the fifth joint, the intersection between the circle and the torus gives the position of the wrist. Figure 3.4 illustrates the idea, with the star points denoting the possible positions of the wrist. As a circle intersects a torus in maximum four points, the origin of the wrist can be placed in four different positions. As every orientation of the wrist has two solutions, we conclude (as shown in the past [Pie68; Ben91]) that this robot has a maximum of eight solutions. We can immediately conclude that four solutions correspond to a positive value of $\det(\mathbf{J})$ as the wrist solutions are separated by a singularity. The geometric explanation allows a visualization of a path in the joint space for change of the inverse kinematic solutions. A trivial method to see

this change of IKS in the joint space is as following:

1. rotate θ_1 to displace the origin of the wrist to the second intersection point
2. move from the current orientation of the wrist to a desired frame
3. this automatically places the fifth joint in the required position, displace θ_5 to align z_6 with the end-effector's z-axis.
4. rotate θ_6 to align the frame with the desired pose

The main difference of the wrist in the middle from other two sub cases is that even though the IKM is decoupled in two different subchains, the end-effector pose cannot be analyzed by decoupling the position and the orientation. It would be ideal if the orientation and position of the end-effector were independent in order to conclude upon the cuspidal nature of the robot, but the form of determinant for wrist in the middle is different from (3.1), and is in the form of:

$$\det(\mathbf{J}) = C_1 \sin\theta_w \, f(\theta_2, \theta_3, \theta_4, \theta_5) \tag{3.2}$$

A simple sufficient condition for such a robot to be noncuspidal is when the D-H parameters are designed such that the circle intersects the torus maximum twice which will limit the number of IKS to four and are always separated by singularity. As all the four joints apart from θ_1 and θ_6 contribute to the determinant of the Jacobian, and there are no distinct components, the analysis for distribution of IKS is not straightforward. This example allows to highlight that the cuspidality analysis of 'simplified' geometries is not easy either. The separation of IKS into different components is only clear in few cases where the determinant factors into distinct components with independent solutions similar to (3.1). We illustrate further two examples of 6R robots with three consecutive axes intersecting in the middle to highlight the possibility of extending geometric analysis for considering noncuspidal cases of 6R serial chains.

Two dimensional singularities

The singularities of a generic 6R serial robot depend on the non-extreme joints only. This is attributed to the reason that the workspace of the robot is symmetrical about the first joint and the last joint of the robot is only responsible for the orientation of the end-effector about its own axis. It is hard to visualize the rank 5 singularities as they are a 3-dimensional manifold in a four dimensional joint space. A simplified case helps us

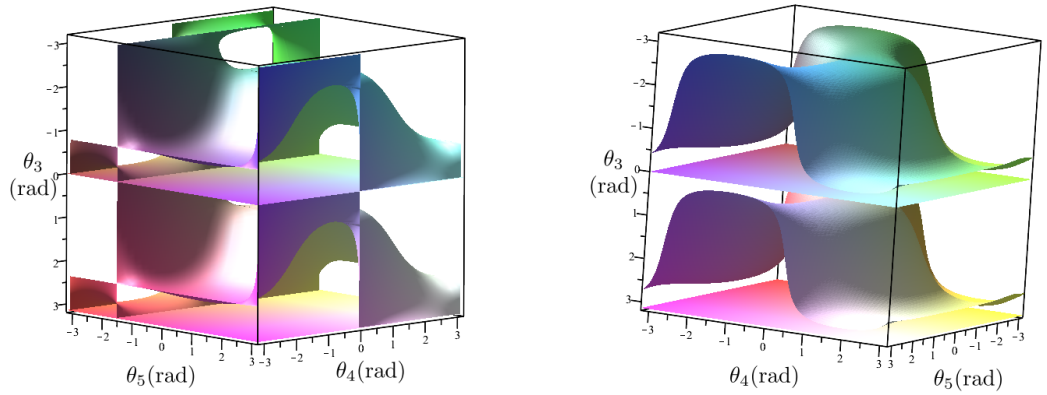

(a) Singularities for an example robot with wrist in the middle. D-H parameters are : $\mathbf{d} = [0, 0, 0, 1, 2, 0]$, $\mathbf{a} = [1, 0, 0, 1, 1, 0]$, $\alpha = [\pi/2, \pi/2, \pi/2, \pi/2, \pi/2, 0]$.

(b) Singularities for an example robot with wrist in the middle. D-H parameters are : $\mathbf{d} = [0, 0, 0, 1, 2, 0]$, $\mathbf{a} = [1, 0, 0, 2, 3, 0]$, $\alpha = [\pi/2, \pi/2, \pi/2, \pi/2, \pi/2, 0]$.

Figure 3.5 – Simplified examples of 6R robots with wrist in the middle such that the rank 4 singularities form a 2 dimensional variety.

in visualizing the joint space with singularities and provides an intuition of the effect of DH parameters on the singularities. One such case with wrist in the middle is when we set d2 = 0 as an additional constraint. The determinant for these parameters is detailed in Appendix A.3. The singularities can be visualized and few examples are illustrated in Figure 3.5.

$\det(\mathbf{J})$ with three components

When the D-H parameters are further constrained such that all the axes are mutually orthogonal and $a_5 = 0$, the $\det(\mathbf{J})$ factors into three components as follows:

$$\begin{aligned}\det(\mathbf{J}) = s_3\left(s_5 d_4 + a_4 c_5\right)\left(s_4 c_3 c_2 d_2 d_5 + c_4 c_3 c_2 a_4 d_2 + s_2 s_4 a_4 d_2 - s_2 c_4 d_2 d_5\right. \\ \left. - s_3 s_4 a_1 d_5 - s_3 c_4 a_1 a_4 + s_3 c_2 d_2 d_4 + c_3 a_1 d_4\right)\end{aligned} \tag{3.3}$$

The three components confirm that there are at least eight aspects in the joint space. As the $\det(\mathbf{J})$ factors, the IKS can be analyzed according to the factors too. Such a robot can be declared non-cuspidal by studying the sign of each component of $\det(\mathbf{J})$. The plot

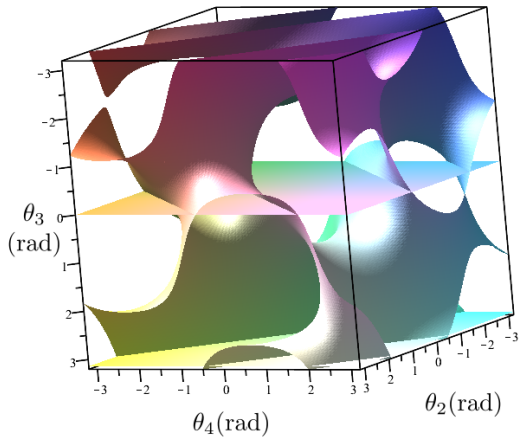

Figure 3.6 – Singularity plot in $\theta_2, \theta_3, \theta_4$ for a robot with wrist in the middle, mutually orthogonal axis with $a_5 = 0$. The component $(2s_5 + c_5)$ is not plotted. D-H parameters are: $\mathbf{d} = [0, 1, 0, 1, 2, d_6], \mathbf{a} = [1, 0, 0, 2, 0, a_6], \alpha = [\pi/2, \pi/2, \pi/2, \pi/2, \pi/2, 0]$.

of the equation (3.3) in θ_2, θ_3, and θ_4 is shown in Figure 3.6. The plot is further divided into 2 parts due to the component $(s_5 d_4 + a_4 c_5)$ along the θ_5 axis.

3.1.4 Planar 3R subchain in 6R robots

Another simplified geometry of 6R robot is when the consecutive three axes are aligned, i.e $\alpha_i = \alpha_{i+1} = 0, i \neq 6$. An existing commercial robot of this geometry is the UR series from Universal Robots. It has been analyzed in [CSEDS20], and shown that this robot has eight connected regions in the joint space with maximum eight IKS that are always separated by singularity. The determinant of the UR robots take the following form:

$$s_3 s_5 \left(c_2 s_3 c_4 d_5 + c_2 s_4 c_3 d_5 - s_2 s_3 s_4 d_5 + s_2 c_4 c_3 d_5 + c_2 c_3 a_3 - s_2 s_3 a_3 + a_2 c_2 + a_1\right) a_2 a_3 \quad (3.4)$$

The geometric analysis of this robot is straightforward, and analyzing each component of the $\det(\mathbf{J})$, it is clear that all IKS correspond to different regions of the aspect. There are two solutions for $\sin\theta_3$, two for $\sin\theta_5$ and (at least) two for the third component, thus verifying that there exist at least eight connected regions in the joint space as each component of the $\det(\mathbf{J})$ cuts the other transversally.

3.2 Cuspidality analysis of generic 6R robots

Deciding cuspidality for a given serial arm allows a designer to take better decisions based on the advantages of the designs and challenges in the path planning of cuspidal robots. Deciding cuspidality in orthogonal 3R serial robots was completely presented in [EOW95] from which the necessary and sufficient condition for a 3R serial *orthogonal* robot to be cuspidal was put forth. Later, the necessary and sufficient condition for cuspidality in generic 3R serial arms was proven using geometric analysis of the IKM [Sal+22b]. These works allowed a designer to integrate a mathematical check for the cuspidality of a robot which can be used in an optimization method during the design process. Recently, a certified algorithm was presented for deciding cuspidality for non redundant nR robots [Cha+22]. It implements various algorithms in computer algebra using methods on real algebraic sets and critical loci of polynomial maps. It uses tools from Real Algebraic Geometry, zero-dimensional parameterizations, to get the sample points in $\mathcal{W}$ such that we have at least a point in each connected region of $\mathcal{W}$. It then investigates the connectivity of the preimages of each of the sample points by implementing one-dimensional parameterizations, roadmap algorithms, which reduce the four dimensional jointspace, $\mathcal{J}$, to a one dimensional graph without the loss of information on connectivity. Though certified, this algorithm is very hard to implement presently and cannot be used with collision constraints.

In this section, the conjecture presented in [IPC98] about two aspects in 6R robots is investigated. Later, the limitations of existing methods to decide cuspidality are discussed, and a generic method that can be applied to all 6R serial robots and incorporate the constraints is proposed. This method is easy to implement and is faster than the certified algorithm in case of a cuspidal robot. Later, we propose a complete framework that can be used for deciding cuspidality of a 6R serial robot. It combines all the previously known results as well as considers the analysis of determinant of the Jacobian in order to accelerate the process.

3.2.1 Number of aspects in 6R robots

In [IPC98], it is claimed that for any 6R robot, the locus of critical points results in only one r-surface and thus the maximum aspects are limited to two. The r-surface is defined as a closed surface formed by the locus of critical points. The argument was based on the analysis of degree of each joint angle in the $\det(\mathbf{J})$ and presented the infeasibility

of multiple r-surfaces. The thesis shows that this statement is incomplete. The following discussion presents a counter example of a 6R robot with more than two aspects formed by non-intersecting locus of critical points.

Counter example to the conjecture

Without motivating the choice of D-H parameters, we simply show a case of generic 6R robot with four aspects in figure 3.7. The term generic is used in the sense that there are no intersections between the singularity manifolds, or isolated singular points in the joint space of the presented robot.

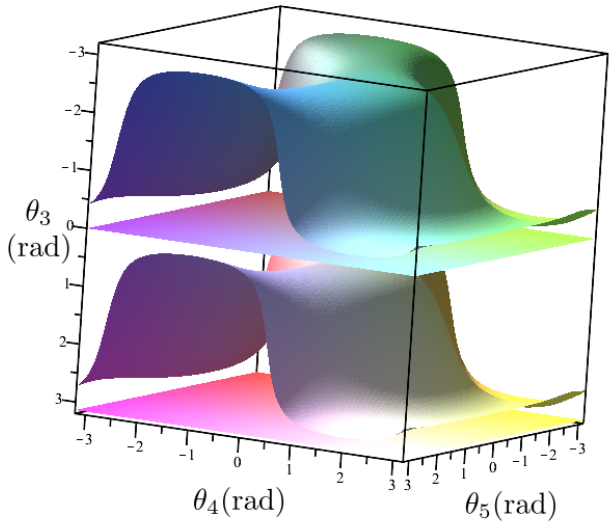

Figure 3.7 – Singularities for the counterexample to [IPC98], a robot with non-intersecting singularities with more than two aspects. D-H parameters are : $\mathbf{d} = [0, 0, 0, 1, 2, 0]$, $\mathbf{a} = [1, 0, 0, 2, 3, 0]$, $\alpha = [\pi/2, \pi/2, \pi/2, \pi/2, \pi/2, 0]$.

Error in the proof

In the proof the r-surfaces refer to the connected components of singularities in the joint space. The analysis of $\det(\mathbf{J})$ is presented to study possible cross sections in the joint

space. It is shown that the det(**J**) is a function of joint angles as follows:

$$\det(\mathbf{J}) = f(t_2^2, t_3^4, t_4^4, t_5^2) \tag{3.5}$$

where $t_i = \tan\frac{\theta_i}{2}$. This is correct, and the proof further discusses the cross section of the singularities in $\theta_2\theta_5$-slice. It argues that the two r-surfaces cannot exist by presenting two cases in which two r-surfaces are present in the joint space. In the first case, it is presented that there cannot be a r-surface enclosed in another as then there will exist a parallel line along θ_5 that intersects the r-surfaces four times which is not possible as the degree of t_5 in det(**J**) is two (refer to figure 3.8). The other case where two r-surfaces exist presents a contradiction about which r-surface has an image of the limit of the workspace (refer to figure 3.9).

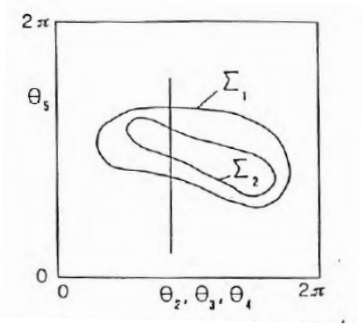

Figure 3.8 – Infeasibility of concentric closed r-surfaces as shown in [IPC98]

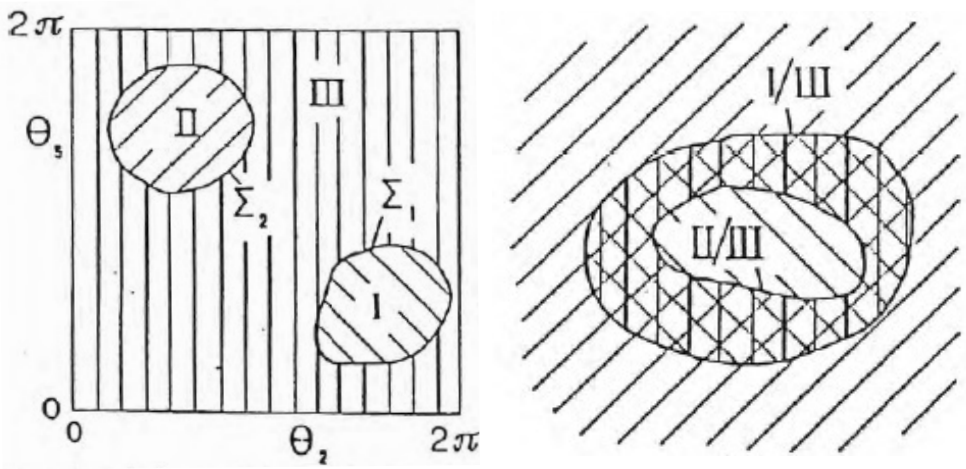

Figure 3.9 – The cross section of joint space and workspace in case of two separated r-surfaces as discussed in [IPC98]

The argument of figure 3.8 is straightforward to verify by studying the form of det(**J**) as mentioned in [IPC98]. The second argument has an error that is an outcome of misinterpreting the joint space. In [IPC98], it is discussed that the r-surfaces should be closed in joint space, $Q \in [0, 2\pi[$. The issue in this argument is that the r-surfaces do not have to form bounded regions in Q to formed closed surfaces as the joint space is a $\mathbb{T}^4$ (refer to figure 3.10). The joint space was not treated as a $\mathbb{T}^4$ in the previous work. This is evident from the argument proposed by the paper presenting the only possible case of existence of 'unique' r-surface as shown in figure 3.11.

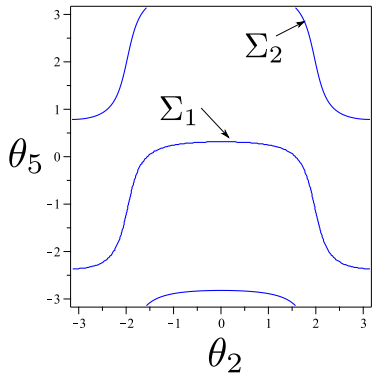

Figure 3.10 – r-surfaces that are closed but do not generate 2 subspace independently

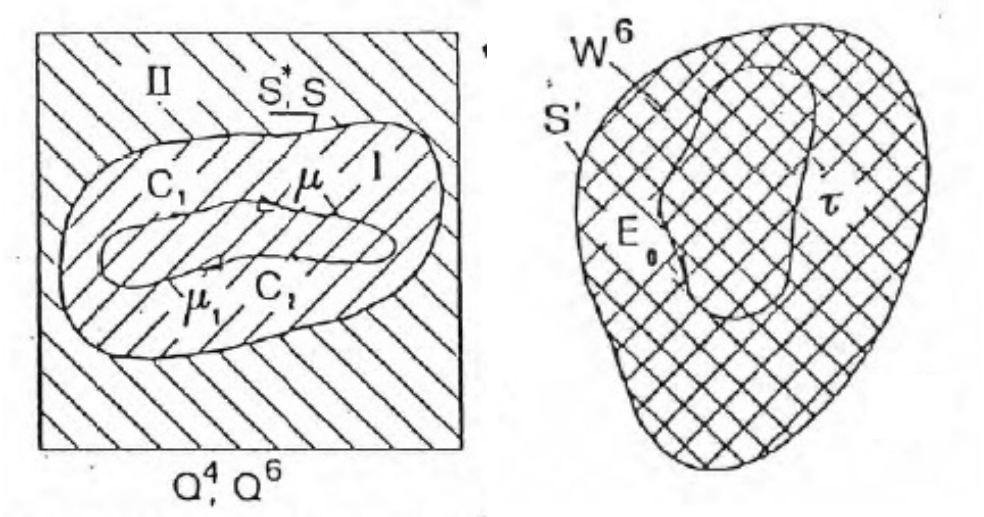

Figure 3.11 – The only possible case of existence of unique r-surface as per [IPC98].

Thus, the assumption that the cross sections shown in figure 3.9 is not possible is erroneous. In fact, neither Σ_1 nor Σ_2 need to be the preimage of the limit of the workspace

as there can exist another r-surface that may correspond to the limit of the workspace and not violate the form of det(**J**). Two counterexamples are presented with the possible r-surface that may map to the limit of the workspace of the robot in figure 3.12. Apart from this, both the r-surfaces can contribute partially to form the limit of the workspace as is the case in 3R robots belonging to the 2(0, 0) homotopy class (refer to [Wen98]).

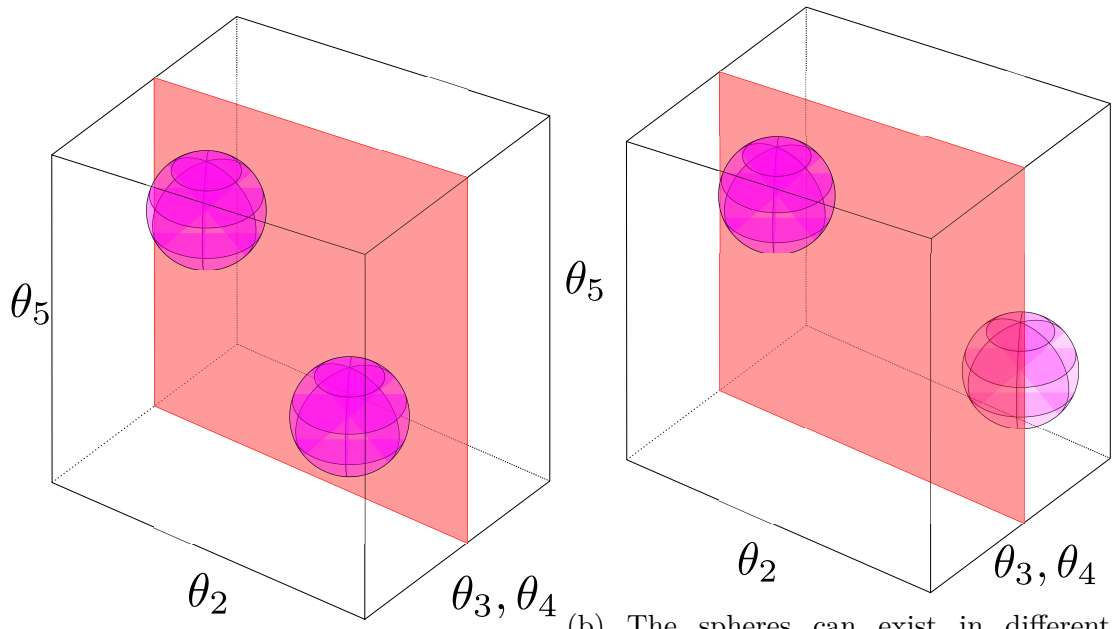

(a) The spheres can exist in same plane.

(b) The spheres can exist in different planes.

Figure 3.12 – The counterexamples showing the possibility of more than two aspects in the joint space. The red plane is a r-surface whose image is the limit of the workspace. The r-surface is not necessarily a plane.

3.2.2 Comment on cuspidality in 6R robots

Conjecture 4. *A generic 6R robot with more than 4 IKS is a cuspidal robot.*

Proof. The proof (in progress) for the presented conjecture uses following two arguments:

1. The form of the determinant of Jacobian matrix of a 6R robot is given as, $\det(\mathbf{J}) = f(t_2^2, t_3^4, t_4^4, t_5^2)$.
2. For a non critical pose in the workspace, the number of IKS with $\det(\mathbf{J}) > 0$ is equal to IKS with $\det(\mathbf{J}) < 0$.

We define following two terms to elucidate the proof:

Definition 18. *Bubble: The singularity manifold that do not encircle the $\mathbb{T}^4$ torus along any generator of the torus is defined as a bubble. A bubble generates an open ball bounded by the bubble only.*

Definition 19. *Sheet: The singularity manifold that is not a bubble is defined as a sheet. A sheet cannot bound any open ball independently.*

Lemma 9. *A single sheet cannot exist in the joint space of a 6R robot.*

Proof. As a sheet cannot enclose any open ball, this type of singularity manifold cannot separate two aspects on its own. A bubble cannot define an aspect with a sheet either as the exterior of bubble is not bound by a bubble and cannot be bound by a single sheet. The only possibility is that two sheets or more than two sheets exist in the joint space. This theorem can be thought as an extension of the Theorem 7 presented in [Wen98]. □

Lemma 10. *There can exist at most four sheets in a joint space of a 6R robot.*

Proof. Upon studying the det($\mathbf{J}$) for a 6R robot, we already know that the maximum degree for any joint angle is four. So there can exist maximum four sheets such that any path parallel to any joint angle θ_i intersects the singularities at maximum four points. □

From Lemma 9 and Lemma 10, it is clear that we have four cases of singularity manifolds depending upon the number of sheets present in the joint space.
Case I: Four sheets exist in the joint space of a 6R robot: In this case, no bubble can co-exist as it will lead to a path parallel to one of the joint angles that will lead to at least six intersections (one from each sheet and at least two from each bubble). The number of aspects present in this case is 4. An example joint space is presented in figure 3.12. So, for a pose in the workspace with more than four IKS, there will be at least one aspect with multiple IKS and thus the robot is cuspidal.
Case II: Three sheets exist in the joint space: In this case, no bubble can co-exist as it will lead to a path parallel to one of the joint angles that will lead to at least five intersections (one from each sheet and at least two from each bubble). The number of aspects present in this case is 3. So if there exist a pose with at least four IKS, then at least one of the three aspects have multiple IKS. This by definition qualifies the robot to be cuspidal.
Case III: No sheets exist in the joint space: In this case n bubbles can exist resulting in n + 1 aspects. If an IKS in each bubble correspond to det($\mathbf{J}$) > 0, then in this case the $(n+1)^{th}$ aspect that is external to all bubbles is the only aspect with det($\mathbf{J}$) < 0. So if the number of IKS is greater than or equal to four, then at least two IKS will exist in the

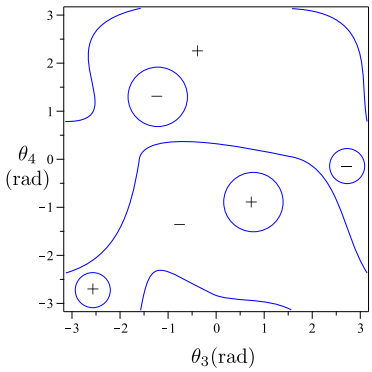

(a) Hypothetical distribution of six IKS such that the aspects external to bubbles are unique.

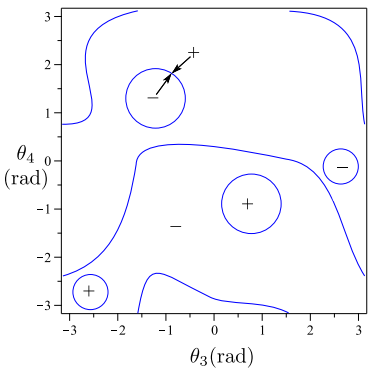

(b) The unique solution meets the IKS in bubble 1

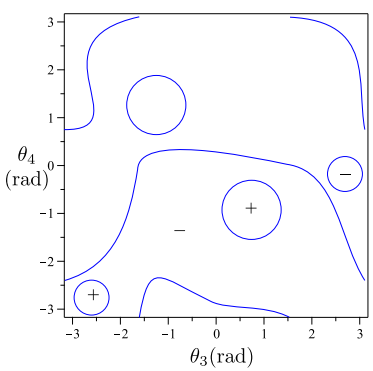

(c) Questionable situation as the solution in the bubble 2 has no IKS to meet at singularity.

$(n+1)^{th}$ aspect. This by definition qualifies the robot to be cuspidal.

Case IV: Two sheets exist in the joint space: In this case we have two aspects generated by the two sheets and n aspects generated by each bubble present in the joint space. In this case, if a pose has more than four IKS then the aspects that are external to the bubbles necessarily contain multiple IKS. This is attributed to the reason that if only one IKS existed in the aspect external to bubbles, then this IKS can meet a singularity boundary associated to one of the bubble and vanish leaving the other IKS belonging to the second bubble without a pair. This is not possible as each IKS is bounded by a singularity and can meet a singularity curve starting from any instance. An illustration of the problem is shown in the figure 3.13. If there are no bubbles then there are upto two aspects and thus a robot with more than 2 IKS will be cuspidal. This suggests that a robot with more than 4 IKS is cuspidal if there exists 2 sheets and n bubbles in the joint space.

□

3.2.3 Effect of constraints

The definition for cuspidality as well as the necessary and sufficient condition for cuspidality in a 3R serial robot is valid without the consideration of joint limits and collision constraints. Figure 3.14 shows an example of a 3R serial robot where we implement joint limits such that the cusp points in the workspace are inaccessible and yet there exists a nonsingular change of solutions. This qualifies the robot as cuspidal without encircling a cusp point. Even though such joint limits are virtual in the aforementioned example, it is helpful to note that the cuspidality analysis should extend beyond checking the nec-

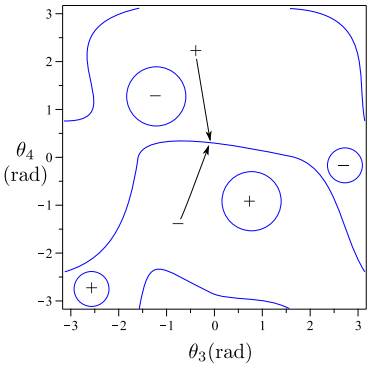

(d) The unique solution meets the IKS from other aspect at a sheet.

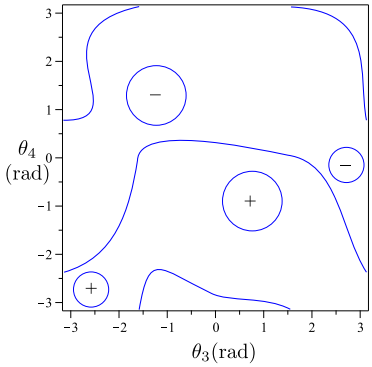

(e) Questionable situation as the solutions in all bubbles have no IKS to meet at singularity.

Figure 3.13 – An example 2D slice in $\theta_3\theta_4$ for the case with sheets and bubbles in the joint space.

essary and sufficient condition only. The certified algorithm proposed in [Cha+22] can incorporate the joint limits as long as the constraints are expressed algebraically. Another important constraint that affects the workspace and cuspidal behavior of a 6R robot is the internal link collisions. The internal collision between links limits the workspace of a robot to a great extent and this impacts the cuspidality analysis. The necessary and sufficient condition as well as the certified algorithm proposed fail to incorporate the collision constraint. The constraints are neither smooth nor algebraically expressible which makes them hard to incorporate in the certified algorithm.

3.2.4 Algorithm for deciding cuspidality

In the next section, we propose an algorithm that is capable of deciding cuspidality of a robot by incorporating both, joint limits as well as internal link collision, constraints. It utilises the known results as well as the determinant analysis of robots to accelerate the process.

Known results on cuspidality

Theorem 7. *For a wrist-partitioned 6R serial robot, i.e, three intersecting consecutive axes, at the beginning or at the end of the robot, the existence of a cusp in the workspace of the 3R serial robot formed by neglecting the wrist is a necessary and sufficient condition*

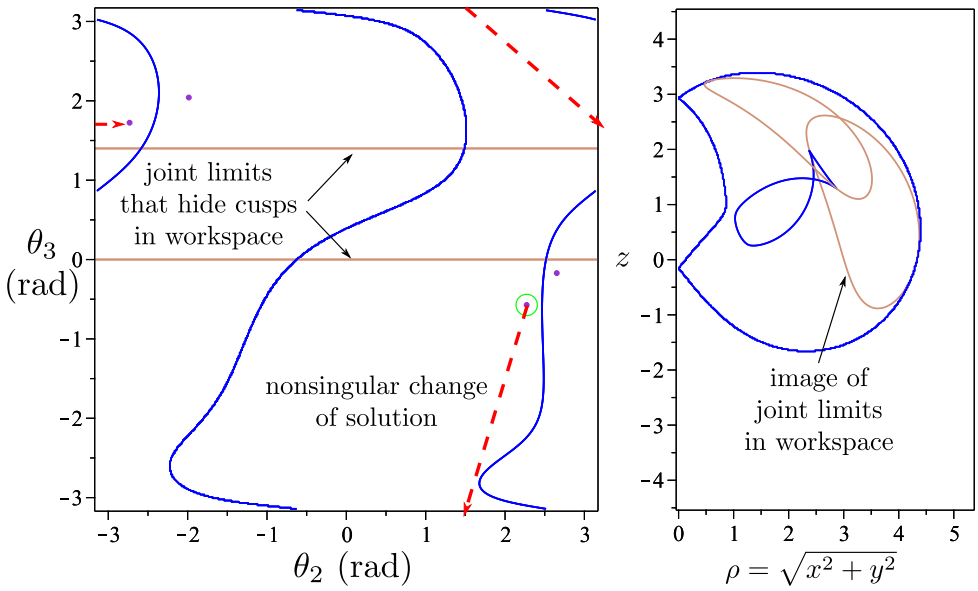

Figure 3.14 – Nonsingular change of solutions in cuspidal robot with joint limits hiding the cusp points. Robot parameters: $\mathbf{d} = [0, 1, 0], \mathbf{a} = [0.8, 1.7, 1.8], \alpha = [\frac{\pi}{6}, \frac{\pi}{3}, 0]$.

for the robot to be cuspidal.

Proof. The results for cuspidality from 3R serial robot can be extended to the 6R serial robots with wrist partition at the end. It is attributed to the reason that the position and orientation for such robots is decoupled. The wrist singularity in such serial robots is well known and the solutions for the orientation are always separated by wrist singularity. This makes the wrist a non-cuspidal robot and so the cuspidal nature of the complete 6R serial robot depends on the cuspidal nature of the 3R serial robot formed by the first three axes only. The necessary and sufficient condition derived for a generic 3R serial robot used the geometric interpretation of the IKM for the proof. It is shown in [Pie68] that this geometric interpretation holds true even for the 6R serial robots with wrist partition in the beginning. It can be readily shown that the analysis done in the $c_3 s_3$-plane in [Sal+22b] can be done in $c_4 s_4$-plane for the robots with wrist in the beginning where c_3, c_4 stands for $\cos\theta_3, \cos\theta_4$ and s_3, s_4 denote $\sin\theta_3, \sin\theta_4$. This suggests that all the theorems proved for a generic 3R serial robot and extended to 6R serial robots with wrist partition at the end can be extended to all 6R serial robots with wrist partition in the beginning as well. The presence of a cusp being a necessary and sufficient condition for a generic 3R serial robot has been already proved [Sal+22b]. The presented theorem is simply an extension of the same. □

Apart from these results, it is also known that UR5 robot is a non-cuspidal robot [CSEDS20] with eight solutions in eight aspects. As it was shown earlier that a generic 6R robot with more than four IKS is cuspidal, it is important to study nongeneric robots whose determinant factors into components. In the next section, we present the importance of analysing the determinant of the Jacobian matrix and present new conditions for a robot to have at least eight aspects.

Determinant analysis

As the number of aspects are governed by the singularities in the joint space, it is of high importance that we study the determinant of the Jacobian matrix of a generic 6R serial robot. A symbolic determinant for a 6R serial robot can be derived by using the preferential Jacobian as mentioned in [KD04]. The analysis of the factors of the determinant of the Jacobian played a fundamental role in orthogonal 3R serial robots. After assigning the D-H parameters in table 3.2, the determinant of a reduced example of wrist partitioned 6R robot with anthropomorphic 3R robot looks like:

$$\det(\mathbf{J}) = \cos\theta_3 \sin\theta_5 \left(f(\theta_2, \theta_3)\right)$$

.

Table 3.2 – The D-H parameters of reduced example of a 6R robot with wrist at the end

i	d_i (mm)	a_i (mm)	α_i (rad)	θ_i (rad)
1	d_1	a_1	$\pi/2$	θ_1
2	0	a_2	0	θ_2
3	0	0	$\pi/2$	θ_3
4	d_4	0	$\pi/2$	θ_4
5	0	0	$\pi/2$	θ_5
6	d_6	a_6	0	θ_6

As the determinant factors in three components it is readily seen that there exists at least eight aspects in the joint space of such robot as $\cos\theta_3$ and $\sin\theta_5$ intersects the other component which produces two aspects. The geometric analysis of IKM further shows that the IKS are separated by the singularities. The determinant of the UR5 architecture

can be obtained in similar fashion. Upon substituting $d_2 = d_3 = d_4 = a_5 = 0$, and $\alpha_1 = \alpha_5 = \frac{\pi}{2}, \alpha_2 = \alpha_3 = 0$, takes the form,

$$\begin{aligned}\det(\mathbf{J}) = &- \sin\theta_3 \sin\theta_5 (\sin\alpha_4 \sin\theta_4 \cos\theta_3 \cos\theta_2 d_5 + \\ &\sin\theta_3 \sin\alpha_4 \cos\theta_4 \cos\theta_2 d_5 + \sin\theta_2 \sin\alpha_4 \cos\theta_4 \cos\theta_3 d_5 - \\ &\sin\theta_2 \sin\theta_3 \sin\alpha_4 \sin\theta_4 d_5 + \cos\theta_4 \cos\theta_3 \cos\theta_2 a_4 - \\ &\sin\theta_3 \sin\theta_4 \cos\theta_2 a_4 - \sin\theta_2 \sin\theta_4 \cos\theta_3 a_4 - \\ &\sin\theta_2 \sin\theta_3 \cos\theta_4 a_4 + \cos\theta_3 \cos\theta_2 a_3 - \sin\theta_2 \sin\theta_3 a_3 + \\ &a_2 \cos\theta_2 + a_1) a_2 a_3 \sin\alpha_4\end{aligned}$$

It can be observed that the determinant is separated in three factors viz, $\sin\theta_3, \sin\theta_5$ and the rest of the component, $g(\theta_2, \theta_3, \theta_4)$. These factors divide jointspace in at least eight aspects which already suggests that the robot is nongeneric. Upon analysis of the IKM, it is verified that such a robot is noncuspidal. As it has been shown in the previous sections, if the determinant factors into at least three components, the number of aspects is at least eight and the geometric analysis of IKM may be able to conclude on cuspidality. This leads to the following question: can we identify 6R robots with simplified architectures such that the $\det(\mathbf{J})$ is factored? The $\det(\mathbf{J})$ is a function of 14 D-H parameters in total that defines the architecture of the robot. These 14 parameters are $d_{2..5}, a_{1..5}, \alpha_{1..5}$, and the classification space is huge. The identification was simplified by providing two values for each parameters. If the parameter is a length parameter, i.e d or a, then it can be either 0 or a symbolic value. For alpha, only $\frac{\pi}{2}$ and 0 values were considered. This analysis investigates the number of components of the $\det(\mathbf{J})$ obtained from the preferential Jacobian. The total number of robots investigated are 2^{14}, and 832 robots were found to be of simplified architecture. The D-H parameters of such robots are mentioned in Appendix A.5. It is to be emphasized that the thesis reports 832 types of robots that are noncuspidal. The symbolic values of the length parameters can take any non zero value and the robot preserves the factored form of $\det(\mathbf{J})$. This result is a doorway to designers for investigating new designs that are non-cuspidal and may have advantages in specific cases. The orthogonal robots have been shown to exhibit better dynamic properties compared with the anthropomorphic architectures [NBW12], and it will be interesting to explore different non-cuspidal designs with simplified IKM.

Generic case of 6R serial robot

Certified algorithm :
Recently, a certified algorithm was presented for deciding cuspidality for non redundant nR robots [Cha+22]. It implements various algorithms in computer algebra using methods on real algebraic sets and critical loci of polynomial maps. It uses tools from Real Algebraic Geometry, zero-dimensional parameterizations, to get the sample points in $\mathcal{W}$ such that we have at least a point in each connected region of $\mathcal{W}$. It then investigates the connectivity of the preimages of each of the sample points by implementing one-dimensional parameterizations, roadmap algorithms, which reduce the four dimensional jointspace, $\mathcal{J}$, to a one dimensional graph without the loss of information on connectivity. Though certified, this algorithm is presently hard to generalize to 6R robots and collision constraints have not been implemented yet. The certified algorithm is presented in Appendix A.4.

Non-certified approach :
As discussed beforehand, the certified algorithm presented in [Cha+22] is hard to implement and is currently not implemented for 6R robots. Furthermore, incorporating collision avoidance is only limited to algebraically expressible constraints. Thus, a different deciding algorithm, similar to [Mar+23], based on solving an optimal-path-planning (OPP) problem is proposed. In order to decide cuspidality, the OPP problem has to be solved for the whole workspace until a connection of at least two IKS is found. The workspace is discretized into a finite $n_{\mathcal{W}}$ points $\mathbf{x}_k \in \mathcal{W}$, $k \in \{1..n_{\mathcal{W}}\}$.

The connectivity problem consists of finding a nonsingular path between two different IKS $(\mathbf{q}_i, \mathbf{q}_j) \in \mathcal{I}_{\mathbf{x}}$. Therefore, a measure of distance to the singularity is required. In the literature various methods to measure the distance exist, such as the kinematic manipulability [Dot+95], condition number, smallest eigenvalue or determinant of the Jacobian to name a few. We use $\det(\mathbf{J})$, since it plays an important role in cuspidality analysis.

Optimal-Path-Planning problem: Given an initial IKS $\mathbf{q}_0 \in \mathcal{I}_{\mathbf{x}}$ to an arbitrary EE-pose $\mathbf{x}$. Find a non-singular path $\mathbf{q}(t)$ connecting $\mathbf{q}_0$ with a valid IKS $\mathbf{q}_1 \in \mathcal{R}_{\mathbf{q}_0,\mathbf{x}}$. The idea is to find a path with the largest distance to the singularity. Therefore, the smallest value of the determinant along the path

$$\inf_t \operatorname{sign}(\det \mathbf{J}(\mathbf{q}_0)) \det \mathbf{J}(\mathbf{q}(t)) \tag{3.6}$$

is maximized. The multiplication with the sign of the initial determinant enables the use of the function inf also for negative values i.e. $\det \mathbf{J}(\mathbf{q}_0) < 0$. A negative value of (3.6)

results in an invalid solution since condition (1.9) is not met. As smooth joint paths $\mathbf{q}(t)$ are desirable, an integrator chain represented by $\mathbf{z}' = \mathbf{f}(\mathbf{z}, \mathbf{u}, t)$, with states

$$\mathbf{z}^T = \left[\mathbf{q}^T,\, (\mathbf{q}')^T,\, (\mathbf{q}'')^T\right]$$

and input $\mathbf{u} = \mathbf{q}'''$ are used to receive a three times differentiable path. The OPP problem is then written as a non-linear optimization problem:

$$\begin{aligned} &\max_{\mathbf{z},\mathbf{u}} \left(\inf_t \operatorname{sign}(\det \mathbf{J}(\mathbf{q}_0)) \det \mathbf{J}(\mathbf{q}(t))\right), \\ &\text{s.t. } \mathbf{z}' = \mathbf{f}(\mathbf{z}, \mathbf{u}, t),\ \mathbf{q}(0) = \mathbf{q}_0,\ \mathbf{q}(1) = \mathbf{q}_1, \\ &\quad \underline{\mathbf{z}} \le \mathbf{z}(t) \le \overline{\mathbf{z}}, \quad \underline{\mathbf{u}} \le \mathbf{u}(t) \le \overline{\mathbf{u}}, \\ &\quad \text{for } t \in [0, 1]. \end{aligned} \tag{3.7}$$

The geometric lower and upper bounds are denoted by $\underline{()}$ and $\overline{()}$. These bounds can be used to incorporate joint limits and influence the geometric derivatives. The OPP problem is solved with a multiple shooting approach [BP84] implemented in MATLAB using CasADi [And+19] and Ipopt [WB06] as solver. It is worth noting that the value of the objective function can be negative at the optimal point.

The Algorithm: The OPP problem is solved for all discrete EE-pose $\mathbf{x}_k$, $k \in \{1..n_{\mathcal{W}}\}$, until a connection between two distinct IKS is found. To this end, the optimization problem (3.7) is solved for a given initial and terminal IKS $\mathbf{q}_0 \in \mathbf{I}_\mathbf{x}$, $\mathbf{q}_1 \in \mathcal{R}_{\mathbf{q}_0,\mathbf{x}}$ of a chosen EE-pose e.g. $\mathbf{x}_0$. If a feasible solution is found (i.e. positive value of the objective) the connectivity problem is solved and the robot is cuspidal. If the optimization is unsuccessful, a different terminal IKS $\mathbf{q}_1 \in \mathcal{R}_{\mathbf{q}_0,\mathbf{x}}$ of the same EE-pose $\mathbf{x}_0$ is chosen and the problem is solved again. If no connection could be found for e.g. $\mathbf{x}_0$, then a different EE-pose $\mathbf{x}_k$,$k \neq 0$, is picked and the procedure is repeated. In the case that all grid points $\mathbf{x}_k$ are checked unsuccessfully no assertion about cuspidality can be made. It is worth noting, that a grid refinement of the workspace (or a different grid) can lead to a proof of cuspidality, since only a finite number of points in the workspace are considered in the procedure. Algorithm 1 details the implementation.

Algorithm 1 Proposed cuspidality deciding algorithm.

Require: Discretized workspace EE-pose $\mathbf{x}_k$, $k \in \{1..n_{\mathcal{W}}\}$
  for all $k \in \{1..n_{\mathcal{W}}\}$ **do**
    - compute IKS and pick initial $\mathbf{q}_0 \in \mathcal{I}_{\mathbf{x}_k}$
    i = 1
    while $\mathbf{q}_i \in \mathcal{R}_{\mathbf{q}_0,\mathbf{x}_k}$ and connectivity_found=False **do**
      - solve OPP problem (3.7)
      if successful **then**
        - connectivity_found = True
      end if
      i = i + 1
    end while
  end for
  if connectivity_found **then**
    - robot is cuspidal
  else
    - no assertion about cuspidality possible
  end if

Numerical subtleties: Algorithm 1 takes care of numerical difficulties encountered by the fact that different revolute joint angles are equal modulo 2π. Since these joints can rotate freely, clockwise as well as counter clockwise rotations must be taken into account. The joint coordinates are defined by a n-torus $\mathbb{T}^n$. Therefore, adding $\pm 2k\pi$ with $k \in \mathbb{N}_0$ does not change the IKS i.e. $\mathbf{x} = \mathbf{f}(\mathbf{q}) = \mathbf{f}(\mathbf{q} \pm 2k\pi)$. For practical applications only solutions within the interval $\mathbf{q} \in [-2\pi, 2\pi]$ have to be considered. Consider planning singularity-free trajectories for a 3R robot connecting the IKS in one aspect, as shown in figure 3.15a. A non-singular trajectory between $\mathbf{q}_1$ and $\mathbf{q}_2$ is readily found. On the other hand, planning a trajectory between $\mathbf{q}_3$ and $\mathbf{q}_4$ without crossing a singularity is not possible, since the OPP problem (3.7) does not consider the periodicity of the joint coordinates. Therefore, adding $\pm 2\pi$ element-wise to the solution $\mathbf{q}_4$ is extended to the interval $[-2\pi, 2\pi]$ as shown in figure 3.15b. Thus, the IKS $\mathbf{q}_3$ and $\mathbf{q}_4$ can be connected by a non-singular trajectory, with a counter clockwise rotation of the third joint.

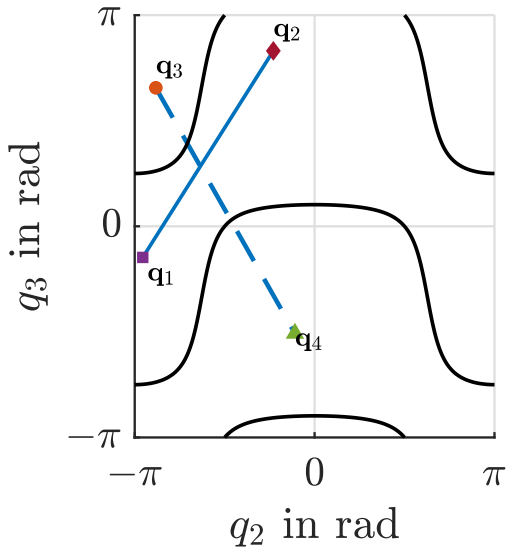

(a) singular connection between IKS $\mathbf{q}_3$ and $\mathbf{q}_4$

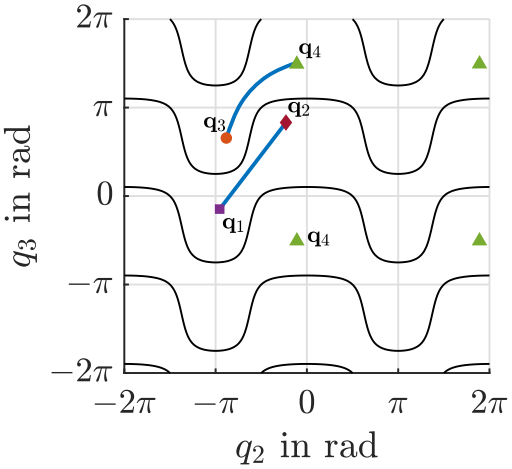

(b) singularity-free connection between IKS $\mathbf{q}_3$ and $\mathbf{q}_4$

Figure 3.15 – Example for considering clockwise and counter clockwise rotations in the IKS.

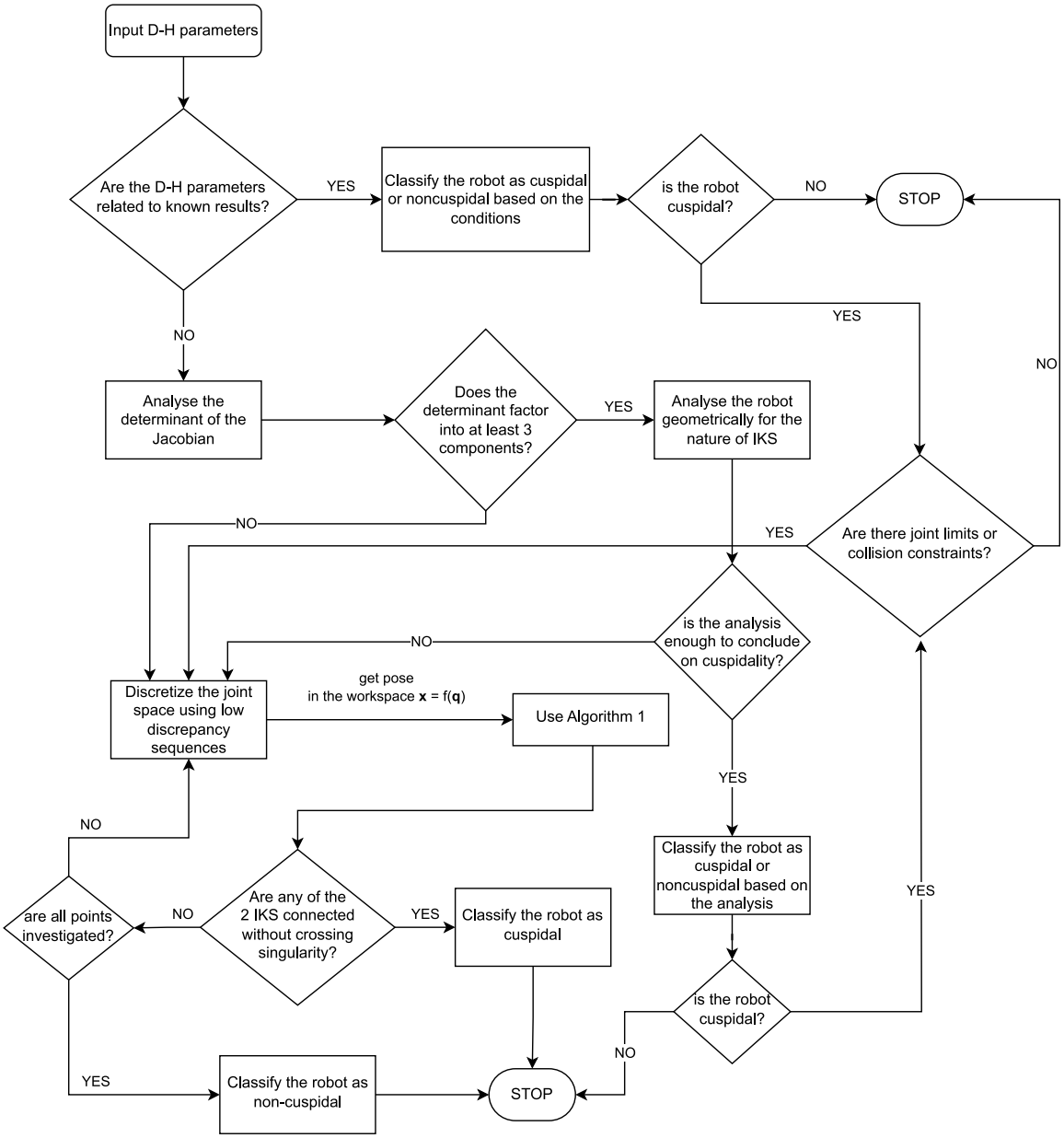

Figure 3.16 – Complete framework for deciding cuspidality for any 6R robot

The self-intersection of singularity manifold accrues more aspects thus leading to a higher possibility of a noncuspidal robot. Such robots are of non-generic type and it has been noted [PL92] that given a class of manipulators, almost all direct kinematic maps, $f : \mathcal{J} \rightarrow \mathcal{W}$, are generic and the nongeneric maps form a thin set of the class. Upon observation of the parameter space for 3R robots, it is not hard to expect that the neighborhood of a nongeneric design almost always leads to a cuspidal robot. This

makes the practical framework very useful as the nongeneric cases are identified with the determinant analysis, and the generic cases are analysed by using the algorithm 1. As the algorithm is fast and conclusive if the robot is cuspidal, the framework presented in figure 3.16 can be automated to decide cuspidality of almost all 6R robots. We have analyzed 10000 robots with varying parameters for cuspidality, and the framework presented in figure 3.16 was able to decide the cuspidal nature of each robot.

Application of the deciding framework We present the results obtained by implementing the deciding framework for cuspidality. The algorithm 1 terminates with few iterations in case of a cuspidal robot. The framework was able to decide upon cuspidal nature of every 6R robot that was given as an input. We have a 14 dimensional parameter space for cuspidality analysis which is not only huge but also impossible to visualize. We choose a specific 3 dimensional parameter space that includes the architecture of almost all types of known commercial robots, to highlight the importance of cuspidality analysis. Figure 3.17 shows the the parameter space with d_5, α_3 and α_4 as the basis. All other D-H parameters for the robot are similar to that of FANUC CRX-10ia/L robot. The cube was discretized into 3240 points and the robot corresponding to each point was analyzed for cuspidality. It was noted that every point inside the cube, i.e. not lying on the faces, correspond to D-H parameters of a cuspidal robot. The robots belonging to the face $ABFE$ are degenerate robots as the det($\mathbf{J}$) is always zero. The face $ADHE$ correspond to anthropomorphic architectures with wrist at end as $d_5 = 0$. It is a known result that the robots on corresponding to the points on the face $ADHE$ except the one at A are noncuspidal. The edge GH corresponds to the robots having anthropomorphic architecture with offset in the wrist. Every robot belonging to edge GH except the point H is a cuspidal robot, suggesting that the addition of an offset to the anthropomorphic architecture almost always leads to a cuspidal robot. The robots corresponding to face $ABCD$ have a 3R subchain as $\alpha_3 = 0$. The edge CD corresponds to UR5 like architecture for a non zero a_3 as $\alpha_4 = \frac{\pi}{2}$. For $a_3 \neq 0$, every robot belonging to the face $ABCD$ except those lying on the edge AB are noncuspidal as the det($\mathbf{J}$) have three factors and the robot has a simplified IKM that can be analyzed geometrically. The face $FGHE$ upon excluding edges GH, HE and EF corresponds to robots with an offset and a non-orthogonal arrangement of the last three joints. One such example of commercial robot is the Jaco robot Gen2 (non-spherical wrist) though in this robot the offset in wrist is generated by non zero a_5 instead of d_5 length. These robots are found to be cuspidal by using the framework proposed in figure 3.16. It is concluded from these results that a robot with generic geometry is almost always a

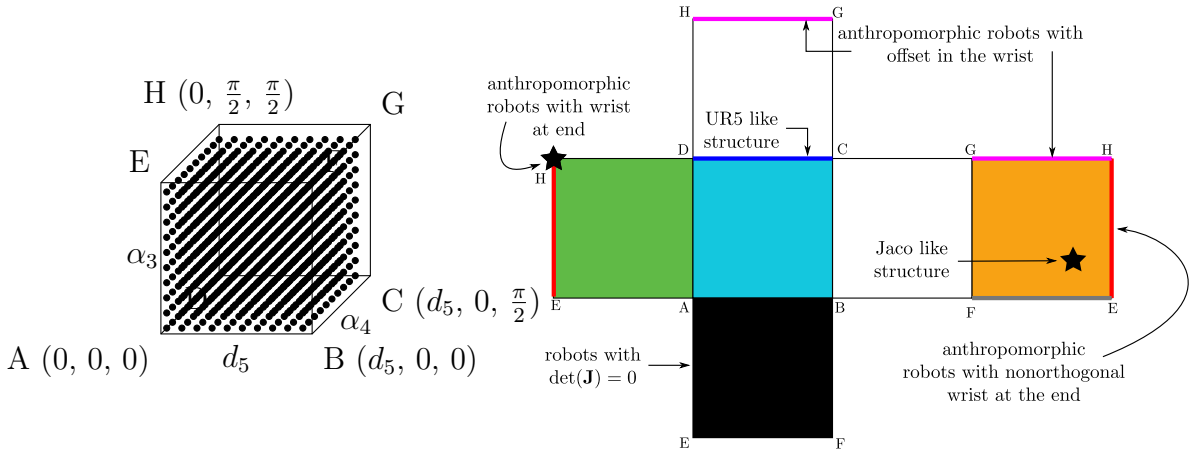

Figure 3.17 – Classification of a 6R robot parameterized in specially chosen three D-H parameters. The rest of the DH parameters match that of FANUC CRX-10ia/L robot.

Table 3.3 – Classification of some of the existing robots according to cuspidal nature.

Robot	Max IKS	Nature
ABB IRB 140, KUKA KR5	8	non cuspidal
UR5, UR10	8	non cuspidal
FANUC CRX-10ia/L	16	cuspidal
Kinova Link6	16	cuspidal
JACO Gen2 (6R version)	12 [1]	cuspidal

cuspidal robot. Extending the framework, some of the existing commercial robots [1] are presented in table 3.3 with the details on maximum IKS present in the workspace, and their cuspidal nature.

3.3 Conclusions

In this chapter, the cuspidality analysis for 6R serial robots is detailed. Considering the majority of designs that exist in industries today, simplified architectures are analysed in the beginning. It is shown that the results for 3R robots can be extended to 6R robots with wrist at the beginning or at the end of the architecture. This is attributed to the reason that the position and orienattion of the end-effector is decoupled in such architectures. The case for wrist in the middle is investigated further highlighting that the rsults of 3R robots are not applicable in this case. Using the geometric interpretation of the kinematic

1. The maximum number of IKS for Jaco Gen2 robot is reported upon searching the workspace with 100,000 points generated by a low discrepancy sequence.

model, a sufficient condition is provided for such architectures to result in noncuspidal robots. A discussion on number of aspects in a generic 6R robot is presented, presenting a counterexample to an existing conjecture. It is further proposed that a generic 6R robot with more than 4 IKS is a cuspidal robot. This conjecture is fundamental to the design of 6R robots to avoid designing cuspidal robots. Given the increasing use of the UR5 architecture, the case of 6R robots with 3R planar subchain is investigated. It is shown that the presence of 3R planar subchain simplifies the det($\mathbf{J}$), thus simplifying the cuspidality analysis. Considering the importance of deciding cuspidality for designing 6R robots, a certified algorithm is presented. Later, a practical framework is presented to decide upon the cuspidal nature of 6R robots. This framework utilizes all the known results, exploits the form of det($\mathbf{J}$), and uses numerical approaches to decide upon cuspidality of a generic 6R robot. The chapter concludes by presenting results of implementing this framework on thousands of generic architectures to further highlight that a generic design most likely leads to a cuspidal robot.

Chapter 4

Path planning in cuspidal robots

In this chapter, we discuss the issues and solutions to the path planning of cuspidal robots. Path planning considering cuspidality is not well-studied as the knowledge about cuspidal robots is limited in industries. Section 4.1 discusses the different issues that can arise in cuspidal robots such as the feasibility as well as repeatability of the path depending on the given path and choice of initial IKS. Later, section 4.2 outlines the different cases that can occur in the path planning problem of cuspidal robots. A path planning framework for 6R cuspidal robots is proposed to address the problems arising in existing commercial/industrial 6R robots. The presented framework allows to utilize the cuspidal robots to their fullest extent while avoiding the dangers of unexpected failure.

4.1 Issues in cuspidal robots

This section focuses on certain issues arising in cuspidal robots due to their geometric properties. The section starts with the definition of configurations, and explains the difference between IKS and configurations. The issues in classifying robots with more than 8 IKS into conventional 8 classes has been highlighted by using a commercially sold robot software. Later, we present a commercial robot widely used in various applications, and the trajectory planning issues occurring with this robot. The feasibility of a path depends on the initial choice of IKS, and some feasible paths are not repeatable. The aim of this section is to motivate the claim that cuspidal robots are not suitable for collaborative tasks and can lead to unexpected behavior if neglected.

4.1.1 Unique configuration identification

A configuration is defined in section 1.2.3 as an IKS that can be uniquely identified geometrically or analytically. This definition was specifically introduced to discuss the problems of unique identification of configurations in a cuspidal robot. A cuspidal robot

by definition has at least one aspect with multiple IKS, and thus at least 2 IKS cannot be uniquely identified at a given time. The issue is exacerbated as the number of aspects decreases as more number of IKS lose the ability to be uniquely identified. As discussed in section 3.2, the offset in the wrist of a 6R serial robot almost always leads to a cuspidal robot. The industrial robots that have an anthropomorphic architecture with an offset in the wrist are almost always cuspidal in nature. We investigate a specific case of such a robot, the CRX-10ia/L robot from FANUC industries (refer to Figure 4.1).

Figure 4.1 – Industrial cobot from FANUC, CRX-10ia/L

The D-H parameters of this robot are: The inverse kinematics of this robot is solved

Table 4.1 – The D-H parameters of the CRX-10ia/L robot

i	d_i (mm)	a_i (mm)	α_i (rad)	θ_i (rad)
1	245	0	$\pi/2$	θ_1
2	260	710	0	θ_2
3	-260	0	$\pi/2$	θ_3
4	540	0	$\pi/2$	θ_4
5	150	0	$\pi/2$	θ_5
6	160	0	0	θ_6

by using HuPf algorithm presented in [HPS07], which provides an algebraic sixteen degree

polynomial for any given generic D-H parameters. It is concluded that this robot has up to sixteen IKS, and an example of these solutions is presented in Figure 4.2.

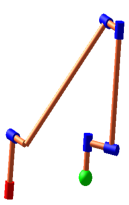

(a) First IKS: θ(rad) = [2.7, 0.87, 2.28, 2.57, 3.14, 0.13]

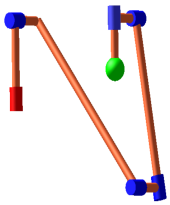

(b) Second IKS: θ(rad) = [-2.88, -0.85, 1.03, 0.03, -0.18, -2.85]

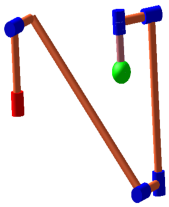

(c) Third IKS: θ(rad) = [-2.94, -0.86, 0.87, -0.54, 0.01, 2.8]

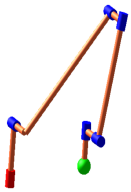

(d) Fourth IKS: θ(rad) = [-0.51, 2.3, 1.02, -0.02, 2.95, -0.49]

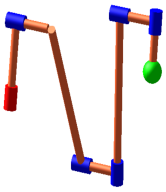

(e) Fifth IKS: θ(rad) = [0.26, -2.3, 2.11, -3.11, -0.18, -2.85]

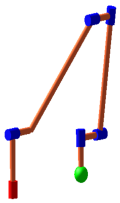

(f) Sixth IKS: θ(rad) = [-2.88, 0.85, 2.12, 0.03, -2.96, -2.91]

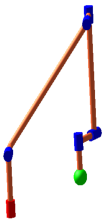

(g) Seventh IKS: θ(rad) = [-2.95, 0.86, 2.28, 0.56, -3.13, 2.78]

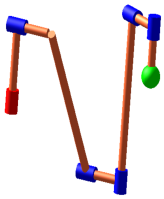

(h) Eight IKS: θ(rad) = [0.2, -2.28, 2.28, 2.6, 0.01, 2.8]

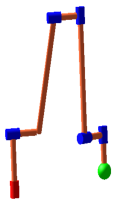

(i) Ninth IKS: θ(rad) = [-0.44, 2.28, 0.86, -0.57, 3.14, 0.13]

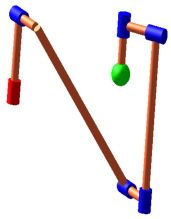

(j) Tenth IKS: θ(rad) = [-0.45, -2.28, 2.27, 0.53, -0.0, 0.08]

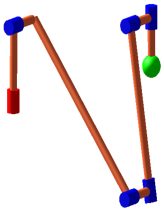

(k) Eleventh IKS: θ(rad) = [2.64, -0.85, 1.03, 3.12, 0.17, -0.52]

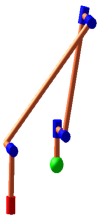

(l) Twelfth IKS: θ(rad) = [2.64, 0.85, 2.12, 3.13, 2.95, -0.49]

In this software, the choice of configurations are provided for the user to choose from. These are binary options between Flip or UnFlip, Up or Down, and Top or Bottom, The user can choose one configuration for each three arrangements. An example configuration

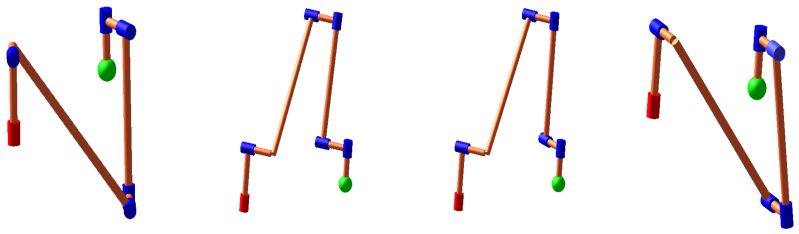

(m) Thirteenth IKS: θ(rad) = [2.69, -0.86, 0.87, -2.61, 0.0, 0.08]

(n) Fourteenth IKS: θ(rad) = [0.26, 2.3, 1.02, -3.11, -2.96, -2.91]

(o) Fifteenth IKS: θ(rad) = [0.2, 2.28, 0.86, -2.58, -3.13, 2.78]

(p) Sixteenth IKS: θ(rad) = [-0.51, -2.3, 2.11, -0.02, 0.17, -0.52]

Figure 4.2 – Sixteen solutions for the CRX-10ia/L robot.

could be N, U, T which can be interpreted as configuration UnFlip-Up-Top, and an example of an IKS in such configuration is provided in Figure 4.3.

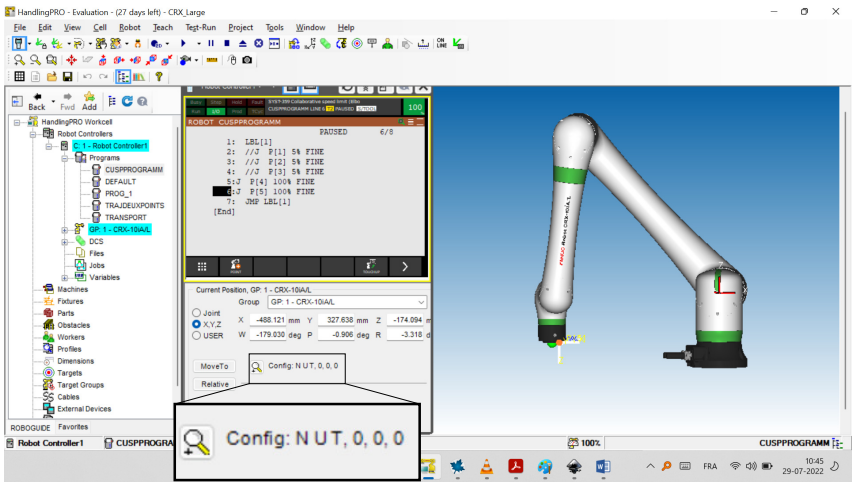

Figure 4.3 – An example IKS for CRX-10ia/L in UnFlip, Up, Top configuration as classified by FANUC

There exists two major problems with such a classification:

1. A maximum eight out of available sixteen solutions are provided by the software
2. sixteen solutions are attempted to be classified into eight categories

The first problem with the IKM implemented in ROBOGUIDE is that it does not provide the complete set of solutions. The user can only choose from up to eight IKS for a given pose of the end-effector. In the example illustrated in Figure 4.2, all the sixteen IKS

respect the joint limits of the robot as well as the collision constraints, but only eight of them are accessible by choosing the three binary choices (2^3). This limits the robot to a great extent and thus fails to motivate the choice of IKS provided to the user. The second problem naturally occurs from trying to fit sixteen solutions in eight unique categories. Moreover, the classification provided by the software is different from the conventional Flip-UnFlip, Right-Left, Up-Down classification. This makes it even harder to interpret the classification and example of such a confusing annotation is illustrated in Figure 4.4. The given configuration is classified as Flip, Down, Bottom configuration, and clearly the classification is counter-intuitive leading to problems for the user to choose the configurations from available limited choices. When the sixteen solutions obtained from the algebraic derivation were input, the configurations defined by the software turned out to be erratic. Among the sixteen solutions the 'configurations' do not repeat uniformly, i.e, the configurations FUT, NDT, FDB, and NUB are unique, while the rest of the configurations have three IKS. All the IKS of an instance with sixteen solutions along with their configuration are presented in Figure 4.5. The solutions can be matched with those in Figure 4.2 for reference, and the underlined captions are the IKS obtained from the ROBOGUIDE software while the IKS without an underline are the solutions missed in the software.

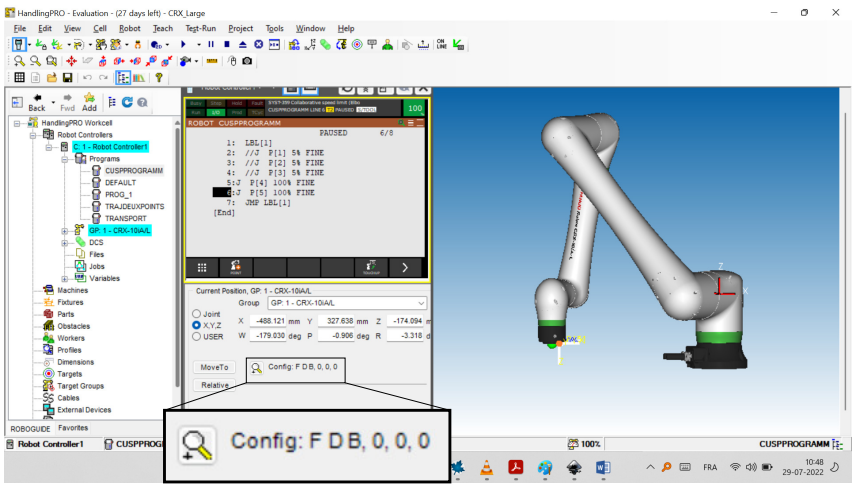

Figure 4.4 – An example IKS for CRX-10ia/L in Flip, Down, Bottom configuration as classified by FANUC

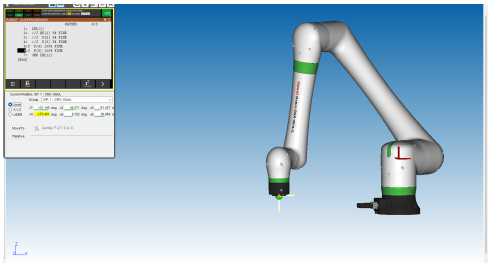

(a) First IKS, configuration: F, U, T

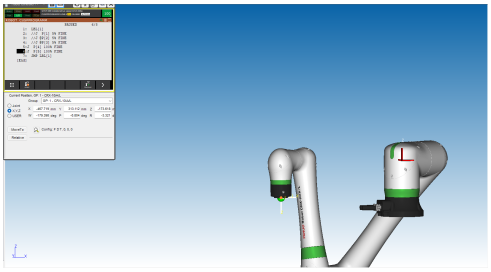

(b) Second IKS, configuration: F, D, T

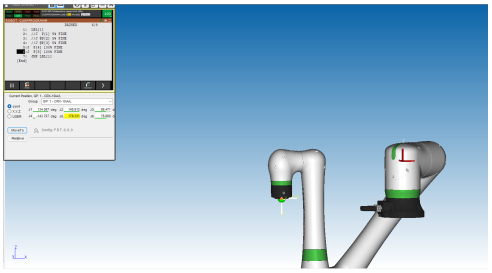

(c) Third IKS, configuration: F, D, T

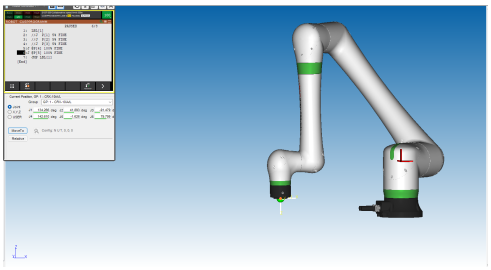

(d) Fourth IKS, configuration: N, U, T

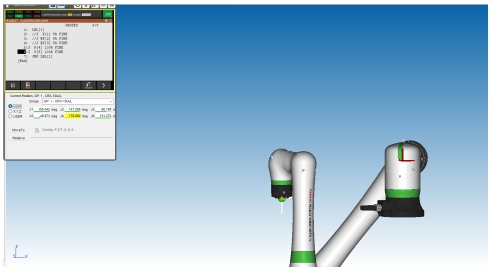

(e) Fifth IKS, configuration: F, D, T

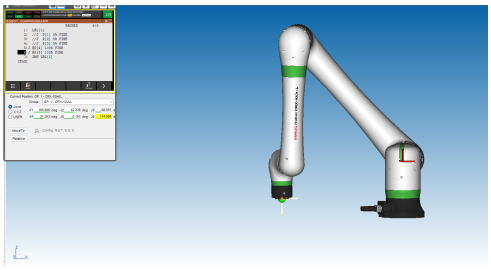

(f) Sixth IKS, configuration: N, U, T

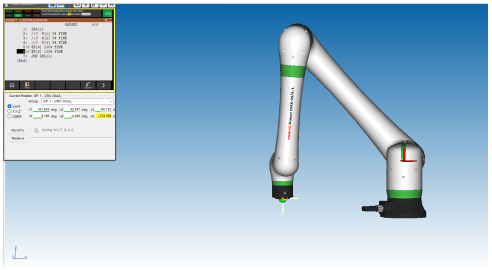

(g) Seventh IKS, configuration: N, U, T

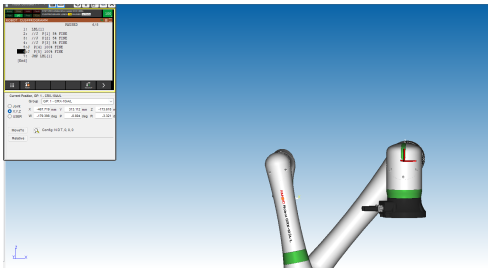

(h) Eight IKS, configuration: N, D, T

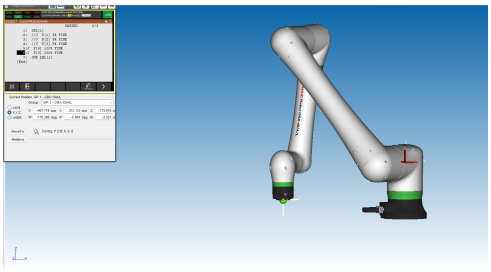

(i) Ninth IKS, configuration: F, D, B

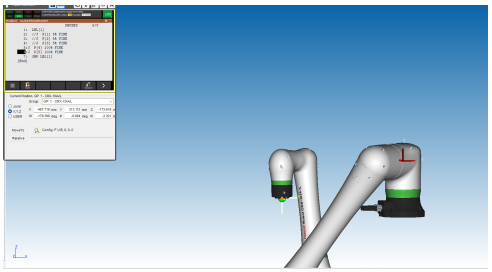

(j) Tenth IKS, configuration: F, U, B

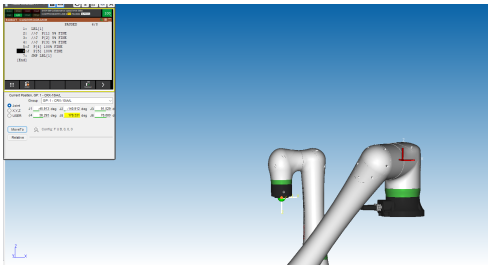

(k) Eleventh IKS, configuration: F, U, B

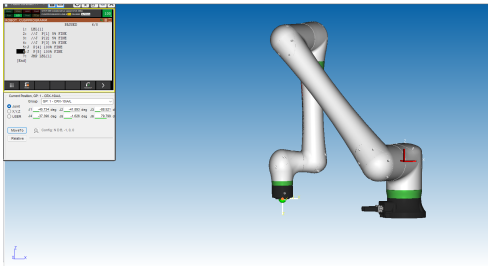

(l) Twelfth IKS, configuration: N, D, B

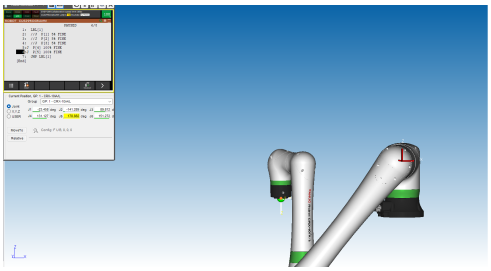

(m) Thirteenth IKS, configuration: F, U, B

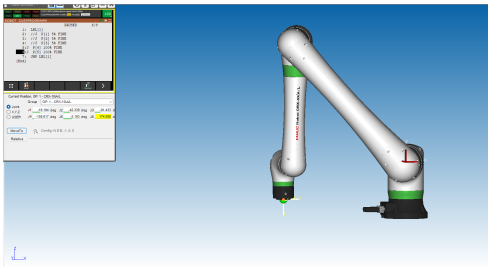

(n) Fourteenth IKS, configuration: N, D, B

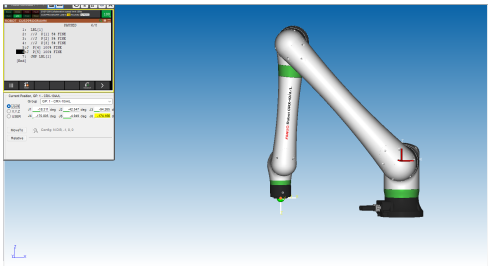

(o) Fifteenth IKS, configuration: N, D, B

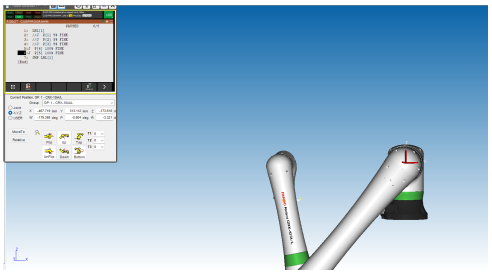

(p) Sixteenth IKS, configuration: N, U, B

Figure 4.5 – Sixteen solutions for the CRX-10ia/L robot with their designated configuration in the ROBOGUIDE software.

The configurations associated with multiple IKS lead to another problem which is specific to the cuspidal property of a robot. To elaborate this issue, the IKS and their

corresponding det(**J**) value is given in table 4.2.

IKS	det(**J**)	configuration	IKS	det(**J**)	configuration
First	positive	F, U, T	Ninth	positive	F, D, B
Second	negative	F, D, T	Tenth	negative	F, U, B
Third	positive	F, D, T	Eleventh	positive	F, U, B
Fourth	negative	N, U, T	Twelfth	negative	N, D, B
Fifth	negative	F, D, T	Thirteenth	negative	F, U, B
Sixth	positive	N, U, T	Fourteenth	positive	N, D, B
Seventh	negative	N, U, T	Fifteenth	negative	N, D, B
Eight	positive	N, D, T	Sixteenth	positive	N, U, B

Table 4.2 – The CRX solutions from Figure 4.5 with their corresponding det(**J**) sign and configurations as assigned by ROBOGUIDE.

From table 4.2, it can be noted that if the two IKS annotated by the same configuration belong to a single aspect, then a nonsingular change of IKS is possible and the program will not even detect this change of IKS. This shortcoming has major consequences on the overall performance as well as safety of the robot. The change of IKS is investigated to prove that indeed the sixteen solutions in Figure 4.5 are present in only two aspects, and thus every IKS with positive det(**J**) can be connected in a nonsingular fashion to an IKS with similar sign of the determinant. As discussed in section 1.2, Figure 4.6 shows the nonsingular paths between IKS in an aspect with positive det(**J**). The given plots are enough to conclude that all the eight IKS whose determinant value is positive can be interconnected, and thus lie in the same aspect. Similar analysis is done for the IKS with negative det(**J**), and plots are illustrated in 4.7. From Figure 4.6 and Figure 4.7, it is concluded that the sixteen solutions presented in Figure 4.2 are separated into two aspects only.

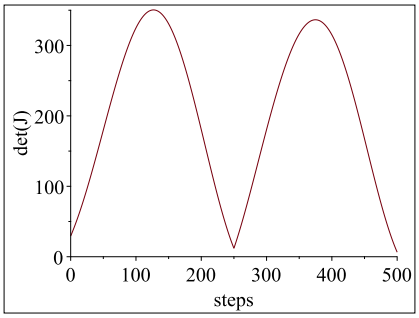

(a) IKS 1 → IKS 6 (Minimum value = 6.43)

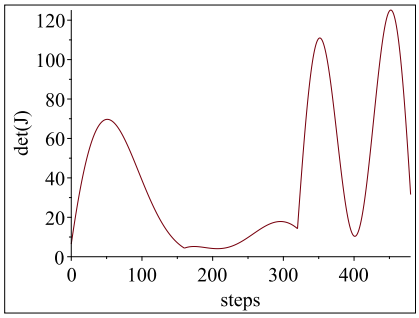

(b) IKS 6 to IKS 8 (Minimum value = 4.08)

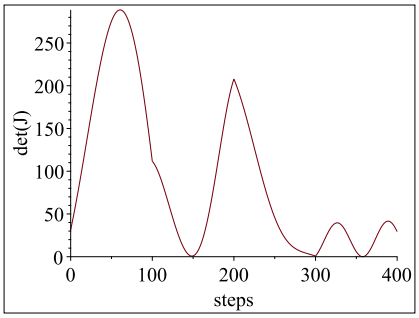

(c) IKS 8 → IKS 9 (Minimum value = 0.006)

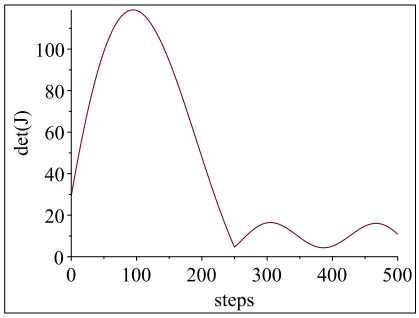

(d) IKS 9 → IKS 11 (Minimum value = 4.3)

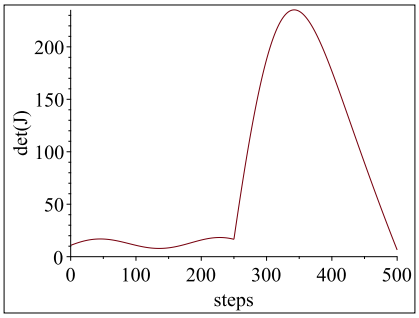

(e) IKS 11 → IKS 14 (Minimum value = 6.43)

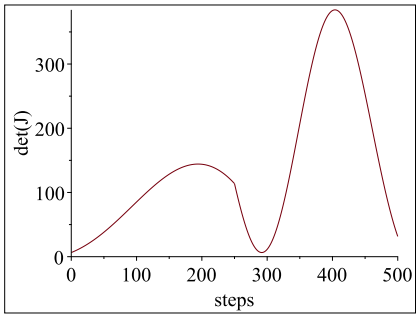

(f) IKS 14 → IKS 16 (Minimum value = 6.46)

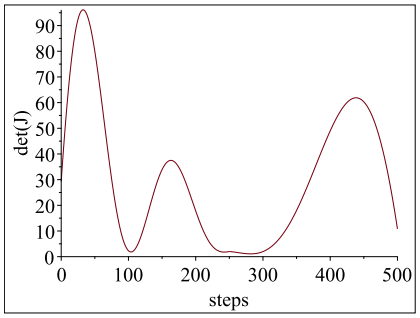

(g) IKS 1 → IKS 3 (Minimum value = 1.09)

Figure 4.6 – The det(**J**) plot to verify nonsingular change of solutions between two IKS of CRX-10ia/L in the aspect with positive det(**J**)

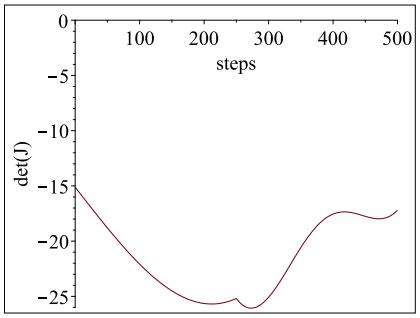

(a) IKS 2 → IKS 5 (Maximum value = -17.19)

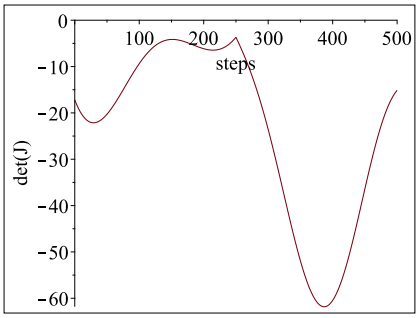

(b) IKS 5 → IKS 10 (Maximum value = -3.67)

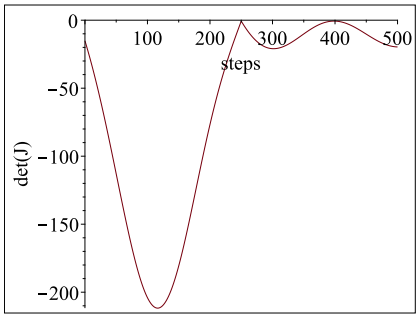

(c) IKS 10 → IKS 12 (Maximum value = -0.668)

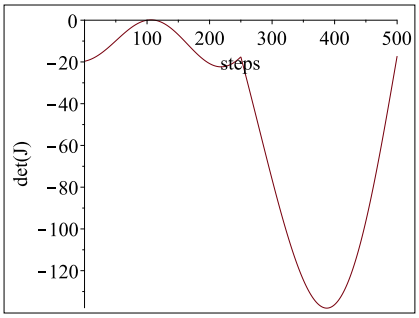

(d) IKS 12 → IKS 13(Maximum value = -17.19)

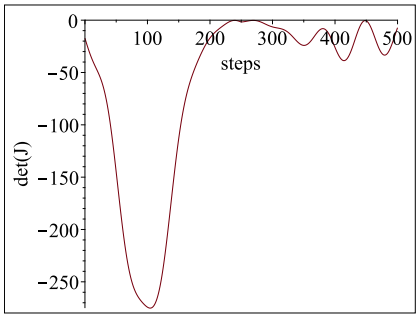

(e) IKS 13 → IKS 15 (Maximum value = -0.216)

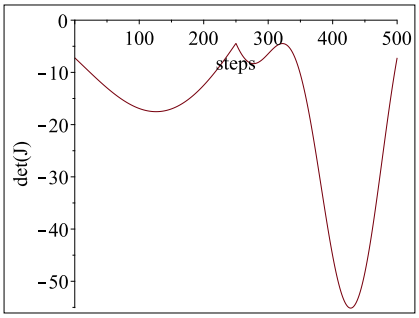

(f) IKS 15 → IKS 7 (Maximum value = -4.43)

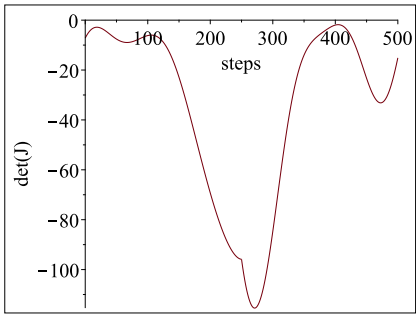

(g) IKS 7 → IKS 10 (Maximum value = -1.81)

Figure 4.7 – The det(**J**) plot to verify nonsingular change of solutions between two IKS of CRX-10ia/L in the aspect with negative det(**J**)

The issue with this is that if the trajectory starts with the fourth solution (refer to Figure 4.2 and table 4.2), there exists a nonsingular path to reach the seventh solution. Both of the IKS are annotated as N, U, T configuration. The consequence of such inaccurate and ambiguous classification is that neither the collision constraints can be guaranteed nor the repeatability of the path is assured. Such errors cause confusion for the user, and further are not safe for operations especially in a collaborative environment. Two solutions are proposed to mitigate the issue discussed in this section:

1. remove the classification of configurations
2. record the pose as well as the joint values to avoid the nonsingular change of solutions going undetected

The first solution is applicable to all cuspidal robots. Not only is it hard to classify IKS for robots whose det($\mathbf{J}$) do not factor into distinct components, but also is impossible for cuspidal robots. This section provides enough motivation for avoiding configuration classification for cuspidal robots. The second solution is an alternative to conventional classification of IKS by configurations. Currently, the program records the end-effector pose and the configuration in which the robot is operating. By remembering the joint values, we circumnavigate the troubles of classification, and the collision constraints can be guaranteed independent of the trajectory information. Though, recording the joint values will not avoid the robot from changing reduced aspects (crossing critical values in the workspace), the robot can at least have an information of its current configuration so that new algorithms can be developed to check collision with environment in real time. The next section discusses the feasibility of a given trajectory depending on the initial choice of IKS for cuspidal robots.

4.1.2 Issues in trajectory planning in cuspidal robots

As shown in previous section, cuspidal robots ask for extra care and caution in trajectory planning, as identifying an *aspect* related to one unique inverse kinematic solution is not possible. The issues related to path following in cuspidal robots are not only related to the algorithms used for trajectory planning, but also due to the inherent property arising from the geometric design of the manipulator. As designers move away from the conventionally implemented wrist-partitioned anthropomorphic architecture, there is a high chance that such robots have completely different kinematic properties. The cuspidality property seems to have been slipped from the consideration of the current designers

around the world [Ver21]. Recently, several industrial 6R robots with a non-spherical wrist have appeared. To the best of our knowledge, the only 6R robots with a non-spherical wrist that have been analyzed for the cuspidal property, are the UR-series robots from Universal Robots. Computer algebraic tools were used to show that these robots have eight aspects with no more than one IKS per aspect [CSEDS20], leading to a conclusion that such robots are non-cuspidal. This is because UR robots have three parallel joint axes, a geometric simplification that was identified by Pieper as a solvability criterion [Pie68]. In the absence of 3 parallel joint axes, 6R robots with a non-spherical wrist are very likely to be cuspidal. In this section, cuspidality is illustrated with the Jaco robot (gen 2, non-spherical wrist) from Kinova robotics, which is used in various applications. The Jaco robot was mainly designed for rehabilitation [Kin] and thus is employed near persons with disability and interacts with them. Multiple IKS that belong to the same aspect are presented, and the implication of cuspidality on path planning is presented in this subsection to highlight the importance of considering cuspidality while designing a robot as well as while implementing such robots in real life. Problems in choosing the initial solution of the path in cuspidal robots, and its consequence, is illustrated with an example path in the workspace of the Jaco robot. The dangers of neglecting the cuspidality are detailed and the rationale behind limiting their use in collaborative environments is motivated too.

Inverse kinematics of Jaco robot

Table 4.3 shows the DH parameter table for the Jaco robot. The parameter d_6 does not affect the inverse kinematic solution, and for the purpose of analysing specifically Jaco robot, $d_6 = 160$ mm. The Jaco robot has an offset in the wrist, and thus a direct decoupled analysis cannot be implemented. Inverse kinematics for such robots with an offset in the

Table 4.3 – The DH parameters of the Jaco robot

i	d_i (mm)	a_i (mm)	α_i (deg)	θ_i (rad)
1	275.5	0	90	θ_1
2	0	410	0	θ_2
3	13.3	207.3	-90	θ_3
4	103.8	0	55	θ_4
5	0	103.8	-55	θ_5
6	160	0	0	θ_6

wrist can be obtained by previously established algorithms for generic 6R robot [RR93; HPS07] or with methods applicable specifically to offset in the wrist [Tri+15; GL14]. In this paper, the results are presented by using the methodology detailed in [GL14] as it is specific to the Jaco design and is easy to implement. Using this method, a 16-degree-polynomial in $\tan\frac{\theta_1}{2}$ is obtained by eliminating the other joint variables. This polynomial with rational parameters is solved with the *Isolate* function [Rou99] in *RootFinding* library available in Maple 2020. Then, straightforward backpropagation is used to obtain the rest of the joint variables.

Number of IKS in the Jaco robot

It is a well-known result that a wrist-partitioned 6R robot has at most eight solutions. This is attributed to the decoupling between the positions and orientation of the end-effector and thus can be solved independently. The first 3R chain forms a regional manipulator and its inverse kinematics can be solved with a four degree inverse kinematics polynomial or two quadratics in cascade. The wrist provides two solutions for each orientation and thus, yields up to eight (4×2) solutions for a wrist-partitioned 6R robot. This does not hold true for robots with an offset in the wrist such as the Jaco robot. A case of end-effector pose with twelve IKS was exhibited in [GL14]. While, in the absence of joint limits and collisions, a pose in a nonsingular configuration of a wrist-partitioned 6R robot has either eight IKS or four IKS, it is shown that the Jaco robot can have two, four, six, eight, ten, or twelve IKS. It can be concluded from this finding that the workspace of the Jaco robot is divided into multiple regions of varying numbers of IKS and thus the trajectory planning for such a robot is a non-trivial problem. This is because a desired path can cross internal boundaries associated with singularities in the workspace and switch between multiple connected regions in the workspace with varying numbers of IKS. Figure 4.8 shows two different 2D slices in the workspace of the Jaco robot with a fixed orientation and z-coordinate. The blue, yellow, dark orchid, green, magenta, and turquoise colors represent the end-effector pose with two, four, six, eight, ten, and twelve solutions, respectively. The slice in fig. 4.8a has regions with two, four, six, and eight solutions. It is worth noting that two voids appear in this slice which is absent in Puma-type robots. The slice in fig. 4.8b has four, six, eight, ten, and twelve solution regions.

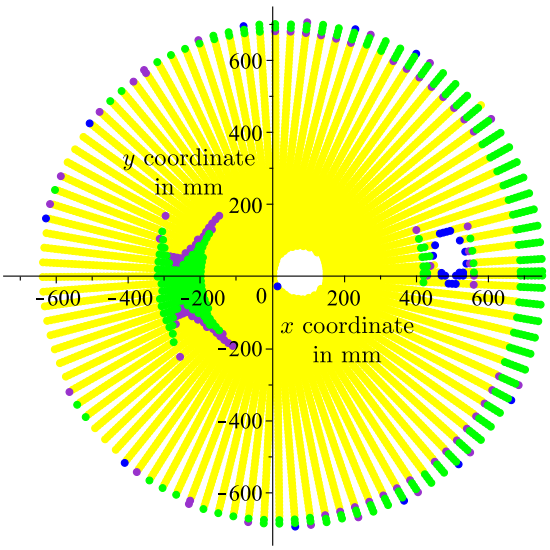

(a) Slice 1. The holes in the workspace correspond to areas with no IKS.

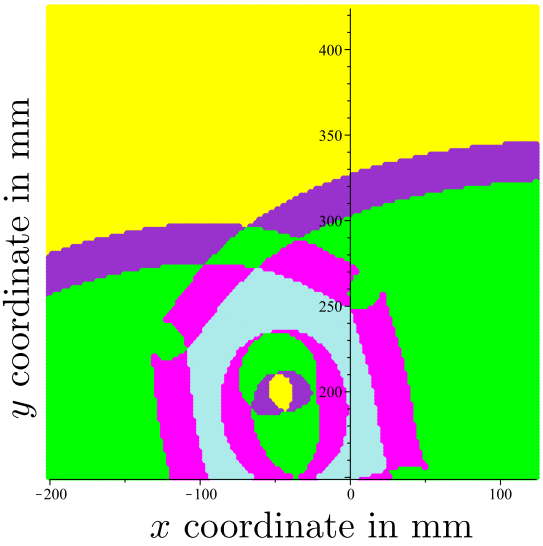

(b) Zoomed section of Slice 2

Figure 4.8 – Regions with different number of IKS in 2D slice (xy-plane) in the workspace of Jaco. The fixed orientation has a quaternion ($\mathbf{h}$) and z-coordinate for the slices:
Slice 1: $\mathbf{h} = 0.2565 + 0.033\hat{\mathbf{i}} + 0.812\hat{\mathbf{j}} + 0.582\hat{\mathbf{k}}$, z = 560.56 mm
Slice 2: $\mathbf{h} = 0.984 + 0.004\hat{\mathbf{i}} + 0.103\hat{\mathbf{j}} + 0.147\hat{\mathbf{k}}$, z = 257.94 mm

Investigating connectivity

The solutions for a particular pose of the end-effector is given in table 4.4 along with the sign of $\det(\mathbf{J})$ at the corresponding joint configuration. To search for a nonsingular change of solutions, a linear interpolation between two IKS with the same determinant value was evaluated. If the determinant value changed sign along the linear interpolation, then the path was divided into three parts and the two non-extreme points of the path were recalculated by using the Nelder-Mead approach [NM65], to find the possible nonsingular change of solutions. This is a working algorithm to determine cuspidality of any robot and is faster to implement when compared to a more robust certified algorithm in [Cha+22]. The advantage of using Nelder-Mead approach to determine the connectivity of the given IKS is that the method is versatile and can adapt to constraints easily. This implies that the working algorithm can be extended to find a nonsingular change of solutions with joint limits and collision constraints of the robot too. Figure 4.9 & 4.10 show the progress of $\det(\mathbf{J})$ along the joint paths obtained from the algorithm. It is apparent that there are six solutions in aspect $\det(\mathbf{J}) > 0$ and six solutions in aspect $\det(\mathbf{J}) < 0$.

IKS ($sign(\det(\mathbf{J}))$)	θ_1 (rad)	θ_2 (rad)	θ_3 (rad)	θ_4 (rad)	θ_5 (rad)	θ_6 (rad)
I (+)	3.0675	1.0545	1.3090	2.4283	-1.2305	-2.3002
II (+)	2.4335	0.0936	1.5741	1.4311	2.3452	0.5391
III (+)	-0.8579	3.0408	1.5721	-1.5912	2.1625	0.5390
IV (+)	2.9132	0.2824	1.9297	-2.1648	-2.9685	-2.7165
V (+)	-0.2812	2.0346	1.8631	-0.5833	-1.0917	-2.4130
VI (+)	-0.2456	2.8156	1.3090	0.4882	-2.8301	-2.3003
VII (-)	-3.1201	0.7082	1.4904	2.62	-1.9637	-1.8817
VIII (-)	2.4730	0.0943	2.0281	-1.4916	-2.4244	2.4362
IX (-)	-0.1583	2.7025	1.4699	-0.0656	-2.5402	-1.9078
X (-)	-0.7501	1.9399	2.0268	-1.4270	0.6212	2.6291
XI (-)	-0.8046	3.0466	1.1135	1.5103	-2.2697	2.4394
XII (-)	2.5338	1.2022	1.1149	1.5839	0.6030	2.6322

Table 4.4 – The 12 IKS of a pose of the Jaco robot for te pose defined below. Orientation: $\mathbf{h} = 0.549 + 0.497\hat{\mathbf{i}} + 0.423\hat{\mathbf{j}} + 0.522\hat{\mathbf{k}}$, position$(x, y, z)$(mm) = (140.49, 47.13, 324.876).

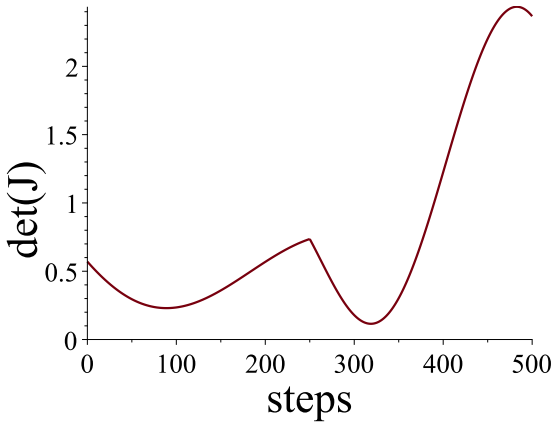

(a) IKS I → II

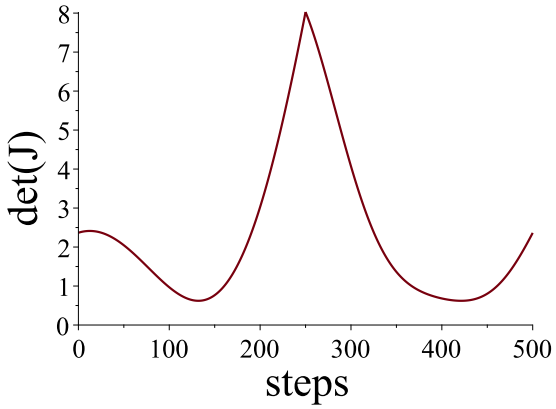

(b) IKS II → III

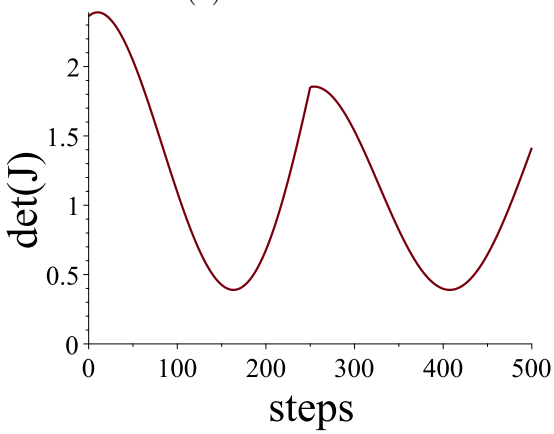

(c) III → IV

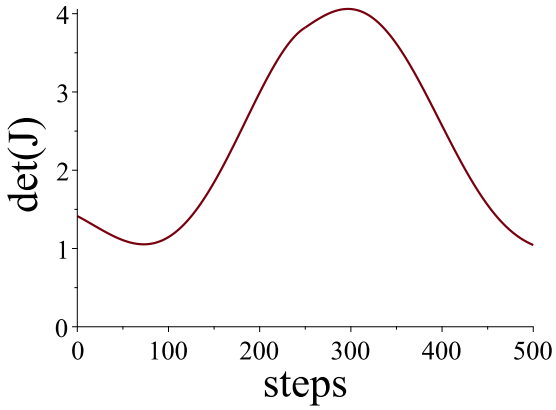

(d) IKS IV → V

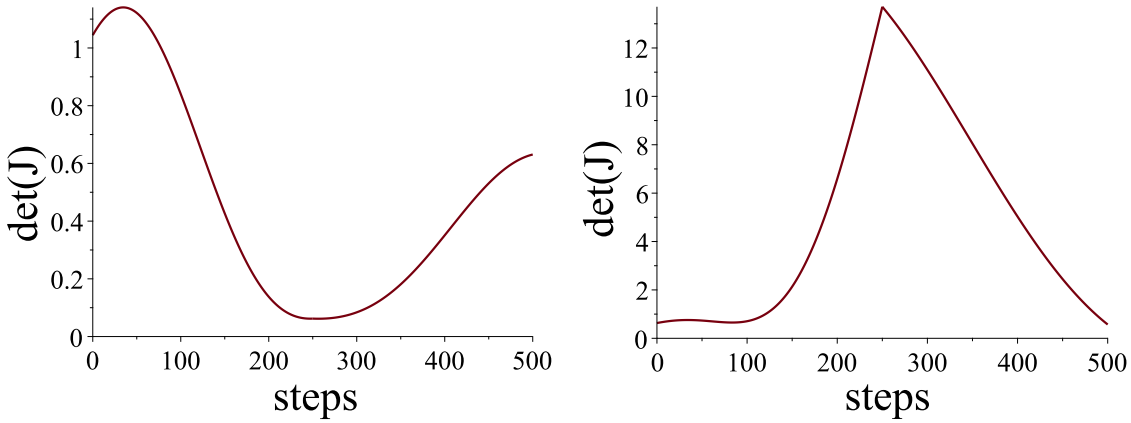

(e) IKS V → VI (f) IKS VI → I

Figure 4.9 – Progress of the det(**J**) for six nonsingular change of solutions in aspect with positive determinant value.

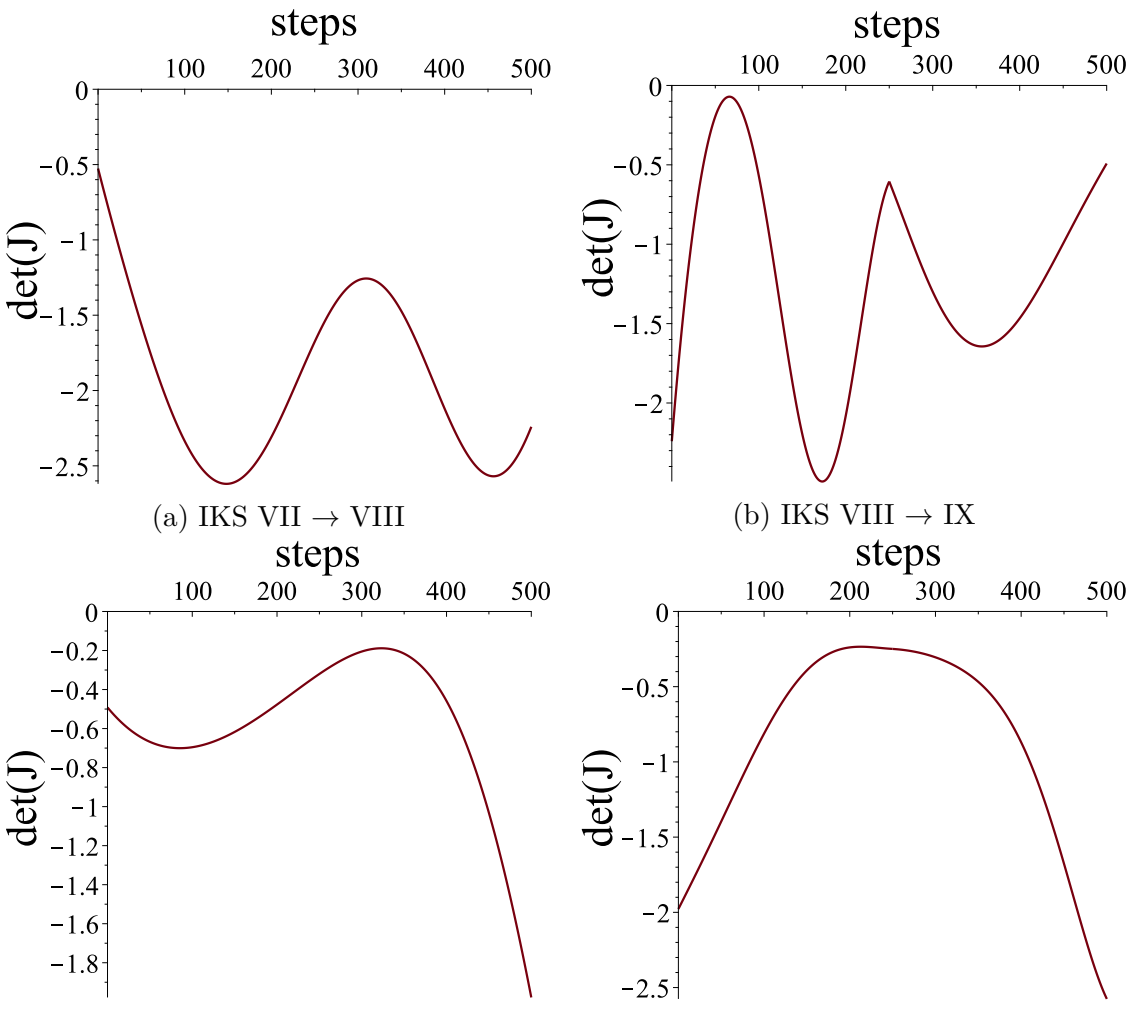

(a) IKS VII → VIII (b) IKS VIII → IX

(c) IKS IX → X (d) IKS X → XI

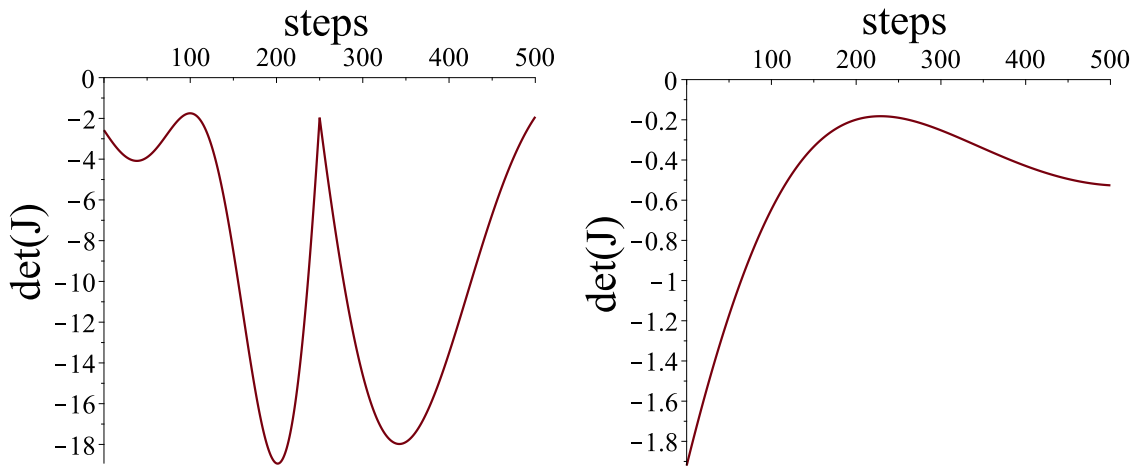

(e) IKS XI → XII

(f) IKS XII → VII

Figure 4.10 – Progress of det(**J**) for six nonsingular change of solutions in aspect with negative determinant value.

Nonsingular change of solutions

The nonsingular change of solutions in 3R robots is well understood and can be anticipated [Wen04]. The nonsingular change of solutions in 3R robots takes place strictly after crossing the locus of critical values (a workspace boundary associated to a singularity) and thus the trajectory passes through regions with different numbers of IKS [Sal+22b]. The existence of reduced aspects in 6R robots is not proven, and thus it is unclear whether a nonsingular change of solutions implies a path that passes through different connected regions in the workspace. The visualization of a nonsingular change of solutions is presented in this subsection to emphasize the impact of the choice of initial IKS on the robot's interaction with the environment. Figure 4.11 shows the end-effector path corresponding to the nonsingular change of solution from VII to VIII (refer to Figure 4.10a). The end-effector path is a closed path. It is straightforward to conclude from Figure 4.11 and Figure 4.10a that the kinematic properties along the desired path are a direct result of the choice of initial IKS.

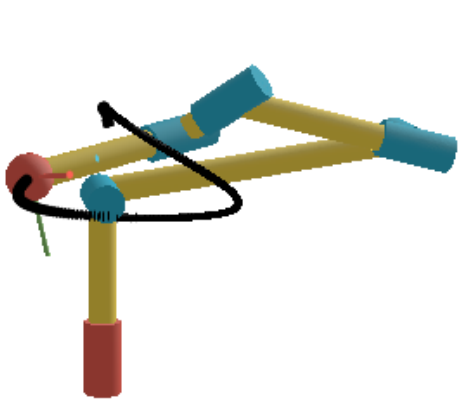

(c) Intermediate path

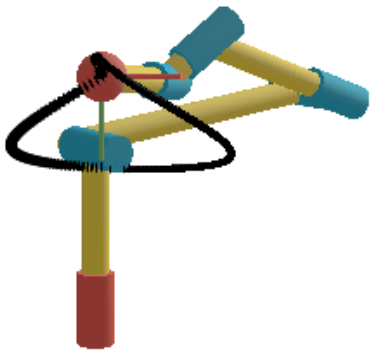

(d) Final solution

Figure 4.11 – Nonsingular change of solutions: IKS VII → VIII.

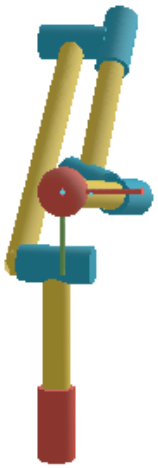

(a) Initial solution

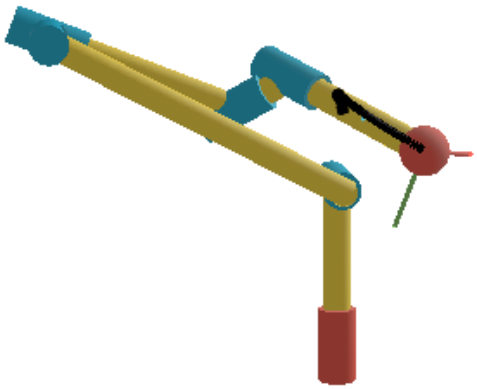

(b) Intermediate path

Feasibility depending on choice of initial IKS

As shown in fig. 4.8, it is known that there are multiple connected regions with varying numbers of IKS. It is well established that when a workspace boundary associated with

a singularity is crossed, at least two solutions disappear (resp. appear) if the robot move toward a region with less IKS (resp. with more IKS) [KS85]. In classical path planning algorithms, a change of solution only occurs when $\det(\mathbf{J})$ changes sign. Thus, an end-effector path can be declared infeasible if $\det(\mathbf{J})$ changes sign. In the case of cuspidal robots, a jump to another IKS in the same aspect can take place without detection, and this jump results into going off the planned end-effector path. Such a behavior has been recorded in the MICO robot earlier but lacks a detailed explanation of the error [Ver21]. It is surprising to note that the issue in path planning of the Jaco Gen 2 robot has not been widely reported. The authors' best guess is that either most of the planning done using this robot is done in the joint space or the solutions are just declared infeasible if a critical value is encountered. The issues in planning were discussed with the company that manufactures the robot, but unfortunately did not culminate into a meaningful conversation.

In order to better explain the issue of choosing a suitable initial IKS, the case of a 3R robot is presented in detail . The workspace and singularities of 3R robots have been extensively presented in [Wen04; Sal+22b], and are revisited briefly here. Figure 1.12 illustrates a closed path path that starts from a pose with four IKS and passes through two connected regions in the workspace. The level set representation [HOC08] of a cross section of the workspace in $(\rho, z, \cos\theta_2)$ corresponding to the two aspects are shown in fig. 4.12b & 4.13b respectively. The dotted line represents the pose of the end-effector and the intersection of this line with the level set representation corresponds to one IKS. $\mathbf{q}_i$ is the IKS in the joint space of the robot and the corresponding point on the level set representation is given as $\mathbf{p}_i$. Depending upon the initial IKS, $\mathbf{q}_i$, the path is either feasible or infeasible. It can be deduced from fig. 1.11, fig. 4.12 and fig. 4.13 that if the trajectory starts from initial IKS $\mathbf{q}_2$ or $\mathbf{q}_3$, the closed path path is infeasible. The path is feasible only if the initial IKS is either $\mathbf{q}_1$ or $\mathbf{q}_4$.

In 3R robots, the transition between regions with 0, 2 and 4 IKS allows one to visualize the level set representation making the analysis easier than for 6R robots. For the Jaco robot, there exists multiple accessibility regions with 6 possible numbers of IKS. This leads to many complicated possibilities and the planned path may include sudden jumps in the joint values. This sudden jump cannot be avoided with a generic planner that is unaware of the cuspidal property of the robot. An example trajectory is shown in Figure 4.14 that crosses regions with 4, 6 and 8 IKS. The trajectory is in the Slice 1 (refer to Figure 4.8a)

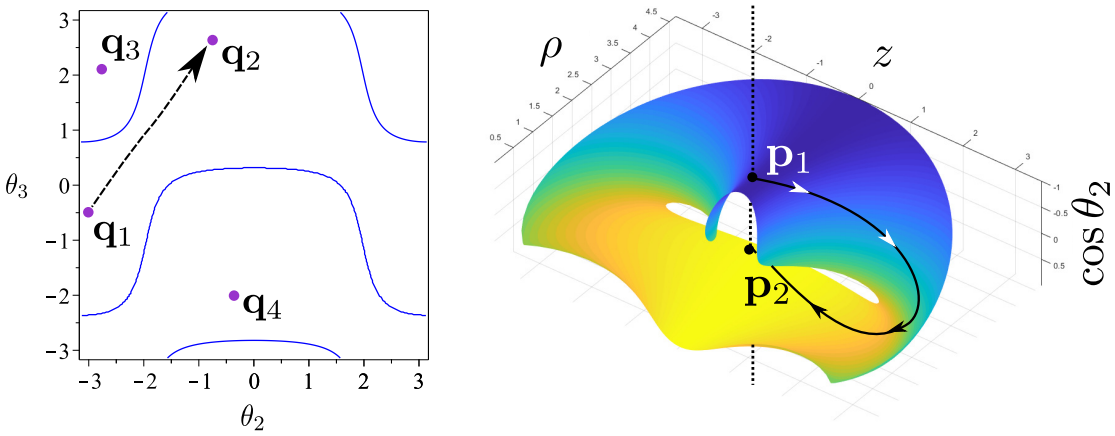

(a) Closed path starting from IKS $\mathbf{q}_1$

(b) Closed path as seen in the level set representation of one aspect

Figure 4.12 – An example of nonsingular change of solutions

and starts from point $\mathbf{a}(-280, 0)$ and passes through point $\mathbf{b}(-280, 200)$, $\mathbf{c}(-120, 200)$ and $\mathbf{d}(-120, 0)$ and returns to $\mathbf{a}$. Figures 4.15 and 4.16 show the time histories of the joint angles along the path. The dotted lines divide the path into four parts and represent the instances when the path crosses a region with a given number of IKS in the workspace. They are labeled as $(i \rightarrow j)$ denoting the change from a region with i solutions to the region with j solutions. The first and the fourth regions correspond to the path in a eight-solution region while the second and third regions correspond to the path in six- and four-solution regions, respectively. The blue color paths in each plot are the solutions in an aspect with $\det(\mathbf{J}) > 0$ while the red paths correspond to $\det(\mathbf{J}) < 0$. In Figure 4.15, $T_i, i = 1..8$ is a trajectory corresponding to each initial IKS. It can be seen that if the robot starts the path from IKS corresponding to T_3, T_4, T_7 or T_8, it soon meets a singularity. If the cuspidality of the robot is not taken into account, a sudden jump will take place to a solution available in the same aspect at the next discrete instance. For example, if the path is initiated from T_4 (resp. from T_3), after the first dotted line, $(8 \rightarrow 6)$, there will be a sudden jump to T_1, T_5 or T_8 (resp. to T_2, T_6 or T_7). In case of trajectory T_7 and T_8, there will be a sudden jump after $(6 \rightarrow 4)$ to T_2 or T_6 and T_1 or T_5, respectively. Some of these jumps are shown by green color lines in Figure 4.15. It is apparent that T_3, T_4, T_7 and T_8 are infeasible.

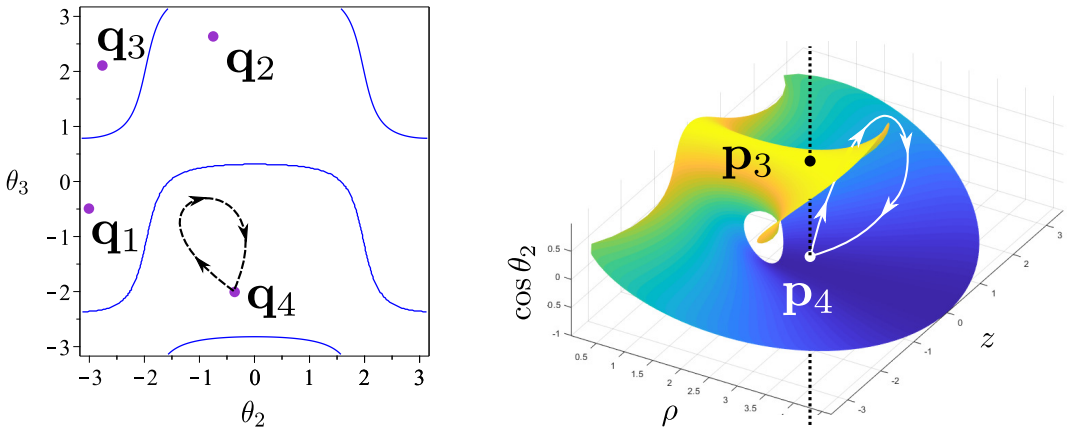

(a) Closed path starting from IKS $\mathbf{q}_4$

(b) Closed path as seen in the level set representation of another aspect

Figure 4.13 – Same path as shown in Figure 4.12, but without changing solutions

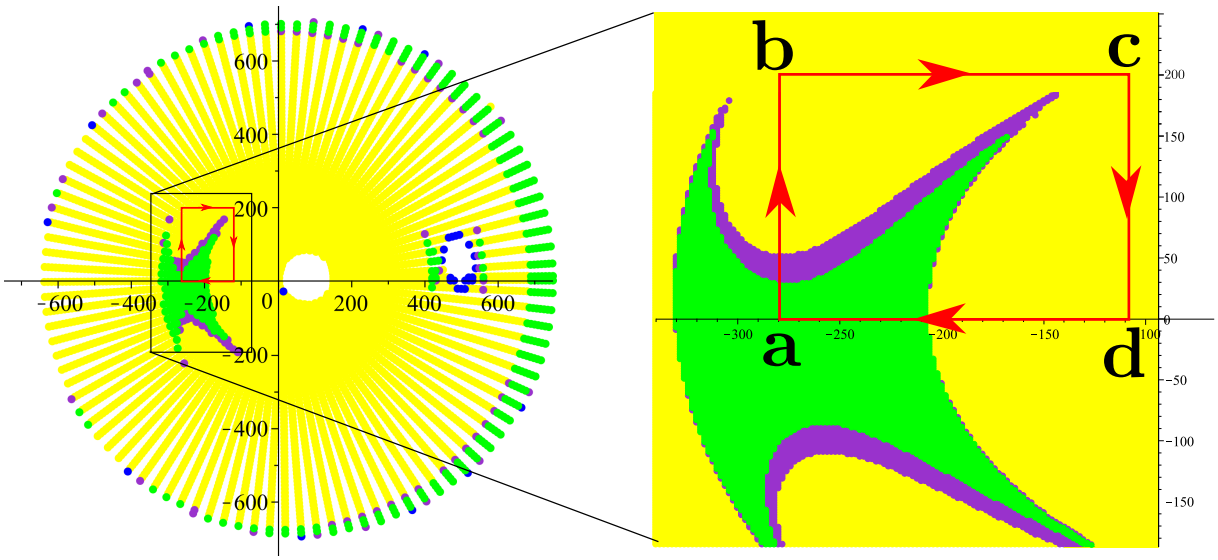

Figure 4.14 – A closed trajectory crossing multiple connected regions in the workspace of Jaco robot

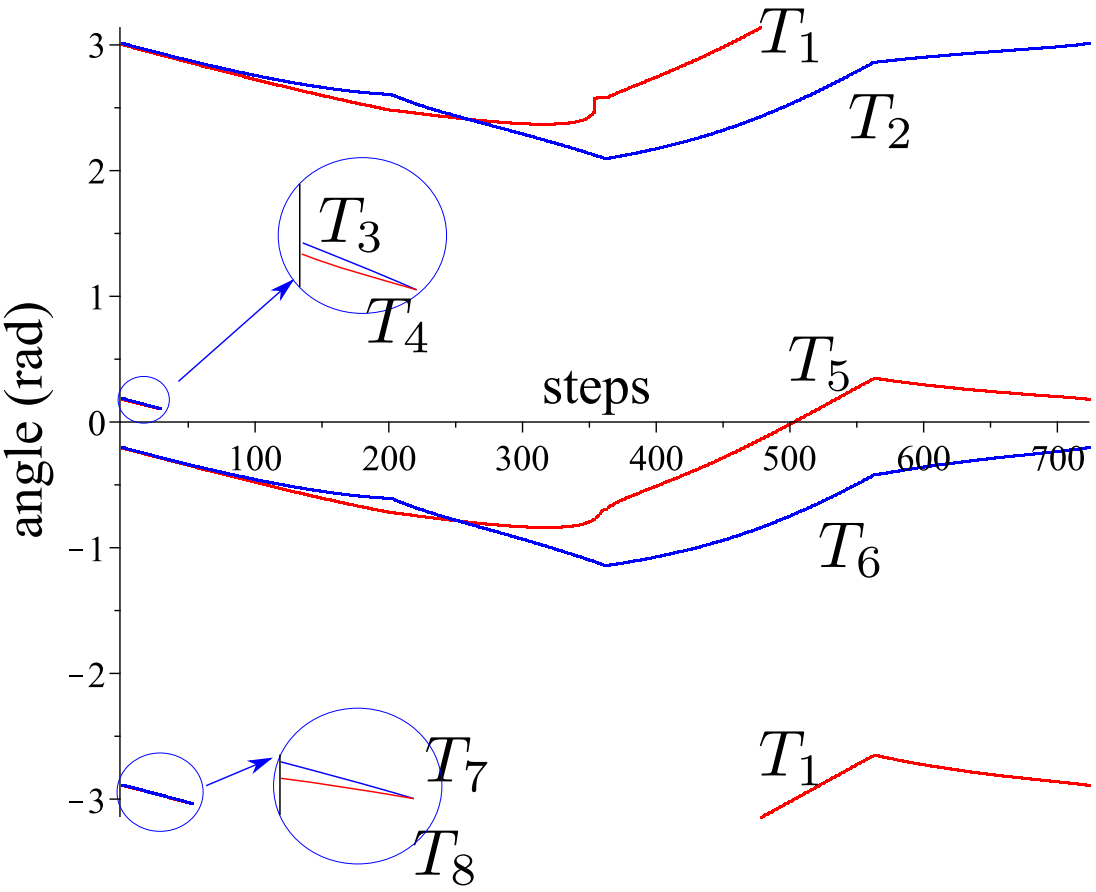

Figure 4.15 – Value of θ_1 along the closed path in fig. 4.14, with regions of 4, 6 and 8 IKS. Blue and red paths correspond to solutions in an aspect with $\det(\mathbf{J}) > 0$ and $\det(\mathbf{J}) < 0$ respectively.

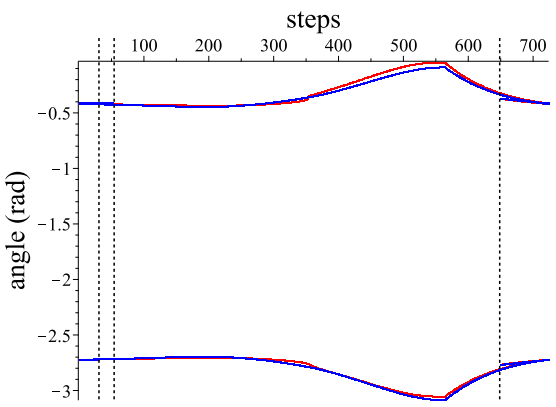

(a) Value of θ_2 along the path

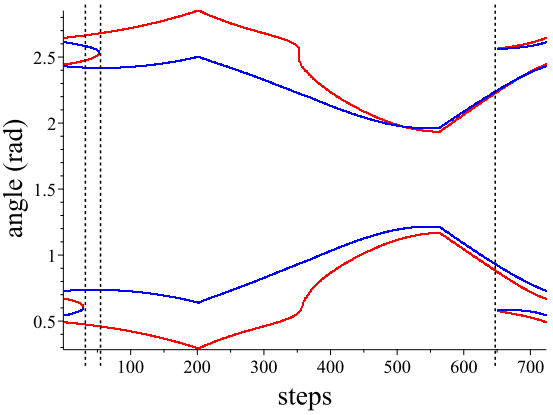

(b) Value of θ_3 along the path

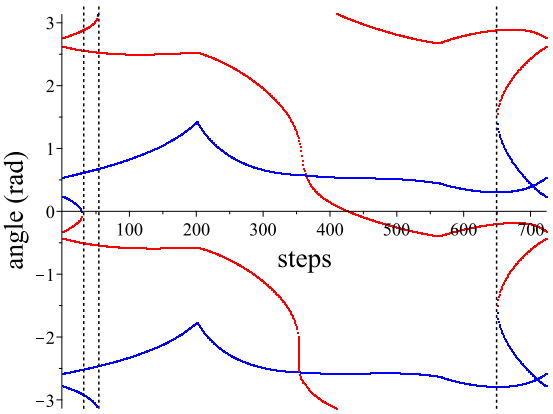

(c) Value of θ_4 along the path

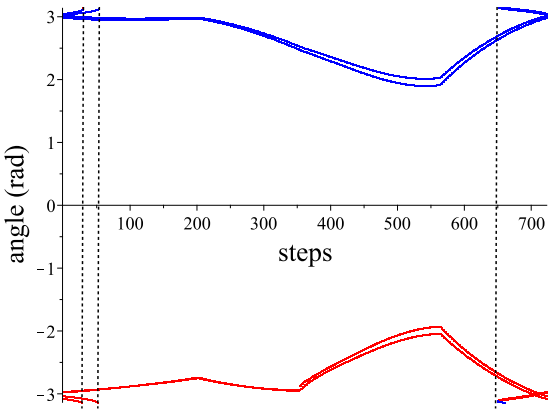

(d) Value of θ_5 along the path

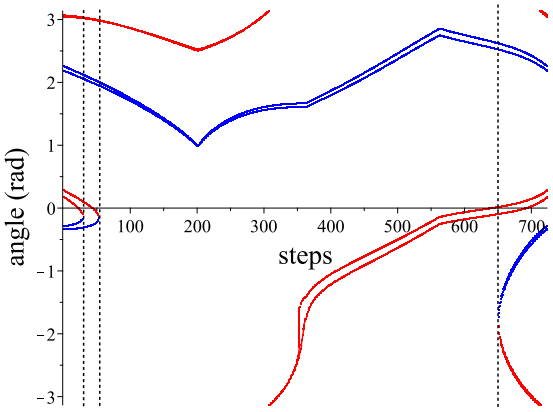

(e) Value of θ_6 along the path

Figure 4.16 – Plot for $\theta_{2...6}$ of all solutions at discretized points along the path in fig. 4.14.

A closed path trajectory in the slice shown in 4.17 that starts from point $\mathbf{a}(-90, 200)$ and passes through $\mathbf{b}(-150, 200)$, $\mathbf{c}(-150, 375)$, $\mathbf{d}(75, 375)$ and $\mathbf{e}(75, 200)$ is bound to sudden jumps and getting off the expected path no matter which initial IKS is chosen. The two examples discussed in this section demonstrate the challenges in path planning for a cuspidal robot. These examples are not related to any special poses, the only condition used to demonstrate the issues in path planning is that it travels through multiple connected regions in the workspace. It suffices to say that the cuspidality analysis is essential particularly in the present scenario when designers choose unconventional designs.

Repeatability depending on choice of initial IKS

Closed paths that do not result in a change of IKS can be repeated infinitely many times, but this is not the case for nonsingular solution changing paths. This dependency of path feasibility and repeatability on the initial IKS pose several challenges in planning

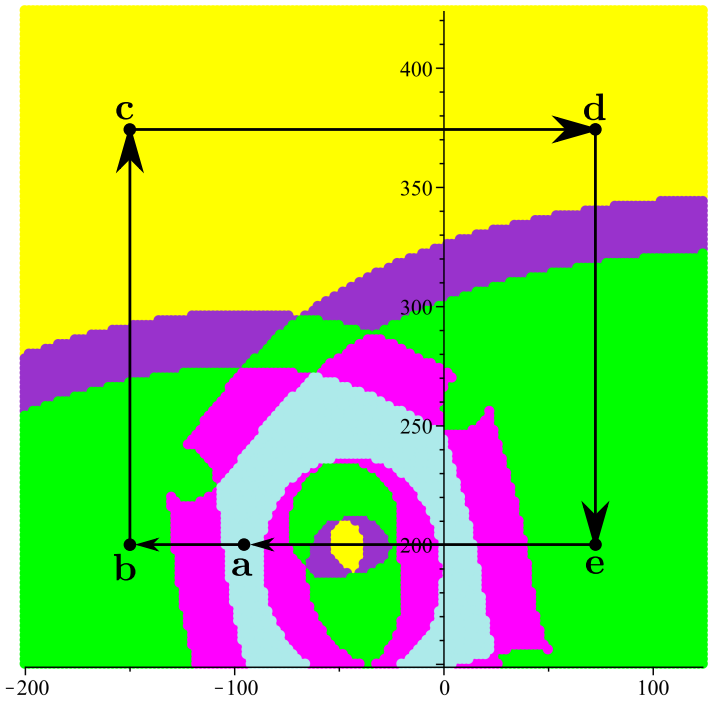

Figure 4.17 – Path in the slice of Jaco that is infeasible no matter the choice of initial IKS

trajectories of 3R and 6R cuspidal robots. In 3R serial robots, a following theorem can be stated:

Theorem 8. *A nonsingular change of solutions in a generic 3R robot is a nonrepeatable path.*

Proof. The proof of this theorem uses theorem 2, and the fact that the number of IKS with $\det(\mathbf{J}) > 0$ is the same as the number of IKS with $\det(\mathbf{J}) < 0$. As it is proved in theorem 2, every IKS of a generic 3R robot lies in a distinct connected region. It has been established in chapter 2.1 that an IKS crosses pseudosingularities while changing solutions in nonsingular fashion. As the maximum number of IKS for a 3R robot is four (refer to $M(t)$ from chapter 2.1), there are at most 2 IKS in an aspect of such a robot. As the preimage of the image of every point on pseudosingularity consists of a critical point too, it is necessary that while crossing the pseudosingularity, the second IKS in the aspect meets the locus of critical points. This implies that if we were to repeat the path starting from the second solution in an aspect, the path would meet a singularity while crossing the component of critical value and thus is an infeasible path. □

Repeatability of a nonsingular change of solutions for 6R robots is different. The dependence of repeatability on initial choice of IKS in Jaco robot is shown by discussing the same path as depicted in Figure 4.14. The repeatability of a path can be studied from Figure 4.15 by following a particular path from the beginning to the end. As the discussed trajectory is a closed path, the initial set of IKS should match the final set of IKS. Path feasibility is a pre-requisite to analyze path repeatability, and for this reason we will consider only the trajectories T_1, T_2, T_5 and T_6. Upon following the continuous path starting from the trajectory T_1 (resp. T_5) whose initial IKS belongs to an aspect with $\det(\mathbf{J}) < 0$, it is clear that it ends up on the initial IKS corresponding to trajectory T_8 (resp. T_4). This signifies a nonsingular change of solutions. It is further noted that this change of solutions will result into a non-repeatable path as trajectory T_8 as well as T_4 are the initial IKS corresponding to infeasible paths. Upon following the trajectory T_2 (resp. T_6), it is noted that they end up on the IKS corresponding to its own path, i.e, IKS corresponding to T_2 (resp. T_6). This path corresponds to a regular path and is thus repeatable. To conclude on the given path in Figure 4.14, trajectories T_2 and T_6 are the only two trajectories out of the eight possibilities that lead to a feasible as well as repeatable path. It is important to highlight that trajectories T_1 and T_5 can qualify as acceptable choices of initial IKS depending upon the tasks requirements on repeatability.

Palindromic robots

As shown in the above example, a nonsingular change of solutions affects the repeatability of the given path. The nonsingular change of solutions in 3R robots is necessarily a nonrepeatable path, but there exists few 6R robots where this is not true. The first robot to exhibit repeatable nonsingular change of solutions was presented in [PCI88]. This robot is a special arrangement of the joints such that the relative joint orientations in subchain formed by first three joints is similar to that of a subchain formed by last three joints (refer to Figure 4.18). Because of the mirrored architecture that resembles palindromes, such a robot is defined as a palindromic robot in the scope of presented work. The D-H parameters for one such robot are given in 4.5. The values for all the joint angles along the path mentioned in table 4.6 is shown Figure 4.19.

i	d_i (mm)	a_i (mm)	α_i (deg)	θ_i (rad)
1	0	0	90	θ_1
2	0	4	0	θ_2
3	0	1	270	θ_3
4	0	0.8	0	θ_4
5	0	0	90	θ_5
6	0	0	0	θ_6

Table 4.5 – The D-H parameters of a robot with palindromic architecture

via point	$\theta_1(deg)$	$\theta_2(deg)$	$\theta_3(deg)$	$\theta_4(deg)$	$\theta_5(deg)$	$\theta_6(deg)$
a	20	40	10	-70	30	0
b	20	36	36	-72	36	0
c	20	72	36	-126	72	0
d	20	72	36	-180	180	0
e	20	72	36	-342	486	0
f	20	108	36	-342	522	0
g	-160	140	-10	-290	510	180

Table 4.6 – The joint values for the via points of nonsingular change of solutions

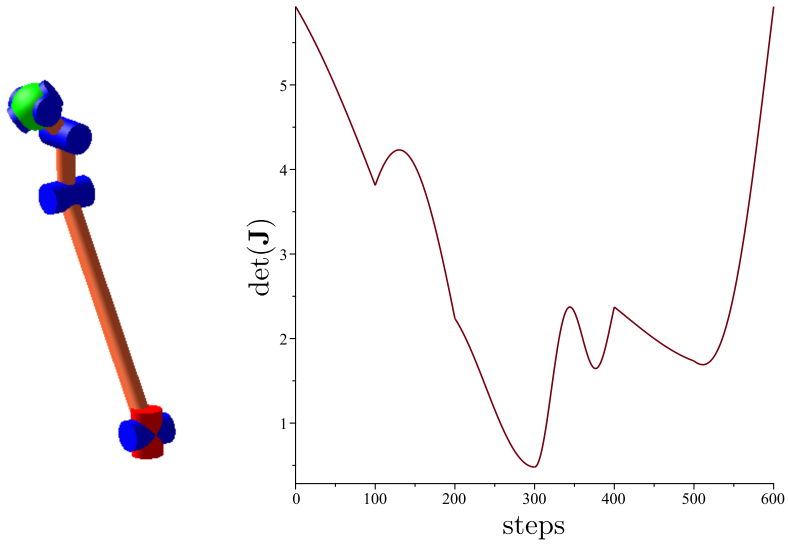

Figure 4.18 – The schematic figure of a palindromic robot and the progress of det(**J**) along the path in table 4.6 confirming a nonsingular change of solutions.

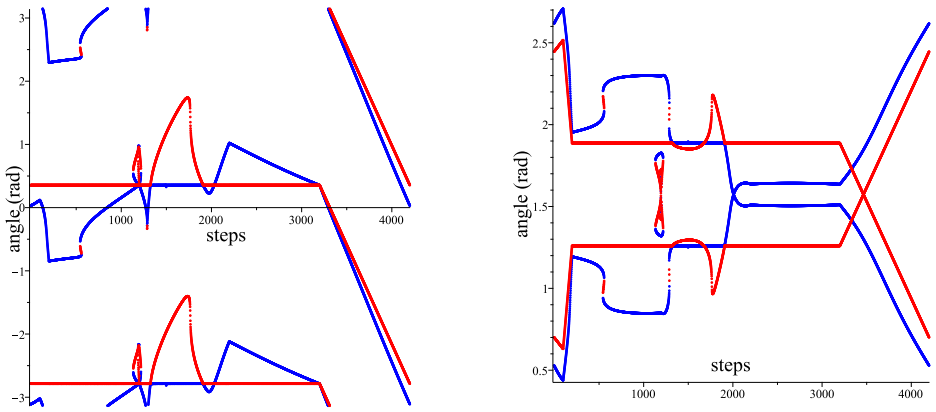

(a) Value of θ_1 along the path

(b) Value of θ_2 along the path

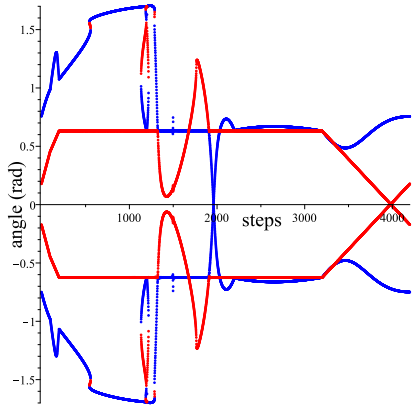

(c) Value of θ_3 along the path

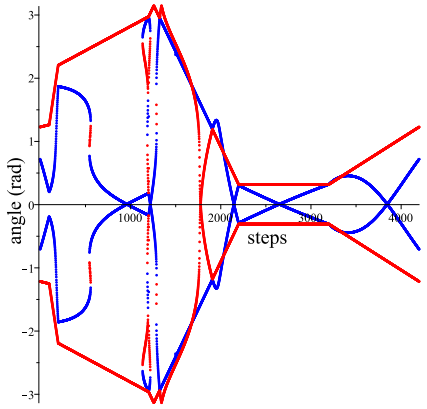

(d) Value of θ_4 along the path

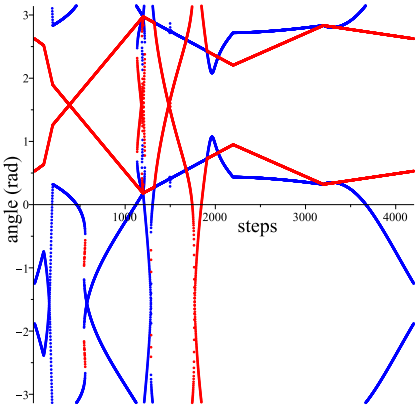

(e) Value of θ_5 along the path

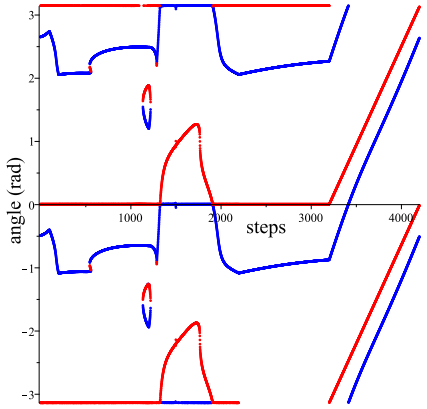

(f) Value of θ_6 along the path

Figure 4.19 – Plot for $\theta_{1...6}$ of all solutions at discretized points for a nonsingular change of solutions that is repeatable.

The property of repeatable nonsingular change of solutions is not applicable to all palindromic robots.

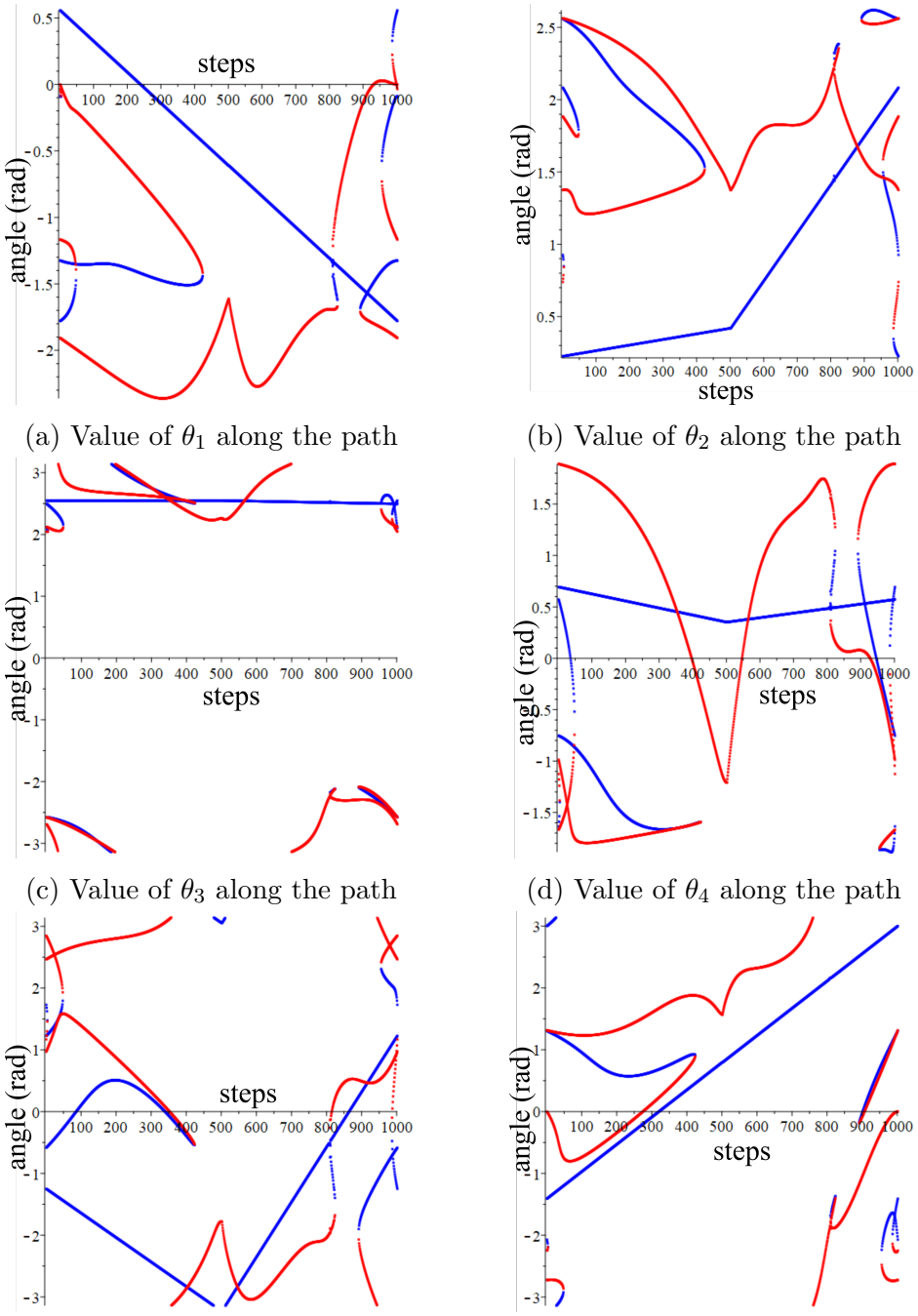

(a) Value of θ_1 along the path

(b) Value of θ_2 along the path

(c) Value of θ_3 along the path

(d) Value of θ_4 along the path

(e) Value of θ_5 along the path

(f) Value of θ_6 along the path

Figure 4.20 – Plot for $\theta_{1...6}$ of all solutions at discretized points for a nonsingular change of solutions that is nonrepeatble.

4.1.3 Problems in collaborative applications

Being aware of the cuspidal property of a robot, the choice of initial IKS may not be a problem if the complete trajectory to be followed and the repeatability condition for the path are known prior to execution. Thus, it is of great importance that such robots are strictly used in environments with pre-planned trajectories. If deployed in collaborative areas (as is the present case for the Jaco robot), such robots are bound to error and can lead to unexpected behavior and unforeseen scenarios. In this section we revisit the infeasible paths in 3R cuspidal robots discussed in [Wen04]. Later, we show that the same issues exist in the 6R robots by showing common trajectories (straight lines with fixed orientation) involved in collaborative task. The aim of this section is to strongly motivate the reason to desist from implementing cuspidal robots in collaborative applications.

Infeasible paths in 3R robots

As discussed in chapter 2.1, the components of critical values have a geometrical interpretation of specific IKS coming together at a tangent point. This implies that if we begin from a particular IKS, then there are certain components of critical values that cannot be crossed. In [Wen04], the different regions of feasible path for a particular 3R robot were presented. It was readily concluded that for such a 3R robot, the trajectory starting from $\mathbf{w}_i$ to $\mathbf{w}_j$ (refer to Figure 4.21) is infeasible no matter the initial choice of IKS (refer to figures 2.5b and 2.5d). If we deploy such a robot in collaborative task where the robot reacts according to the user, this robot will not be able to comply to certain movements. The multiple connected regions with varying number of IKS is a common observation in cuspidal robots, and thus it is impossible to guarantee that a robot will comply to a user as needed.

Infeasible paths in 6R commercial robots

In section 4.1.2, the infeasibility of certain paths was shown in the Jaco robot. Figures 4.14 and 4.15 clearly present feasible and infeasible paths. In this section, we present an infeasible path in the CRX-10ia/L workspace (see Figure 4.22). The feasibility of the trajectories, $\mathbf{w}_i \rightarrow \mathbf{w}_j$ and $\mathbf{w}_a \rightarrow \mathbf{w}_b$ is dependent on the initial choice of IKS. This is because a region with 4 IKS must be crossed, while the path starts from a region with 8 IKS and thus 4 IKS are lost. Interestingly, the trajectory $\mathbf{w}_k \rightarrow \mathbf{w}_l$ is a feasible trajectory no matter the initial choice of IKS. This is attributed to the reason that in

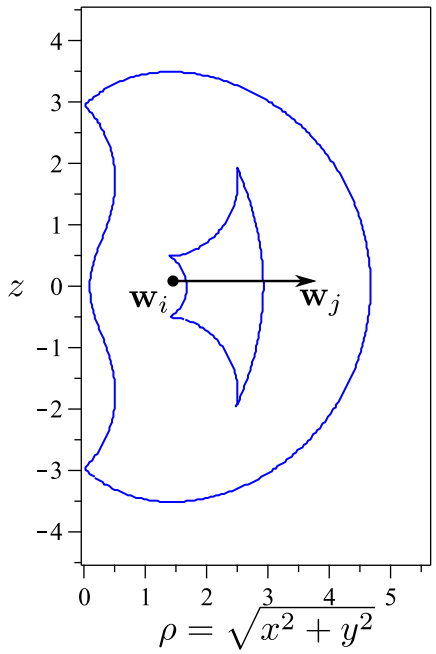

Figure 4.21 – An example infeasible path in 3R robot.
Robot parameters: d = [0, 1, 0], a = [1, 2, $\frac{3}{2}$], α = [-$\frac{\pi}{2}$, $\frac{\pi}{2}$, 0].

trajectory $\mathbf{w}_k \rightarrow \mathbf{w}_l$, we start from an instance with 8 IKS and cross boundaries to enter region with 12 IKS. This implies that upon crossing the boundary, we gain more IKS and thus the continuity of the path is not disturbed upon this. The plots of thetas for all trajectory $\mathbf{w}_i \rightarrow \mathbf{w}_j$ (respectively $\mathbf{w}_k \rightarrow \mathbf{w}_l$ and $\mathbf{w}_a \rightarrow \mathbf{w}_b$) is given in Figure 4.23 (respectively Figure 4.24 and Figure 4.25). The most complicated trajectory of the above three examples is the trajectory $\mathbf{w}_a \rightarrow \mathbf{w}_b$ which passes through regions with 16, 12, 8 and 4 IKS. It is clear from the analysis of the trajectory that at most 4 out of the initial 16 IKS qualify for continuous paths. The eligible 4 IKS are completely dependent on the path followed and the components of critical values crossed. If the trajectory is known beforehand, then one can analyze and decide a trajectory planning algorithm that considers a nonsingular change of solutions too. To the author's knowledge the only work that incorporates nonsingular change of solutions in a time optimal point to point trajectories was recently reported [Mar+23].

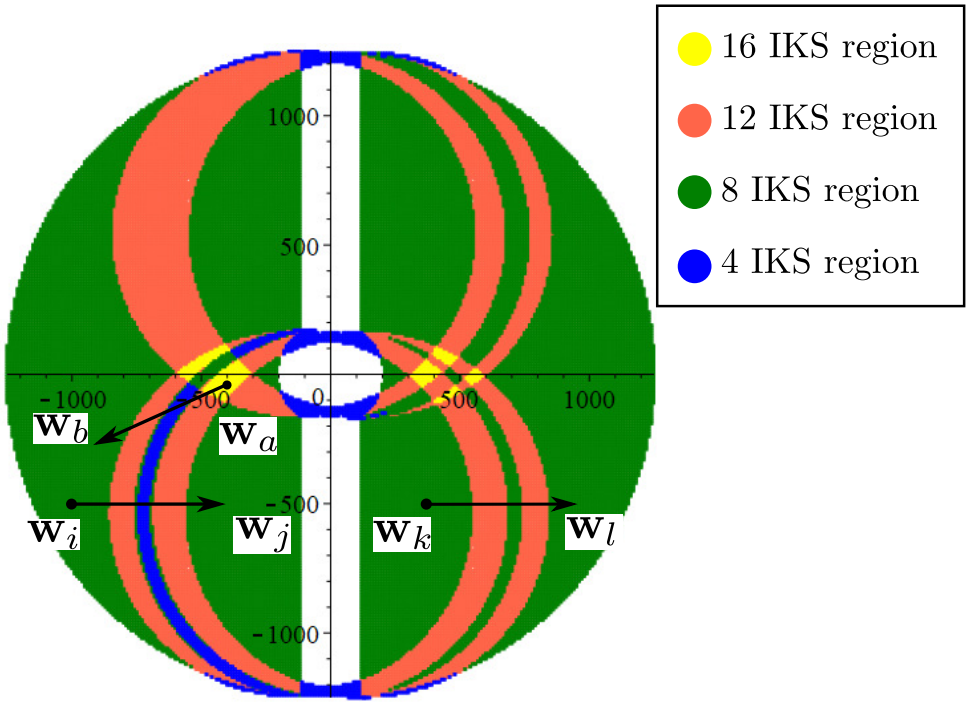

Figure 4.22 – 2-D slice in (xz - plane) of the workspace for CRX-10ia/L with $y = 0.05m$ and orientation as equivalent angle axis representation = 0.195400(0.816$\hat{\mathbf{i}}$ -0.011$\hat{\mathbf{j}}$ + 0.014$\hat{\mathbf{k}}$).

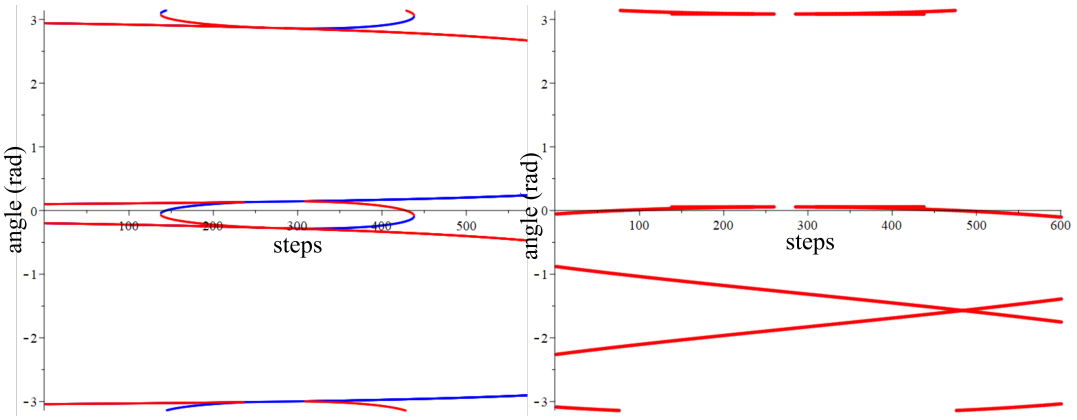

(a) Value of θ_1 along the path

(b) Value of θ_2 along the path

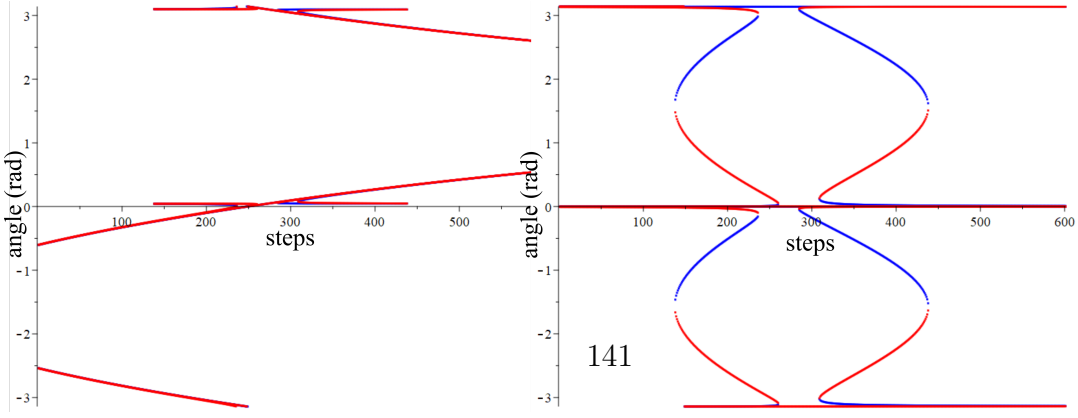

(c) Value of θ_3 along the path

(d) Value of θ_4 along the path

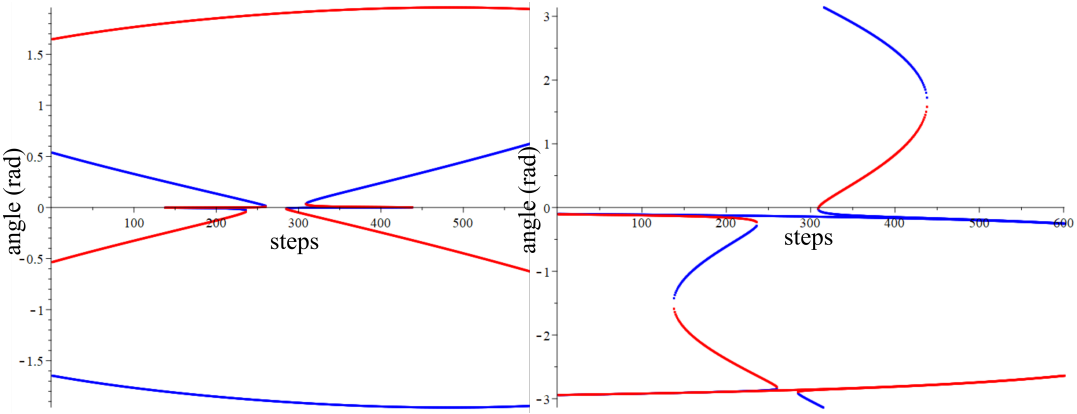

(e) Value of θ_5 along the path (f) Value of θ_6 along the path

Figure 4.23 – Plot for $\theta_{1...6}$ of all solutions at discretized points along the trajectory $\mathbf{w}_i \rightarrow \mathbf{w}_j$.

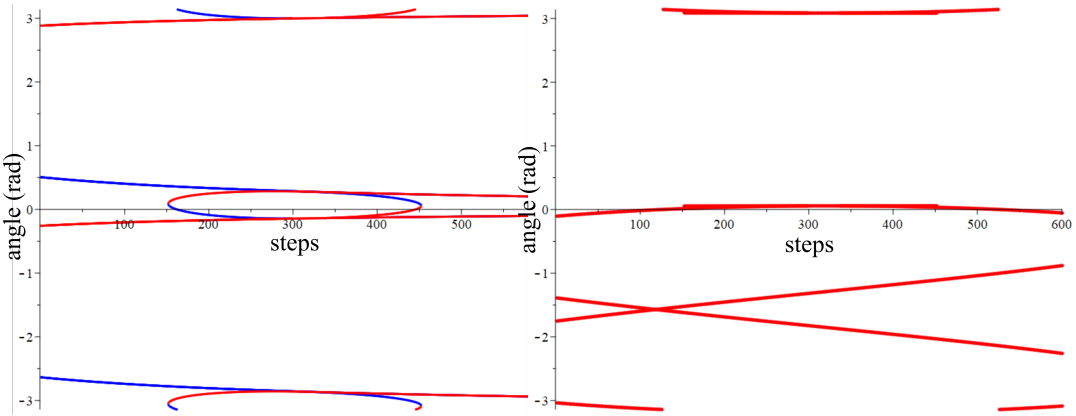

(a) Value of θ_1 along the path (b) Value of θ_2 along the path

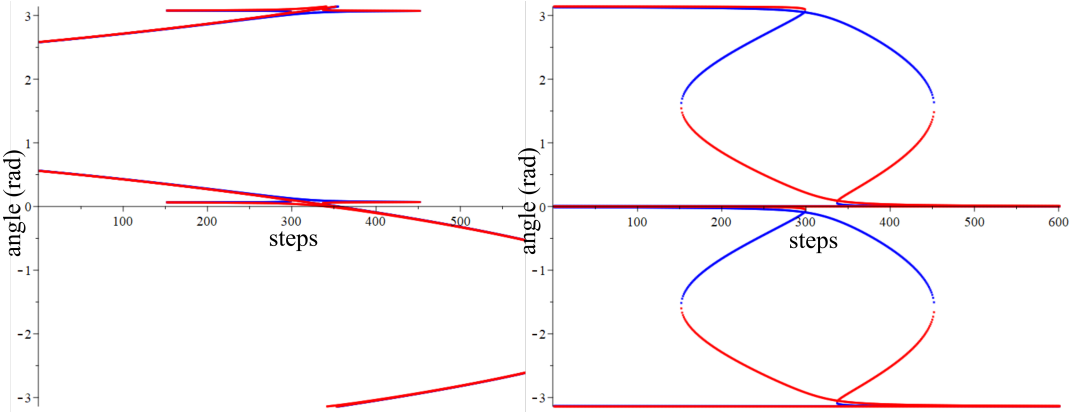

(c) Value of θ_3 along the path (d) Value of θ_4 along the path

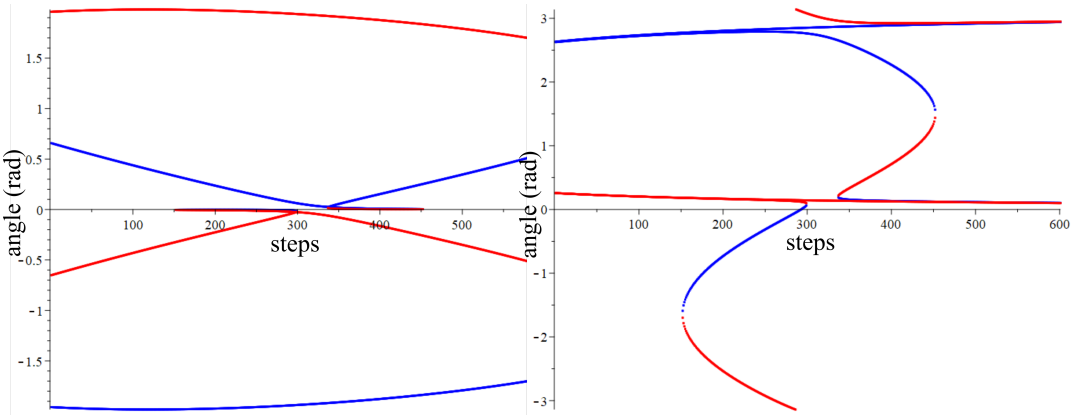

(e) Value of θ_5 along the path (f) Value of θ_6 along the path

Figure 4.24 – Plot for $\theta_{1...6}$ of all solutions at discretized points along the trajectory $\mathbf{w}_k \rightarrow \mathbf{w}_l$.

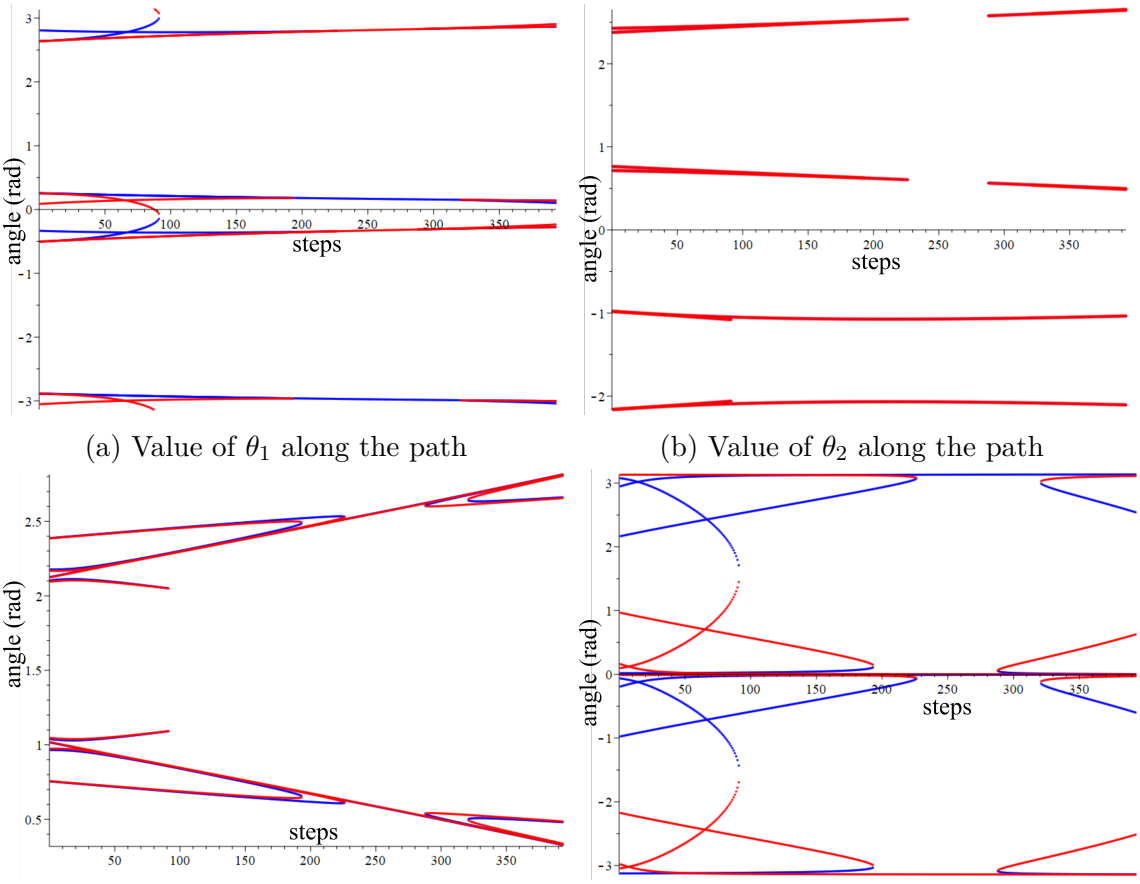

(a) Value of θ_1 along the path (b) Value of θ_2 along the path

(c) Value of θ_3 along the path (d) Value of θ_4 along the path

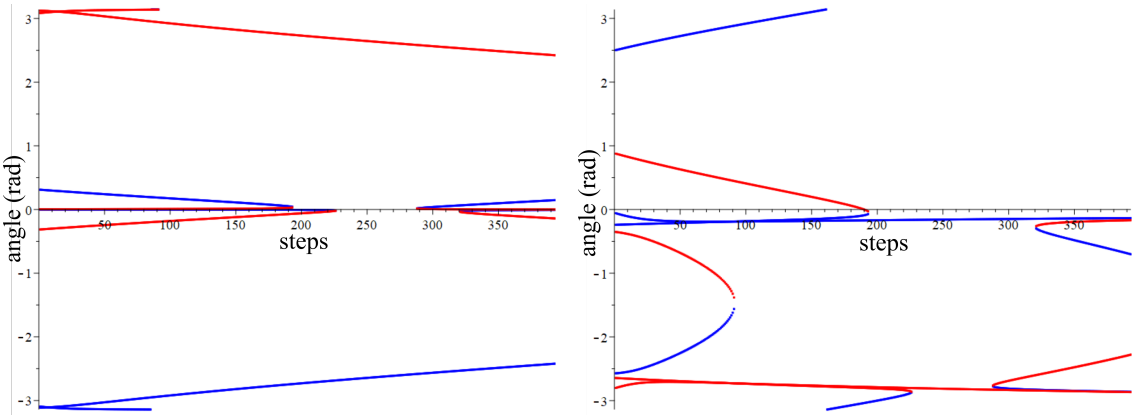

(e) Value of θ_5 along the path

(f) Value of θ_6 along the path

Figure 4.25 – Plot for $\theta_{1...6}$ of all solutions at discretized points along the trajectory $\mathbf{w}_a \rightarrow \mathbf{w}_b$.

4.2 Path planning framework for cuspidal robots

In this section, we present the different types of paths occuring due to the presence of multiple regions of IKS in the workspace of a cuspidal robot. Different scenarios are put forth to highlight the classification of these path. The path planning framework for cuspidal robots is then presented at the end of the section. The proposed framework can be implemented on existing commercial cuspidal robots to mitigate any issues in path planning.

4.2.1 Types of paths

In a wrist-partitioned 6R serial robot, a given path is either feasible or infeasible depending upon the constraints provided. A path can be declared infeasible due to multiple reasons such as unreachable poses in the path, joint limits and internal collisions. It is important to note that if a path is infeasible for such a robot, it is not possible to change the IKS that can execute the desired path without crossing a singularity. A feasible path for these robots is always repeatable as even in the case of a closed loop path, the robots do not undergo nonsingular change of solutions, and thus path feasibility implies path repeatability. This is not true for cuspidal robots, and the path feasibility is dependent upon the initial IKS as discussed in section 4.1. As cuspidal robots can undergo a nonsingular change of solutions while performing a closed loop path, a feasible

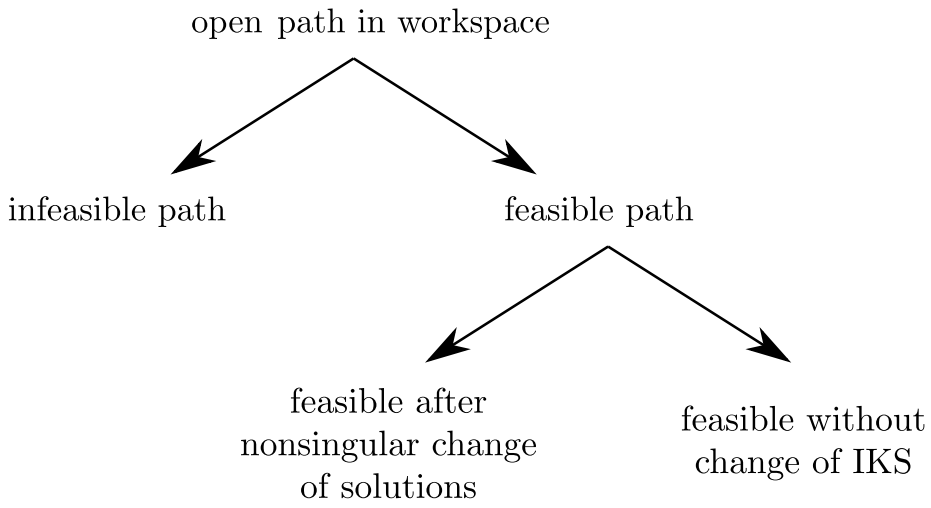

Figure 4.26 – The classification of possible open paths in cuspidal robots.

path may not be necessarily repeatable. An example of a feasible but non-repeatable path in a commercial cuspidal robot was discussed in [SCW23] and other examples are detailed in previous section. If the path in the workspace is an open path such as a point-to-point path, the given path is either feasible or infeasible. The feasibility of a given open path is dependent on the initial IKS and the possibility of changing the IKS before executing the path. The case of changing IKS making an infeasible path feasible is of prime importance in commercial cuspidal robots that are used in collaborative tasks. The complete classification of possible paths for a cuspidal robot is presented in Figure 4.26 and Figure 4.27.

Infeasible path: The path defined in the workspace which cannot be traversed starting from a defined IKS is termed as an infeasible path.
Feasible path: The path defined in the workspace which can be traversed starting from a defined IKS is termed as a feasible path.

If the path is a closed loop in workspace, then we have further classification of feasible paths depending on their repeatability. The definitions for repeatable and non-repeatable paths is given in section 1.2. The repeatable paths can either correspond to a regular path (see section 1.2) or a nonsingular change of solutions. An example of each type of the mentioned paths are illustrated in Figure 4.28.

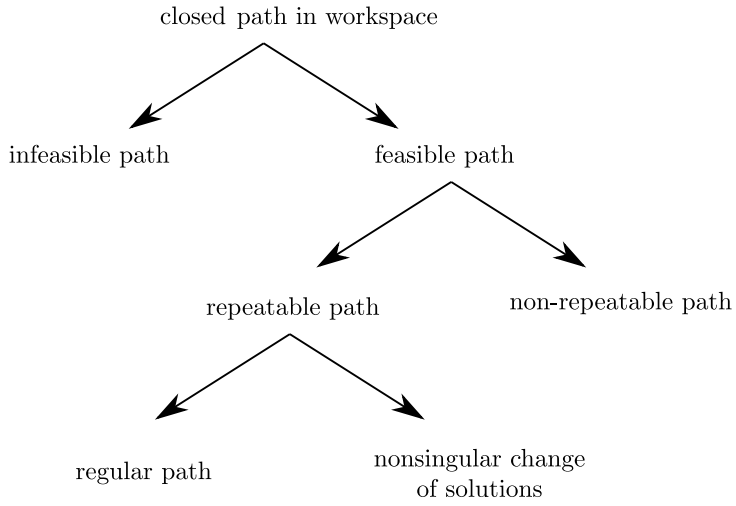

Figure 4.27 – The classification of possible closed paths in cuspidal robots.

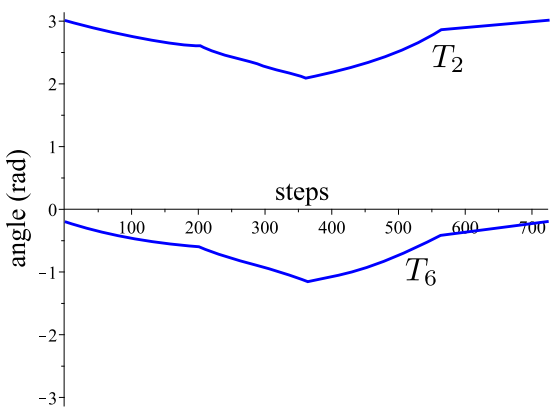

(a) Regular path

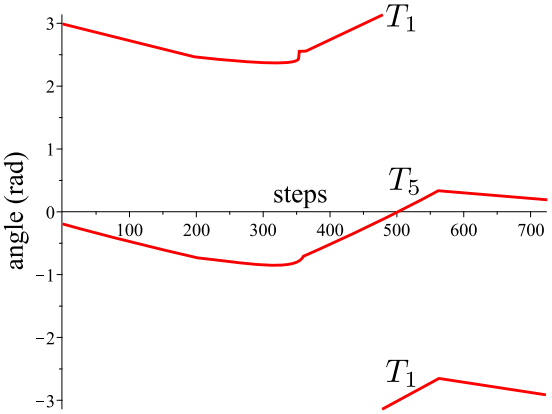

(b) Nonsingular change of solutions path that is non-repeatable

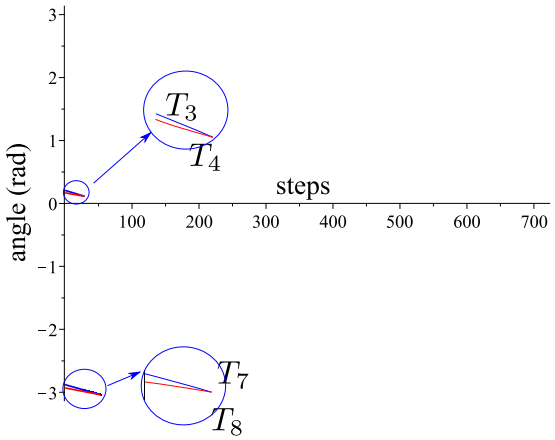

(c) An infeasible path

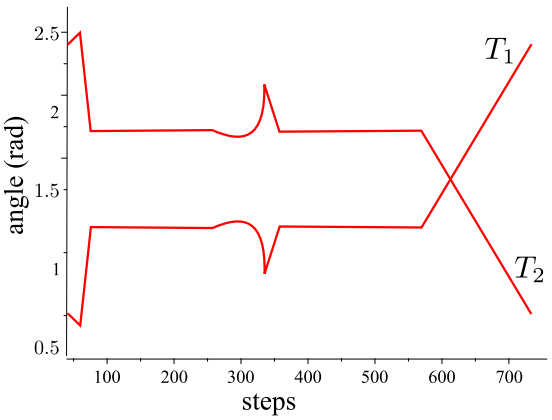

(d) The nonsingular change of solution that is repeatable path

Figure 4.28 – The types of path possible in a cuspidal robot

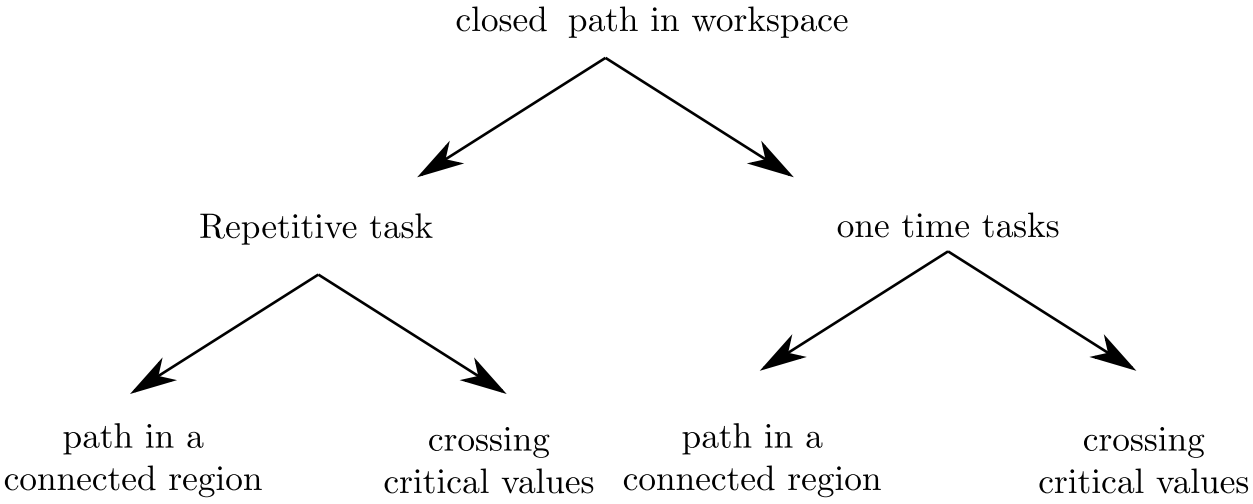

Figure 4.29 – The classification of possible scenarios of closed paths in cuspidal robots.

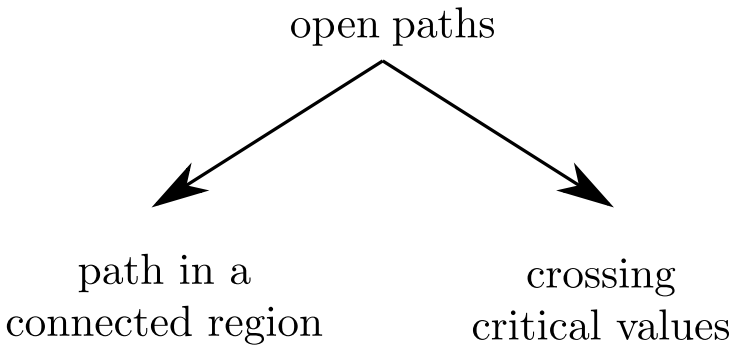

Figure 4.30 – The classification of possible scenarios of open paths in cuspidal robots.

4.2.2 Types of scenarios

As discussed in previous section, there exists more types of path in a cuspidal robot than a noncuspidal robot. The direct implication of this fact is that we encounter different scenarios in the path planning as well. The scenarios familiar with the industrial applications are pick and place operations, repetitive tasks forming a closed path (e.g. welding, surface inspection) or point-to-point trajectories. We will discuss path planning in the workspace only as the paths in the joint space are simpler and can cross singularities. The different scenarios in cuspidal robots are illustrated in Figure 4.29 and 4.30.

Scenarios in closed paths: These scenarios are often encountered in welding or inspection application. The robot is expected to follow a given path in the workspace and return to its initial pose. Such paths can be repetitive in nature such as welding in an assembly line or can be one time tasks such as inspecting a unique part. In the case of non

repetitive tasks, a path leading to a nonsingular change of solutions is acceptable while the repetitive tasks should be regular paths to be declared as feasible. In special cases where the nonsingular change of solutions is repeatable, such paths can be declared fit for repetitive tasks but may face issues such as collisions with the environment. For this reason, a path specified in the workspace has to be analyzed for the intersection with critical values. If the path exists in a connected region of a workspace, it is a regular path. In case the path intersects the critical values, it is important to verify the initial IKS as well as compare it with the final IKS. An example of a closed loop path crossing critical values is shown in Figure 4.14. It can be observed that in order to complete the closed loop path, it is important to start the path from the IKS corresponding to either T_1, T_2, T_5 or T_6. Furthermore, if the task is repetitive then IKS belonging to T_1 and T_5 are to be discarded. It is clear from this illustration that for a given path to be declared as feasible, the choice of initial IKS plays a crucial role in cuspidal robots.

Scenarios in open paths: These scenarios are simpler than the closed loop paths. A typical example of this scenario is an open path of a welding that starts at a point and terminates at another point. In such case the robot is not expected to return to its initial pose. In case the path belongs to a connected region in the workspace, it is always feasible and the feasibility of the paths that cross the critical values depends on the choice of initial IKS. A continuous path in the workspace of a cuspidal robot is not guaranteed if it crosses two distinct components of critical values [Wen04].

4.2.3 Path planning framework

Based on the types of paths and scenarios in cuspidal robots as shown in previous subsections, we propose a path planning framework for cuspidal robots. This framework addresses all the scenarios discussed in previous subsection. The framework proposed can be implemented to existing commercial cuspidal robots such as JACO Gen2 robot from Kinova robotics, CRX series from FANUC and many others. The framework is divided into two parts; the first part deals with the open paths in the workspace and the second part with the scenarios related to closed loop paths in the workspace.
Framework for open paths: The flowchart in Figure 4.31 explains the framework to be adapted in case of open paths for a cuspidal robot. The main consideration in such cases is the intersection of the path with the critical values. In case the path intersects the critical values, we can check the connectivity of the path starting of every IKS of the

initial pose of the path. As we know that the number of IKS either increase or decreases upon crossing a critical value and traveling from a region with lower number of IKS is never a problem as we gain extra IKS. This fact is used to accelerate the connectivity check for the feasibility of different initial IKS. We propose to choose an instance along the path that corresponds to a region with the least IKS. The connectivity of every IKS at this instance with the initial IKS is investigated and in case a connected path exists the forward connectivity of the IKS at this instance with the final IKS is investigated. If the IKS is connected to both initial as well as final IKS then such path is declared feasible. After repeating this for every IKS of the instance, we optimise the feasible paths to choose the one for execution. *Framework for closed paths*: The flowchart in Figure 4.32 explains the framework to be adapted in case of closed paths for a cuspidal robot. This case presents more scenarios and the choices are complicated. As already shown, a given closed path can be feasible and yet not repeatable. The main consideration in such cases is whether a nonsingular change of solutions is acceptable for declaring a path feasible. The feasibility of a path can be checked in the same manner as discussed in the framework for open paths. A connected path is not enough to declare the feasibility and the type of task should be known beforehand in order to optimise and execute a given closed path in the workspace. This framework proposes all the cases that can occur in commercial robots and as highlighted in [SCW23], it is important to consider cuspidality in path planning to avoid dangerous situations.

The types of paths, the different scenarios and the framework proposed for path planning in cuspidal robots clearly suggests that the complete path to be followed should be known prior to execution. This implies that cuspidal robots are NOT suitable for compliance tasks where the path to be followed depends on the agent acting on the robot and thus is calculated in real time. This is an important observation and a contribution of the paper as all the commercial cuspidal robots that exist in the industry exist under the category of collaborative robots or 'cobots'.

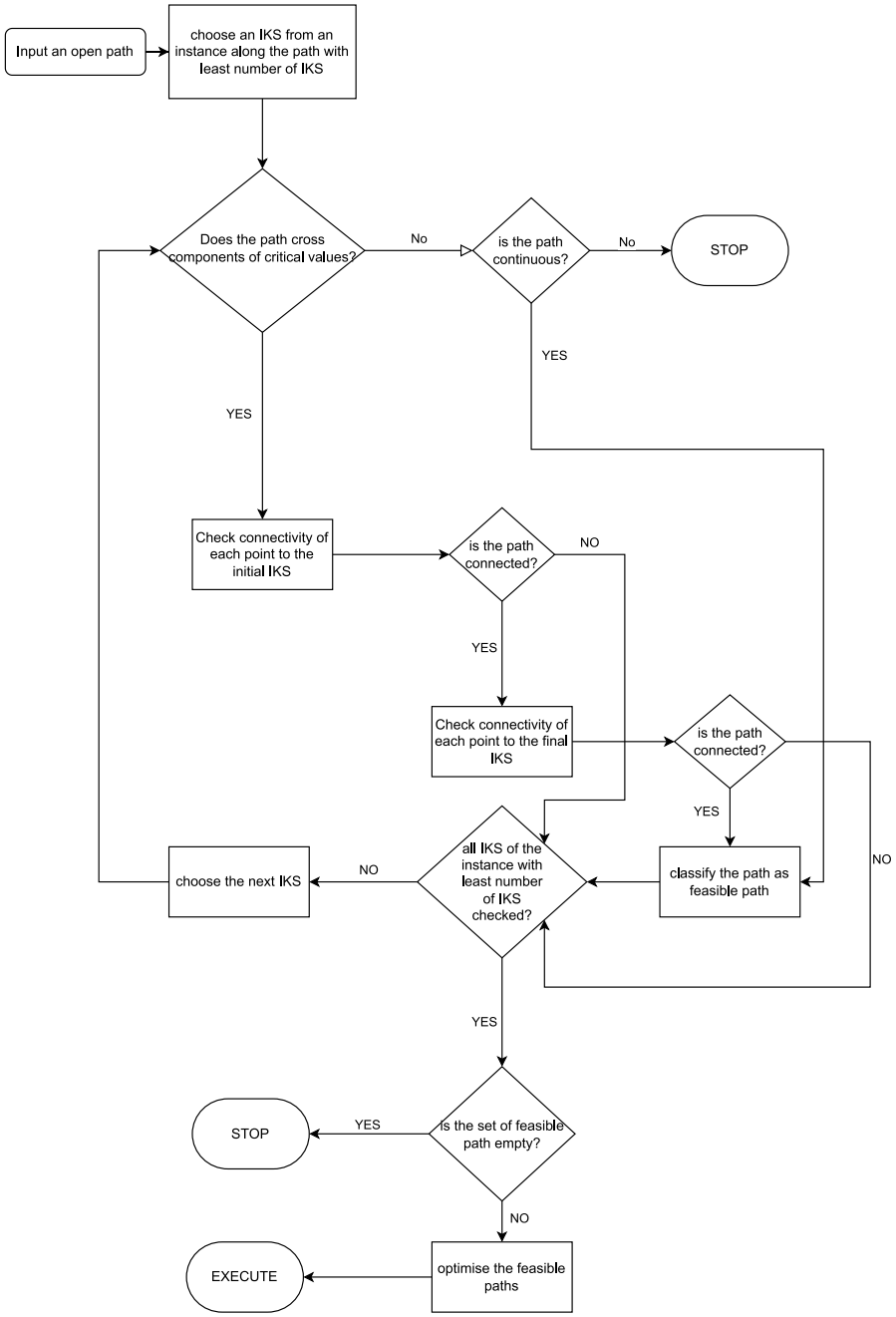

Figure 4.31 – The framework for scenarios with open paths in cuspidal robots.

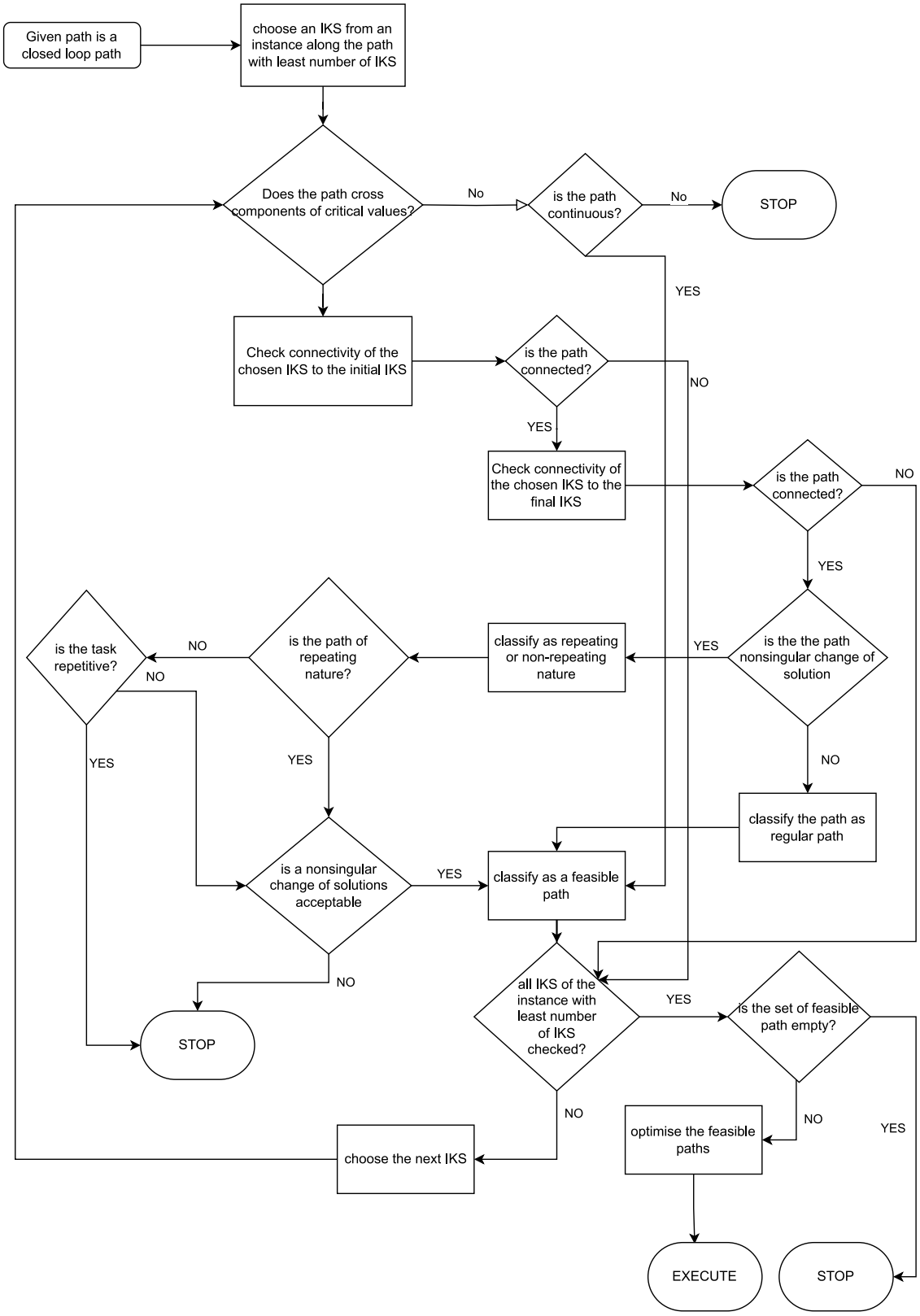

Figure 4.32 – The framework for scenarios with closed loop paths in cuspidal robots.

4.3 Conclusions

In this chapter, the issues in path planning pertinent to cuspidal robots are discussed. The issues such as mislabeling of 'configurations', incorrect calculations of IKS due to numerical methods are highlighted using existing commercial cuspidal robots as example. Later, the major issues such as the dependence of a path feasibility as well as path repeatability on the choice of initial IKS are discussed. All of the above issues prove to be dangerous in collaborative application and the discontinuity in paths while crossing internal locus of critical values is discussed with examples of linear paths in the workspace of an existing commercial robot. Different cases occuring in the path planning of cuspidal robots are presented highlighting the importance of special care while designing path planning algorithms for cuspidal robots. Though cuspidal robots can be used in industrial applications in a controlled environment, such robots are clearly dangerous and cannot predict the feasibility of a path without knowledge about the complete path to be executed. Considering all the problems in 6R cuspidal robot, we propose a framework for path planning in cuspidal robots. This framework considers different cases arising in cuspidal robots and takes into account a possible nonsingular change of solution to be executed in order to make a given path feasible and repeatable. The results discussed in this chapter clearly prove that the cuspidality should be seriously considered while executing tasks in cuspidal robots, and such robots should be completely avoided for the tasks that require executing path online or reacting to an external agents.

CONCLUSIONS

Synopsis

The presented doctoral thesis investigated on the cuspidality analysis of 3R and 6R serial robots. Geometric interpretation of the IKM for 3R serial robots provided a geometric interpretation of IKS in 3R robots. A comparative analysis of singularities and nonsingular change of solutions in the joint space, workspace and the $c_3 s_3$- plane led the proof for necessary and sufficient condition for a *generic* 3R robot to be cuspidal. The existence of reduced aspects for generic 3R robot was shown to be true using similar analysis. The geometric analysis further proposed new classification criteria that are intuitive and easy to calculate. This allowed multiple sufficient conditions for cuspidal and noncuspidal robots. The geometric analysis was further used to answer on the non-existence of 3(0, 0) and 4(0, 0) homotopy classes thus confirming that the maximum number of aspects for a generic 3R robot is four.

The analysis of 6R robots was done in two phases. Simplified geometries involving either a wrist or a 3R planar subchain were investigated using geometric methods and analysis of the determinant of the Jacobian matrix. The analysis further showed that the theorems proved for generic 3R serial robots apply for 6R robots with wrist at the either of the extreme positions as well. It was shown with an example of wrist in the middle that not all simplified geometries lead to easy analysis of cuspidality. It was further proved that the presence of a 3R planar chain always results into the determinant having three distinct factors. In second phase of analysis, the claim of two aspects in a generic 6R robot was refuted by showing examples of 2-dimensional non-intersecting varieties that separate the joint space in more than two regions. Later, the building blocks of deciding cuspidality were explained and both, certified as well as numerical, approaches were presented to decide upon cuspidality of nR nonredundant robots. A complete framework for this purpose was presented that utilizes the known results, simpler analysis coupled with numerical and certified algorithms to make the identification process implementable. It was shown through this analysis that almost all of the generic robots are cuspidal in nature.

Later, cuspidal robots existing in industries were analyzed to highlight major issues

in cuspidal robots that remain unattended. The issues in misidentification of configurations in cuspidal robots were shown with an industrial robot FANUC CRX-10ia/L. The problems in annotating sixteen solutions into eight categories was illustrated through an example to further motivate the problem existing in the industrial software. The existence of multiple regions with varying IKS was shown to be a typical case for cupidal robots. The consequence of crossing these regions on path planning of cuspidal robots was highlighted through a known commercial robot, Kinova Jaco Gen2 (non-spherical wrist). The dependence of feasibility as well as repeatability on the choice of initial IKS in cuspidal robots was presented, and different types of scenarios specific to path planning in cuspidal robots were discussed. An extensive path planning framework for cuspidal robots was proposed that considers cuspidality as well as all the possible scenarios related to cuspidal robots. A time optimal point-to-point trajectory was planned for an industrial robot to motivate the application of the proposed path planning framework.

The contributions of this doctoral thesis are summarized as follows:

Contributions

1. Proof of reduced aspects in generic 3R robots

The existence of reduced aspects in generic 3R robot was proved by using the geometric interpretation of the IKM. It was proved that every IKS in 3R robot lies in distinct region bounded by singularities and pseudosingularities. The proof of this statement was helpful in the proof of necessary and sufficient condition for a 3R robot to be cuspidal. The existence of reduced aspects was utilised to comment upon the maximum aspects in 3R robot too.

2. Proof of necessary and sufficient condition for a generic 3R robot to be cuspidal

The existence of a cusp in the locus of critical values of IKM of a 3R robot was shown to be a necessary and sufficient condition for a 3R robot to be cuspidal. It uses the geometric interpretation of IKM, the existence of reduced aspects as well as the sufficient condition already proven for generic 3R robots. This result is one of the most fundamental contributions of the thesis as we closed the conjecture for the condition of 3R robot to be cuspidal.

3. Multiple sufficient conditions for a robot to be cuspidal or noncuspidal

Extending further the geometric interpretation of IKM for 3R robot, the thesis presented various cases for a 3R robot to be either cuspidal or noncuspidal. The conditions derived are simple and intuitive. A clear advantage of classification based on geometry is that the analysis is generic and is applicable the greater number of classes of robot as compared to analytic conditions whose efficiency is challenged as we deviate from orthogonal architecture.

4. The maximum number of aspects in a generic 3R robot is four

The homotopy based classification of 3R robots presented in [Pag08] suspected the existence of 3(0, 0) and 4(0, 0) type of robots. The existence of 4(0, 0) robot suggested that it was possible for a generic 3R robot to have up to 5 aspects. The thesis presented a brief comment on the nonexistence of both, 3(0, 0) and 4(0, 0), classes of robot by using the geometric interpretation as well as the existence of reduced aspects. This concluded that the maximum number of aspects in generic 3R robot is four.

5. Cuspidality analysis of simplified 6r geometries

The thesis presented cuspidality analysis of simplified architectures of 6R robot. These robots are widely used in industries due to their simple architecture and simplifications in their kinematic analysis. The thesis extended the known results for robot with wrist at end to 6R robots with wrist at the beginning as well as in the middle of the architecture. It was shown that the cuspidality analysis of the architecture with wrist in middle is not straightforward and requires careful consideration. It was further shown by analysing $\det(\mathbf{J})$ that the presence of a 3R subchain in the architecture further simplifies the IKM and certain architectures of this class can result into noncuspidal robots.

6. Certified as well as numerical algorithms for deciding cuspidality of a nR non redundant robot

The thesis presented a certified algorithm for deciding cuspidality in 6R robots. Considering the issues in implementation, the thesis presented a numerical approach that considers the known results combined with $\det(\mathbf{J})$ analysis to accelerate the process. The numerical approach used discretization of the workspace and used HuPf algorithm to get

all the IKS of the end-effector instance. These IKS were then checked for connectivity by implementing an optimization methodology.

7. Issues in path planning of commercial cuspidal robots

The cuspidal robots have multiple regions with varying number of IKS in the workspace. Crossing these regions results into various cases that need consideration for a 6R robot. The dependence of feasibility as well as repeatability of a path on the choice of starting IKS was emphasized by showing an example from an existing commercial cuspidal robot. The thesis highlighted issues related to unique identification of 'configurations' in a commercial robot software. The thesis presented an important remark regarding the unsuitability of cuuspidal robots in collaborative applications.

8. Path planning framework for cuspidal robots

Considering the issues in 6R cuspidal robots, the thesis proposed a path planning framework for a 6R cuspidal robots. The framework considers all the cases arising in a cuspidal robot and is capable of suggesting a choice of IKS leading to a feasible and repeatable path. The framework can be used to utilise the existing commercial cuspidal robots to the best of their ability by avoiding unexpected behavior arising due to the cuspidality of a robot.

4.3.1 Future works

The work presented in the thesis closed some conjectures, and at the same time opened many questions related to cuspidality in nonredundant robots. Some of the possible extensions of the work are presented as follows:

Complete classification of generic 3R robots

The geometric interpretation of the IKM of 3R robot allows greater insights into cuspidality analysis of 3R robots. Many sufficient conditions were derived for a robot to be a binary or a quaternary robot through this analysis. A complete geometric classification of 3R robots can be done in the future.

Further study of palindromic robots

The robots discussed in chapter 4 with palindromic arrangement of motors resulted into a repeatable paths that was a nonsingular change of solutions as well. This is an interesting result and the properties of such robots can be studied in depth to understand the relation between the arrangement the nonsingular change of solutions.

Designing simplified architectures

In section 3.2, the thesis presented various robot classes whose det($\mathbf{J}$) factors into at least three components. This implies that there exists at least eight aspects in such robots. The robots analysed had either an orthogonal or parallel axes arrangement. As industries tend to have an offset in the wrist at the end for cobots, the future work can consider designs that are noncuspidal and an offset at the end of the architecture. Generic conditions on D-H parameters can be found by using the symbolic expression of det($\mathbf{J}$) such that factors into three components. The analysis of IKM using Study parameters might lead to insights on the nature of distribution of IKS depending on the architecture of the robot.

Identification of a noncuspidal 6R generic robot

In chapter 3, the thesis presented Conjecture 4 which stated that a generic 6R robot with more than 4 IKS is a cuspidal robot. The future work can study the 6R robots that are binary and generic. This work requires deeper analysis into theoretical kinematics and tools from algebraic geometry, geometric algebra and homotopy are envisaged in the study. It will be of great interest to the designers of robot architectures to have a necessary condition for a 6R robot to be noncuspidal. This will allow the designers with a reduced catalog of parameters to choose from leading to easier kinematic analysis and noncuspidal designs. This is important as the robots are collaborating more than ever with humans, and it is important that the next cobot we design is noncuspidal. One direction to be followed can be to prove that there does not exist a generic 6R robots will less than or equal to 4 IKS. This will imply that nongenericity in 6R robots is a necessary condition for cuspidality.

PUBLICATIONS RELATED TO THE DOCTORAL THESIS

Journal publications

[1] Durgesh Haribhau Salunkhe, Christoforos Spartalis, Jose Capco, Damien Chablat, Philippe Wenger, Necessary and sufficient condition for a generic 3R serial manipulator to be cuspidal, Mechanism and Machine Theory, Volume 171, 2022, https://doi.org/10.1016/j.mechmachtheory.2022.104729

[2] [Submitted] Durgesh Haribhau Salunkhe, Tobias Marauli, Andreas Müller, Damien Chablat, Philippe Wenger, 6R cuspidal robots: issues, identification, and path planning framework, International Journal of Robotics Research, 2023

Conference proceedings

[1] Durgesh Haribhau Salunkhe, Jose Capco, Damien Chablat, Philippe Wenger (2022). Geometry Based Analysis of 3R Serial Robots. In: Altuzarra, O., Kecskeméthy, A. (eds) Advances in Robot Kinematics 2022. ARK 2022. Springer Proceedings in Advanced Robotics, vol 24. Springer, Cham. https://doi.org/10.1007/978-3-031-08140-8_8

[2] Damien Chablat, Rémi Prébet, Mohab Safey El Din, Durgesh Haribhau Salunkhe, and Philippe Wenger. 2022. Deciding Cuspidality of Manipulators through Computer Algebra and Algorithms in Real Algebraic Geometry. In Proceedings of the 2022 International Symposium on Symbolic and Algebraic Computation (ISSAC '22). Association for Computing Machinery, New York, NY, USA, 439–448. https://doi.org/10.1145/3476446.3535477

[3] Durgesh Haribhau Salunkhe, Damien Chablat, and Philippe Wenger, Trajectory planning issues in cuspidal commercial robots, 2023 IEEE International Conference on Robotics and Automation (ICRA), London, United Kingdom, 2023, pp. 7426-7432, doi: 10.1109/ICRA48891.2023.10161444.

[4] Tobias Marauli, Durgesh Haribhau Salunkhe, Hubert Gattringer, Andreas Múller, Damien Chablat, Philippe Wenger, Time-Optimal Point-To-Point Motion Planning and Assembly Mode Change of Cuspidal Manipulators: Application to 3R and 6R Robots, 2023 IEEE/RSJ International Conference on Intelligent Robots and Systems (IROS), Detroit, United States of America, 2023

Appendix

A.1 IKM of a 3R serial chain

The symbolic conic equation for the inverse kinematic polynomial of a 3R serial chain is:

$$\frac{2\,a_2\,a_3^2\,c_3\,d_2\,s_3\,sa_2}{a_1^2}+\frac{2\,a_3\,ca_2\,d_2^2\,d_3\,s_3\,sa_2}{a_1^2}+\frac{2\,a_2\,a_3\,c_3\,ca_2\,d_2\,d_3}{a_1^2}+\frac{2\,a_3\,ca_1^2\,ca_2\,d_3\,s_3\,sa_2}{sa_1^2}-$$
$$d_3^2\,sa_2^2+\frac{a_3^2\,d_2^2\,s_3^2\,sa_2^2}{a_1^2}+\frac{a_3^3\,d_2\,s_3\,sa_2}{a_1^2}+\frac{a_3\,d_2^3\,s_3\,sa_2}{a_1^2}+\frac{a_2^2\,ca_2\,d_2\,d_3}{a_1^2}+\frac{a_2\,a_3\,c_3\,d_2^2}{a_1^2}+$$
$$\frac{a_2\,a_3\,c_3\,d_3^2}{a_1^2}+\frac{a_3^2\,ca_2\,d_2\,d_3}{a_1^2}+\frac{a_3^2\,ca_1^2\,s_3^2\,sa_2^2}{sa_1^2}+\frac{2\,ca_1^2\,ca_2\,d_2\,d_3}{sa_1^2}+2\,a_3\,ca_2\,d_3\,s_3\,sa_2+\frac{a_2^2\,a_3^2\,c_3^2}{a_1^2}+$$
$$\frac{ca_2^2\,d_2^2\,d_3^2}{a_1^2}+\frac{a_2^3\,a_3\,c_3}{a_1^2}+\frac{a_2\,a_3^3\,c_3}{a_1^2}+\frac{ca_2\,d_2^3\,d_3}{a_1^2}+\frac{ca_2\,d_2\,d_3^3}{a_1^2}+\frac{ca_1^2\,ca_2^2\,d_3^2}{sa_1^2}+$$
$$a_3\,d_2\,s_3\,sa_2-a_3^2\,c_3^2+\frac{a_2^4}{(4\,a_1^2)}+\frac{a_3^4}{(4\,a_1^2)}+\frac{d_2^4}{(4\,a_1^2)}+\frac{d_3^4}{(4\,a_1^2)}-a_3^2\,ca_2^2\,s_3^2+\frac{ca_1^2\,d_2^2}{sa_1^2}+$$
$$ca_2\,d_2\,d_3-a_2\,a_3\,c_3+\frac{a_2^2\,a_3\,d_2\,s_3\,sa_2}{a_1^2}+\frac{a_3\,d_2\,d_3^2\,s_3\,sa_2}{a_1^2}+\frac{2\,a_3\,ca_1^2\,d_2\,s_3\,sa_2}{sa_1^2}+\frac{a_1^2}{4}-$$
$$\frac{a_2^2}{2}+\frac{d_3^2}{2}+\frac{d_2^2}{2}+\frac{a_3^2}{2}-\frac{R}{2}+\frac{a_2^2\,d_3^2}{(2\,a_1^2)}+\frac{a_2^2\,a_3^2}{(2\,a_1^2)}+\frac{d_2^2\,d_3^2}{(2\,a_1^2)}+\frac{a_3^2\,d_3^2}{(2\,a_1^2)}+\frac{a_3^2\,d_2^2}{(2\,a_1^2)}+$$
$$\frac{a_2^2\,d_2^2}{(2\,a_1^2)}-\frac{d_3^2\,R}{(2\,a_1^2)}-\frac{d_2^2\,R}{(2\,a_1^2)}-\frac{a_3^2\,R}{(2\,a_1^2)}-\frac{a_2^2\,R}{(2\,a_1^2)}+\frac{R^2}{(4\,a_1^2)}-\frac{2\,ca_1\,ca_2\,d_3\,z}{sa_1^2}-\frac{a_2\,a_3\,c_3\,R}{a_1^2}-$$
$$\frac{ca_2\,d_2\,d_3\,R}{a_1^2}+\frac{z^2}{sa_1^2}-\frac{2\,ca_1\,d_2\,z}{sa_1^2}-\frac{a_3\,d_2\,R\,s_3\,sa_2}{a_1^2}-\frac{2\,a_3\,ca_1\,z\,s_3\,sa_2}{sa_1^2} \tag{A.1}$$

Here, sa_1 and sa_2 stands for $\sin\alpha_1$ and $\sin\alpha_2$, and ca_1 and ca_2 stands for $\cos\alpha_1$ and $\cos\alpha_2$. $a_{1..3}$, $d_{1..3}$ are the D-H parameters for the 3R serial robot. Let x, y, z be the x, y and z-coordinates of the end-effector position, $R = x^2 + y^2 + z^2$. c_3 stands for $\cos\theta_3$ and s_3 stands for $\sin\theta_3$.

If (A.1) is rearranged as:

$$A_{xx}\, c_3^2 + 2A_{xy}\, c_3 s_3 + A_{yy}\, s_3^2 + 2B_x\, c_3 + 2B_y\, s_3 + C = 0 \tag{A.2}$$

then,

$$A_{xx} = -a_3^2 + \frac{a_2^2\, a_3^2}{a_1^2} \tag{A.3}$$

$$A_{xy} = \frac{2\, a_2\, a_3^2\, d_2\, sa_2}{a_1^2} \tag{A.4}$$

$$A_{yy} = \frac{a_3^2 d_2^2\, sa_2^2}{a_1^2} + \frac{a_3^2\, ca_1^2\, sa_2^2}{sa_1^2} - a_3^2\, ca_2^2 \tag{A.5}$$

$$B_x = -a_2 a_3 + \frac{a_2 a_3 d_2^2}{a_1^2} + \frac{a_2 a_3 d_3^2}{a_1^2} - \frac{a_2 a_3\, R}{a_1^2} + \frac{a_2^3 a_3}{a_1^2} + \frac{a_2 a_3^3}{a_1^2} + \frac{2 a_2 a_3 ca_2 d_2 d_3}{a_1^2} \tag{A.6}$$

$$B_y = \frac{a_3^3\, d_2\, sa_2}{a_1^2} + \frac{a_3\, d_2^3\, sa_2}{a_1^2} + a_3\, d_2\, sa_2 + \frac{2\, a_3\, ca_2\, d_2^2\, d_3\, sa_2}{a_1^2} + \frac{2\, a_3\, ca_1^2\, ca_2\, d_3\, sa_2}{sa_1^2} \tag{A.7}$$

$$+ \frac{a_2^2\, a_3\, d_2\, sa_2}{a_1^2} + \frac{a_3\, d_2\, d_3^2\, sa_2}{a_1^2} - \frac{a_3\, d_2\, R\, sa_2}{a_1^2} + \frac{2\, a_3\, ca_1^2\, d_2\, sa_2}{sa_1^2} - \tag{A.8}$$

$$\frac{2\, a_3\, ca_1\, z\, sa_2}{sa_1^2} + 2\, a_3\, ca_2\, d_3\, sa_2 \tag{A.9}$$

$$C = \frac{1}{4\, a_1^2\, sa_1^2}\, ((d_3^4 + 4\, ca_2\, d_2\, d_3^3 + \tag{A.10}$$

$$((4\, ca_2^2 + 2)\, d_2^2 + (-4\, sa_2^2 + 2)\, a_1^2 + 2\, a_2^2 + 2\, a_3^2 - 2\, R)\, d_3^2 + \tag{A.11}$$

$$4\, d_2\, ca_2\, (a_1^2 + a_2^2 + a_3^2 + d_2^2 - R)\, d3 + (a_1^2 - 2\, a_1\, a_2 + a_2^2 + a_3^2 + d_2^2 - R) \tag{A.12}$$

$$(a_1^2 + 2\, a_1\, a_2 + a_2^2 + a_3^2 + d_2^2 - R))\, sa_1^2 + 4\, a_1^2\, (ca_1\, ca_2\, d_3 + ca_1\, d_2 - z)^2) \tag{A.13}$$

A.2 Geometric analysis of 3R serial robots

$$\begin{aligned} f(z) = {} & -a_1^2\, sa_1^4\, sa_2^2 + a_1^2\, sa_1^2\, sa_2^4 + a_2^2\, sa_1^4\, sa_2^2 - a_2^2\, sa_1^2\, sa_2^4 + a_3^2\, sa_1^4\, sa_2^2 - a_3^2\, sa_1^2\, sa_2^4 + \\ & d_3^2\, sa_1^4\, sa_2^2 - d_3^2\, sa_1^2\, sa_2^4 + 2\, \sqrt{a_1^2\, sa_1^2 - a_1^2\, sa_2^2 - a_2^2\, sa_1^2 + a_2^2\, sa_2^2}\, d_3\, ca_2\, sa_2\, sa_1^3 - \\ & 2\, ca_1\, \sqrt{a_1^2\, sa_1^2 - a_1^2\, sa_2^2 - a_2^2\, sa_1^2 + a_2^2\, sa_2^2}\, sa_1\, sa_2^3\, \mathbf{z} + a_1^2\, sa_1^4 - \\ & a_1^2\, sa_2^4 - a_2^2\, sa_1^4 + a_2^2\, sa_2^4 \end{aligned} \tag{A.14}$$

Here, sa_1 and sa_2 stands for $\sin\alpha_1$ and $\sin\alpha_2$, and ca_1 and ca_2 stands for $\cos\alpha_1$ and $\cos\alpha_2$.

$a_{1..3}$, $d_{1..3}$ are the D-H parameters for the 3R serial robot. $\mathbf{z}$ is emboldened to highlight the function is dependent on z, and does not mean that $\mathbf{z}$ is a vector.

A.3 Determinant of Jacobian matrix

The symbolic expression for the determinant of the Jacobian with the wrist in the middle and $d_2 = 0$:

$$
\begin{aligned}
\det \mathbf{J} = {} & \sin(\alpha_2)\sin(\theta_3)\sin(\alpha_3)(-\sin(\alpha_2)\cos(\alpha_3)\cos(\theta_4)(\cos(\alpha_4))^2\cos(\theta_3)\sin(\theta_5)\sin(\alpha_5)d_4\,d_5 \\
& + \sin(\alpha_2)\cos(\alpha_3)\cos(\theta_4)(\cos(\alpha_4))^2\cos(\theta_3)\cos(\theta_5)\cos(\alpha_5)a_5\,d_4 + \sin(\alpha_2)\sin(\alpha_3)\sin(\alpha_4)\cos(\alpha_4) \\
& \cos(\theta_3)\sin(\theta_5)\sin(\alpha_5)d_4\,d_5 - \sin(\alpha_2)\sin(\alpha_3)\sin(\alpha_4)\cos(\alpha_4)\cos(\theta_3)\cos(\theta_5)\cos(\alpha_5)a_5\,d_4 + \sin(\alpha_2) \\
& \sin(\alpha_3)\cos(\alpha_4)\cos(\theta_3)\cos(\theta_5)\sin(\alpha_5)a_4\,d_5 + \sin(\alpha_2)\cos(\alpha_3)\cos(\theta_4)\cos(\theta_3) \\
& \sin(\theta_5)\sin(\alpha_5)d_4\,d_5 - \sin(\alpha_2)\cos(\alpha_3)\cos(\theta_4)\cos(\theta_3)\cos(\theta_5)\cos(\alpha_5)a_5\,d_4 - \cos(\alpha_2)\sin(\alpha_3) \\
& \sin(\theta_4)\sin(\alpha_4)\sin(\theta_5)\sin(\alpha_5)a_4\,d_4 - \cos(\alpha_2)\sin(\alpha_3)\sin(\alpha_4)\cos(\theta_4)\cos(\alpha_4)\sin(\alpha_5)a_5\,d_4 \\
& + \cos(\alpha_2)\sin(\alpha_3)\sin(\alpha_4)\cos(\theta_4)\sin(\theta_5)\cos(\alpha_5)a_4\,a_5 + \cos(\alpha_2)\sin(\alpha_3)\sin(\alpha_4)\cos(\theta_4)\cos(\theta_5) \\
& \sin(\alpha_5)a_4\,d_5 - \cos(\alpha_2)\cos(\alpha_3)\sin(\alpha_4)\cos(\alpha_4)\sin(\theta_5)\sin(\alpha_5)d_4\,d_5 + \cos(\alpha_2)\cos(\alpha_3)\sin(\alpha_4) \\
& \cos(\alpha_4)\cos(\theta_5)\cos(\alpha_5)a_5\,d_4 + \sin(\alpha_2)\sin(\theta_3)\sin(\theta_4)(\cos(\alpha_4))^2\sin(\theta_5)\sin(\alpha_5)d_4\,d_5 - \sin(\alpha_2) \\
& \sin(\theta_3)\sin(\theta_4)(\cos(\alpha_4))^2\cos(\theta_5)\cos(\alpha_5)a_5\,d_4 - \cos(\alpha_2)\sin(\alpha_3)\cos(\theta_4)(\cos(\alpha_4))^2\sin(\theta_5)\sin(\alpha_5) \\
& d_4\,d_5 + \cos(\alpha_2)\sin(\alpha_3)\cos(\theta_4)(\cos(\alpha_4))^2\cos(\theta_5)\cos(\alpha_5)a_5\,d_4 + \sin(\alpha_2)\sin(\theta_3)\sin(\theta_4)\sin(\alpha_4) \\
& \cos(\alpha_4)\sin(\alpha_5)a_5\,d_4 - \sin(\alpha_2)\sin(\theta_3)\sin(\theta_4)\sin(\alpha_4)\sin(\theta_5)\cos(\alpha_5)a_4\,a_5 - \sin(\alpha_2)\sin(\theta_3)\sin(\theta_4) \\
& \sin(\alpha_4)\cos(\theta_5)\sin(\alpha_5)a_4\,d_5 - \sin(\alpha_2)\sin(\theta_3)\sin(\alpha_4)\cos(\theta_4)\sin(\theta_5)\sin(\alpha_5)a_4\,d_4 + \\
& \sin(\alpha_2)\sin(\alpha_3)\cos(\alpha_4)\cos(\theta_3)\sin(\theta_5)\cos(\alpha_5)a_4\,a_5 - \cos(\alpha_2)\cos(\alpha_3)\sin(\alpha_5) \\
& a_5\,d_4 - \sin(\alpha_2)\sin(\theta_4)\cos(\alpha_3)\sin(\alpha_4)\cos(\theta_3)\sin(\theta_5)\sin(\alpha_5)a_4\,d_4 - \sin(\alpha_2)\cos(\alpha_3)\sin(\alpha_4)\cos(\theta_4) \\
& \cos(\alpha_4)\cos(\theta_3)\sin(\alpha_5)a_5\,d_4 + \sin(\alpha_2)\cos(\alpha_3)\sin(\alpha_4)\cos(\theta_4)\cos(\theta_3)\sin(\theta_5)\cos(\alpha_5)a_4\,a_5 \\
& + \sin(\alpha_2)\cos(\alpha_3)\sin(\alpha_4)\cos(\theta_4)\cos(\theta_3)\cos(\theta_5)\sin(\alpha_5)a_4\,d_5 - \\
& \sin(\alpha_2)\sin(\theta_4)\cos(\alpha_3)\cos(\theta_3)\sin(\alpha_5)a_4\,a_5 + \cos(\alpha_2)\sin(\alpha_3)\cos(\theta_4)\sin(\theta_5)\sin(\alpha_5)d_4\,d_5 - \cos \\
& (\alpha_2)\sin(\alpha_3)\cos(\theta_4)\cos(\theta_5)\cos(\alpha_5)a_5\,d_4 - \cos(\alpha_2)\cos(\alpha_3)\cos(\alpha_4)\sin(\theta_5)\cos(\alpha_5)a_4\,a_5 - \cos(\alpha_2) \\
& \cos(\alpha_3)\cos(\alpha_4)\cos(\theta_5)\sin(\alpha_5)a_4\,d_5 + \sin(\alpha_2)\sin(\alpha_3)\sin(\alpha_4)\cos(\theta_3)\sin(\theta_5)\sin \\
& (\alpha_5){d_4}^2 - \sin(\alpha_2)\sin(\alpha_3)(\cos(\alpha_4))^2\cos(\theta_3)\sin(\alpha_5)a_5 \\
& d_4 - \sin(\alpha_2)\sin(\theta_4)\cos(\alpha_3)\cos(\theta_3)\cos(\theta_5)\sin(\alpha_5){a_4}^2 - \sin(\alpha_2)\sin(\theta_3)\sin \\
& (\theta_4)\sin(\theta_5)\sin(\alpha_5)d_4\,d_5 + \sin(\alpha_2)\sin(\theta_3)\sin(\theta_4)\cos(\theta_5)\cos(\alpha_5)a_5\,d_4 + \sin \\
& (\alpha_2)\sin(\alpha_3)\cos(\theta_3)\cos(\theta_5)\sin(\alpha_5)a_4\,d_4) \\
& + \sin(\alpha_2)\sin(\theta_3)\sin(\alpha_3)(-\sin(\alpha_2)\sin(\theta_3)\cos(\theta_4)\cos(\theta_5)\sin \\
& (\alpha_5){a_4}^2 - \cos(\alpha_2)\sin(\alpha_3)\sin(\theta_4)\cos(\theta_5)\sin(\alpha_5){a_4}^2 - \cos(\alpha_2) \\
& \cos(\alpha_3)\sin(\alpha_4)\sin(\theta_5)\sin(\alpha_5)d_4^2 + \cos(\alpha_2)\cos(\alpha_3) \\
& (\cos(\alpha_4))^2\sin(\alpha_5)a_5\,d_4 - \sin(\alpha_2)\sin(\theta_3)\cos(\theta_4)\sin(\alpha_5) \\
& a_4\,a_5 + \sin(\alpha_2)\sin(\alpha_3)\cos(\theta_3)\sin(\alpha_5)a_5\,d_4 - \cos(\alpha_2)\sin \\
& (\alpha_3)\sin(\theta_4)\sin(\alpha_5)a_4\,a_5 - \cos(\alpha_2)\cos(\alpha_3)\cos(\theta_5)\sin(\alpha_5)a_4\,d_4)a_1
\end{aligned}
\tag{A.15}
$$

A.4 Certified algorithm to decide cuspidality of 6R robots

Problem statement Let $\boldsymbol{f} = (f_1, \ldots, f_s)$ be a sequence of polynomials in $\mathbb{Q}[x_1, \ldots, x_n]$ and $V = \boldsymbol{V}(\boldsymbol{f}) \subset \mathbb{C}^n$ be the algebraic set it defines (i.e. the set of common complex solutions to the f_i's). We denote by $V_{\mathbb{R}} = V \cap \mathbb{R}^n$ the real trace of V. Let $\mathcal{R} = (r_1, \ldots, r_d)$ be a sequence of polynomials in $\mathbb{Q}[x_1, \ldots, x_n]$. By a slight abuse of notation, we still denote by $\mathcal{R}$ the map

$$\mathcal{R} : \boldsymbol{y} \in \mathbb{C}^n \mapsto (r_1(\boldsymbol{y}), \ldots, r_d(\boldsymbol{y})) \in \mathbb{C}^d.$$

In the following algorithm, we make the following assumption:

(A) the ideal generated by $\boldsymbol{f}$, which we denote by $\langle \boldsymbol{f} \rangle$, is radical and equidimensional of dimension d and $V_{\mathbb{R}}$ is not contained in the singular set of V.

We denote by $\mathrm{crit}(\mathcal{R}, V)$ the union of the set of *critical points* of the restriction of $\mathcal{R}$ to V and the set of *singular points* of V (see e.g. [SEDS17, Appendix A.2.] for a definition of these objects). Further, we denote by $\mathrm{sval}(\mathcal{R}, V)$ the set of *singular values* of the restriction of $\mathcal{R}$ to V, i.e. the image by $\mathcal{R}$ of the set $\mathrm{crit}(\mathcal{R}, V)$:

$$\mathrm{sval}(\mathcal{R}, V) = \mathcal{R}(\mathrm{crit}(\mathcal{R}, V)).$$

Under assumption (A), the set $\mathrm{crit}(\mathcal{R}, V)$ is the set of common complex solutions to the polynomials in $\boldsymbol{f}$ and the set of minors of size n of the Jacobian matrix $\mathrm{Jac}[\boldsymbol{f}, \mathcal{R}]$ associated to $\boldsymbol{f}, \mathcal{R}$ (see e.g. [SEDS17, Lemma A.2.]).

The restriction of the map $\mathcal{R}$ to V is said to be proper at a point $\boldsymbol{y} \in \mathbb{C}^d$ if there exists a ball $B \subset \mathbb{C}^d$ containing $\boldsymbol{y}$ such that $\mathcal{R}^{-1}(B) \cap V$ is closed and bounded. The restriction of $\mathcal{R}$ to V is said to be proper if it is proper at every point of $\mathbb{C}^d$.

We denote by $\mathrm{nprop}(\mathcal{R}, V)$ be the set of points of $\mathbb{C}^d$ at which $\mathcal{R}$ is *not* proper. According to [Jel99, Theorem 3.8.] it is contained in a proper algebraic set of $\mathbb{C}^d$.

Finally we denote by $\mathrm{atyp}(\mathcal{R}, V)$ the set of *atypical values* of the restriction of $\mathcal{R}$ to V, that is the union $\mathrm{sval}(\mathcal{R}, V) \cup \mathrm{nprop}(\mathcal{R}, V)$, and let

$$\mathcal{R}, V) = \mathcal{R}^{-1}(\mathrm{atyp}(\mathcal{R}, V)) \cap V$$

the set of *special points* of the restriction of $\mathcal{R}$ to V that map to atypical values. We denote by $\overline{\mathrm{atyp}(\mathcal{R}, V)}^z$ the Zariski closure in $\mathbb{C}^d$ of the set of atypical values.

Following the formalism introduced in [Wen92], we say that the restriction of the map $\mathcal{R}$ to $V_{\mathbb{R}}$ is *cuspidal* if there exist two distinct points $\boldsymbol{y}$ and $\boldsymbol{y}'$ in $V_{\mathbb{R}}$ such that the following holds:

(i) $\mathcal{R}(\boldsymbol{y}) = \mathcal{R}(\boldsymbol{y}')$;

(ii) there exists a connected component$C$ of $V_{\mathbb{R}} - \mathrm{crit}(\mathcal{R}, V)$ which contains both $\boldsymbol{y}$ and $\boldsymbol{y}'$.

If two such points $\boldsymbol{y}$ and $\boldsymbol{y}'$ exist, we say that they form a *cuspidal couple* of the restriction of $\mathcal{R}$ to $V_{\mathbb{R}}$. Note that such a couple is not unique in general. The following algorithm 2 takes as input $\boldsymbol{f}$ and $\mathcal{R}$, satisfying (A) and which decides the cuspidality of the restriction of $\mathcal{R}$ to the real solution set $V_{\mathbb{R}} = V \cap \mathbb{R}^n$ where $V = \boldsymbol{V}(\boldsymbol{f})$.

It proceeds by computing a zero-dimensional parametrization $\mathscr{P}$ of a set of points that provides cuspidal couples of the restriction of $\mathcal{R}$ to $V_{\mathbb{R}}$ whenever such a couple exists. In other words, if no cuspidal couple can be found among $Z(\mathscr{P})$, then the restriction of $\mathcal{R}$ to $V_{\mathbb{R}}$ is not cuspidal.

Hence, to solve our cuspidality problem, it suffices to compute a graph which is isotopy equivalent to a roadmap of $V_{\mathbb{R}} - \mathrm{crit}(\mathcal{R}, V)$ connecting the points of $Z(\mathscr{P})$ that lie in the same connected componentof $V_{\mathbb{R}} - \mathrm{crit}(\mathcal{R}, V)$.

In addition to the high-level procedures presented in the previous section, we use here some basic subroutines to manipulate rational parametrizations, polynomials and graphs. In the following, $\mathscr{P}_\emptyset$ will denote a zero-dimensional parametrization of $\mathbb{R}^n$ encoding the empty set, and () will denote the empty sequence. Besides, given a polynomial sequence $\boldsymbol{h} = (h_i)_{1 \leq i \leq \iota}$ we will note $\pm\boldsymbol{h} = (\pm h_i)_{1 \leq i \leq \iota}$.

The procedure Union takes as input two zero-dimensional parametrizations $\mathscr{P}$ and $\mathscr{P}'$ of degree $\delta_{\mathscr{P}}$ and $\delta_{\mathscr{P}'}$ and returns a zero-dimensional parametrization of $Z(\mathscr{P}) \cup Z(\mathscr{P}')$ of degree $\delta_{\mathscr{P}} + \delta_{\mathscr{P}'}$. See [SEDS17, Lemma J.3.] for a description of this procedure.

The procedures Crit and AtypicalValues take as input a polynomial map $\mathcal{R}$ and a finite sequence of polynomials $\boldsymbol{h}$. Assuming that $\boldsymbol{h}$ satisfies assumption (A), these two procedures output finite sequences of polynomials whose complex zero-sets are respectively $\mathrm{crit}(\mathcal{R}, \boldsymbol{V}(\boldsymbol{h}))$ and a proper subset of $\mathbb{C}^d$ containing $\overline{\mathrm{atyp}(\mathcal{R}, \boldsymbol{V}(\boldsymbol{h}))}^z$. We refer to [SEDS17, Lemma A.2] for a description of Crit.

Let $\mathscr{G} = (\mathcal{V}, \mathcal{E})$ be a graph and let $v, v' \in \mathcal{V}$ be two vertices. We say that v and v' are connected in $\mathscr{G}$ if there exists a sequence $(v_1, \ldots, v_m)$ of vertices in $\mathcal{V}$ such that for all $1 \leq i < m$,

$$v_1 = v, \quad v_2 = v' \quad \text{and} \quad \{v_i, v_{i+1}\} \in \mathcal{E}.$$

The procedure GraphConnected takes as input $\mathscr{G} = (\mathcal{V}, \mathcal{E})$ and (v, v') and outputs `True` if and only if v and v' are connected in $\mathscr{G}$. Else it outputs `False`. This subroutine is classic among graph problems, and can be done using well-know algorithms such as the breadth-first search algorithm [Cor+09, Section 22.2].

Algorithm 2 Cuspidality algorithm

Require: Two sequences $\boldsymbol{f} = (f_1, \ldots, f_s)$ and $\mathcal{R} = (r_1, \ldots, r_d)$ of polynomials in $\mathbb{Q}[x_1, \ldots, x_n]$ that satisfy assumption (A).

Ensure: A decision, `True` or `False`, on the cuspidality of the restriction of $\mathcal{R}$ to $V_{\mathbb{R}} = V \cap \mathbb{R}^n$ where $V = \boldsymbol{V}(\boldsymbol{f})$.

$\boldsymbol{g} \leftarrow$AtypicalValues$(\mathcal{R}, \boldsymbol{f})$;
$\mathcal{Q} \leftarrow$SamplePointsRational$(\boldsymbol{g})$;
$\mathscr{P} \leftarrow \mathscr{P}_{\emptyset}$;
for $\boldsymbol{q} = (\boldsymbol{q}_1, \ldots, \boldsymbol{q}_d) \in \mathcal{Q}$ **do**
    $\mathcal{R}_{\boldsymbol{q}} \leftarrow (r_1 - \boldsymbol{q}_1, \ldots, r_d - \boldsymbol{q}_d)$;
    $\mathscr{P}_{\boldsymbol{q}} \leftarrow$SamplePoints$((\boldsymbol{f}, \mathcal{R}_{\boldsymbol{q}}), ())$;
    $\mathscr{P} \leftarrow$Union$(\mathscr{P}, \mathscr{P}_{\boldsymbol{q}})$;
end for
$\Delta \leftarrow$ Crit$(\mathcal{R}, \boldsymbol{f})$;
$\mathscr{R} \leftarrow$Roadmap$(\boldsymbol{f}, \pm\Delta, \mathscr{P})$;
$\left(\mathscr{G} = (\mathcal{V}, \mathcal{E}), \text{Vert}_{\mathscr{G}}\right) \leftarrow$GraphIsotop$(\mathscr{R}, \pm\Delta, \mathscr{P})$;
for $\boldsymbol{q} \in \mathcal{Q}$ **do**
    $\mathcal{V}_{\boldsymbol{q}} \leftarrow$Vert$_{\mathscr{G}}(\mathscr{P}_{\boldsymbol{q}})$;
    for $(\boldsymbol{v}_1, \boldsymbol{v}_2) \in \mathcal{V}_{\boldsymbol{q}}^2$ **do**
        if GraphConnected$((\boldsymbol{v}_1, \boldsymbol{v}_2), \mathscr{G})$ and $\boldsymbol{v}_1 \neq \boldsymbol{v}_2$ **then**
            return `True`;
        end if
    end for
end for
return `False`.

A.5 Simplified architectures with $\det(\mathbf{J})$ with three components

d_1	d_2	d_3	d_4	d_5	d_6	a_1	a_2	a_3	a_4	a_5	a_6	α_1	α_2	α_3	α_4	α_5	α_6
d_1	d_2	d_3	d_4	d_5	d_6	a_1	a_2	a_3	a_4	a_5	a_6	$\frac{\pi}{2}$	$\frac{\pi}{2}$	$\frac{\pi}{2}$	0	0	α_6
d_1	d_2	d_3	d_4	d_5	d_6	a_1	a_2	a_3	a_4	a_5	a_6	$\frac{\pi}{2}$	$\frac{\pi}{2}$	0	0	$\frac{\pi}{2}$	α_6
d_1	d_2	d_3	d_4	d_5	d_6	a_1	a_2	a_3	a_4	a_5	a_6	$\frac{\pi}{2}$	0	$\frac{\pi}{2}$	0	0	α_6
d_1	d_2	d_3	d_4	d_5	d_6	a_1	a_2	a_3	a_4	a_5	a_6	$\frac{\pi}{2}$	0	0	$\frac{\pi}{2}$	$\frac{\pi}{2}$	α_6
d_1	d_2	d_3	d_4	d_5	d_6	a_1	a_2	a_3	a_4	a_5	a_6	$\frac{\pi}{2}$	0	0	$\frac{\pi}{2}$	0	α_6
d_1	d_2	d_3	d_4	d_5	d_6	a_1	a_2	a_3	a_4	a_5	a_6	0	$\frac{\pi}{2}$	$\frac{\pi}{2}$	0	0	α_6
d_1	d_2	d_3	d_4	d_5	d_6	a_1	a_2	a_3	a_4	a_5	a_6	0	$\frac{\pi}{2}$	0	0	$\frac{\pi}{2}$	α_6
d_1	d_2	d_3	d_4	d_5	d_6	a_1	a_2	a_3	a_4	a_5	a_6	0	0	$\frac{\pi}{2}$	$\frac{\pi}{2}$	$\frac{\pi}{2}$	α_6
d_1	d_2	d_3	d_4	d_5	d_6	a_1	a_2	a_3	a_4	a_5	a_6	0	0	$\frac{\pi}{2}$	$\frac{\pi}{2}$	0	α_6
d_1	d_2	d_3	d_4	d_5	d_6	a_1	a_2	a_3	a_4	a_5	a_6	0	0	$\frac{\pi}{2}$	0	$\frac{\pi}{2}$	α_6
d_1	d_2	d_3	d_4	d_5	d_6	a_1	a_2	a_3	a_4	0	a_6	$\frac{\pi}{2}$	$\frac{\pi}{2}$	0	0	$\frac{\pi}{2}$	α_6
d_1	d_2	d_3	d_4	d_5	d_6	a_1	a_2	a_3	a_4	0	a_6	$\frac{\pi}{2}$	0	0	$\frac{\pi}{2}$	$\frac{\pi}{2}$	α_6
d_1	d_2	d_3	d_4	d_5	d_6	a_1	a_2	a_3	a_4	0	a_6	0	$\frac{\pi}{2}$	0	0	$\frac{\pi}{2}$	α_6
d_1	d_2	d_3	d_4	d_5	d_6	a_1	a_2	a_3	a_4	0	a_6	0	0	$\frac{\pi}{2}$	$\frac{\pi}{2}$	$\frac{\pi}{2}$	α_6
d_1	d_2	d_3	d_4	d_5	d_6	a_1	a_2	a_3	a_4	0	a_6	0	0	$\frac{\pi}{2}$	0	$\frac{\pi}{2}$	α_6
d_1	d_2	d_3	d_4	d_5	d_6	a_1	a_2	a_3	0	a_5	a_6	$\frac{\pi}{2}$	0	0	$\frac{\pi}{2}$	$\frac{\pi}{2}$	α_6
d_1	d_2	d_3	d_4	d_5	d_6	a_1	a_2	a_3	0	a_5	a_6	$\frac{\pi}{2}$	0	0	$\frac{\pi}{2}$	0	α_6
d_1	d_2	d_3	d_4	d_5	d_6	a_1	a_2	a_3	0	a_5	a_6	0	0	$\frac{\pi}{2}$	$\frac{\pi}{2}$	$\frac{\pi}{2}$	α_6
d_1	d_2	d_3	d_4	d_5	d_6	a_1	a_2	a_3	0	a_5	a_6	0	0	$\frac{\pi}{2}$	$\frac{\pi}{2}$	0	α_6
d_1	d_2	d_3	d_4	d_5	d_6	a_1	a_2	a_3	0	0	a_6	$\frac{\pi}{2}$	0	0	$\frac{\pi}{2}$	$\frac{\pi}{2}$	α_6
d_1	d_2	d_3	d_4	d_5	d_6	a_1	a_2	a_3	0	0	a_6	0	0	$\frac{\pi}{2}$	$\frac{\pi}{2}$	$\frac{\pi}{2}$	α_6
d_1	d_2	d_3	d_4	d_5	d_6	a_1	a_2	0	a_4	a_5	a_6	$\frac{\pi}{2}$	$\frac{\pi}{2}$	$\frac{\pi}{2}$	0	0	α_6
d_1	d_2	d_3	d_4	d_5	d_6	a_1	a_2	0	a_4	a_5	a_6	$\frac{\pi}{2}$	0	$\frac{\pi}{2}$	0	0	α_6
d_1	d_2	d_3	d_4	d_5	d_6	a_1	a_2	0	a_4	a_5	a_6	0	$\frac{\pi}{2}$	$\frac{\pi}{2}$	0	0	α_6
d_1	d_2	d_3	d_4	d_5	d_6	a_1	a_2	0	a_4	a_5	a_6	0	0	$\frac{\pi}{2}$	$\frac{\pi}{2}$	$\frac{\pi}{2}$	α_6
d_1	d_2	d_3	d_4	d_5	d_6	a_1	a_2	0	a_4	a_5	a_6	0	0	$\frac{\pi}{2}$	$\frac{\pi}{2}$	0	α_6
d_1	d_2	d_3	d_4	d_5	d_6	a_1	a_2	0	a_4	a_5	a_6	0	0	$\frac{\pi}{2}$	0	$\frac{\pi}{2}$	α_6
d_1	d_2	d_3	d_4	d_5	d_6	a_1	a_2	0	a_4	0	a_6	0	0	$\frac{\pi}{2}$	$\frac{\pi}{2}$	$\frac{\pi}{2}$	α_6
d_1	d_2	d_3	d_4	d_5	d_6	a_1	a_2	0	a_4	0	a_6	0	0	$\frac{\pi}{2}$	0	$\frac{\pi}{2}$	α_6
d_1	d_2	d_3	d_4	d_5	d_6	a_1	a_2	0	0	a_5	a_6	0	0	$\frac{\pi}{2}$	$\frac{\pi}{2}$	$\frac{\pi}{2}$	α_6
d_1	d_2	d_3	d_4	d_5	d_6	a_1	a_2	0	0	a_5	a_6	0	0	$\frac{\pi}{2}$	$\frac{\pi}{2}$	0	α_6
d_1	d_2	d_3	d_4	d_5	d_6	a_1	a_2	0	0	0	a_6	0	0	$\frac{\pi}{2}$	$\frac{\pi}{2}$	$\frac{\pi}{2}$	α_6
d_1	d_2	d_3	d_4	d_5	d_6	a_1	0	a_3	a_4	a_5	a_6	$\frac{\pi}{2}$	$\frac{\pi}{2}$	$\frac{\pi}{2}$	0	0	α_6
d_1	d_2	d_3	d_4	d_5	d_6	a_1	0	a_3	a_4	a_5	a_6	$\frac{\pi}{2}$	$\frac{\pi}{2}$	0	0	$\frac{\pi}{2}$	α_6
d_1	d_2	d_3	d_4	d_5	d_6	a_1	0	a_3	a_4	a_5	a_6	0	$\frac{\pi}{2}$	$\frac{\pi}{2}$	0	0	α_6
d_1	d_2	d_3	d_4	d_5	d_6	a_1	0	a_3	a_4	a_5	a_6	0	$\frac{\pi}{2}$	0	0	$\frac{\pi}{2}$	α_6
d_1	d_2	d_3	d_4	d_5	d_6	a_1	0	a_3	a_4	0	a_6	$\frac{\pi}{2}$	$\frac{\pi}{2}$	0	0	$\frac{\pi}{2}$	α_6
d_1	d_2	d_3	d_4	d_5	d_6	a_1	0	a_3	a_4	0	a_6	0	$\frac{\pi}{2}$	0	0	$\frac{\pi}{2}$	α_6
d_1	d_2	d_3	d_4	d_5	d_6	a_1	0	0	a_4	a_5	a_6	$\frac{\pi}{2}$	$\frac{\pi}{2}$	$\frac{\pi}{2}$	0	0	α_6
d_1	d_2	d_3	d_4	d_5	d_6	a_1	0	0	a_4	a_5	a_6	0	$\frac{\pi}{2}$	$\frac{\pi}{2}$	0	0	α_6
d_1	d_2	d_3	d_4	0	d_6	a_1	a_2	a_3	a_4	a_5	a_6	$\frac{\pi}{2}$	$\frac{\pi}{2}$	$\frac{\pi}{2}$	0	0	α_6
d_1	d_2	d_3	d_4	0	d_6	a_1	a_2	a_3	a_4	a_5	a_6	$\frac{\pi}{2}$	$\frac{\pi}{2}$	0	0	$\frac{\pi}{2}$	α_6
d_1	d_2	d_3	d_4	0	d_6	a_1	a_2	a_3	a_4	a_5	a_6	$\frac{\pi}{2}$	0	$\frac{\pi}{2}$	0	0	α_6

Table A.1 – The D-H parameter values of robots whose det(**J**) factors into three components.

d_1	d_2	d_3	d_4	d_5	d_6	a_1	a_2	a_3	a_4	a_5	a_6	α_1	α_2	α_3	α_4	α_5	α_6
d_1	d_2	d_3	d_4	0	d_6	a_1	a_2	a_3	a_4	a_5	a_6	$\frac{\pi}{2}$	0	0	$\frac{\pi}{2}$	$\frac{\pi}{2}$	α_6
d_1	d_2	d_3	d_4	0	d_6	a_1	a_2	a_3	a_4	a_5	a_6	$\frac{\pi}{2}$	0	0	$\frac{\pi}{2}$	0	α_6
d_1	d_2	d_3	d_4	0	d_6	a_1	a_2	a_3	a_4	a_5	a_6	0	$\frac{\pi}{2}$	$\frac{\pi}{2}$	0	0	α_6
d_1	d_2	d_3	d_4	0	d_6	a_1	a_2	a_3	a_4	a_5	a_6	0	$\frac{\pi}{2}$	0	0	$\frac{\pi}{2}$	α_6
d_1	d_2	d_3	d_4	0	d_6	a_1	a_2	a_3	a_4	a_5	a_6	0	0	$\frac{\pi}{2}$	$\frac{\pi}{2}$	$\frac{\pi}{2}$	α_6
d_1	d_2	d_3	d_4	0	d_6	a_1	a_2	a_3	a_4	a_5	a_6	0	0	$\frac{\pi}{2}$	$\frac{\pi}{2}$	0	α_6
d_1	d_2	d_3	d_4	0	d_6	a_1	a_2	a_3	a_4	a_5	a_6	0	0	$\frac{\pi}{2}$	0	$\frac{\pi}{2}$	α_6
d_1	d_2	d_3	d_4	0	d_6	a_1	a_2	a_3	a_4	0	a_6	$\frac{\pi}{2}$	$\frac{\pi}{2}$	0	0	$\frac{\pi}{2}$	α_6
d_1	d_2	d_3	d_4	0	d_6	a_1	a_2	a_3	a_4	0	a_6	$\frac{\pi}{2}$	0	0	$\frac{\pi}{2}$	$\frac{\pi}{2}$	α_6
d_1	d_2	d_3	d_4	0	d_6	a_1	a_2	a_3	a_4	0	a_6	0	$\frac{\pi}{2}$	0	0	$\frac{\pi}{2}$	α_6
d_1	d_2	d_3	d_4	0	d_6	a_1	a_2	a_3	a_4	0	a_6	0	0	$\frac{\pi}{2}$	$\frac{\pi}{2}$	$\frac{\pi}{2}$	α_6
d_1	d_2	d_3	d_4	0	d_6	a_1	a_2	a_3	a_4	0	a_6	0	0	$\frac{\pi}{2}$	0	$\frac{\pi}{2}$	α_6
d_1	d_2	d_3	d_4	0	d_6	a_1	a_2	a_3	0	a_5	a_6	$\frac{\pi}{2}$	0	0	$\frac{\pi}{2}$	$\frac{\pi}{2}$	α_6
d_1	d_2	d_3	d_4	0	d_6	a_1	a_2	a_3	0	a_5	a_6	$\frac{\pi}{2}$	0	0	$\frac{\pi}{2}$	0	α_6
d_1	d_2	d_3	d_4	0	d_6	a_1	a_2	a_3	0	a_5	a_6	0	0	$\frac{\pi}{2}$	$\frac{\pi}{2}$	$\frac{\pi}{2}$	α_6
d_1	d_2	d_3	d_4	0	d_6	a_1	a_2	a_3	0	a_5	a_6	0	0	$\frac{\pi}{2}$	$\frac{\pi}{2}$	0	α_6
d_1	d_2	d_3	d_4	0	d_6	a_1	a_2	a_3	0	0	a_6	$\frac{\pi}{2}$	0	0	$\frac{\pi}{2}$	$\frac{\pi}{2}$	α_6
d_1	d_2	d_3	d_4	0	d_6	a_1	a_2	a_3	0	0	a_6	0	$\frac{\pi}{2}$	0	$\frac{\pi}{2}$	$\frac{\pi}{2}$	α_6
d_1	d_2	d_3	d_4	0	d_6	a_1	a_2	0	a_4	a_5	a_6	$\frac{\pi}{2}$	$\frac{\pi}{2}$	$\frac{\pi}{2}$	0	0	α_6
d_1	d_2	d_3	d_4	0	d_6	a_1	a_2	0	a_4	a_5	a_6	$\frac{\pi}{2}$	0	$\frac{\pi}{2}$	0	0	α_6
d_1	d_2	d_3	d_4	0	d_6	a_1	a_2	0	a_4	a_5	a_6	0	$\frac{\pi}{2}$	$\frac{\pi}{2}$	0	0	α_6
d_1	d_2	d_3	d_4	0	d_6	a_1	a_2	0	a_4	a_5	a_6	0	0	$\frac{\pi}{2}$	$\frac{\pi}{2}$	$\frac{\pi}{2}$	α_6
d_1	d_2	d_3	d_4	0	d_6	a_1	a_2	0	a_4	a_5	a_6	0	0	$\frac{\pi}{2}$	$\frac{\pi}{2}$	0	α_6
d_1	d_2	d_3	d_4	0	d_6	a_1	a_2	0	a_4	a_5	a_6	0	0	$\frac{\pi}{2}$	0	$\frac{\pi}{2}$	α_6
d_1	d_2	d_3	d_4	0	d_6	a_1	a_2	0	a_4	0	a_6	0	0	$\frac{\pi}{2}$	$\frac{\pi}{2}$	$\frac{\pi}{2}$	α_6
d_1	d_2	d_3	d_4	0	d_6	a_1	a_2	0	a_4	0	a_6	0	0	$\frac{\pi}{2}$	0	$\frac{\pi}{2}$	α_6
d_1	d_2	d_3	d_4	0	d_6	a_1	a_2	0	0	a_5	a_6	0	0	$\frac{\pi}{2}$	$\frac{\pi}{2}$	$\frac{\pi}{2}$	α_6
d_1	d_2	d_3	d_4	0	d_6	a_1	a_2	0	0	a_5	a_6	0	0	$\frac{\pi}{2}$	$\frac{\pi}{2}$	0	α_6
d_1	d_2	d_3	d_4	0	d_6	a_1	a_2	0	0	0	a_6	$\frac{\pi}{2}$	0	$\frac{\pi}{2}$	$\frac{\pi}{2}$	$\frac{\pi}{2}$	α_6
d_1	d_2	d_3	d_4	0	d_6	a_1	a_2	0	0	0	a_6	0	$\frac{\pi}{2}$	$\frac{\pi}{2}$	$\frac{\pi}{2}$	$\frac{\pi}{2}$	α_6
d_1	d_2	d_3	d_4	0	d_6	a_1	0	a_3	a_4	a_5	a_6	$\frac{\pi}{2}$	$\frac{\pi}{2}$	$\frac{\pi}{2}$	0	0	α_6
d_1	d_2	d_3	d_4	0	d_6	a_1	0	a_3	a_4	a_5	a_6	$\frac{\pi}{2}$	$\frac{\pi}{2}$	0	0	$\frac{\pi}{2}$	α_6
d_1	d_2	d_3	d_4	0	d_6	a_1	0	a_3	a_4	a_5	a_6	0	$\frac{\pi}{2}$	$\frac{\pi}{2}$	0	0	α_6
d_1	d_2	d_3	d_4	0	d_6	a_1	0	a_3	a_4	a_5	a_6	0	$\frac{\pi}{2}$	0	0	$\frac{\pi}{2}$	α_6
d_1	d_2	d_3	d_4	0	d_6	a_1	0	a_3	a_4	0	a_6	$\frac{\pi}{2}$	$\frac{\pi}{2}$	0	0	$\frac{\pi}{2}$	α_6
d_1	d_2	d_3	d_4	0	d_6	a_1	0	a_3	a_4	0	a_6	0	$\frac{\pi}{2}$	0	0	$\frac{\pi}{2}$	α_6
d_1	d_2	d_3	d_4	0	d_6	a_1	0	a_3	0	0	a_6	$\frac{\pi}{2}$	$\frac{\pi}{2}$	0	$\frac{\pi}{2}$	$\frac{\pi}{2}$	α_6
d_1	d_2	d_3	d_4	0	d_6	a_1	0	a_3	0	0	a_6	0	$\frac{\pi}{2}$	0	$\frac{\pi}{2}$	$\frac{\pi}{2}$	α_6
d_1	d_2	d_3	d_4	0	d_6	a_1	0	0	a_4	a_5	a_6	$\frac{\pi}{2}$	$\frac{\pi}{2}$	$\frac{\pi}{2}$	0	0	α_6
d_1	d_2	d_3	d_4	0	d_6	a_1	0	0	a_4	a_5	a_6	0	$\frac{\pi}{2}$	$\frac{\pi}{2}$	0	0	α_6
d_1	d_2	d_3	d_4	0	d_6	a_1	0	0	0	0	a_6	$\frac{\pi}{2}$	$\frac{\pi}{2}$	$\frac{\pi}{2}$	$\frac{\pi}{2}$	$\frac{\pi}{2}$	α_6
d_1	d_2	d_3	d_4	0	d_6	a_1	0	0	0	0	a_6	0	$\frac{\pi}{2}$	$\frac{\pi}{2}$	$\frac{\pi}{2}$	$\frac{\pi}{2}$	α_6
d_1	d_2	d_3	0	d_5	d_6	a_1	a_2	a_3	a_4	a_5	a_6	$\frac{\pi}{2}$	$\frac{\pi}{2}$	$\frac{\pi}{2}$	0	0	α_6

Table A.2 – The D-H parameter values of robots whose $\det(\mathbf{J})$ factors into three components.

d_1	d_2	d_3	d_4	d_5	d_6	a_1	a_2	a_3	a_4	a_5	a_6	α_1	α_2	α_3	α_4	α_5	α_6
d_1	d_2	d_3	0	d_5	d_6	a_1	a_2	a_3	a_4	a_5	a_6	$\frac{\pi}{2}$	$\frac{\pi}{2}$	0	0	$\frac{\pi}{2}$	α_6
d_1	d_2	d_3	0	d_5	d_6	a_1	a_2	a_3	a_4	a_5	a_6	$\frac{\pi}{2}$	0	$\frac{\pi}{2}$	0	0	α_6
d_1	d_2	d_3	0	d_5	d_6	a_1	a_2	a_3	a_4	a_5	a_6	$\frac{\pi}{2}$	0	0	$\frac{\pi}{2}$	$\frac{\pi}{2}$	α_6
d_1	d_2	d_3	0	d_5	d_6	a_1	a_2	a_3	a_4	a_5	a_6	$\frac{\pi}{2}$	0	0	$\frac{\pi}{2}$	0	α_6
d_1	d_2	d_3	0	d_5	d_6	a_1	a_2	a_3	a_4	a_5	a_6	0	$\frac{\pi}{2}$	$\frac{\pi}{2}$	0	0	α_6
d_1	d_2	d_3	0	d_5	d_6	a_1	a_2	a_3	a_4	a_5	a_6	0	$\frac{\pi}{2}$	0	0	$\frac{\pi}{2}$	α_6
d_1	d_2	d_3	0	d_5	d_6	a_1	a_2	a_3	a_4	a_5	a_6	0	0	$\frac{\pi}{2}$	$\frac{\pi}{2}$	$\frac{\pi}{2}$	α_6
d_1	d_2	d_3	0	d_5	d_6	a_1	a_2	a_3	a_4	a_5	a_6	0	0	$\frac{\pi}{2}$	$\frac{\pi}{2}$	0	α_6
d_1	d_2	d_3	0	d_5	d_6	a_1	a_2	a_3	a_4	a_5	a_6	0	0	$\frac{\pi}{2}$	0	$\frac{\pi}{2}$	α_6
d_1	d_2	d_3	0	d_5	d_6	a_1	a_2	a_3	a_4	0	a_6	$\frac{\pi}{2}$	$\frac{\pi}{2}$	0	0	$\frac{\pi}{2}$	α_6
d_1	d_2	d_3	0	d_5	d_6	a_1	a_2	a_3	a_4	0	a_6	$\frac{\pi}{2}$	0	0	$\frac{\pi}{2}$	$\frac{\pi}{2}$	α_6
d_1	d_2	d_3	0	d_5	d_6	a_1	a_2	a_3	a_4	0	a_6	0	$\frac{\pi}{2}$	0	0	$\frac{\pi}{2}$	α_6
d_1	d_2	d_3	0	d_5	d_6	a_1	a_2	a_3	a_4	0	a_6	0	0	$\frac{\pi}{2}$	$\frac{\pi}{2}$	$\frac{\pi}{2}$	α_6
d_1	d_2	d_3	0	d_5	d_6	a_1	a_2	a_3	a_4	0	a_6	0	0	$\frac{\pi}{2}$	0	$\frac{\pi}{2}$	α_6
d_1	d_2	d_3	0	d_5	d_6	a_1	a_2	a_3	0	a_5	a_6	$\frac{\pi}{2}$	0	0	$\frac{\pi}{2}$	$\frac{\pi}{2}$	α_6
d_1	d_2	d_3	0	d_5	d_6	a_1	a_2	a_3	0	a_5	a_6	$\frac{\pi}{2}$	0	0	$\frac{\pi}{2}$	0	α_6
d_1	d_2	d_3	0	d_5	d_6	a_1	a_2	a_3	0	a_5	a_6	0	0	$\frac{\pi}{2}$	$\frac{\pi}{2}$	$\frac{\pi}{2}$	α_6
d_1	d_2	d_3	0	d_5	d_6	a_1	a_2	a_3	0	a_5	a_6	0	0	$\frac{\pi}{2}$	$\frac{\pi}{2}$	0	α_6
d_1	d_2	d_3	0	d_5	d_6	a_1	a_2	a_3	0	0	a_6	$\frac{\pi}{2}$	0	0	$\frac{\pi}{2}$	$\frac{\pi}{2}$	α_6
d_1	d_2	d_3	0	d_5	d_6	a_1	a_2	a_3	0	0	a_6	0	0	$\frac{\pi}{2}$	$\frac{\pi}{2}$	$\frac{\pi}{2}$	α_6
d_1	d_2	d_3	0	d_5	d_6	a_1	a_2	0	a_4	a_5	a_6	$\frac{\pi}{2}$	$\frac{\pi}{2}$	$\frac{\pi}{2}$	0	0	α_6
d_1	d_2	d_3	0	d_5	d_6	a_1	a_2	0	a_4	a_5	a_6	$\frac{\pi}{2}$	0	$\frac{\pi}{2}$	0	0	α_6
d_1	d_2	d_3	0	d_5	d_6	a_1	a_2	0	a_4	a_5	a_6	0	$\frac{\pi}{2}$	$\frac{\pi}{2}$	0	0	α_6
d_1	d_2	d_3	0	d_5	d_6	a_1	a_2	0	a_4	a_5	a_6	0	0	$\frac{\pi}{2}$	$\frac{\pi}{2}$	$\frac{\pi}{2}$	α_6
d_1	d_2	d_3	0	d_5	d_6	a_1	a_2	0	a_4	a_5	a_6	0	0	$\frac{\pi}{2}$	0	$\frac{\pi}{2}$	α_6
d_1	d_2	d_3	0	d_5	d_6	a_1	a_2	0	a_4	0	a_6	0	0	$\frac{\pi}{2}$	$\frac{\pi}{2}$	$\frac{\pi}{2}$	α_6
d_1	d_2	d_3	0	d_5	d_6	a_1	a_2	0	a_4	0	a_6	0	0	$\frac{\pi}{2}$	0	$\frac{\pi}{2}$	α_6
d_1	d_2	d_3	0	d_5	d_6	a_1	a_2	0	0	a_5	a_6	0	$\frac{\pi}{2}$	$\frac{\pi}{2}$	$\frac{\pi}{2}$	$\frac{\pi}{2}$	α_6
d_1	d_2	d_3	0	d_5	d_6	a_1	a_2	0	0	a_5	a_6	0	$\frac{\pi}{2}$	$\frac{\pi}{2}$	$\frac{\pi}{2}$	0	α_6
d_1	d_2	d_3	0	d_5	d_6	a_1	a_2	0	0	a_5	a_6	0	0	$\frac{\pi}{2}$	$\frac{\pi}{2}$	$\frac{\pi}{2}$	α_6
d_1	d_2	d_3	0	d_5	d_6	a_1	a_2	0	0	0	a_6	0	$\frac{\pi}{2}$	$\frac{\pi}{2}$	$\frac{\pi}{2}$	$\frac{\pi}{2}$	α_6
d_1	d_2	d_3	0	d_5	d_6	a_1	a_2	0	0	0	a_6	0	0	$\frac{\pi}{2}$	$\frac{\pi}{2}$	$\frac{\pi}{2}$	α_6
d_1	d_2	d_3	0	d_5	d_6	a_1	0	a_3	a_4	a_5	a_6	$\frac{\pi}{2}$	$\frac{\pi}{2}$	$\frac{\pi}{2}$	0	0	α_6
d_1	d_2	d_3	0	d_5	d_6	a_1	0	a_3	a_4	a_5	a_6	$\frac{\pi}{2}$	$\frac{\pi}{2}$	0	0	$\frac{\pi}{2}$	α_6
d_1	d_2	d_3	0	d_5	d_6	a_1	0	a_3	a_4	a_5	a_6	0	$\frac{\pi}{2}$	$\frac{\pi}{2}$	0	0	α_6
d_1	d_2	d_3	0	d_5	d_6	a_1	0	a_3	a_4	a_5	a_6	0	$\frac{\pi}{2}$	0	0	$\frac{\pi}{2}$	α_6
d_1	d_2	d_3	0	d_5	d_6	a_1	0	a_3	a_4	0	a_6	$\frac{\pi}{2}$	$\frac{\pi}{2}$	0	0	$\frac{\pi}{2}$	α_6
d_1	d_2	d_3	0	d_5	d_6	a_1	0	a_3	a_4	0	a_6	0	$\frac{\pi}{2}$	0	0	$\frac{\pi}{2}$	α_6
d_1	d_2	d_3	0	d_5	d_6	a_1	0	0	a_4	a_5	a_6	$\frac{\pi}{2}$	$\frac{\pi}{2}$	$\frac{\pi}{2}$	0	0	α_6
d_1	d_2	d_3	0	d_5	d_6	a_1	0	0	a_4	a_5	a_6	0	$\frac{\pi}{2}$	$\frac{\pi}{2}$	0	0	α_6
d_1	d_2	d_3	0	d_5	d_6	a_1	0	0	0	a_5	a_6	0	$\frac{\pi}{2}$	$\frac{\pi}{2}$	$\frac{\pi}{2}$	$\frac{\pi}{2}$	α_6

Table A.3 – The D-H parameter values of robots whose det(**J**) factors into three components.

d_1	d_2	d_3	d_4	d_5	d_6	a_1	a_2	a_3	a_4	a_5	a_6	α_1	α_2	α_3	α_4	α_5	α_6
d_1	d_2	d_3	0	d_5	d_6	a_1	0	0	0	a_5	a_6	0	$\frac{\pi}{2}$	$\frac{\pi}{2}$	$\frac{\pi}{2}$	0	α_6
d_1	d_2	d_3	0	d_5	d_6	a_1	0	0	0	0	a_6	0	$\frac{\pi}{2}$	$\frac{\pi}{2}$	$\frac{\pi}{2}$	$\frac{\pi}{2}$	α_6
d_1	d_2	d_3	0	0	d_6	a_1	a_2	a_3	a_4	a_5	a_6	$\frac{\pi}{2}$	$\frac{\pi}{2}$	$\frac{\pi}{2}$	0	0	α_6
d_1	d_2	d_3	0	0	d_6	a_1	a_2	a_3	a_4	a_5	a_6	$\frac{\pi}{2}$	$\frac{\pi}{2}$	0	0	$\frac{\pi}{2}$	α_6
d_1	d_2	d_3	0	0	d_6	a_1	a_2	a_3	a_4	a_5	a_6	$\frac{\pi}{2}$	0	$\frac{\pi}{2}$	0	0	α_6
d_1	d_2	d_3	0	0	d_6	a_1	a_2	a_3	a_4	a_5	a_6	$\frac{\pi}{2}$	0	0	$\frac{\pi}{2}$	$\frac{\pi}{2}$	α_6
d_1	d_2	d_3	0	0	d_6	a_1	a_2	a_3	a_4	a_5	a_6	$\frac{\pi}{2}$	0	0	$\frac{\pi}{2}$	0	α_6
d_1	d_2	d_3	0	0	d_6	a_1	a_2	a_3	a_4	a_5	a_6	0	$\frac{\pi}{2}$	$\frac{\pi}{2}$	0	0	α_6
d_1	d_2	d_3	0	0	d_6	a_1	a_2	a_3	a_4	a_5	a_6	0	$\frac{\pi}{2}$	0	0	$\frac{\pi}{2}$	α_6
d_1	d_2	d_3	0	0	d_6	a_1	a_2	a_3	a_4	a_5	a_6	0	0	$\frac{\pi}{2}$	$\frac{\pi}{2}$	$\frac{\pi}{2}$	α_6
d_1	d_2	d_3	0	0	d_6	a_1	a_2	a_3	a_4	a_5	a_6	0	0	$\frac{\pi}{2}$	$\frac{\pi}{2}$	0	α_6
d_1	d_2	d_3	0	0	d_6	a_1	a_2	a_3	a_4	a_5	a_6	0	0	$\frac{\pi}{2}$	0	$\frac{\pi}{2}$	α_6
d_1	d_2	d_3	0	0	d_6	a_1	a_2	a_3	a_4	0	a_6	$\frac{\pi}{2}$	$\frac{\pi}{2}$	0	0	$\frac{\pi}{2}$	α_6
d_1	d_2	d_3	0	0	d_6	a_1	a_2	a_3	a_4	0	a_6	$\frac{\pi}{2}$	0	0	$\frac{\pi}{2}$	$\frac{\pi}{2}$	α_6
d_1	d_2	d_3	0	0	d_6	a_1	a_2	a_3	a_4	0	a_6	0	$\frac{\pi}{2}$	0	0	$\frac{\pi}{2}$	α_6
d_1	d_2	d_3	0	0	d_6	a_1	a_2	a_3	a_4	0	a_6	0	0	$\frac{\pi}{2}$	$\frac{\pi}{2}$	$\frac{\pi}{2}$	α_6
d_1	d_2	d_3	0	0	d_6	a_1	a_2	a_3	a_4	0	a_6	0	0	$\frac{\pi}{2}$	0	$\frac{\pi}{2}$	α_6
d_1	d_2	d_3	0	0	d_6	a_1	a_2	a_3	0	a_5	a_6	$\frac{\pi}{2}$	0	0	$\frac{\pi}{2}$	$\frac{\pi}{2}$	α_6
d_1	d_2	d_3	0	0	d_6	a_1	a_2	a_3	0	a_5	a_6	$\frac{\pi}{2}$	0	0	$\frac{\pi}{2}$	0	α_6
d_1	d_2	d_3	0	0	d_6	a_1	a_2	a_3	0	a_5	a_6	0	0	$\frac{\pi}{2}$	$\frac{\pi}{2}$	$\frac{\pi}{2}$	α_6
d_1	d_2	d_3	0	0	d_6	a_1	a_2	a_3	0	a_5	a_6	0	0	$\frac{\pi}{2}$	$\frac{\pi}{2}$	0	α_6
d_1	d_2	d_3	0	0	d_6	a_1	a_2	a_3	0	0	a_6	$\frac{\pi}{2}$	0	$\frac{\pi}{2}$	$\frac{\pi}{2}$	$\frac{\pi}{2}$	α_6
d_1	d_2	d_3	0	0	d_6	a_1	a_2	a_3	0	0	a_6	$\frac{\pi}{2}$	0	0	$\frac{\pi}{2}$	$\frac{\pi}{2}$	α_6
d_1	d_2	d_3	0	0	d_6	a_1	a_2	a_3	0	0	a_6	0	$\frac{\pi}{2}$	$\frac{\pi}{2}$	$\frac{\pi}{2}$	$\frac{\pi}{2}$	α_6
d_1	d_2	d_3	0	0	d_6	a_1	a_2	a_3	0	0	a_6	0	$\frac{\pi}{2}$	0	$\frac{\pi}{2}$	$\frac{\pi}{2}$	α_6
d_1	d_2	d_3	0	0	d_6	a_1	a_2	0	a_4	a_5	a_6	$\frac{\pi}{2}$	$\frac{\pi}{2}$	$\frac{\pi}{2}$	0	0	α_6
d_1	d_2	d_3	0	0	d_6	a_1	a_2	0	a_4	a_5	a_6	$\frac{\pi}{2}$	0	$\frac{\pi}{2}$	0	0	α_6
d_1	d_2	d_3	0	0	d_6	a_1	a_2	0	a_4	a_5	a_6	0	$\frac{\pi}{2}$	$\frac{\pi}{2}$	0	0	α_6
d_1	d_2	d_3	0	0	d_6	a_1	a_2	0	a_4	a_5	a_6	0	0	$\frac{\pi}{2}$	$\frac{\pi}{2}$	$\frac{\pi}{2}$	α_6
d_1	d_2	d_3	0	0	d_6	a_1	a_2	0	a_4	a_5	a_6	0	0	$\frac{\pi}{2}$	$\frac{\pi}{2}$	0	α_6
d_1	d_2	d_3	0	0	d_6	a_1	a_2	0	a_4	a_5	a_6	0	0	$\frac{\pi}{2}$	0	$\frac{\pi}{2}$	α_6
d_1	d_2	d_3	0	0	d_6	a_1	a_2	0	a_4	0	a_6	0	0	$\frac{\pi}{2}$	$\frac{\pi}{2}$	$\frac{\pi}{2}$	α_6
d_1	d_2	d_3	0	0	d_6	a_1	a_2	0	a_4	0	a_6	0	0	$\frac{\pi}{2}$	0	$\frac{\pi}{2}$	α_6
d_1	d_2	d_3	0	0	d_6	a_1	a_2	0	0	a_5	a_6	0	$\frac{\pi}{2}$	$\frac{\pi}{2}$	$\frac{\pi}{2}$	$\frac{\pi}{2}$	α_6
d_1	d_2	d_3	0	0	d_6	a_1	a_2	0	0	a_5	a_6	0	$\frac{\pi}{2}$	$\frac{\pi}{2}$	$\frac{\pi}{2}$	0	α_6
d_1	d_2	d_3	0	0	d_6	a_1	a_2	0	0	a_5	a_6	0	0	$\frac{\pi}{2}$	$\frac{\pi}{2}$	$\frac{\pi}{2}$	α_6
d_1	d_2	d_3	0	0	d_6	a_1	a_2	0	0	a_5	a_6	0	0	$\frac{\pi}{2}$	$\frac{\pi}{2}$	0	α_6
d_1	d_2	d_3	0	0	d_6	a_1	0	a_3	a_4	a_5	a_6	$\frac{\pi}{2}$	$\frac{\pi}{2}$	$\frac{\pi}{2}$	0	0	α_6
d_1	d_2	d_3	0	0	d_6	a_1	0	a_3	a_4	a_5	a_6	$\frac{\pi}{2}$	$\frac{\pi}{2}$	0	0	$\frac{\pi}{2}$	α_6
d_1	d_2	d_3	0	0	d_6	a_1	0	a_3	a_4	a_5	a_6	0	$\frac{\pi}{2}$	$\frac{\pi}{2}$	0	0	α_6
d_1	d_2	d_3	0	0	d_6	a_1	0	a_3	a_4	a_5	a_6	0	$\frac{\pi}{2}$	0	0	$\frac{\pi}{2}$	α_6
d_1	d_2	d_3	0	0	d_6	a_1	0	a_3	a_4	0	a_6	$\frac{\pi}{2}$	$\frac{\pi}{2}$	0	0	$\frac{\pi}{2}$	α_6
d_1	d_2	d_3	0	0	d_6	a_1	0	a_3	a_4	0	a_6	0	$\frac{\pi}{2}$	0	0	$\frac{\pi}{2}$	α_6

Table A.4 – The D-H parameter values of robots whose det(**J**) factors into three components.

d_1	d_2	d_3	d_4	d_5	d_6	a_1	a_2	a_3	a_4	a_5	a_6	α_1	α_2	α_3	α_4	α_5	α_6
d_1	d_2	d_3	0	0	d_6	a_1	0	a_3	0	0	a_6	$\frac{\pi}{2}$	$\frac{\pi}{2}$	$\frac{\pi}{2}$	$\frac{\pi}{2}$	$\frac{\pi}{2}$	α_6
d_1	d_2	d_3	0	0	d_6	a_1	0	a_3	0	0	a_6	$\frac{\pi}{2}$	$\frac{\pi}{2}$	0	$\frac{\pi}{2}$	$\frac{\pi}{2}$	α_6
d_1	d_2	d_3	0	0	d_6	a_1	0	a_3	0	0	a_6	0	$\frac{\pi}{2}$	$\frac{\pi}{2}$	$\frac{\pi}{2}$	$\frac{\pi}{2}$	α_6
d_1	d_2	d_3	0	0	d_6	a_1	0	a_3	0	0	a_6	0	$\frac{\pi}{2}$	0	$\frac{\pi}{2}$	$\frac{\pi}{2}$	α_6
d_1	d_2	d_3	0	0	d_6	a_1	0	0	a_4	a_5	a_6	$\frac{\pi}{2}$	$\frac{\pi}{2}$	$\frac{\pi}{2}$	0	0	α_6
d_1	d_2	d_3	0	0	d_6	a_1	0	0	a_4	a_5	a_6	0	$\frac{\pi}{2}$	$\frac{\pi}{2}$	0	0	α_6
d_1	d_2	d_3	0	0	d_6	a_1	0	0	0	a_5	a_6	0	$\frac{\pi}{2}$	$\frac{\pi}{2}$	$\frac{\pi}{2}$	$\frac{\pi}{2}$	α_6
d_1	d_2	d_3	0	0	d_6	a_1	0	0	0	a_5	a_6	0	$\frac{\pi}{2}$	$\frac{\pi}{2}$	$\frac{\pi}{2}$	0	α_6
d_1	d_2	0	d_4	d_5	d_6	a_1	a_2	a_3	a_4	a_5	a_6	$\frac{\pi}{2}$	$\frac{\pi}{2}$	$\frac{\pi}{2}$	0	0	α_6
d_1	d_2	0	d_4	d_5	d_6	a_1	a_2	a_3	a_4	a_5	a_6	$\frac{\pi}{2}$	$\frac{\pi}{2}$	0	0	$\frac{\pi}{2}$	α_6
d_1	d_2	0	d_4	d_5	d_6	a_1	a_2	a_3	a_4	a_5	a_6	$\frac{\pi}{2}$	0	$\frac{\pi}{2}$	0	0	α_6
d_1	d_2	0	d_4	d_5	d_6	a_1	a_2	a_3	a_4	a_5	a_6	$\frac{\pi}{2}$	0	0	$\frac{\pi}{2}$	$\frac{\pi}{2}$	α_6
d_1	d_2	0	d_4	d_5	d_6	a_1	a_2	a_3	a_4	a_5	a_6	$\frac{\pi}{2}$	0	0	$\frac{\pi}{2}$	0	α_6
d_1	d_2	0	d_4	d_5	d_6	a_1	a_2	a_3	a_4	a_5	a_6	0	$\frac{\pi}{2}$	$\frac{\pi}{2}$	0	0	α_6
d_1	d_2	0	d_4	d_5	d_6	a_1	a_2	a_3	a_4	a_5	a_6	0	$\frac{\pi}{2}$	0	0	$\frac{\pi}{2}$	α_6
d_1	d_2	0	d_4	d_5	d_6	a_1	a_2	a_3	a_4	a_5	a_6	0	0	$\frac{\pi}{2}$	$\frac{\pi}{2}$	$\frac{\pi}{2}$	α_6
d_1	d_2	0	d_4	d_5	d_6	a_1	a_2	a_3	a_4	a_5	a_6	0	0	$\frac{\pi}{2}$	$\frac{\pi}{2}$	0	α_6
d_1	d_2	0	d_4	d_5	d_6	a_1	a_2	a_3	a_4	a_5	a_6	0	0	$\frac{\pi}{2}$	0	$\frac{\pi}{2}$	α_6
d_1	d_2	0	d_4	d_5	d_6	a_1	a_2	a_3	a_4	0	a_6	$\frac{\pi}{2}$	$\frac{\pi}{2}$	0	0	$\frac{\pi}{2}$	α_6
d_1	d_2	0	d_4	d_5	d_6	a_1	a_2	a_3	a_4	0	a_6	$\frac{\pi}{2}$	0	0	$\frac{\pi}{2}$	$\frac{\pi}{2}$	α_6
d_1	d_2	0	d_4	d_5	d_6	a_1	a_2	a_3	a_4	0	a_6	0	$\frac{\pi}{2}$	0	0	$\frac{\pi}{2}$	α_6
d_1	d_2	0	d_4	d_5	d_6	a_1	a_2	a_3	a_4	0	a_6	0	0	$\frac{\pi}{2}$	$\frac{\pi}{2}$	$\frac{\pi}{2}$	α_6
d_1	d_2	0	d_4	d_5	d_6	a_1	a_2	a_3	a_4	0	a_6	0	0	$\frac{\pi}{2}$	0	$\frac{\pi}{2}$	α_6
d_1	d_2	0	d_4	d_5	d_6	a_1	a_2	a_3	0	a_5	a_6	$\frac{\pi}{2}$	0	0	$\frac{\pi}{2}$	$\frac{\pi}{2}$	α_6
d_1	d_2	0	d_4	d_5	d_6	a_1	a_2	a_3	0	a_5	a_6	$\frac{\pi}{2}$	0	0	$\frac{\pi}{2}$	0	α_6
d_1	d_2	0	d_4	d_5	d_6	a_1	a_2	a_3	0	a_5	a_6	0	0	$\frac{\pi}{2}$	$\frac{\pi}{2}$	$\frac{\pi}{2}$	α_6
d_1	d_2	0	d_4	d_5	d_6	a_1	a_2	a_3	0	a_5	a_6	0	0	$\frac{\pi}{2}$	$\frac{\pi}{2}$	0	α_6
d_1	d_2	0	d_4	d_5	d_6	a_1	a_2	a_3	0	0	a_6	$\frac{\pi}{2}$	0	0	$\frac{\pi}{2}$	$\frac{\pi}{2}$	α_6
d_1	d_2	0	d_4	d_5	d_6	a_1	a_2	a_3	0	0	a_6	0	0	$\frac{\pi}{2}$	$\frac{\pi}{2}$	$\frac{\pi}{2}$	α_6
d_1	d_2	0	d_4	d_5	d_6	a_1	a_2	0	a_4	a_5	a_6	$\frac{\pi}{2}$	$\frac{\pi}{2}$	$\frac{\pi}{2}$	0	0	α_6
d_1	d_2	0	d_4	d_5	d_6	a_1	a_2	0	a_4	a_5	a_6	$\frac{\pi}{2}$	0	$\frac{\pi}{2}$	0	0	α_6
d_1	d_2	0	d_4	d_5	d_6	a_1	a_2	0	a_4	a_5	a_6	0	$\frac{\pi}{2}$	$\frac{\pi}{2}$	0	0	α_6
d_1	d_2	0	d_4	d_5	d_6	a_1	a_2	0	a_4	a_5	a_6	0	0	$\frac{\pi}{2}$	$\frac{\pi}{2}$	$\frac{\pi}{2}$	α_6
d_1	d_2	0	d_4	d_5	d_6	a_1	a_2	0	a_4	a_5	a_6	0	0	$\frac{\pi}{2}$	$\frac{\pi}{2}$	0	α_6
d_1	d_2	0	d_4	d_5	d_6	a_1	a_2	0	a_4	a_5	a_6	0	0	$\frac{\pi}{2}$	0	$\frac{\pi}{2}$	α_6
d_1	d_2	0	d_4	d_5	d_6	a_1	a_2	0	a_4	0	a_6	0	0	$\frac{\pi}{2}$	$\frac{\pi}{2}$	$\frac{\pi}{2}$	α_6
d_1	d_2	0	d_4	d_5	d_6	a_1	a_2	0	a_4	0	a_6	0	0	$\frac{\pi}{2}$	0	$\frac{\pi}{2}$	α_6
d_1	d_2	0	d_4	d_5	d_6	a_1	a_2	0	0	a_5	a_6	0	0	$\frac{\pi}{2}$	$\frac{\pi}{2}$	$\frac{\pi}{2}$	α_6
d_1	d_2	0	d_4	d_5	d_6	a_1	a_2	0	0	a_5	a_6	0	0	$\frac{\pi}{2}$	$\frac{\pi}{2}$	0	α_6
d_1	d_2	0	d_4	d_5	d_6	a_1	a_2	0	0	0	a_6	0	0	$\frac{\pi}{2}$	$\frac{\pi}{2}$	$\frac{\pi}{2}$	α_6
d_1	d_2	0	d_4	d_5	d_6	a_1	0	a_3	a_4	a_5	a_6	$\frac{\pi}{2}$	$\frac{\pi}{2}$	$\frac{\pi}{2}$	0	0	α_6
d_1	d_2	0	d_4	d_5	d_6	a_1	0	a_3	a_4	a_5	a_6	$\frac{\pi}{2}$	$\frac{\pi}{2}$	0	0	$\frac{\pi}{2}$	α_6
d_1	d_2	0	d_4	d_5	d_6	a_1	0	a_3	a_4	a_5	a_6	0	$\frac{\pi}{2}$	$\frac{\pi}{2}$	0	0	α_6

Table A.5 – The D-H parameter values of robots whose det(**J**) factors into three components.

d_1	d_2	d_3	d_4	d_5	d_6	a_1	a_2	a_3	a_4	a_5	a_6	α_1	α_2	α_3	α_4	α_5	α_6
d_1	d_2	0	d_4	d_5	d_6	a_1	0	a_3	a_4	a_5	a_6	0	$\frac{\pi}{2}$	0	0	$\frac{\pi}{2}$	α_6
d_1	d_2	0	d_4	d_5	d_6	a_1	0	a_3	a_4	0	a_6	$\frac{\pi}{2}$	$\frac{\pi}{2}$	0	0	$\frac{\pi}{2}$	α_6
d_1	d_2	0	d_4	d_5	d_6	a_1	0	a_3	a_4	0	a_6	0	$\frac{\pi}{2}$	0	0	$\frac{\pi}{2}$	α_6
d_1	d_2	0	d_4	d_5	d_6	a_1	0	0	a_4	a_5	a_6	$\frac{\pi}{2}$	$\frac{\pi}{2}$	$\frac{\pi}{2}$	$\frac{\pi}{2}$	0	α_6
d_1	d_2	0	d_4	d_5	d_6	a_1	0	0	a_4	a_5	a_6	$\frac{\pi}{2}$	$\frac{\pi}{2}$	$\frac{\pi}{2}$	0	0	α_6
d_1	d_2	0	d_4	d_5	d_6	a_1	0	0	a_4	a_5	a_6	0	$\frac{\pi}{2}$	$\frac{\pi}{2}$	$\frac{\pi}{2}$	0	α_6
d_1	d_2	0	d_4	d_5	d_6	a_1	0	0	a_4	a_5	a_6	0	$\frac{\pi}{2}$	$\frac{\pi}{2}$	0	0	α_6
d_1	d_2	0	d_4	d_5	d_6	a_1	0	0	a_4	0	a_6	$\frac{\pi}{2}$	$\frac{\pi}{2}$	$\frac{\pi}{2}$	$\frac{\pi}{2}$	$\frac{\pi}{2}$	α_6
d_1	d_2	0	d_4	d_5	d_6	a_1	0	0	a_4	0	a_6	$\frac{\pi}{2}$	$\frac{\pi}{2}$	$\frac{\pi}{2}$	0	$\frac{\pi}{2}$	α_6
d_1	d_2	0	d_4	d_5	d_6	a_1	0	0	a_4	0	a_6	0	$\frac{\pi}{2}$	$\frac{\pi}{2}$	$\frac{\pi}{2}$	$\frac{\pi}{2}$	α_6
d_1	d_2	0	d_4	d_5	d_6	a_1	0	0	a_4	0	a_6	0	$\frac{\pi}{2}$	$\frac{\pi}{2}$	0	$\frac{\pi}{2}$	α_6
d_1	d_2	0	d_4	d_5	d_6	a_1	0	0	0	a_5	a_6	$\frac{\pi}{2}$	$\frac{\pi}{2}$	$\frac{\pi}{2}$	$\frac{\pi}{2}$	0	α_6
d_1	d_2	0	d_4	d_5	d_6	a_1	0	0	0	a_5	a_6	0	$\frac{\pi}{2}$	$\frac{\pi}{2}$	$\frac{\pi}{2}$	0	α_6
d_1	d_2	0	d_4	d_5	d_6	a_1	0	0	0	0	a_6	$\frac{\pi}{2}$	$\frac{\pi}{2}$	$\frac{\pi}{2}$	$\frac{\pi}{2}$	$\frac{\pi}{2}$	α_6
d_1	d_2	0	d_4	d_5	d_6	a_1	0	0	0	0	a_6	0	$\frac{\pi}{2}$	$\frac{\pi}{2}$	$\frac{\pi}{2}$	$\frac{\pi}{2}$	α_6
d_1	d_2	0	d_4	0	d_6	a_1	a_2	a_3	a_4	a_5	a_6	$\frac{\pi}{2}$	$\frac{\pi}{2}$	$\frac{\pi}{2}$	0	0	α_6
d_1	d_2	0	d_4	0	d_6	a_1	a_2	a_3	a_4	a_5	a_6	$\frac{\pi}{2}$	$\frac{\pi}{2}$	0	0	$\frac{\pi}{2}$	α_6
d_1	d_2	0	d_4	0	d_6	a_1	a_2	a_3	a_4	a_5	a_6	$\frac{\pi}{2}$	0	$\frac{\pi}{2}$	0	0	α_6
d_1	d_2	0	d_4	0	d_6	a_1	a_2	a_3	a_4	a_5	a_6	$\frac{\pi}{2}$	0	0	$\frac{\pi}{2}$	$\frac{\pi}{2}$	α_6
d_1	d_2	0	d_4	0	d_6	a_1	a_2	a_3	a_4	a_5	a_6	$\frac{\pi}{2}$	0	0	$\frac{\pi}{2}$	0	α_6
d_1	d_2	0	d_4	0	d_6	a_1	a_2	a_3	a_4	a_5	a_6	0	$\frac{\pi}{2}$	$\frac{\pi}{2}$	0	0	α_6
d_1	d_2	0	d_4	0	d_6	a_1	a_2	a_3	a_4	a_5	a_6	0	$\frac{\pi}{2}$	0	0	$\frac{\pi}{2}$	α_6
d_1	d_2	0	d_4	0	d_6	a_1	a_2	a_3	a_4	a_5	a_6	0	0	$\frac{\pi}{2}$	$\frac{\pi}{2}$	$\frac{\pi}{2}$	α_6
d_1	d_2	0	d_4	0	d_6	a_1	a_2	a_3	a_4	a_5	a_6	0	0	$\frac{\pi}{2}$	$\frac{\pi}{2}$	0	α_6
d_1	d_2	0	d_4	0	d_6	a_1	a_2	a_3	a_4	a_5	a_6	0	0	$\frac{\pi}{2}$	0	$\frac{\pi}{2}$	α_6
d_1	d_2	0	d_4	0	d_6	a_1	a_2	a_3	a_4	0	a_6	$\frac{\pi}{2}$	$\frac{\pi}{2}$	0	0	$\frac{\pi}{2}$	α_6
d_1	d_2	0	d_4	0	d_6	a_1	a_2	a_3	a_4	0	a_6	$\frac{\pi}{2}$	0	0	$\frac{\pi}{2}$	$\frac{\pi}{2}$	α_6
d_1	d_2	0	d_4	0	d_6	a_1	a_2	a_3	a_4	0	a_6	0	$\frac{\pi}{2}$	0	0	$\frac{\pi}{2}$	α_6
d_1	d_2	0	d_4	0	d_6	a_1	a_2	a_3	a_4	0	a_6	0	0	$\frac{\pi}{2}$	$\frac{\pi}{2}$	$\frac{\pi}{2}$	α_6
d_1	d_2	0	d_4	0	d_6	a_1	a_2	a_3	a_4	0	a_6	0	0	$\frac{\pi}{2}$	0	$\frac{\pi}{2}$	α_6
d_1	d_2	0	d_4	0	d_6	a_1	a_2	a_3	0	a_5	a_6	$\frac{\pi}{2}$	0	0	$\frac{\pi}{2}$	$\frac{\pi}{2}$	α_6
d_1	d_2	0	d_4	0	d_6	a_1	a_2	a_3	0	a_5	a_6	$\frac{\pi}{2}$	0	0	$\frac{\pi}{2}$	0	α_6
d_1	d_2	0	d_4	0	d_6	a_1	a_2	a_3	0	a_5	a_6	0	0	$\frac{\pi}{2}$	$\frac{\pi}{2}$	$\frac{\pi}{2}$	α_6
d_1	d_2	0	d_4	0	d_6	a_1	a_2	a_3	0	a_5	a_6	0	0	$\frac{\pi}{2}$	$\frac{\pi}{2}$	0	α_6
d_1	d_2	0	d_4	0	d_6	a_1	a_2	a_3	0	0	a_6	$\frac{\pi}{2}$	0	0	$\frac{\pi}{2}$	$\frac{\pi}{2}$	α_6
d_1	d_2	0	d_4	0	d_6	a_1	a_2	a_3	0	0	a_6	0	$\frac{\pi}{2}$	$\frac{\pi}{2}$	$\frac{\pi}{2}$	$\frac{\pi}{2}$	α_6
d_1	d_2	0	d_4	0	d_6	a_1	a_2	a_3	0	0	a_6	0	$\frac{\pi}{2}$	0	$\frac{\pi}{2}$	$\frac{\pi}{2}$	α_6
d_1	d_2	0	d_4	0	d_6	a_1	a_2	0	a_4	a_5	a_6	$\frac{\pi}{2}$	$\frac{\pi}{2}$	$\frac{\pi}{2}$	0	0	α_6
d_1	d_2	0	d_4	0	d_6	a_1	a_2	0	a_4	a_5	a_6	$\frac{\pi}{2}$	0	$\frac{\pi}{2}$	0	0	α_6
d_1	d_2	0	d_4	0	d_6	a_1	a_2	0	a_4	a_5	a_6	0	$\frac{\pi}{2}$	$\frac{\pi}{2}$	0	0	α_6
d_1	d_2	0	d_4	0	d_6	a_1	a_2	0	a_4	a_5	a_6	0	0	$\frac{\pi}{2}$	$\frac{\pi}{2}$	$\frac{\pi}{2}$	α_6
d_1	d_2	0	d_4	0	d_6	a_1	a_2	0	a_4	a_5	a_6	0	0	$\frac{\pi}{2}$	$\frac{\pi}{2}$	0	α_6
d_1	d_2	0	d_4	0	d_6	a_1	a_2	0	a_4	a_5	a_6	0	0	$\frac{\pi}{2}$	0	$\frac{\pi}{2}$	α_6

Table A.6 – The D-H parameter values of robots whose det(**J**) factors into three components.

d_1	d_2	d_3	d_4	d_5	d_6	a_1	a_2	a_3	a_4	a_5	a_6	α_1	α_2	α_3	α_4	α_5	α_6
d_1	d_2	0	d_4	0	d_6	a_1	a_2	0	a_4	0	a_6	0	0	$\frac{\pi}{2}$	$\frac{\pi}{2}$	$\frac{\pi}{2}$	α_6
d_1	d_2	0	d_4	0	d_6	a_1	a_2	0	a_4	0	a_6	0	0	$\frac{\pi}{2}$	0	$\frac{\pi}{2}$	α_6
d_1	d_2	0	d_4	0	d_6	a_1	a_2	0	0	a_5	a_6	0	$\frac{\pi}{2}$	$\frac{\pi}{2}$	$\frac{\pi}{2}$	$\frac{\pi}{2}$	α_6
d_1	d_2	0	d_4	0	d_6	a_1	a_2	0	0	a_5	a_6	0	0	$\frac{\pi}{2}$	$\frac{\pi}{2}$	$\frac{\pi}{2}$	α_6
d_1	d_2	0	d_4	0	d_6	a_1	a_2	0	0	a_5	a_6	0	0	$\frac{\pi}{2}$	$\frac{\pi}{2}$	0	α_6
d_1	d_2	0	d_4	0	d_6	a_1	a_2	0	0	0	a_6	$\frac{\pi}{2}$	0	$\frac{\pi}{2}$	$\frac{\pi}{2}$	$\frac{\pi}{2}$	α_6
d_1	d_2	0	d_4	0	d_6	a_1	a_2	0	0	0	a_6	0	$\frac{\pi}{2}$	$\frac{\pi}{2}$	$\frac{\pi}{2}$	$\frac{\pi}{2}$	α_6
d_1	d_2	0	d_4	0	d_6	a_1	0	a_3	a_4	a_5	a_6	$\frac{\pi}{2}$	$\frac{\pi}{2}$	$\frac{\pi}{2}$	0	0	α_6
d_1	d_2	0	d_4	0	d_6	a_1	0	a_3	a_4	a_5	a_6	$\frac{\pi}{2}$	$\frac{\pi}{2}$	0	0	$\frac{\pi}{2}$	α_6
d_1	d_2	0	d_4	0	d_6	a_1	0	a_3	a_4	a_5	a_6	0	$\frac{\pi}{2}$	$\frac{\pi}{2}$	0	0	α_6
d_1	d_2	0	d_4	0	d_6	a_1	0	a_3	a_4	a_5	a_6	0	$\frac{\pi}{2}$	0	0	$\frac{\pi}{2}$	α_6
d_1	d_2	0	d_4	0	d_6	a_1	0	a_3	a_4	0	a_6	$\frac{\pi}{2}$	$\frac{\pi}{2}$	0	0	$\frac{\pi}{2}$	α_6
d_1	d_2	0	d_4	0	d_6	a_1	0	a_3	a_4	0	a_6	0	$\frac{\pi}{2}$	0	0	$\frac{\pi}{2}$	α_6
d_1	d_2	0	d_4	0	d_6	a_1	0	a_3	0	0	a_6	$\frac{\pi}{2}$	$\frac{\pi}{2}$	0	$\frac{\pi}{2}$	$\frac{\pi}{2}$	α_6
d_1	d_2	0	d_4	0	d_6	a_1	0	a_3	0	0	a_6	0	$\frac{\pi}{2}$	$\frac{\pi}{2}$	$\frac{\pi}{2}$	$\frac{\pi}{2}$	α_6
d_1	d_2	0	d_4	0	d_6	a_1	0	a_3	0	0	a_6	0	$\frac{\pi}{2}$	0	$\frac{\pi}{2}$	$\frac{\pi}{2}$	α_6
d_1	d_2	0	d_4	0	d_6	a_1	0	0	a_4	a_5	a_6	$\frac{\pi}{2}$	$\frac{\pi}{2}$	$\frac{\pi}{2}$	$\frac{\pi}{2}$	$\frac{\pi}{2}$	α_6
d_1	d_2	0	d_4	0	d_6	a_1	0	0	a_4	a_5	a_6	$\frac{\pi}{2}$	$\frac{\pi}{2}$	$\frac{\pi}{2}$	$\frac{\pi}{2}$	0	α_6
d_1	d_2	0	d_4	0	d_6	a_1	0	0	a_4	a_5	a_6	$\frac{\pi}{2}$	$\frac{\pi}{2}$	$\frac{\pi}{2}$	0	0	α_6
d_1	d_2	0	d_4	0	d_6	a_1	0	0	a_4	a_5	a_6	0	$\frac{\pi}{2}$	$\frac{\pi}{2}$	$\frac{\pi}{2}$	$\frac{\pi}{2}$	α_6
d_1	d_2	0	d_4	0	d_6	a_1	0	0	a_4	a_5	a_6	0	$\frac{\pi}{2}$	$\frac{\pi}{2}$	$\frac{\pi}{2}$	0	α_6
d_1	d_2	0	d_4	0	d_6	a_1	0	0	a_4	a_5	a_6	0	$\frac{\pi}{2}$	$\frac{\pi}{2}$	0	0	α_6
d_1	d_2	0	d_4	0	d_6	a_1	0	0	a_4	0	a_6	$\frac{\pi}{2}$	$\frac{\pi}{2}$	$\frac{\pi}{2}$	$\frac{\pi}{2}$	$\frac{\pi}{2}$	α_6
d_1	d_2	0	d_4	0	d_6	a_1	0	0	a_4	0	a_6	$\frac{\pi}{2}$	$\frac{\pi}{2}$	$\frac{\pi}{2}$	0	$\frac{\pi}{2}$	α_6
d_1	d_2	0	d_4	0	d_6	a_1	0	0	a_4	0	a_6	0	$\frac{\pi}{2}$	$\frac{\pi}{2}$	$\frac{\pi}{2}$	$\frac{\pi}{2}$	α_6
d_1	d_2	0	d_4	0	d_6	a_1	0	0	a_4	0	a_6	0	$\frac{\pi}{2}$	$\frac{\pi}{2}$	0	$\frac{\pi}{2}$	α_6
d_1	d_2	0	d_4	0	d_6	a_1	0	0	0	a_5	a_6	$\frac{\pi}{2}$	$\frac{\pi}{2}$	$\frac{\pi}{2}$	$\frac{\pi}{2}$	$\frac{\pi}{2}$	α_6
d_1	d_2	0	d_4	0	d_6	a_1	0	0	0	a_5	a_6	$\frac{\pi}{2}$	$\frac{\pi}{2}$	$\frac{\pi}{2}$	$\frac{\pi}{2}$	0	α_6
d_1	d_2	0	d_4	0	d_6	a_1	0	0	0	a_5	a_6	0	$\frac{\pi}{2}$	$\frac{\pi}{2}$	$\frac{\pi}{2}$	$\frac{\pi}{2}$	α_6
d_1	d_2	0	d_4	0	d_6	a_1	0	0	0	0	a_6	$\frac{\pi}{2}$	$\frac{\pi}{2}$	$\frac{\pi}{2}$	$\frac{\pi}{2}$	$\frac{\pi}{2}$	α_6
d_1	d_2	0	d_4	0	d_6	a_1	0	0	0	0	a_6	0	$\frac{\pi}{2}$	$\frac{\pi}{2}$	$\frac{\pi}{2}$	$\frac{\pi}{2}$	α_6
d_1	d_2	0	0	d_5	d_6	a_1	a_2	a_3	a_4	a_5	a_6	$\frac{\pi}{2}$	$\frac{\pi}{2}$	$\frac{\pi}{2}$	0	0	α_6
d_1	d_2	0	0	d_5	d_6	a_1	a_2	a_3	a_4	a_5	a_6	$\frac{\pi}{2}$	$\frac{\pi}{2}$	0	0	$\frac{\pi}{2}$	α_6
d_1	d_2	0	0	d_5	d_6	a_1	a_2	a_3	a_4	a_5	a_6	$\frac{\pi}{2}$	0	$\frac{\pi}{2}$	0	0	α_6
d_1	d_2	0	0	d_5	d_6	a_1	a_2	a_3	a_4	a_5	a_6	$\frac{\pi}{2}$	0	0	$\frac{\pi}{2}$	$\frac{\pi}{2}$	α_6
d_1	d_2	0	0	d_5	d_6	a_1	a_2	a_3	a_4	a_5	a_6	$\frac{\pi}{2}$	0	0	$\frac{\pi}{2}$	0	α_6
d_1	d_2	0	0	d_5	d_6	a_1	a_2	a_3	a_4	a_5	a_6	0	$\frac{\pi}{2}$	$\frac{\pi}{2}$	0	0	α_6
d_1	d_2	0	0	d_5	d_6	a_1	a_2	a_3	a_4	a_5	a_6	0	$\frac{\pi}{2}$	0	0	$\frac{\pi}{2}$	α_6
d_1	d_2	0	0	d_5	d_6	a_1	a_2	a_3	a_4	a_5	a_6	0	0	$\frac{\pi}{2}$	$\frac{\pi}{2}$	$\frac{\pi}{2}$	α_6
d_1	d_2	0	0	d_5	d_6	a_1	a_2	a_3	a_4	a_5	a_6	0	0	$\frac{\pi}{2}$	$\frac{\pi}{2}$	0	α_6
d_1	d_2	0	0	d_5	d_6	a_1	a_2	a_3	a_4	a_5	a_6	0	0	$\frac{\pi}{2}$	0	$\frac{\pi}{2}$	α_6
d_1	d_2	0	0	d_5	d_6	a_1	a_2	a_3	a_4	0	a_6	$\frac{\pi}{2}$	$\frac{\pi}{2}$	0	0	$\frac{\pi}{2}$	α_6

Table A.7 – The D-H parameter values of robots whose det(**J**) factors into three components.

d_1	d_2	d_3	d_4	d_5	d_6	a_1	a_2	a_3	a_4	a_5	a_6	α_1	α_2	α_3	α_4	α_5	α_6
d_1	d_2	0	0	d_5	d_6	a_1	a_2	a_3	a_4	0	a_6	$\frac{\pi}{2}$	0	0	$\frac{\pi}{2}$	$\frac{\pi}{2}$	α_6
d_1	d_2	0	0	d_5	d_6	a_1	a_2	a_3	a_4	0	a_6	0	$\frac{\pi}{2}$	0	0	$\frac{\pi}{2}$	α_6
d_1	d_2	0	0	d_5	d_6	a_1	a_2	a_3	a_4	0	a_6	0	0	$\frac{\pi}{2}$	$\frac{\pi}{2}$	$\frac{\pi}{2}$	α_6
d_1	d_2	0	0	d_5	d_6	a_1	a_2	a_3	a_4	0	a_6	0	0	$\frac{\pi}{2}$	0	$\frac{\pi}{2}$	α_6
d_1	d_2	0	0	d_5	d_6	a_1	a_2	a_3	0	a_5	a_6	$\frac{\pi}{2}$	0	0	$\frac{\pi}{2}$	$\frac{\pi}{2}$	α_6
d_1	d_2	0	0	d_5	d_6	a_1	a_2	a_3	0	a_5	a_6	$\frac{\pi}{2}$	0	0	$\frac{\pi}{2}$	0	α_6
d_1	d_2	0	0	d_5	d_6	a_1	a_2	a_3	0	a_5	a_6	0	0	$\frac{\pi}{2}$	$\frac{\pi}{2}$	$\frac{\pi}{2}$	α_6
d_1	d_2	0	0	d_5	d_6	a_1	a_2	a_3	0	a_5	a_6	0	0	$\frac{\pi}{2}$	$\frac{\pi}{2}$	0	α_6
d_1	d_2	0	0	d_5	d_6	a_1	a_2	a_3	0	0	a_6	$\frac{\pi}{2}$	0	0	$\frac{\pi}{2}$	$\frac{\pi}{2}$	α_6
d_1	d_2	0	0	d_5	d_6	a_1	a_2	a_3	0	0	a_6	0	0	$\frac{\pi}{2}$	$\frac{\pi}{2}$	$\frac{\pi}{2}$	α_6
d_1	d_2	0	0	d_5	d_6	a_1	a_2	0	a_4	a_5	a_6	$\frac{\pi}{2}$	$\frac{\pi}{2}$	$\frac{\pi}{2}$	0	0	α_6
d_1	d_2	0	0	d_5	d_6	a_1	a_2	0	a_4	a_5	a_6	$\frac{\pi}{2}$	0	$\frac{\pi}{2}$	0	0	α_6
d_1	d_2	0	0	d_5	d_6	a_1	a_2	0	a_4	a_5	a_6	0	$\frac{\pi}{2}$	$\frac{\pi}{2}$	0	0	α_6
d_1	d_2	0	0	d_5	d_6	a_1	a_2	0	a_4	a_5	a_6	0	0	$\frac{\pi}{2}$	$\frac{\pi}{2}$	$\frac{\pi}{2}$	α_6
d_1	d_2	0	0	d_5	d_6	a_1	a_2	0	a_4	a_5	a_6	0	0	$\frac{\pi}{2}$	$\frac{\pi}{2}$	0	α_6
d_1	d_2	0	0	d_5	d_6	a_1	a_2	0	a_4	a_5	a_6	0	0	$\frac{\pi}{2}$	0	$\frac{\pi}{2}$	α_6
d_1	d_2	0	0	d_5	d_6	a_1	a_2	0	a_4	0	a_6	0	0	$\frac{\pi}{2}$	$\frac{\pi}{2}$	$\frac{\pi}{2}$	α_6
d_1	d_2	0	0	d_5	d_6	a_1	a_2	0	a_4	0	a_6	0	0	$\frac{\pi}{2}$	0	$\frac{\pi}{2}$	α_6
d_1	d_2	0	0	d_5	d_6	a_1	a_2	0	0	a_5	a_6	0	$\frac{\pi}{2}$	$\frac{\pi}{2}$	$\frac{\pi}{2}$	$\frac{\pi}{2}$	α_6
d_1	d_2	0	0	d_5	d_6	a_1	a_2	0	0	a_5	a_6	0	$\frac{\pi}{2}$	$\frac{\pi}{2}$	$\frac{\pi}{2}$	0	α_6
d_1	d_2	0	0	d_5	d_6	a_1	a_2	0	0	a_5	a_6	0	0	$\frac{\pi}{2}$	$\frac{\pi}{2}$	$\frac{\pi}{2}$	α_6
d_1	d_2	0	0	d_5	d_6	a_1	a_2	0	0	a_5	a_6	0	0	$\frac{\pi}{2}$	$\frac{\pi}{2}$	0	α_6
d_1	d_2	0	0	d_5	d_6	a_1	a_2	0	0	0	a_6	0	$\frac{\pi}{2}$	$\frac{\pi}{2}$	$\frac{\pi}{2}$	$\frac{\pi}{2}$	α_6
d_1	d_2	0	0	d_5	d_6	a_1	a_2	0	0	0	a_6	0	0	$\frac{\pi}{2}$	$\frac{\pi}{2}$	$\frac{\pi}{2}$	α_6
d_1	d_2	0	0	d_5	d_6	a_1	0	a_3	a_4	a_5	a_6	$\frac{\pi}{2}$	$\frac{\pi}{2}$	$\frac{\pi}{2}$	0	0	α_6
d_1	d_2	0	0	d_5	d_6	a_1	0	a_3	a_4	a_5	a_6	$\frac{\pi}{2}$	$\frac{\pi}{2}$	0	0	$\frac{\pi}{2}$	α_6
d_1	d_2	0	0	d_5	d_6	a_1	0	a_3	a_4	a_5	a_6	0	$\frac{\pi}{2}$	$\frac{\pi}{2}$	0	0	α_6
d_1	d_2	0	0	d_5	d_6	a_1	0	a_3	a_4	a_5	a_6	0	$\frac{\pi}{2}$	0	0	$\frac{\pi}{2}$	α_6
d_1	d_2	0	0	d_5	d_6	a_1	0	a_3	a_4	0	a_6	$\frac{\pi}{2}$	$\frac{\pi}{2}$	0	0	$\frac{\pi}{2}$	α_6
d_1	d_2	0	0	d_5	d_6	a_1	0	a_3	a_4	0	a_6	0	$\frac{\pi}{2}$	0	0	$\frac{\pi}{2}$	α_6
d_1	d_2	0	0	d_5	d_6	a_1	0	0	a_4	a_5	a_6	$\frac{\pi}{2}$	$\frac{\pi}{2}$	$\frac{\pi}{2}$	$\frac{\pi}{2}$	0	α_6
d_1	d_2	0	0	d_5	d_6	a_1	0	0	a_4	a_5	a_6	$\frac{\pi}{2}$	$\frac{\pi}{2}$	$\frac{\pi}{2}$	0	0	α_6
d_1	d_2	0	0	d_5	d_6	a_1	0	0	a_4	a_5	a_6	0	$\frac{\pi}{2}$	$\frac{\pi}{2}$	$\frac{\pi}{2}$	0	α_6
d_1	d_2	0	0	d_5	d_6	a_1	0	0	a_4	a_5	a_6	0	$\frac{\pi}{2}$	$\frac{\pi}{2}$	$\frac{\pi}{2}$	$\frac{\pi}{2}$	α_6
d_1	d_2	0	0	d_5	d_6	a_1	0	0	a_4	0	a_6	$\frac{\pi}{2}$	$\frac{\pi}{2}$	$\frac{\pi}{2}$	$\frac{\pi}{2}$	0	α_6
d_1	d_2	0	0	d_5	d_6	a_1	0	0	a_4	0	a_6	$\frac{\pi}{2}$	$\frac{\pi}{2}$	$\frac{\pi}{2}$	0	$\frac{\pi}{2}$	α_6
d_1	d_2	0	0	d_5	d_6	a_1	0	0	a_4	0	a_6	0	$\frac{\pi}{2}$	$\frac{\pi}{2}$	$\frac{\pi}{2}$	$\frac{\pi}{2}$	α_6
d_1	d_2	0	0	d_5	d_6	a_1	0	0	a_4	0	a_6	0	$\frac{\pi}{2}$	$\frac{\pi}{2}$	0	$\frac{\pi}{2}$	α_6
d_1	d_2	0	0	0	d_6	a_1	a_2	a_3	a_4	a_5	a_6	$\frac{\pi}{2}$	$\frac{\pi}{2}$	$\frac{\pi}{2}$	0	0	α_6
d_1	d_2	0	0	0	d_6	a_1	a_2	a_3	a_4	a_5	a_6	$\frac{\pi}{2}$	$\frac{\pi}{2}$	0	0	$\frac{\pi}{2}$	α_6
d_1	d_2	0	0	0	d_6	a_1	a_2	a_3	a_4	a_5	a_6	$\frac{\pi}{2}$	0	$\frac{\pi}{2}$	0	0	α_6
d_1	d_2	0	0	0	d_6	a_1	a_2	a_3	a_4	a_5	a_6	$\frac{\pi}{2}$	0	0	$\frac{\pi}{2}$	$\frac{\pi}{2}$	α_6
d_1	d_2	0	0	0	d_6	a_1	a_2	a_3	a_4	a_5	a_6	$\frac{\pi}{2}$	0	0	$\frac{\pi}{2}$	0	α_6

Table A.8 – The D-H parameter values of robots whose det(**J**) factors into three components.

d_1	d_2	d_3	d_4	d_5	d_6	a_1	a_2	a_3	a_4	a_5	a_6	α_1	α_2	α_3	α_4	α_5	α_6
d_1	d_2	0	0	0	d_6	a_1	a_2	a_3	a_4	a_5	a_6	0	$\frac{\pi}{2}$	$\frac{\pi}{2}$	0	0	α_6
d_1	d_2	0	0	0	d_6	a_1	a_2	a_3	a_4	a_5	a_6	0	$\frac{\pi}{2}$	0	0	$\frac{\pi}{2}$	α_6
d_1	d_2	0	0	0	d_6	a_1	a_2	a_3	a_4	a_5	a_6	0	0	$\frac{\pi}{2}$	$\frac{\pi}{2}$	$\frac{\pi}{2}$	α_6
d_1	d_2	0	0	0	d_6	a_1	a_2	a_3	a_4	a_5	a_6	0	0	$\frac{\pi}{2}$	$\frac{\pi}{2}$	0	α_6
d_1	d_2	0	0	0	d_6	a_1	a_2	a_3	a_4	a_5	a_6	0	0	$\frac{\pi}{2}$	0	$\frac{\pi}{2}$	α_6
d_1	d_2	0	0	0	d_6	a_1	a_2	a_3	a_4	0	a_6	$\frac{\pi}{2}$	$\frac{\pi}{2}$	0	0	$\frac{\pi}{2}$	α_6
d_1	d_2	0	0	0	d_6	a_1	a_2	a_3	a_4	0	a_6	$\frac{\pi}{2}$	0	0	$\frac{\pi}{2}$	$\frac{\pi}{2}$	α_6
d_1	d_2	0	0	0	d_6	a_1	a_2	a_3	a_4	0	a_6	0	$\frac{\pi}{2}$	0	0	$\frac{\pi}{2}$	α_6
d_1	d_2	0	0	0	d_6	a_1	a_2	a_3	a_4	0	a_6	0	0	$\frac{\pi}{2}$	$\frac{\pi}{2}$	$\frac{\pi}{2}$	α_6
d_1	d_2	0	0	0	d_6	a_1	a_2	a_3	a_4	0	a_6	0	0	$\frac{\pi}{2}$	0	$\frac{\pi}{2}$	α_6
d_1	d_2	0	0	0	d_6	a_1	a_2	a_3	0	a_5	a_6	$\frac{\pi}{2}$	0	0	$\frac{\pi}{2}$	$\frac{\pi}{2}$	α_6
d_1	d_2	0	0	0	d_6	a_1	a_2	a_3	0	a_5	a_6	$\frac{\pi}{2}$	0	0	$\frac{\pi}{2}$	0	α_6
d_1	d_2	0	0	0	d_6	a_1	a_2	a_3	0	a_5	a_6	0	0	$\frac{\pi}{2}$	$\frac{\pi}{2}$	$\frac{\pi}{2}$	α_6
d_1	d_2	0	0	0	d_6	a_1	a_2	a_3	0	a_5	a_6	0	0	$\frac{\pi}{2}$	$\frac{\pi}{2}$	0	α_6
d_1	d_2	0	0	0	d_6	a_1	a_2	a_3	0	0	a_6	$\frac{\pi}{2}$	$\frac{\pi}{2}$	$\frac{\pi}{2}$	$\frac{\pi}{2}$	$\frac{\pi}{2}$	α_6
d_1	d_2	0	0	0	d_6	a_1	a_2	a_3	0	0	a_6	$\frac{\pi}{2}$	$\frac{\pi}{2}$	0	$\frac{\pi}{2}$	$\frac{\pi}{2}$	α_6
d_1	d_2	0	0	0	d_6	a_1	a_2	a_3	0	0	a_6	$\frac{\pi}{2}$	0	$\frac{\pi}{2}$	$\frac{\pi}{2}$	$\frac{\pi}{2}$	α_6
d_1	d_2	0	0	0	d_6	a_1	a_2	a_3	0	0	a_6	$\frac{\pi}{2}$	0	0	$\frac{\pi}{2}$	$\frac{\pi}{2}$	α_6
d_1	d_2	0	0	0	d_6	a_1	a_2	a_3	0	0	a_6	0	$\frac{\pi}{2}$	$\frac{\pi}{2}$	$\frac{\pi}{2}$	$\frac{\pi}{2}$	α_6
d_1	d_2	0	0	0	d_6	a_1	a_2	a_3	0	0	a_6	0	$\frac{\pi}{2}$	0	$\frac{\pi}{2}$	$\frac{\pi}{2}$	α_6
d_1	d_2	0	0	0	d_6	a_1	a_2	0	a_4	a_5	a_6	$\frac{\pi}{2}$	$\frac{\pi}{2}$	$\frac{\pi}{2}$	0	0	α_6
d_1	d_2	0	0	0	d_6	a_1	a_2	0	a_4	a_5	a_6	$\frac{\pi}{2}$	0	$\frac{\pi}{2}$	0	0	α_6
d_1	d_2	0	0	0	d_6	a_1	a_2	0	a_4	a_5	a_6	0	$\frac{\pi}{2}$	$\frac{\pi}{2}$	0	0	α_6
d_1	d_2	0	0	0	d_6	a_1	a_2	0	a_4	a_5	a_6	0	0	$\frac{\pi}{2}$	$\frac{\pi}{2}$	$\frac{\pi}{2}$	α_6
d_1	d_2	0	0	0	d_6	a_1	a_2	0	a_4	a_5	a_6	0	0	$\frac{\pi}{2}$	$\frac{\pi}{2}$	0	α_6
d_1	d_2	0	0	0	d_6	a_1	a_2	0	a_4	a_5	a_6	0	0	$\frac{\pi}{2}$	0	$\frac{\pi}{2}$	α_6
d_1	d_2	0	0	0	d_6	a_1	a_2	0	a_4	0	a_6	0	0	$\frac{\pi}{2}$	$\frac{\pi}{2}$	$\frac{\pi}{2}$	α_6
d_1	d_2	0	0	0	d_6	a_1	a_2	0	a_4	0	a_6	0	0	$\frac{\pi}{2}$	0	$\frac{\pi}{2}$	α_6
d_1	d_2	0	0	0	d_6	a_1	a_2	0	0	a_5	a_6	0	$\frac{\pi}{2}$	$\frac{\pi}{2}$	$\frac{\pi}{2}$	$\frac{\pi}{2}$	α_6
d_1	d_2	0	0	0	d_6	a_1	a_2	0	0	a_5	a_6	0	$\frac{\pi}{2}$	$\frac{\pi}{2}$	$\frac{\pi}{2}$	0	α_6
d_1	d_2	0	0	0	d_6	a_1	a_2	0	0	a_5	a_6	0	0	$\frac{\pi}{2}$	$\frac{\pi}{2}$	$\frac{\pi}{2}$	α_6
d_1	d_2	0	0	0	d_6	a_1	a_2	0	0	a_5	a_6	0	0	$\frac{\pi}{2}$	$\frac{\pi}{2}$	0	α_6
d_1	d_2	0	0	0	d_6	a_1	0	a_3	a_4	a_5	a_6	$\frac{\pi}{2}$	$\frac{\pi}{2}$	$\frac{\pi}{2}$	0	0	α_6
d_1	d_2	0	0	0	d_6	a_1	0	a_3	a_4	a_5	a_6	$\frac{\pi}{2}$	$\frac{\pi}{2}$	0	0	$\frac{\pi}{2}$	α_6
d_1	d_2	0	0	0	d_6	a_1	0	a_3	a_4	a_5	a_6	0	$\frac{\pi}{2}$	$\frac{\pi}{2}$	0	0	α_6
d_1	d_2	0	0	0	d_6	a_1	0	a_3	a_4	a_5	a_6	0	$\frac{\pi}{2}$	0	0	$\frac{\pi}{2}$	α_6
d_1	d_2	0	0	0	d_6	a_1	0	a_3	a_4	0	a_6	$\frac{\pi}{2}$	$\frac{\pi}{2}$	0	0	$\frac{\pi}{2}$	α_6
d_1	d_2	0	0	0	d_6	a_1	0	a_3	a_4	0	a_6	0	$\frac{\pi}{2}$	0	0	$\frac{\pi}{2}$	α_6
d_1	d_2	0	0	0	d_6	a_1	0	a_3	0	0	a_6	$\frac{\pi}{2}$	$\frac{\pi}{2}$	$\frac{\pi}{2}$	$\frac{\pi}{2}$	$\frac{\pi}{2}$	α_6
d_1	d_2	0	0	0	d_6	a_1	0	a_3	0	0	a_6	$\frac{\pi}{2}$	$\frac{\pi}{2}$	0	$\frac{\pi}{2}$	$\frac{\pi}{2}$	α_6
d_1	d_2	0	0	0	d_6	a_1	0	a_3	0	0	a_6	0	$\frac{\pi}{2}$	$\frac{\pi}{2}$	$\frac{\pi}{2}$	$\frac{\pi}{2}$	α_6
d_1	d_2	0	0	0	d_6	a_1	0	a_3	0	0	a_6	0	$\frac{\pi}{2}$	0	$\frac{\pi}{2}$	$\frac{\pi}{2}$	α_6
d_1	d_2	0	0	0	d_6	a_1	0	0	a_4	a_5	a_6	$\frac{\pi}{2}$	$\frac{\pi}{2}$	$\frac{\pi}{2}$	$\frac{\pi}{2}$	$\frac{\pi}{2}$	α_6

Table A.9 – The D-H parameter values of robots whose det(**J**) factors into three components.

d_1	d_2	d_3	d_4	d_5	d_6	a_1	a_2	a_3	a_4	a_5	a_6	α_1	α_2	α_3	α_4	α_5	α_6
d_1	d_2	0	0	0	d_6	a_1	0	0	a_4	a_5	a_6	$\frac{\pi}{2}$	$\frac{\pi}{2}$	$\frac{\pi}{2}$	$\frac{\pi}{2}$	0	α_6
d_1	d_2	0	0	0	d_6	a_1	0	0	a_4	a_5	a_6	$\frac{\pi}{2}$	$\frac{\pi}{2}$	$\frac{\pi}{2}$	0	$\frac{\pi}{2}$	α_6
d_1	d_2	0	0	0	d_6	a_1	0	0	a_4	a_5	a_6	$\frac{\pi}{2}$	$\frac{\pi}{2}$	$\frac{\pi}{2}$	0	0	α_6
d_1	d_2	0	0	0	d_6	a_1	0	0	a_4	a_5	a_6	0	$\frac{\pi}{2}$	$\frac{\pi}{2}$	$\frac{\pi}{2}$	$\frac{\pi}{2}$	α_6
d_1	d_2	0	0	0	d_6	a_1	0	0	a_4	a_5	a_6	0	$\frac{\pi}{2}$	$\frac{\pi}{2}$	$\frac{\pi}{2}$	0	α_6
d_1	d_2	0	0	0	d_6	a_1	0	0	a_4	a_5	a_6	0	$\frac{\pi}{2}$	$\frac{\pi}{2}$	0	$\frac{\pi}{2}$	α_6
d_1	d_2	0	0	0	d_6	a_1	0	0	a_4	a_5	a_6	0	$\frac{\pi}{2}$	$\frac{\pi}{2}$	0	0	α_6
d_1	d_2	0	0	0	d_6	a_1	0	0	a_4	0	a_6	$\frac{\pi}{2}$	$\frac{\pi}{2}$	$\frac{\pi}{2}$	$\frac{\pi}{2}$	$\frac{\pi}{2}$	α_6
d_1	d_2	0	0	0	d_6	a_1	0	0	a_4	0	a_6	$\frac{\pi}{2}$	$\frac{\pi}{2}$	$\frac{\pi}{2}$	0	$\frac{\pi}{2}$	α_6
d_1	d_2	0	0	0	d_6	a_1	0	0	a_4	0	a_6	0	$\frac{\pi}{2}$	$\frac{\pi}{2}$	$\frac{\pi}{2}$	$\frac{\pi}{2}$	α_6
d_1	d_2	0	0	0	d_6	a_1	0	0	a_4	0	a_6	0	$\frac{\pi}{2}$	$\frac{\pi}{2}$	0	$\frac{\pi}{2}$	α_6
d_1	0	d_3	d_4	d_5	d_6	a_1	a_2	a_3	a_4	a_5	a_6	$\frac{\pi}{2}$	$\frac{\pi}{2}$	$\frac{\pi}{2}$	0	0	α_6
d_1	0	d_3	d_4	d_5	d_6	a_1	a_2	a_3	a_4	a_5	a_6	$\frac{\pi}{2}$	$\frac{\pi}{2}$	0	0	$\frac{\pi}{2}$	α_6
d_1	0	d_3	d_4	d_5	d_6	a_1	a_2	a_3	a_4	a_5	a_6	$\frac{\pi}{2}$	0	$\frac{\pi}{2}$	0	0	α_6
d_1	0	d_3	d_4	d_5	d_6	a_1	a_2	a_3	a_4	a_5	a_6	$\frac{\pi}{2}$	0	0	$\frac{\pi}{2}$	$\frac{\pi}{2}$	α_6
d_1	0	d_3	d_4	d_5	d_6	a_1	a_2	a_3	a_4	a_5	a_6	$\frac{\pi}{2}$	0	0	$\frac{\pi}{2}$	0	α_6
d_1	0	d_3	d_4	d_5	d_6	a_1	a_2	a_3	a_4	a_5	a_6	0	$\frac{\pi}{2}$	$\frac{\pi}{2}$	0	0	α_6
d_1	0	d_3	d_4	d_5	d_6	a_1	a_2	a_3	a_4	a_5	a_6	0	$\frac{\pi}{2}$	0	0	$\frac{\pi}{2}$	α_6
d_1	0	d_3	d_4	d_5	d_6	a_1	a_2	a_3	a_4	a_5	a_6	0	0	$\frac{\pi}{2}$	$\frac{\pi}{2}$	$\frac{\pi}{2}$	α_6
d_1	0	d_3	d_4	d_5	d_6	a_1	a_2	a_3	a_4	a_5	a_6	0	0	$\frac{\pi}{2}$	$\frac{\pi}{2}$	0	α_6
d_1	0	d_3	d_4	d_5	d_6	a_1	a_2	a_3	a_4	a_5	a_6	0	0	$\frac{\pi}{2}$	0	$\frac{\pi}{2}$	α_6
d_1	0	d_3	d_4	d_5	d_6	a_1	a_2	a_3	a_4	0	a_6	$\frac{\pi}{2}$	$\frac{\pi}{2}$	0	0	$\frac{\pi}{2}$	α_6
d_1	0	d_3	d_4	d_5	d_6	a_1	a_2	a_3	a_4	0	a_6	$\frac{\pi}{2}$	0	0	$\frac{\pi}{2}$	$\frac{\pi}{2}$	α_6
d_1	0	d_3	d_4	d_5	d_6	a_1	a_2	a_3	a_4	0	a_6	0	$\frac{\pi}{2}$	0	0	$\frac{\pi}{2}$	α_6
d_1	0	d_3	d_4	d_5	d_6	a_1	a_2	a_3	a_4	0	a_6	0	0	$\frac{\pi}{2}$	$\frac{\pi}{2}$	$\frac{\pi}{2}$	α_6
d_1	0	d_3	d_4	d_5	d_6	a_1	a_2	a_3	a_4	0	a_6	0	0	$\frac{\pi}{2}$	0	$\frac{\pi}{2}$	α_6
d_1	0	d_3	d_4	d_5	d_6	a_1	a_2	a_3	0	a_5	a_6	$\frac{\pi}{2}$	0	0	$\frac{\pi}{2}$	$\frac{\pi}{2}$	α_6
d_1	0	d_3	d_4	d_5	d_6	a_1	a_2	a_3	0	a_5	a_6	$\frac{\pi}{2}$	0	0	$\frac{\pi}{2}$	0	α_6
d_1	0	d_3	d_4	d_5	d_6	a_1	a_2	a_3	0	a_5	a_6	0	0	$\frac{\pi}{2}$	$\frac{\pi}{2}$	$\frac{\pi}{2}$	α_6
d_1	0	d_3	d_4	d_5	d_6	a_1	a_2	a_3	0	a_5	a_6	0	0	$\frac{\pi}{2}$	$\frac{\pi}{2}$	0	α_6
d_1	0	d_3	d_4	d_5	d_6	a_1	a_2	a_3	0	0	a_6	$\frac{\pi}{2}$	0	0	$\frac{\pi}{2}$	$\frac{\pi}{2}$	α_6
d_1	0	d_3	d_4	d_5	d_6	a_1	a_2	a_3	0	0	a_6	0	0	$\frac{\pi}{2}$	$\frac{\pi}{2}$	$\frac{\pi}{2}$	α_6
d_1	0	d_3	d_4	d_5	d_6	a_1	a_2	0	a_4	a_5	a_6	$\frac{\pi}{2}$	$\frac{\pi}{2}$	$\frac{\pi}{2}$	0	0	α_6
d_1	0	d_3	d_4	d_5	d_6	a_1	a_2	0	a_4	a_5	a_6	$\frac{\pi}{2}$	0	$\frac{\pi}{2}$	0	0	α_6
d_1	0	d_3	d_4	d_5	d_6	a_1	a_2	0	a_4	a_5	a_6	0	$\frac{\pi}{2}$	$\frac{\pi}{2}$	0	0	α_6
d_1	0	d_3	d_4	d_5	d_6	a_1	a_2	0	a_4	a_5	a_6	0	0	$\frac{\pi}{2}$	$\frac{\pi}{2}$	$\frac{\pi}{2}$	α_6
d_1	0	d_3	d_4	d_5	d_6	a_1	a_2	0	a_4	a_5	a_6	0	0	$\frac{\pi}{2}$	$\frac{\pi}{2}$	0	α_6
d_1	0	d_3	d_4	d_5	d_6	a_1	a_2	0	a_4	a_5	a_6	0	0	$\frac{\pi}{2}$	0	$\frac{\pi}{2}$	α_6
d_1	0	d_3	d_4	d_5	d_6	a_1	a_2	0	a_4	0	a_6	0	0	$\frac{\pi}{2}$	$\frac{\pi}{2}$	$\frac{\pi}{2}$	α_6
d_1	0	d_3	d_4	d_5	d_6	a_1	a_2	0	a_4	0	a_6	0	0	$\frac{\pi}{2}$	0	$\frac{\pi}{2}$	α_6
d_1	0	d_3	d_4	d_5	d_6	a_1	a_2	0	0	a_5	a_6	0	0	$\frac{\pi}{2}$	$\frac{\pi}{2}$	$\frac{\pi}{2}$	α_6
d_1	0	d_3	d_4	d_5	d_6	a_1	a_2	0	0	a_5	a_6	0	0	$\frac{\pi}{2}$	$\frac{\pi}{2}$	0	α_6
d_1	0	d_3	d_4	d_5	d_6	a_1	a_2	0	0	0	a_6	0	0	$\frac{\pi}{2}$	$\frac{\pi}{2}$	$\frac{\pi}{2}$	α_6

Table A.10 – The D-H parameter values of robots whose det(**J**) factors into three components.

d_1	d_2	d_3	d_4	d_5	d_6	a_1	a_2	a_3	a_4	a_5	a_6	α_1	α_2	α_3	α_4	α_5	α_6
d_1	0	d_3	d_4	d_5	d_6	a_1	0	a_3	a_4	a_5	a_6	$\frac{\pi}{2}$	$\frac{\pi}{2}$	$\frac{\pi}{2}$	0	0	α_6
d_1	0	d_3	d_4	d_5	d_6	a_1	0	a_3	a_4	a_5	a_6	$\frac{\pi}{2}$	$\frac{\pi}{2}$	0	0	$\frac{\pi}{2}$	α_6
d_1	0	d_3	d_4	d_5	d_6	a_1	0	a_3	a_4	a_5	a_6	0	$\frac{\pi}{2}$	$\frac{\pi}{2}$	0	0	α_6
d_1	0	d_3	d_4	d_5	d_6	a_1	0	a_3	a_4	a_5	a_6	0	$\frac{\pi}{2}$	0	0	$\frac{\pi}{2}$	α_6
d_1	0	d_3	d_4	d_5	d_6	a_1	0	a_3	a_4	0	a_6	$\frac{\pi}{2}$	$\frac{\pi}{2}$	0	0	$\frac{\pi}{2}$	α_6
d_1	0	d_3	d_4	d_5	d_6	a_1	0	a_3	a_4	0	a_6	0	$\frac{\pi}{2}$	0	0	$\frac{\pi}{2}$	α_6
d_1	0	d_3	d_4	d_5	d_6	a_1	0	0	a_4	a_5	a_6	$\frac{\pi}{2}$	$\frac{\pi}{2}$	$\frac{\pi}{2}$	0	0	α_6
d_1	0	d_3	d_4	d_5	d_6	a_1	0	0	a_4	a_5	a_6	0	$\frac{\pi}{2}$	$\frac{\pi}{2}$	0	0	α_6
d_1	0	d_3	d_4	0	d_6	a_1	a_2	a_3	a_4	a_5	a_6	$\frac{\pi}{2}$	$\frac{\pi}{2}$	$\frac{\pi}{2}$	0	0	α_6
d_1	0	d_3	d_4	0	d_6	a_1	a_2	a_3	a_4	a_5	a_6	$\frac{\pi}{2}$	$\frac{\pi}{2}$	0	0	$\frac{\pi}{2}$	α_6
d_1	0	d_3	d_4	0	d_6	a_1	a_2	a_3	a_4	a_5	a_6	$\frac{\pi}{2}$	0	$\frac{\pi}{2}$	0	0	α_6
d_1	0	d_3	d_4	0	d_6	a_1	a_2	a_3	a_4	a_5	a_6	$\frac{\pi}{2}$	0	0	$\frac{\pi}{2}$	$\frac{\pi}{2}$	α_6
d_1	0	d_3	d_4	0	d_6	a_1	a_2	a_3	a_4	a_5	a_6	$\frac{\pi}{2}$	0	0	$\frac{\pi}{2}$	0	α_6
d_1	0	d_3	d_4	0	d_6	a_1	a_2	a_3	a_4	a_5	a_6	0	$\frac{\pi}{2}$	$\frac{\pi}{2}$	0	0	α_6
d_1	0	d_3	d_4	0	d_6	a_1	a_2	a_3	a_4	a_5	a_6	0	$\frac{\pi}{2}$	0	0	$\frac{\pi}{2}$	α_6
d_1	0	d_3	d_4	0	d_6	a_1	a_2	a_3	a_4	a_5	a_6	0	0	$\frac{\pi}{2}$	$\frac{\pi}{2}$	$\frac{\pi}{2}$	α_6
d_1	0	d_3	d_4	0	d_6	a_1	a_2	a_3	a_4	a_5	a_6	0	0	$\frac{\pi}{2}$	$\frac{\pi}{2}$	0	α_6
d_1	0	d_3	d_4	0	d_6	a_1	a_2	a_3	a_4	a_5	a_6	0	0	$\frac{\pi}{2}$	0	$\frac{\pi}{2}$	α_6
d_1	0	d_3	d_4	0	d_6	a_1	a_2	a_3	a_4	0	a_6	$\frac{\pi}{2}$	$\frac{\pi}{2}$	0	0	$\frac{\pi}{2}$	α_6
d_1	0	d_3	d_4	0	d_6	a_1	a_2	a_3	a_4	0	a_6	$\frac{\pi}{2}$	0	0	$\frac{\pi}{2}$	$\frac{\pi}{2}$	α_6
d_1	0	d_3	d_4	0	d_6	a_1	a_2	a_3	a_4	0	a_6	0	$\frac{\pi}{2}$	0	0	$\frac{\pi}{2}$	α_6
d_1	0	d_3	d_4	0	d_6	a_1	a_2	a_3	a_4	0	a_6	0	0	$\frac{\pi}{2}$	$\frac{\pi}{2}$	$\frac{\pi}{2}$	α_6
d_1	0	d_3	d_4	0	d_6	a_1	a_2	a_3	a_4	0	a_6	0	0	$\frac{\pi}{2}$	0	$\frac{\pi}{2}$	α_6
d_1	0	d_3	d_4	0	d_6	a_1	a_2	a_3	0	a_5	a_6	$\frac{\pi}{2}$	0	0	$\frac{\pi}{2}$	$\frac{\pi}{2}$	α_6
d_1	0	d_3	d_4	0	d_6	a_1	a_2	a_3	0	a_5	a_6	$\frac{\pi}{2}$	0	0	$\frac{\pi}{2}$	0	α_6
d_1	0	d_3	d_4	0	d_6	a_1	a_2	a_3	0	a_5	a_6	0	0	$\frac{\pi}{2}$	$\frac{\pi}{2}$	$\frac{\pi}{2}$	α_6
d_1	0	d_3	d_4	0	d_6	a_1	a_2	a_3	0	a_5	a_6	0	0	$\frac{\pi}{2}$	$\frac{\pi}{2}$	0	α_6
d_1	0	d_3	d_4	0	d_6	a_1	a_2	a_3	0	0	a_6	$\frac{\pi}{2}$	$\frac{\pi}{2}$	0	$\frac{\pi}{2}$	$\frac{\pi}{2}$	α_6
d_1	0	d_3	d_4	0	d_6	a_1	a_2	a_3	0	0	a_6	$\frac{\pi}{2}$	0	0	$\frac{\pi}{2}$	$\frac{\pi}{2}$	α_6
d_1	0	d_3	d_4	0	d_6	a_1	a_2	a_3	0	0	a_6	0	$\frac{\pi}{2}$	0	$\frac{\pi}{2}$	$\frac{\pi}{2}$	α_6
d_1	0	d_3	d_4	0	d_6	a_1	a_2	0	a_4	a_5	a_6	$\frac{\pi}{2}$	$\frac{\pi}{2}$	$\frac{\pi}{2}$	0	0	α_6
d_1	0	d_3	d_4	0	d_6	a_1	a_2	0	a_4	a_5	a_6	$\frac{\pi}{2}$	0	$\frac{\pi}{2}$	0	0	α_6
d_1	0	d_3	d_4	0	d_6	a_1	a_2	0	a_4	a_5	a_6	0	$\frac{\pi}{2}$	$\frac{\pi}{2}$	0	0	α_6
d_1	0	d_3	d_4	0	d_6	a_1	a_2	0	a_4	a_5	a_6	0	0	$\frac{\pi}{2}$	$\frac{\pi}{2}$	$\frac{\pi}{2}$	α_6
d_1	0	d_3	d_4	0	d_6	a_1	a_2	0	a_4	a_5	a_6	0	0	$\frac{\pi}{2}$	$\frac{\pi}{2}$	0	α_6
d_1	0	d_3	d_4	0	d_6	a_1	a_2	0	a_4	a_5	a_6	0	0	$\frac{\pi}{2}$	0	$\frac{\pi}{2}$	α_6
d_1	0	d_3	d_4	0	d_6	a_1	a_2	0	a_4	0	a_6	0	0	$\frac{\pi}{2}$	$\frac{\pi}{2}$	$\frac{\pi}{2}$	α_6
d_1	0	d_3	d_4	0	d_6	a_1	a_2	0	a_4	0	a_6	0	0	$\frac{\pi}{2}$	0	$\frac{\pi}{2}$	α_6
d_1	0	d_3	d_4	0	d_6	a_1	a_2	0	0	a_5	a_6	0	0	$\frac{\pi}{2}$	$\frac{\pi}{2}$	$\frac{\pi}{2}$	α_6
d_1	0	d_3	d_4	0	d_6	a_1	a_2	0	0	a_5	a_6	0	0	$\frac{\pi}{2}$	$\frac{\pi}{2}$	0	α_6
d_1	0	d_3	d_4	0	d_6	a_1	a_2	0	0	0	a_6	$\frac{\pi}{2}$	$\frac{\pi}{2}$	$\frac{\pi}{2}$	$\frac{\pi}{2}$	$\frac{\pi}{2}$	α_6
d_1	0	d_3	d_4	0	d_6	a_1	a_2	0	0	0	a_6	$\frac{\pi}{2}$	0	$\frac{\pi}{2}$	$\frac{\pi}{2}$	$\frac{\pi}{2}$	α_6
d_1	0	d_3	d_4	0	d_6	a_1	a_2	0	0	0	a_6	0	$\frac{\pi}{2}$	$\frac{\pi}{2}$	$\frac{\pi}{2}$	$\frac{\pi}{2}$	α_6

Table A.11 – The D-H parameter values of robots whose det(**J**) factors into three components.

d_1	d_2	d_3	d_4	d_5	d_6	a_1	a_2	a_3	a_4	a_5	a_6	α_1	α_2	α_3	α_4	α_5	α_6
d_1	0	d_3	d_4	0	d_6	a_1	0	a_3	a_4	a_5	a_6	$\frac{\pi}{2}$	$\frac{\pi}{2}$	$\frac{\pi}{2}$	0	0	α_6
d_1	0	d_3	d_4	0	d_6	a_1	0	a_3	a_4	a_5	a_6	$\frac{\pi}{2}$	$\frac{\pi}{2}$	0	0	$\frac{\pi}{2}$	α_6
d_1	0	d_3	d_4	0	d_6	a_1	0	a_3	a_4	a_5	a_6	0	$\frac{\pi}{2}$	$\frac{\pi}{2}$	0	0	α_6
d_1	0	d_3	d_4	0	d_6	a_1	0	a_3	a_4	a_5	a_6	0	$\frac{\pi}{2}$	0	0	$\frac{\pi}{2}$	α_6
d_1	0	d_3	d_4	0	d_6	a_1	0	a_3	a_4	0	a_6	$\frac{\pi}{2}$	$\frac{\pi}{2}$	0	0	$\frac{\pi}{2}$	α_6
d_1	0	d_3	d_4	0	d_6	a_1	0	a_3	a_4	0	a_6	0	$\frac{\pi}{2}$	0	0	$\frac{\pi}{2}$	α_6
d_1	0	d_3	d_4	0	d_6	a_1	0	a_3	0	0	a_6	$\frac{\pi}{2}$	$\frac{\pi}{2}$	0	$\frac{\pi}{2}$	$\frac{\pi}{2}$	α_6
d_1	0	d_3	d_4	0	d_6	a_1	0	a_3	0	0	a_6	0	$\frac{\pi}{2}$	0	$\frac{\pi}{2}$	$\frac{\pi}{2}$	α_6
d_1	0	d_3	d_4	0	d_6	a_1	0	0	a_4	a_5	a_6	$\frac{\pi}{2}$	$\frac{\pi}{2}$	$\frac{\pi}{2}$	0	0	α_6
d_1	0	d_3	d_4	0	d_6	a_1	0	0	a_4	a_5	a_6	0	$\frac{\pi}{2}$	$\frac{\pi}{2}$	0	0	α_6
d_1	0	d_3	d_4	0	d_6	a_1	0	0	0	0	a_6	$\frac{\pi}{2}$	$\frac{\pi}{2}$	$\frac{\pi}{2}$	$\frac{\pi}{2}$	$\frac{\pi}{2}$	α_6
d_1	0	d_3	d_4	0	d_6	a_1	0	0	0	0	a_6	0	$\frac{\pi}{2}$	$\frac{\pi}{2}$	$\frac{\pi}{2}$	$\frac{\pi}{2}$	α_6
d_1	0	d_3	0	d_5	d_6	a_1	a_2	a_3	a_4	a_5	a_6	$\frac{\pi}{2}$	$\frac{\pi}{2}$	$\frac{\pi}{2}$	0	0	α_6
d_1	0	d_3	0	d_5	d_6	a_1	a_2	a_3	a_4	a_5	a_6	$\frac{\pi}{2}$	$\frac{\pi}{2}$	0	0	$\frac{\pi}{2}$	α_6
d_1	0	d_3	0	d_5	d_6	a_1	a_2	a_3	a_4	a_5	a_6	$\frac{\pi}{2}$	0	$\frac{\pi}{2}$	0	0	α_6
d_1	0	d_3	0	d_5	d_6	a_1	a_2	a_3	a_4	a_5	a_6	$\frac{\pi}{2}$	0	0	$\frac{\pi}{2}$	$\frac{\pi}{2}$	α_6
d_1	0	d_3	0	d_5	d_6	a_1	a_2	a_3	a_4	a_5	a_6	$\frac{\pi}{2}$	0	0	$\frac{\pi}{2}$	0	α_6
d_1	0	d_3	0	d_5	d_6	a_1	a_2	a_3	a_4	a_5	a_6	0	$\frac{\pi}{2}$	$\frac{\pi}{2}$	0	0	α_6
d_1	0	d_3	0	d_5	d_6	a_1	a_2	a_3	a_4	a_5	a_6	0	$\frac{\pi}{2}$	0	0	$\frac{\pi}{2}$	α_6
d_1	0	d_3	0	d_5	d_6	a_1	a_2	a_3	a_4	a_5	a_6	0	0	$\frac{\pi}{2}$	$\frac{\pi}{2}$	$\frac{\pi}{2}$	α_6
d_1	0	d_3	0	d_5	d_6	a_1	a_2	a_3	a_4	a_5	a_6	0	0	$\frac{\pi}{2}$	$\frac{\pi}{2}$	0	α_6
d_1	0	d_3	0	d_5	d_6	a_1	a_2	a_3	a_4	a_5	a_6	0	0	$\frac{\pi}{2}$	0	$\frac{\pi}{2}$	α_6
d_1	0	d_3	0	d_5	d_6	a_1	a_2	a_3	a_4	0	a_6	$\frac{\pi}{2}$	$\frac{\pi}{2}$	0	0	$\frac{\pi}{2}$	α_6
d_1	0	d_3	0	d_5	d_6	a_1	a_2	a_3	a_4	0	a_6	$\frac{\pi}{2}$	0	0	$\frac{\pi}{2}$	$\frac{\pi}{2}$	α_6
d_1	0	d_3	0	d_5	d_6	a_1	a_2	a_3	a_4	0	a_6	0	$\frac{\pi}{2}$	0	0	$\frac{\pi}{2}$	α_6
d_1	0	d_3	0	d_5	d_6	a_1	a_2	a_3	a_4	0	a_6	0	0	$\frac{\pi}{2}$	$\frac{\pi}{2}$	$\frac{\pi}{2}$	α_6
d_1	0	d_3	0	d_5	d_6	a_1	a_2	a_3	a_4	0	a_6	0	0	$\frac{\pi}{2}$	0	$\frac{\pi}{2}$	α_6
d_1	0	d_3	0	d_5	d_6	a_1	a_2	a_3	0	a_5	a_6	$\frac{\pi}{2}$	0	0	$\frac{\pi}{2}$	$\frac{\pi}{2}$	α_6
d_1	0	d_3	0	d_5	d_6	a_1	a_2	a_3	0	a_5	a_6	$\frac{\pi}{2}$	0	0	$\frac{\pi}{2}$	0	α_6
d_1	0	d_3	0	d_5	d_6	a_1	a_2	a_3	0	a_5	a_6	0	0	$\frac{\pi}{2}$	$\frac{\pi}{2}$	$\frac{\pi}{2}$	α_6
d_1	0	d_3	0	d_5	d_6	a_1	a_2	a_3	0	a_5	a_6	0	0	$\frac{\pi}{2}$	$\frac{\pi}{2}$	0	α_6
d_1	0	d_3	0	d_5	d_6	a_1	a_2	a_3	0	0	a_6	$\frac{\pi}{2}$	0	0	$\frac{\pi}{2}$	$\frac{\pi}{2}$	α_6
d_1	0	d_3	0	d_5	d_6	a_1	a_2	a_3	0	0	a_6	0	0	$\frac{\pi}{2}$	$\frac{\pi}{2}$	$\frac{\pi}{2}$	α_6
d_1	0	d_3	0	d_5	d_6	a_1	a_2	0	a_4	a_5	a_6	$\frac{\pi}{2}$	$\frac{\pi}{2}$	$\frac{\pi}{2}$	0	0	α_6
d_1	0	d_3	0	d_5	d_6	a_1	a_2	0	a_4	a_5	a_6	$\frac{\pi}{2}$	0	$\frac{\pi}{2}$	0	0	α_6
d_1	0	d_3	0	d_5	d_6	a_1	a_2	0	a_4	a_5	a_6	0	$\frac{\pi}{2}$	$\frac{\pi}{2}$	0	0	α_6
d_1	0	d_3	0	d_5	d_6	a_1	a_2	0	a_4	a_5	a_6	0	0	$\frac{\pi}{2}$	$\frac{\pi}{2}$	$\frac{\pi}{2}$	α_6
d_1	0	d_3	0	d_5	d_6	a_1	a_2	0	a_4	a_5	a_6	0	0	$\frac{\pi}{2}$	0	$\frac{\pi}{2}$	α_6
d_1	0	d_3	0	d_5	d_6	a_1	a_2	0	a_4	a_5	a_6	0	0	$\frac{\pi}{2}$	0	0	α_6
d_1	0	d_3	0	d_5	d_6	a_1	a_2	0	a_4	0	a_6	0	0	$\frac{\pi}{2}$	$\frac{\pi}{2}$	$\frac{\pi}{2}$	α_6
d_1	0	d_3	0	d_5	d_6	a_1	a_2	0	a_4	0	a_6	0	0	$\frac{\pi}{2}$	0	$\frac{\pi}{2}$	α_6
d_1	0	d_3	0	d_5	d_6	a_1	a_2	0	0	a_5	a_6	$\frac{\pi}{2}$	$\frac{\pi}{2}$	$\frac{\pi}{2}$	$\frac{\pi}{2}$	$\frac{\pi}{2}$	α_6
d_1	0	d_3	0	d_5	d_6	a_1	a_2	0	0	a_5	a_6	$\frac{\pi}{2}$	$\frac{\pi}{2}$	$\frac{\pi}{2}$	$\frac{\pi}{2}$	0	α_6
d_1	0	d_3	0	d_5	d_6	a_1	a_2	0	0	a_5	a_6	0	$\frac{\pi}{2}$	$\frac{\pi}{2}$	$\frac{\pi}{2}$	$\frac{\pi}{2}$	α_6
d_1	0	d_3	0	d_5	d_6	a_1	a_2	0	0	a_5	a_6	0	$\frac{\pi}{2}$	$\frac{\pi}{2}$	$\frac{\pi}{2}$	0	α_6
d_1	0	d_3	0	d_5	d_6	a_1	a_2	0	0	a_5	a_6	0	0	$\frac{\pi}{2}$	$\frac{\pi}{2}$	$\frac{\pi}{2}$	α_6

Table A.12 – The D-H parameter values of robots whose det(**J**) factors into three components.

d_1	d_2	d_3	d_4	d_5	d_6	a_1	a_2	a_3	a_4	a_5	a_6	α_1	α_2	α_3	α_4	α_5	α_6
d_1	0	d_3	0	d_5	d_6	a_1	a_2	0	0	a_5	a_6	0	0	$\frac{\pi}{2}$	$\frac{\pi}{2}$	0	α_6
d_1	0	d_3	0	d_5	d_6	a_1	a_2	0	0	0	a_6	$\frac{\pi}{2}$	$\frac{\pi}{2}$	$\frac{\pi}{2}$	$\frac{\pi}{2}$	$\frac{\pi}{2}$	α_6
d_1	0	d_3	0	d_5	d_6	a_1	a_2	0	0	0	a_6	0	$\frac{\pi}{2}$	$\frac{\pi}{2}$	$\frac{\pi}{2}$	$\frac{\pi}{2}$	α_6
d_1	0	d_3	0	d_5	d_6	a_1	a_2	0	0	0	a_6	0	0	$\frac{\pi}{2}$	$\frac{\pi}{2}$	$\frac{\pi}{2}$	α_6
d_1	0	d_3	0	d_5	d_6	a_1	0	a_3	a_4	a_5	a_6	$\frac{\pi}{2}$	$\frac{\pi}{2}$	$\frac{\pi}{2}$	0	0	α_6
d_1	0	d_3	0	d_5	d_6	a_1	0	a_3	a_4	a_5	a_6	$\frac{\pi}{2}$	$\frac{\pi}{2}$	0	0	$\frac{\pi}{2}$	α_6
d_1	0	d_3	0	d_5	d_6	a_1	0	a_3	a_4	a_5	a_6	0	$\frac{\pi}{2}$	$\frac{\pi}{2}$	0	0	α_6
d_1	0	d_3	0	d_5	d_6	a_1	0	a_3	a_4	a_5	a_6	0	$\frac{\pi}{2}$	0	0	$\frac{\pi}{2}$	α_6
d_1	0	d_3	0	d_5	d_6	a_1	0	a_3	a_4	0	a_6	$\frac{\pi}{2}$	$\frac{\pi}{2}$	0	0	$\frac{\pi}{2}$	α_6
d_1	0	d_3	0	d_5	d_6	a_1	0	a_3	a_4	0	a_6	0	$\frac{\pi}{2}$	0	0	$\frac{\pi}{2}$	α_6
d_1	0	d_3	0	d_5	d_6	a_1	0	0	a_4	a_5	a_6	$\frac{\pi}{2}$	$\frac{\pi}{2}$	$\frac{\pi}{2}$	$\frac{\pi}{2}$	0	α_6
d_1	0	d_3	0	d_5	d_6	a_1	0	0	a_4	a_5	a_6	$\frac{\pi}{2}$	$\frac{\pi}{2}$	$\frac{\pi}{2}$	0	0	α_6
d_1	0	d_3	0	d_5	d_6	a_1	0	0	a_4	a_5	a_6	0	$\frac{\pi}{2}$	$\frac{\pi}{2}$	0	0	α_6
d_1	0	d_3	0	d_5	d_6	a_1	0	0	a_4	0	a_6	$\frac{\pi}{2}$	$\frac{\pi}{2}$	$\frac{\pi}{2}$	$\frac{\pi}{2}$	$\frac{\pi}{2}$	α_6
d_1	0	d_3	0	d_5	d_6	a_1	0	0	0	a_5	a_6	$\frac{\pi}{2}$	$\frac{\pi}{2}$	$\frac{\pi}{2}$	$\frac{\pi}{2}$	$\frac{\pi}{2}$	α_6
d_1	0	d_3	0	d_5	d_6	a_1	0	0	0	a_5	a_6	$\frac{\pi}{2}$	$\frac{\pi}{2}$	$\frac{\pi}{2}$	$\frac{\pi}{2}$	0	α_6
d_1	0	d_3	0	d_5	d_6	a_1	0	0	0	a_5	a_6	0	$\frac{\pi}{2}$	$\frac{\pi}{2}$	$\frac{\pi}{2}$	$\frac{\pi}{2}$	α_6
d_1	0	d_3	0	d_5	d_6	a_1	0	0	0	a_5	a_6	0	$\frac{\pi}{2}$	$\frac{\pi}{2}$	$\frac{\pi}{2}$	0	α_6
d_1	0	d_3	0	d_5	d_6	a_1	0	0	0	0	a_6	$\frac{\pi}{2}$	$\frac{\pi}{2}$	$\frac{\pi}{2}$	$\frac{\pi}{2}$	$\frac{\pi}{2}$	α_6
d_1	0	d_3	0	d_5	d_6	a_1	0	0	0	0	a_6	0	$\frac{\pi}{2}$	$\frac{\pi}{2}$	$\frac{\pi}{2}$	$\frac{\pi}{2}$	α_6
d_1	0	d_3	0	0	d_6	a_1	a_2	a_3	a_4	a_5	a_6	$\frac{\pi}{2}$	$\frac{\pi}{2}$	$\frac{\pi}{2}$	0	0	α_6
d_1	0	d_3	0	0	d_6	a_1	a_2	a_3	a_4	a_5	a_6	$\frac{\pi}{2}$	$\frac{\pi}{2}$	0	0	$\frac{\pi}{2}$	α_6
d_1	0	d_3	0	0	d_6	a_1	a_2	a_3	a_4	a_5	a_6	$\frac{\pi}{2}$	0	$\frac{\pi}{2}$	0	0	α_6
d_1	0	d_3	0	0	d_6	a_1	a_2	a_3	a_4	a_5	a_6	$\frac{\pi}{2}$	0	0	$\frac{\pi}{2}$	$\frac{\pi}{2}$	α_6
d_1	0	d_3	0	0	d_6	a_1	a_2	a_3	a_4	a_5	a_6	$\frac{\pi}{2}$	0	0	$\frac{\pi}{2}$	0	α_6
d_1	0	d_3	0	0	d_6	a_1	a_2	a_3	a_4	a_5	a_6	0	$\frac{\pi}{2}$	$\frac{\pi}{2}$	0	0	α_6
d_1	0	d_3	0	0	d_6	a_1	a_2	a_3	a_4	a_5	a_6	0	$\frac{\pi}{2}$	0	0	$\frac{\pi}{2}$	α_6
d_1	0	d_3	0	0	d_6	a_1	a_2	a_3	a_4	a_5	a_6	0	0	$\frac{\pi}{2}$	$\frac{\pi}{2}$	$\frac{\pi}{2}$	α_6
d_1	0	d_3	0	0	d_6	a_1	a_2	a_3	a_4	a_5	a_6	0	0	$\frac{\pi}{2}$	0	$\frac{\pi}{2}$	α_6
d_1	0	d_3	0	0	d_6	a_1	a_2	a_3	a_4	0	a_6	$\frac{\pi}{2}$	$\frac{\pi}{2}$	0	0	$\frac{\pi}{2}$	α_6
d_1	0	d_3	0	0	d_6	a_1	a_2	a_3	a_4	0	a_6	$\frac{\pi}{2}$	0	0	$\frac{\pi}{2}$	$\frac{\pi}{2}$	α_6
d_1	0	d_3	0	0	d_6	a_1	a_2	a_3	a_4	0	a_6	0	$\frac{\pi}{2}$	0	0	$\frac{\pi}{2}$	α_6
d_1	0	d_3	0	0	d_6	a_1	a_2	a_3	a_4	0	a_6	0	0	$\frac{\pi}{2}$	$\frac{\pi}{2}$	$\frac{\pi}{2}$	α_6
d_1	0	d_3	0	0	d_6	a_1	a_2	a_3	a_4	0	a_6	0	0	$\frac{\pi}{2}$	0	$\frac{\pi}{2}$	α_6
d_1	0	d_3	0	0	d_6	a_1	a_2	a_3	0	a_5	a_6	$\frac{\pi}{2}$	0	0	$\frac{\pi}{2}$	$\frac{\pi}{2}$	α_6
d_1	0	d_3	0	0	d_6	a_1	a_2	a_3	0	a_5	a_6	$\frac{\pi}{2}$	0	0	$\frac{\pi}{2}$	0	α_6
d_1	0	d_3	0	0	d_6	a_1	a_2	a_3	0	a_5	a_6	0	0	$\frac{\pi}{2}$	$\frac{\pi}{2}$	$\frac{\pi}{2}$	α_6
d_1	0	d_3	0	0	d_6	a_1	a_2	a_3	0	a_5	a_6	0	0	$\frac{\pi}{2}$	$\frac{\pi}{2}$	0	α_6
d_1	0	d_3	0	0	d_6	a_1	a_2	a_3	0	0	a_6	$\frac{\pi}{2}$	$\frac{\pi}{2}$	$\frac{\pi}{2}$	$\frac{\pi}{2}$	$\frac{\pi}{2}$	α_6
d_1	0	d_3	0	0	d_6	a_1	a_2	a_3	0	0	a_6	$\frac{\pi}{2}$	$\frac{\pi}{2}$	0	$\frac{\pi}{2}$	$\frac{\pi}{2}$	α_6
d_1	0	d_3	0	0	d_6	a_1	a_2	a_3	0	0	a_6	$\frac{\pi}{2}$	0	$\frac{\pi}{2}$	$\frac{\pi}{2}$	$\frac{\pi}{2}$	α_6
d_1	0	d_3	0	0	d_6	a_1	a_2	a_3	0	0	a_6	$\frac{\pi}{2}$	0	0	$\frac{\pi}{2}$	$\frac{\pi}{2}$	α_6
d_1	0	d_3	0	0	d_6	a_1	a_2	a_3	0	0	a_6	0	$\frac{\pi}{2}$	$\frac{\pi}{2}$	$\frac{\pi}{2}$	$\frac{\pi}{2}$	α_6
d_1	0	d_3	0	0	d_6	a_1	a_2	a_3	0	0	a_6	0	$\frac{\pi}{2}$	0	$\frac{\pi}{2}$	$\frac{\pi}{2}$	α_6
d_1	0	d_3	0	0	d_6	a_1	a_2	0	a_4	a_5	a_6	$\frac{\pi}{2}$	$\frac{\pi}{2}$	$\frac{\pi}{2}$	0	0	α_6

Table A.13 – The D-H parameter values of robots whose det(**J**) factors into three components.

d_1	d_2	d_3	d_4	d_5	d_6	a_1	a_2	a_3	a_4	a_5	a_6	α_1	α_2	α_3	α_4	α_5	α_6
d_1	0	d_3	0	0	d_6	a_1	a_2	0	a_4	a_5	a_6	0	0	$\frac{\pi}{2}$	$\frac{\pi}{2}$	0	α_6
d_1	0	d_3	0	0	d_6	a_1	a_2	0	a_4	a_5	a_6	0	0	$\frac{\pi}{2}$	0	$\frac{\pi}{2}$	α_6
d_1	0	d_3	0	0	d_6	a_1	a_2	0	a_4	0	a_6	0	0	$\frac{\pi}{2}$	$\frac{\pi}{2}$	$\frac{\pi}{2}$	α_6
d_1	0	d_3	0	0	d_6	a_1	a_2	0	a_4	0	a_6	0	0	$\frac{\pi}{2}$	0	$\frac{\pi}{2}$	α_6
d_1	0	d_3	0	0	d_6	a_1	a_2	0	0	a_5	a_6	$\frac{\pi}{2}$	$\frac{\pi}{2}$	$\frac{\pi}{2}$	$\frac{\pi}{2}$	$\frac{\pi}{2}$	α_6
d_1	0	d_3	0	0	d_6	a_1	a_2	0	0	a_5	a_6	$\frac{\pi}{2}$	$\frac{\pi}{2}$	$\frac{\pi}{2}$	$\frac{\pi}{2}$	0	α_6
d_1	0	d_3	0	0	d_6	a_1	a_2	0	0	a_5	a_6	0	$\frac{\pi}{2}$	$\frac{\pi}{2}$	$\frac{\pi}{2}$	$\frac{\pi}{2}$	α_6
d_1	0	d_3	0	0	d_6	a_1	a_2	0	0	a_5	a_6	0	$\frac{\pi}{2}$	$\frac{\pi}{2}$	$\frac{\pi}{2}$	0	α_6
d_1	0	d_3	0	0	d_6	a_1	a_2	0	0	a_5	a_6	0	0	$\frac{\pi}{2}$	$\frac{\pi}{2}$	$\frac{\pi}{2}$	α_6
d_1	0	d_3	0	0	d_6	a_1	a_2	0	0	a_5	a_6	0	0	$\frac{\pi}{2}$	$\frac{\pi}{2}$	0	α_6
d_1	0	d_3	0	0	d_6	a_1	0	a_3	a_4	a_5	a_6	$\frac{\pi}{2}$	$\frac{\pi}{2}$	$\frac{\pi}{2}$	0	0	α_6
d_1	0	d_3	0	0	d_6	a_1	0	a_3	a_4	a_5	a_6	$\frac{\pi}{2}$	$\frac{\pi}{2}$	0	0	$\frac{\pi}{2}$	α_6
d_1	0	d_3	0	0	d_6	a_1	0	a_3	a_4	a_5	a_6	0	$\frac{\pi}{2}$	$\frac{\pi}{2}$	0	0	α_6
d_1	0	d_3	0	0	d_6	a_1	0	a_3	a_4	a_5	a_6	0	$\frac{\pi}{2}$	0	0	$\frac{\pi}{2}$	α_6
d_1	0	d_3	0	0	d_6	a_1	0	a_3	a_4	0	a_6	$\frac{\pi}{2}$	$\frac{\pi}{2}$	0	0	$\frac{\pi}{2}$	α_6
d_1	0	d_3	0	0	d_6	a_1	0	a_3	a_4	0	a_6	0	$\frac{\pi}{2}$	0	0	$\frac{\pi}{2}$	α_6
d_1	0	d_3	0	0	d_6	a_1	0	a_3	0	0	a_6	$\frac{\pi}{2}$	$\frac{\pi}{2}$	$\frac{\pi}{2}$	$\frac{\pi}{2}$	$\frac{\pi}{2}$	α_6
d_1	0	d_3	0	0	d_6	a_1	0	a_3	0	0	a_6	$\frac{\pi}{2}$	$\frac{\pi}{2}$	0	$\frac{\pi}{2}$	$\frac{\pi}{2}$	α_6
d_1	0	d_3	0	0	d_6	a_1	0	a_3	0	0	a_6	0	$\frac{\pi}{2}$	$\frac{\pi}{2}$	$\frac{\pi}{2}$	$\frac{\pi}{2}$	α_6
d_1	0	d_3	0	0	d_6	a_1	0	a_3	0	0	a_6	0	$\frac{\pi}{2}$	0	$\frac{\pi}{2}$	$\frac{\pi}{2}$	α_6
d_1	0	d_3	0	0	d_6	a_1	0	0	a_4	a_5	a_6	$\frac{\pi}{2}$	$\frac{\pi}{2}$	$\frac{\pi}{2}$	$\frac{\pi}{2}$	$\frac{\pi}{2}$	α_6
d_1	0	d_3	0	0	d_6	a_1	0	0	a_4	a_5	a_6	$\frac{\pi}{2}$	$\frac{\pi}{2}$	$\frac{\pi}{2}$	$\frac{\pi}{2}$	0	α_6
d_1	0	d_3	0	0	d_6	a_1	0	0	a_4	a_5	a_6	$\frac{\pi}{2}$	$\frac{\pi}{2}$	$\frac{\pi}{2}$	0	$\frac{\pi}{2}$	α_6
d_1	0	d_3	0	0	d_6	a_1	0	0	a_4	a_5	a_6	$\frac{\pi}{2}$	$\frac{\pi}{2}$	$\frac{\pi}{2}$	0	0	α_6
d_1	0	d_3	0	0	d_6	a_1	0	0	a_4	a_5	a_6	0	$\frac{\pi}{2}$	$\frac{\pi}{2}$	0	0	α_6
d_1	0	d_3	0	0	d_6	a_1	0	0	a_4	0	a_6	$\frac{\pi}{2}$	$\frac{\pi}{2}$	$\frac{\pi}{2}$	$\frac{\pi}{2}$	$\frac{\pi}{2}$	α_6
d_1	0	d_3	0	0	d_6	a_1	0	0	a_4	0	a_6	$\frac{\pi}{2}$	$\frac{\pi}{2}$	$\frac{\pi}{2}$	0	$\frac{\pi}{2}$	α_6
d_1	0	d_3	0	0	d_6	a_1	0	0	0	a_5	a_6	$\frac{\pi}{2}$	$\frac{\pi}{2}$	$\frac{\pi}{2}$	$\frac{\pi}{2}$	$\frac{\pi}{2}$	α_6
d_1	0	d_3	0	0	d_6	a_1	0	0	0	a_5	a_6	$\frac{\pi}{2}$	$\frac{\pi}{2}$	$\frac{\pi}{2}$	$\frac{\pi}{2}$	0	α_6
d_1	0	d_3	0	0	d_6	a_1	0	0	0	a_5	a_6	0	$\frac{\pi}{2}$	$\frac{\pi}{2}$	$\frac{\pi}{2}$	$\frac{\pi}{2}$	α_6
d_1	0	d_3	0	0	d_6	a_1	0	0	0	a_5	a_6	0	$\frac{\pi}{2}$	$\frac{\pi}{2}$	$\frac{\pi}{2}$	0	α_6
d_1	0	0	d_4	d_5	d_6	a_1	a_2	a_3	a_4	a_5	a_6	$\frac{\pi}{2}$	$\frac{\pi}{2}$	$\frac{\pi}{2}$	0	0	α_6
d_1	0	0	d_4	d_5	d_6	a_1	a_2	a_3	a_4	a_5	a_6	$\frac{\pi}{2}$	$\frac{\pi}{2}$	0	0	$\frac{\pi}{2}$	α_6
d_1	0	0	d_4	d_5	d_6	a_1	a_2	a_3	a_4	a_5	a_6	$\frac{\pi}{2}$	0	$\frac{\pi}{2}$	0	0	α_6
d_1	0	0	d_4	d_5	d_6	a_1	a_2	a_3	a_4	a_5	a_6	$\frac{\pi}{2}$	0	0	$\frac{\pi}{2}$	$\frac{\pi}{2}$	α_6
d_1	0	0	d_4	d_5	d_6	a_1	a_2	a_3	a_4	a_5	a_6	$\frac{\pi}{2}$	0	0	$\frac{\pi}{2}$	0	α_6
d_1	0	0	d_4	d_5	d_6	a_1	a_2	a_3	a_4	a_5	a_6	0	$\frac{\pi}{2}$	$\frac{\pi}{2}$	0	0	α_6
d_1	0	0	d_4	d_5	d_6	a_1	a_2	a_3	a_4	a_5	a_6	0	$\frac{\pi}{2}$	0	0	$\frac{\pi}{2}$	α_6
d_1	0	0	d_4	d_5	d_6	a_1	a_2	a_3	a_4	a_5	a_6	0	0	$\frac{\pi}{2}$	$\frac{\pi}{2}$	$\frac{\pi}{2}$	α_6
d_1	0	0	d_4	d_5	d_6	a_1	a_2	a_3	a_4	a_5	a_6	0	0	$\frac{\pi}{2}$	$\frac{\pi}{2}$	0	α_6
d_1	0	0	d_4	d_5	d_6	a_1	a_2	a_3	a_4	a_5	a_6	0	0	$\frac{\pi}{2}$	0	$\frac{\pi}{2}$	α_6
d_1	0	0	d_4	d_5	d_6	a_1	a_2	a_3	a_4	0	a_6	$\frac{\pi}{2}$	$\frac{\pi}{2}$	0	0	$\frac{\pi}{2}$	α_6
d_1	0	0	d_4	d_5	d_6	a_1	a_2	a_3	a_4	0	a_6	$\frac{\pi}{2}$	0	0	$\frac{\pi}{2}$	$\frac{\pi}{2}$	α_6

Table A.14 – The D-H parameter values of robots whose det(**J**) factors into three components.

d_1	d_2	d_3	d_4	d_5	d_6	a_1	a_2	a_3	a_4	a_5	a_6	α_1	α_2	α_3	α_4	α_5	α_6
d_1	0	d_3	0	d_5	d_6	a_1	a_2	0	0	a_5	a_6	0	$\frac{\pi}{2}$	$\frac{\pi}{2}$	$\frac{\pi}{2}$	$\frac{\pi}{2}$	α_6
d_1	0	d_3	0	d_5	d_6	a_1	a_2	0	0	a_5	a_6	0	$\frac{\pi}{2}$	$\frac{\pi}{2}$	$\frac{\pi}{2}$	0	α_6
d_1	0	d_3	0	d_5	d_6	a_1	a_2	0	0	a_5	a_6	0	0	$\frac{\pi}{2}$	$\frac{\pi}{2}$	$\frac{\pi}{2}$	α_6
d_1	0	d_3	0	d_5	d_6	a_1	a_2	0	0	a_5	a_6	0	0	$\frac{\pi}{2}$	$\frac{\pi}{2}$	0	α_6
d_1	0	d_3	0	d_5	d_6	a_1	a_2	0	0	0	a_6	$\frac{\pi}{2}$	$\frac{\pi}{2}$	$\frac{\pi}{2}$	$\frac{\pi}{2}$	$\frac{\pi}{2}$	α_6
d_1	0	d_3	0	d_5	d_6	a_1	a_2	0	0	0	a_6	0	$\frac{\pi}{2}$	$\frac{\pi}{2}$	$\frac{\pi}{2}$	$\frac{\pi}{2}$	α_6
d_1	0	d_3	0	d_5	d_6	a_1	a_2	0	0	0	a_6	0	0	$\frac{\pi}{2}$	$\frac{\pi}{2}$	$\frac{\pi}{2}$	α_6
d_1	0	d_3	0	d_5	d_6	a_1	0	a_3	a_4	a_5	a_6	$\frac{\pi}{2}$	$\frac{\pi}{2}$	$\frac{\pi}{2}$	0	0	α_6
d_1	0	d_3	0	d_5	d_6	a_1	0	a_3	a_4	a_5	a_6	$\frac{\pi}{2}$	$\frac{\pi}{2}$	0	0	$\frac{\pi}{2}$	α_6
d_1	0	d_3	0	d_5	d_6	a_1	0	a_3	a_4	a_5	a_6	0	$\frac{\pi}{2}$	$\frac{\pi}{2}$	0	0	α_6
d_1	0	d_3	0	d_5	d_6	a_1	0	a_3	a_4	a_5	a_6	0	$\frac{\pi}{2}$	0	0	$\frac{\pi}{2}$	α_6
d_1	0	d_3	0	d_5	d_6	a_1	0	a_3	a_4	0	a_6	$\frac{\pi}{2}$	$\frac{\pi}{2}$	0	0	$\frac{\pi}{2}$	α_6
d_1	0	d_3	0	d_5	d_6	a_1	0	a_3	a_4	0	a_6	0	$\frac{\pi}{2}$	0	0	$\frac{\pi}{2}$	α_6
d_1	0	d_3	0	d_5	d_6	a_1	0	0	a_4	a_5	a_6	$\frac{\pi}{2}$	$\frac{\pi}{2}$	$\frac{\pi}{2}$	$\frac{\pi}{2}$	$\frac{\pi}{2}$	α_6
d_1	0	d_3	0	d_5	d_6	a_1	0	0	a_4	a_5	a_6	$\frac{\pi}{2}$	$\frac{\pi}{2}$	$\frac{\pi}{2}$	0	0	α_6
d_1	0	d_3	0	d_5	d_6	a_1	0	0	a_4	a_5	a_6	0	$\frac{\pi}{2}$	$\frac{\pi}{2}$	0	0	α_6
d_1	0	d_3	0	d_5	d_6	a_1	0	0	a_4	0	a_6	$\frac{\pi}{2}$	$\frac{\pi}{2}$	$\frac{\pi}{2}$	$\frac{\pi}{2}$	$\frac{\pi}{2}$	α_6
d_1	0	d_3	0	d_5	d_6	a_1	0	0	0	a_5	a_6	$\frac{\pi}{2}$	$\frac{\pi}{2}$	$\frac{\pi}{2}$	$\frac{\pi}{2}$	$\frac{\pi}{2}$	α_6
d_1	0	d_3	0	d_5	d_6	a_1	0	0	0	a_5	a_6	$\frac{\pi}{2}$	$\frac{\pi}{2}$	$\frac{\pi}{2}$	$\frac{\pi}{2}$	0	α_6
d_1	0	d_3	0	d_5	d_6	a_1	0	0	0	a_5	a_6	0	$\frac{\pi}{2}$	$\frac{\pi}{2}$	$\frac{\pi}{2}$	$\frac{\pi}{2}$	α_6
d_1	0	d_3	0	d_5	d_6	a_1	0	0	0	a_5	a_6	0	$\frac{\pi}{2}$	$\frac{\pi}{2}$	$\frac{\pi}{2}$	0	α_6
d_1	0	d_3	0	d_5	d_6	a_1	0	0	0	0	a_6	$\frac{\pi}{2}$	$\frac{\pi}{2}$	$\frac{\pi}{2}$	$\frac{\pi}{2}$	$\frac{\pi}{2}$	α_6
d_1	0	d_3	0	d_5	d_6	a_1	0	0	0	0	a_6	0	$\frac{\pi}{2}$	$\frac{\pi}{2}$	$\frac{\pi}{2}$	$\frac{\pi}{2}$	α_6
d_1	0	d_3	0	0	d_6	a_1	a_2	a_3	a_4	a_5	a_6	$\frac{\pi}{2}$	$\frac{\pi}{2}$	$\frac{\pi}{2}$	0	0	α_6
d_1	0	d_3	0	0	d_6	a_1	a_2	a_3	a_4	a_5	a_6	$\frac{\pi}{2}$	$\frac{\pi}{2}$	0	0	$\frac{\pi}{2}$	α_6
d_1	0	d_3	0	0	d_6	a_1	a_2	a_3	a_4	a_5	a_6	$\frac{\pi}{2}$	0	$\frac{\pi}{2}$	0	0	α_6
d_1	0	d_3	0	0	d_6	a_1	a_2	a_3	a_4	a_5	a_6	$\frac{\pi}{2}$	0	0	$\frac{\pi}{2}$	$\frac{\pi}{2}$	α_6
d_1	0	d_3	0	0	d_6	a_1	a_2	a_3	a_4	a_5	a_6	$\frac{\pi}{2}$	0	0	$\frac{\pi}{2}$	0	α_6
d_1	0	d_3	0	0	d_6	a_1	a_2	a_3	a_4	a_5	a_6	$\frac{\pi}{2}$	0	0	$\frac{\pi}{2}$	$\frac{\pi}{2}$	α_6
d_1	0	d_3	0	0	d_6	a_1	a_2	a_3	a_4	0	a_6	$\frac{\pi}{2}$	$\frac{\pi}{2}$	0	0	$\frac{\pi}{2}$	α_6
d_1	0	d_3	0	0	d_6	a_1	a_2	a_3	a_4	0	a_6	$\frac{\pi}{2}$	0	0	$\frac{\pi}{2}$	$\frac{\pi}{2}$	α_6
d_1	0	d_3	0	0	d_6	a_1	a_2	a_3	a_4	0	a_6	0	$\frac{\pi}{2}$	0	0	$\frac{\pi}{2}$	α_6
d_1	0	d_3	0	0	d_6	a_1	a_2	a_3	a_4	0	a_6	0	0	$\frac{\pi}{2}$	$\frac{\pi}{2}$	$\frac{\pi}{2}$	α_6
d_1	0	d_3	0	0	d_6	a_1	a_2	a_3	a_4	0	a_6	0	0	$\frac{\pi}{2}$	0	$\frac{\pi}{2}$	α_6
d_1	0	d_3	0	0	d_6	a_1	a_2	a_3	0	a_5	a_6	$\frac{\pi}{2}$	0	0	$\frac{\pi}{2}$	$\frac{\pi}{2}$	α_6
d_1	0	d_3	0	0	d_6	a_1	a_2	a_3	0	a_5	a_6	$\frac{\pi}{2}$	0	0	$\frac{\pi}{2}$	0	α_6
d_1	0	d_3	0	0	d_6	a_1	a_2	a_3	0	a_5	a_6	0	0	$\frac{\pi}{2}$	$\frac{\pi}{2}$	$\frac{\pi}{2}$	α_6
d_1	0	d_3	0	0	d_6	a_1	a_2	a_3	0	a_5	a_6	0	0	$\frac{\pi}{2}$	$\frac{\pi}{2}$	0	α_6
d_1	0	d_3	0	0	d_6	a_1	a_2	a_3	0	0	a_6	$\frac{\pi}{2}$	$\frac{\pi}{2}$	$\frac{\pi}{2}$	$\frac{\pi}{2}$	$\frac{\pi}{2}$	α_6
d_1	0	0	d_4	d_5	d_6	a_1	a_2	a_3	0	0	a_6	0	0	$\frac{\pi}{2}$	$\frac{\pi}{2}$	$\frac{\pi}{2}$	α_6
d_1	0	0	d_4	d_5	d_6	a_1	a_2	0	a_4	a_5	a_6	$\frac{\pi}{2}$	$\frac{\pi}{2}$	$\frac{\pi}{2}$	0	0	α_6
d_1	0	0	d_4	d_5	d_6	a_1	a_2	0	a_4	a_5	a_6	$\frac{\pi}{2}$	0	$\frac{\pi}{2}$	0	0	α_6
d_1	0	0	d_4	d_5	d_6	a_1	a_2	0	a_4	a_5	a_6	0	$\frac{\pi}{2}$	$\frac{\pi}{2}$	0	0	α_6

Table A.15 – The D-H parameter values of robots whose det(**J**) factors into three components.

d_1	d_2	d_3	d_4	d_5	d_6	a_1	a_2	a_3	a_4	a_5	a_6	α_1	α_2	α_3	α_4	α_5	α_6
d_1	0	d_3	0	0	d_6	a_1	a_2	a_3	0	0	a_6	$\frac{\pi}{2}$	$\frac{\pi}{2}$	0	$\frac{\pi}{2}$	$\frac{\pi}{2}$	α_6
d_1	0	d_3	0	0	d_6	a_1	a_2	a_3	0	0	a_6	$\frac{\pi}{2}$	0	$\frac{\pi}{2}$	$\frac{\pi}{2}$	$\frac{\pi}{2}$	α_6
d_1	0	d_3	0	0	d_6	a_1	a_2	a_3	0	0	a_6	$\frac{\pi}{2}$	0	0	$\frac{\pi}{2}$	$\frac{\pi}{2}$	α_6
d_1	0	d_3	0	0	d_6	a_1	a_2	a_3	0	0	a_6	0	$\frac{\pi}{2}$	$\frac{\pi}{2}$	$\frac{\pi}{2}$	$\frac{\pi}{2}$	α_6
d_1	0	d_3	0	0	d_6	a_1	a_2	a_3	0	0	a_6	0	$\frac{\pi}{2}$	0	$\frac{\pi}{2}$	$\frac{\pi}{2}$	α_6
d_1	0	d_3	0	0	d_6	a_1	a_2	0	a_4	a_5	a_6	$\frac{\pi}{2}$	$\frac{\pi}{2}$	$\frac{\pi}{2}$	0	0	α_6
d_1	0	d_3	0	0	d_6	a_1	a_2	0	a_4	a_5	a_6	$\frac{\pi}{2}$	0	$\frac{\pi}{2}$	0	0	α_6
d_1	0	d_3	0	0	d_6	a_1	a_2	0	a_4	a_5	a_6	0	$\frac{\pi}{2}$	$\frac{\pi}{2}$	0	0	α_6
d_1	0	d_3	0	0	d_6	a_1	a_2	0	a_4	a_5	a_6	0	0	$\frac{\pi}{2}$	$\frac{\pi}{2}$	$\frac{\pi}{2}$	α_6
d_1	0	d_3	0	0	d_6	a_1	a_2	0	a_4	a_5	a_6	0	0	$\frac{\pi}{2}$	$\frac{\pi}{2}$	0	α_6
d_1	0	d_3	0	0	d_6	a_1	a_2	0	a_4	a_5	a_6	0	0	$\frac{\pi}{2}$	0	$\frac{\pi}{2}$	α_6
d_1	0	d_3	0	0	d_6	a_1	a_2	0	a_4	0	a_6	0	0	$\frac{\pi}{2}$	$\frac{\pi}{2}$	$\frac{\pi}{2}$	α_6
d_1	0	d_3	0	0	d_6	a_1	a_2	0	a_4	0	a_6	0	0	$\frac{\pi}{2}$	0	$\frac{\pi}{2}$	α_6
d_1	0	d_3	0	0	d_6	a_1	a_2	0	0	a_5	a_6	$\frac{\pi}{2}$	$\frac{\pi}{2}$	$\frac{\pi}{2}$	$\frac{\pi}{2}$	$\frac{\pi}{2}$	α_6
d_1	0	d_3	0	0	d_6	a_1	a_2	0	0	a_5	a_6	$\frac{\pi}{2}$	$\frac{\pi}{2}$	$\frac{\pi}{2}$	$\frac{\pi}{2}$	0	α_6
d_1	0	d_3	0	0	d_6	a_1	a_2	0	0	a_5	a_6	0	$\frac{\pi}{2}$	$\frac{\pi}{2}$	$\frac{\pi}{2}$	$\frac{\pi}{2}$	α_6
d_1	0	d_3	0	0	d_6	a_1	a_2	0	0	a_5	a_6	0	$\frac{\pi}{2}$	$\frac{\pi}{2}$	$\frac{\pi}{2}$	0	α_6
d_1	0	d_3	0	0	d_6	a_1	a_2	0	0	a_5	a_6	0	0	$\frac{\pi}{2}$	$\frac{\pi}{2}$	$\frac{\pi}{2}$	α_6
d_1	0	d_3	0	0	d_6	a_1	a_2	0	0	a_5	a_6	0	0	$\frac{\pi}{2}$	$\frac{\pi}{2}$	0	α_6
d_1	0	d_3	0	0	d_6	a_1	0	a_3	a_4	a_5	a_6	$\frac{\pi}{2}$	$\frac{\pi}{2}$	$\frac{\pi}{2}$	0	0	α_6
d_1	0	d_3	0	0	d_6	a_1	0	a_3	a_4	a_5	a_6	$\frac{\pi}{2}$	$\frac{\pi}{2}$	0	0	$\frac{\pi}{2}$	α_6
d_1	0	d_3	0	0	d_6	a_1	0	a_3	a_4	a_5	a_6	0	$\frac{\pi}{2}$	$\frac{\pi}{2}$	0	0	α_6
d_1	0	d_3	0	0	d_6	a_1	0	a_3	a_4	a_5	a_6	0	$\frac{\pi}{2}$	0	0	$\frac{\pi}{2}$	α_6
d_1	0	d_3	0	0	d_6	a_1	0	a_3	a_4	0	a_6	$\frac{\pi}{2}$	$\frac{\pi}{2}$	0	0	$\frac{\pi}{2}$	α_6
d_1	0	d_3	0	0	d_6	a_1	0	a_3	a_4	0	a_6	0	$\frac{\pi}{2}$	0	0	$\frac{\pi}{2}$	α_6
d_1	0	d_3	0	0	d_6	a_1	0	a_3	0	0	a_6	$\frac{\pi}{2}$	$\frac{\pi}{2}$	$\frac{\pi}{2}$	$\frac{\pi}{2}$	$\frac{\pi}{2}$	α_6
d_1	0	d_3	0	0	d_6	a_1	0	a_3	0	0	a_6	$\frac{\pi}{2}$	$\frac{\pi}{2}$	0	$\frac{\pi}{2}$	$\frac{\pi}{2}$	α_6
d_1	0	d_3	0	0	d_6	a_1	0	a_3	0	0	a_6	0	$\frac{\pi}{2}$	$\frac{\pi}{2}$	$\frac{\pi}{2}$	$\frac{\pi}{2}$	α_6
d_1	0	d_3	0	0	d_6	a_1	0	a_3	0	0	a_6	0	$\frac{\pi}{2}$	0	$\frac{\pi}{2}$	$\frac{\pi}{2}$	α_6
d_1	0	d_3	0	0	d_6	a_1	0	0	a_4	a_5	a_6	$\frac{\pi}{2}$	$\frac{\pi}{2}$	$\frac{\pi}{2}$	$\frac{\pi}{2}$	$\frac{\pi}{2}$	α_6
d_1	0	d_3	0	0	d_6	a_1	0	0	a_4	a_5	a_6	$\frac{\pi}{2}$	$\frac{\pi}{2}$	$\frac{\pi}{2}$	$\frac{\pi}{2}$	0	α_6
d_1	0	d_3	0	0	d_6	a_1	0	0	a_4	a_5	a_6	$\frac{\pi}{2}$	$\frac{\pi}{2}$	$\frac{\pi}{2}$	0	$\frac{\pi}{2}$	α_6
d_1	0	d_3	0	0	d_6	a_1	0	0	a_4	a_5	a_6	$\frac{\pi}{2}$	$\frac{\pi}{2}$	$\frac{\pi}{2}$	0	0	α_6
d_1	0	d_3	0	0	d_6	a_1	0	0	a_4	a_5	a_6	0	$\frac{\pi}{2}$	$\frac{\pi}{2}$	0	0	α_6
d_1	0	d_3	0	0	d_6	a_1	0	0	a_4	0	a_6	$\frac{\pi}{2}$	$\frac{\pi}{2}$	$\frac{\pi}{2}$	$\frac{\pi}{2}$	$\frac{\pi}{2}$	α_6
d_1	0	d_3	0	0	d_6	a_1	0	0	a_4	0	a_6	$\frac{\pi}{2}$	$\frac{\pi}{2}$	$\frac{\pi}{2}$	0	$\frac{\pi}{2}$	α_6
d_1	0	d_3	0	0	d_6	a_1	0	0	0	a_5	a_6	$\frac{\pi}{2}$	$\frac{\pi}{2}$	$\frac{\pi}{2}$	$\frac{\pi}{2}$	$\frac{\pi}{2}$	α_6
d_1	0	d_3	0	0	d_6	a_1	0	0	0	a_5	a_6	$\frac{\pi}{2}$	$\frac{\pi}{2}$	$\frac{\pi}{2}$	$\frac{\pi}{2}$	0	α_6
d_1	0	d_3	0	0	d_6	a_1	0	0	0	a_5	a_6	0	$\frac{\pi}{2}$	$\frac{\pi}{2}$	$\frac{\pi}{2}$	$\frac{\pi}{2}$	α_6
d_1	0	d_3	0	0	d_6	a_1	0	0	0	a_5	a_6	0	$\frac{\pi}{2}$	$\frac{\pi}{2}$	$\frac{\pi}{2}$	0	α_6
d_1	0	0	d_4	d_5	d_6	a_1	a_2	a_3	a_4	a_5	a_6	$\frac{\pi}{2}$	$\frac{\pi}{2}$	$\frac{\pi}{2}$	0	0	α_6
d_1	0	0	d_4	d_5	d_6	a_1	a_2	a_3	a_4	a_5	a_6	$\frac{\pi}{2}$	$\frac{\pi}{2}$	0	0	$\frac{\pi}{2}$	α_6
d_1	0	0	d_4	d_5	d_6	a_1	a_2	a_3	a_4	a_5	a_6	$\frac{\pi}{2}$	0	$\frac{\pi}{2}$	0	0	α_6

Table A.16 – The D-H parameter values of robots whose det(**J**) factors into three components.

d_1	d_2	d_3	d_4	d_5	d_6	a_1	a_2	a_3	a_4	a_5	a_6	α_1	α_2	α_3	α_4	α_5	α_6
d_1	0	0	d_4	d_5	d_6	a_1	a_2	a_3	a_4	a_5	a_6	$\frac{\pi}{2}$	0	0	$\frac{\pi}{2}$	$\frac{\pi}{2}$	α_6
d_1	0	0	d_4	d_5	d_6	a_1	a_2	a_3	a_4	a_5	a_6	$\frac{\pi}{2}$	0	0	$\frac{\pi}{2}$	0	α_6
d_1	0	0	d_4	d_5	d_6	a_1	a_2	a_3	a_4	a_5	a_6	0	$\frac{\pi}{2}$	$\frac{\pi}{2}$	0	0	α_6
d_1	0	0	d_4	d_5	d_6	a_1	a_2	a_3	a_4	a_5	a_6	0	$\frac{\pi}{2}$	0	0	$\frac{\pi}{2}$	α_6
d_1	0	0	d_4	d_5	d_6	a_1	a_2	a_3	a_4	a_5	a_6	0	0	$\frac{\pi}{2}$	$\frac{\pi}{2}$	$\frac{\pi}{2}$	α_6
d_1	0	0	d_4	d_5	d_6	a_1	a_2	a_3	a_4	a_5	a_6	0	0	$\frac{\pi}{2}$	$\frac{\pi}{2}$	0	α_6
d_1	0	0	d_4	d_5	d_6	a_1	a_2	a_3	a_4	a_5	a_6	0	0	$\frac{\pi}{2}$	0	$\frac{\pi}{2}$	α_6
d_1	0	0	d_4	d_5	d_6	a_1	a_2	a_3	a_4	0	a_6	$\frac{\pi}{2}$	$\frac{\pi}{2}$	0	0	$\frac{\pi}{2}$	α_6
d_1	0	0	d_4	d_5	d_6	a_1	a_2	a_3	a_4	0	a_6	$\frac{\pi}{2}$	0	0	$\frac{\pi}{2}$	$\frac{\pi}{2}$	α_6
d_1	0	0	d_4	d_5	d_6	a_1	a_2	a_3	a_4	0	a_6	0	$\frac{\pi}{2}$	0	0	$\frac{\pi}{2}$	α_6
d_1	0	0	d_4	d_5	d_6	a_1	a_2	a_3	a_4	0	a_6	0	0	$\frac{\pi}{2}$	$\frac{\pi}{2}$	$\frac{\pi}{2}$	α_6
d_1	0	0	d_4	d_5	d_6	a_1	a_2	a_3	a_4	0	a_6	0	0	$\frac{\pi}{2}$	0	$\frac{\pi}{2}$	α_6
d_1	0	0	d_4	d_5	d_6	a_1	a_2	a_3	0	a_5	a_6	$\frac{\pi}{2}$	0	0	$\frac{\pi}{2}$	$\frac{\pi}{2}$	α_6
d_1	0	0	d_4	d_5	d_6	a_1	a_2	a_3	0	a_5	a_6	$\frac{\pi}{2}$	0	0	$\frac{\pi}{2}$	0	α_6
d_1	0	0	d_4	d_5	d_6	a_1	a_2	a_3	0	a_5	a_6	0	0	$\frac{\pi}{2}$	$\frac{\pi}{2}$	$\frac{\pi}{2}$	α_6
d_1	0	0	d_4	d_5	d_6	a_1	a_2	a_3	0	a_5	a_6	0	0	$\frac{\pi}{2}$	$\frac{\pi}{2}$	0	α_6
d_1	0	0	d_4	d_5	d_6	a_1	a_2	a_3	0	0	a_6	$\frac{\pi}{2}$	0	0	$\frac{\pi}{2}$	$\frac{\pi}{2}$	α_6
d_1	0	0	d_4	d_5	d_6	a_1	a_2	a_3	0	0	a_6	0	0	$\frac{\pi}{2}$	$\frac{\pi}{2}$	$\frac{\pi}{2}$	α_6
d_1	0	0	d_4	d_5	d_6	a_1	a_2	0	a_4	a_5	a_6	$\frac{\pi}{2}$	$\frac{\pi}{2}$	$\frac{\pi}{2}$	0	0	α_6
d_1	0	0	d_4	d_5	d_6	a_1	a_2	0	a_4	a_5	a_6	$\frac{\pi}{2}$	0	$\frac{\pi}{2}$	0	0	α_6
d_1	0	0	d_4	d_5	d_6	a_1	a_2	0	a_4	a_5	a_6	0	$\frac{\pi}{2}$	$\frac{\pi}{2}$	0	0	α_6
d_1	0	0	d_4	d_5	d_6	a_1	a_2	0	a_4	a_5	a_6	0	0	$\frac{\pi}{2}$	$\frac{\pi}{2}$	$\frac{\pi}{2}$	α_6
d_1	0	0	d_4	d_5	d_6	a_1	a_2	0	a_4	a_5	a_6	0	0	$\frac{\pi}{2}$	$\frac{\pi}{2}$	0	α_6
d_1	0	0	d_4	d_5	d_6	a_1	a_2	0	a_4	a_5	a_6	0	0	$\frac{\pi}{2}$	0	$\frac{\pi}{2}$	α_6
d_1	0	0	d_4	d_5	d_6	a_1	a_2	0	a_4	0	a_6	0	0	$\frac{\pi}{2}$	$\frac{\pi}{2}$	$\frac{\pi}{2}$	α_6
d_1	0	0	d_4	d_5	d_6	a_1	a_2	0	a_4	0	a_6	0	0	$\frac{\pi}{2}$	0	$\frac{\pi}{2}$	α_6
d_1	0	0	d_4	d_5	d_6	a_1	a_2	0	0	a_5	a_6	0	0	$\frac{\pi}{2}$	$\frac{\pi}{2}$	$\frac{\pi}{2}$	α_6
d_1	0	0	d_4	d_5	d_6	a_1	a_2	0	a_4	a_5	a_6	0	0	$\frac{\pi}{2}$	$\frac{\pi}{2}$	$\frac{\pi}{2}$	α_6
d_1	0	0	d_4	d_5	d_6	a_1	a_2	0	a_4	a_5	a_6	0	0	$\frac{\pi}{2}$	$\frac{\pi}{2}$	0	α_6
d_1	0	0	d_4	d_5	d_6	a_1	a_2	0	a_4	a_5	a_6	0	0	$\frac{\pi}{2}$	0	$\frac{\pi}{2}$	α_6
d_1	0	0	d_4	d_5	d_6	a_1	a_2	0	a_4	0	a_6	0	0	$\frac{\pi}{2}$	$\frac{\pi}{2}$	$\frac{\pi}{2}$	α_6
d_1	0	0	d_4	d_5	d_6	a_1	a_2	0	a_4	0	a_6	0	0	$\frac{\pi}{2}$	0	$\frac{\pi}{2}$	α_6
d_1	0	0	d_4	d_5	d_6	a_1	a_2	0	0	a_5	a_6	0	0	$\frac{\pi}{2}$	$\frac{\pi}{2}$	$\frac{\pi}{2}$	α_6
d_1	0	d_3	0	0	d_6	a_1	a_2	0	a_4	a_5	a_6	$\frac{\pi}{2}$	0	$\frac{\pi}{2}$	0	0	α_6
d_1	0	d_3	0	0	d_6	a_1	a_2	0	a_4	a_5	a_6	0	$\frac{\pi}{2}$	$\frac{\pi}{2}$	0	0	α_6
d_1	0	d_3	0	0	d_6	a_1	a_2	0	a_4	a_5	a_6	0	0	$\frac{\pi}{2}$	$\frac{\pi}{2}$	$\frac{\pi}{2}$	α_6
d_1	0	0	d_4	d_5	d_6	a_1	a_2	a_3	a_4	0	a_6	0	$\frac{\pi}{2}$	0	0	$\frac{\pi}{2}$	α_6
d_1	0	0	d_4	d_5	d_6	a_1	a_2	a_3	a_4	0	a_6	0	0	$\frac{\pi}{2}$	$\frac{\pi}{2}$	$\frac{\pi}{2}$	α_6
d_1	0	0	d_4	d_5	d_6	a_1	a_2	a_3	a_4	0	a_6	0	0	$\frac{\pi}{2}$	0	$\frac{\pi}{2}$	α_6
d_1	0	0	d_4	d_5	d_6	a_1	a_2	a_3	0	a_5	a_6	$\frac{\pi}{2}$	0	0	$\frac{\pi}{2}$	$\frac{\pi}{2}$	α_6
d_1	0	0	d_4	d_5	d_6	a_1	a_2	a_3	0	a_5	a_6	$\frac{\pi}{2}$	0	0	$\frac{\pi}{2}$	0	α_6
d_1	0	0	d_4	d_5	d_6	a_1	a_2	a_3	0	a_5	a_6	0	0	$\frac{\pi}{2}$	$\frac{\pi}{2}$	$\frac{\pi}{2}$	α_6
d_1	0	0	d_4	d_5	d_6	a_1	a_2	a_3	0	a_5	a_6	0	0	$\frac{\pi}{2}$	$\frac{\pi}{2}$	0	α_6
d_1	0	0	d_4	d_5	d_6	a_1	a_2	a_3	0	0	a_6	$\frac{\pi}{2}$	0	0	$\frac{\pi}{2}$	$\frac{\pi}{2}$	α_6

Table A.17 – The D-H parameter values of robots whose det(**J**) factors into three components.

d_1	d_2	d_3	d_4	d_5	d_6	a_1	a_2	a_3	a_4	a_5	a_6	α_1	α_2	α_3	α_4	α_5	α_6
d_1	0	0	d_4	d_5	d_6	a_1	a_2	0	0	a_5	a_6	0	0	$\frac{\pi}{2}$	$\frac{\pi}{2}$	0	α_6
d_1	0	0	d_4	d_5	d_6	a_1	a_2	0	0	0	a_6	0	0	$\frac{\pi}{2}$	$\frac{\pi}{2}$	$\frac{\pi}{2}$	α_6
d_1	0	0	d_4	d_5	d_6	a_1	0	a_3	a_4	a_5	a_6	$\frac{\pi}{2}$	$\frac{\pi}{2}$	$\frac{\pi}{2}$	0	0	α_6
d_1	0	0	d_4	d_5	d_6	a_1	0	a_3	a_4	a_5	a_6	$\frac{\pi}{2}$	$\frac{\pi}{2}$	0	0	$\frac{\pi}{2}$	α_6
d_1	0	0	d_4	d_5	d_6	a_1	0	a_3	a_4	a_5	a_6	0	$\frac{\pi}{2}$	$\frac{\pi}{2}$	0	0	α_6
d_1	0	0	d_4	d_5	d_6	a_1	0	a_3	a_4	a_5	a_6	0	$\frac{\pi}{2}$	0	0	$\frac{\pi}{2}$	α_6
d_1	0	0	d_4	d_5	d_6	a_1	0	a_3	a_4	0	a_6	$\frac{\pi}{2}$	$\frac{\pi}{2}$	0	0	$\frac{\pi}{2}$	α_6
d_1	0	0	d_4	d_5	d_6	a_1	0	a_3	a_4	0	a_6	0	$\frac{\pi}{2}$	0	0	$\frac{\pi}{2}$	α_6
d_1	0	0	d_4	d_5	d_6	a_1	0	0	a_4	a_5	a_6	$\frac{\pi}{2}$	$\frac{\pi}{2}$	$\frac{\pi}{2}$	$\frac{\pi}{2}$	0	α_6
d_1	0	0	d_4	d_5	d_6	a_1	0	0	a_4	a_5	a_6	$\frac{\pi}{2}$	$\frac{\pi}{2}$	$\frac{\pi}{2}$	0	0	α_6
d_1	0	0	d_4	d_5	d_6	a_1	0	0	a_4	a_5	a_6	0	$\frac{\pi}{2}$	$\frac{\pi}{2}$	$\frac{\pi}{2}$	0	α_6
d_1	0	0	d_4	d_5	d_6	a_1	0	0	a_4	a_5	a_6	0	$\frac{\pi}{2}$	$\frac{\pi}{2}$	0	0	α_6
d_1	0	0	d_4	d_5	d_6	a_1	0	0	a_4	0	a_6	$\frac{\pi}{2}$	$\frac{\pi}{2}$	$\frac{\pi}{2}$	$\frac{\pi}{2}$	$\frac{\pi}{2}$	α_6
d_1	0	0	d_4	d_5	d_6	a_1	0	0	a_4	0	a_6	$\frac{\pi}{2}$	$\frac{\pi}{2}$	$\frac{\pi}{2}$	0	$\frac{\pi}{2}$	α_6
d_1	0	0	d_4	d_5	d_6	a_1	0	0	a_4	0	a_6	0	$\frac{\pi}{2}$	$\frac{\pi}{2}$	$\frac{\pi}{2}$	$\frac{\pi}{2}$	α_6
d_1	0	0	d_4	d_5	d_6	a_1	0	0	0	a_5	a_6	$\frac{\pi}{2}$	$\frac{\pi}{2}$	$\frac{\pi}{2}$	$\frac{\pi}{2}$	0	α_6
d_1	0	0	d_4	d_5	d_6	a_1	0	0	0	a_5	a_6	0	$\frac{\pi}{2}$	$\frac{\pi}{2}$	$\frac{\pi}{2}$	0	α_6
d_1	0	0	d_4	d_5	d_6	a_1	0	0	0	0	a_6	$\frac{\pi}{2}$	$\frac{\pi}{2}$	$\frac{\pi}{2}$	$\frac{\pi}{2}$	$\frac{\pi}{2}$	α_6
d_1	0	0	d_4	d_5	d_6	a_1	0	0	0	0	a_6	0	$\frac{\pi}{2}$	$\frac{\pi}{2}$	$\frac{\pi}{2}$	$\frac{\pi}{2}$	α_6
d_1	0	0	d_4	0	d_6	a_1	a_2	a_3	a_4	a_5	a_6	$\frac{\pi}{2}$	$\frac{\pi}{2}$	$\frac{\pi}{2}$	0	0	α_6
d_1	0	0	d_4	0	d_6	a_1	a_2	a_3	a_4	a_5	a_6	$\frac{\pi}{2}$	$\frac{\pi}{2}$	0	0	$\frac{\pi}{2}$	α_6
d_1	0	0	d_4	0	d_6	a_1	a_2	a_3	a_4	a_5	a_6	$\frac{\pi}{2}$	0	$\frac{\pi}{2}$	0	0	α_6
d_1	0	0	d_4	0	d_6	a_1	a_2	a_3	a_4	a_5	a_6	$\frac{\pi}{2}$	0	0	$\frac{\pi}{2}$	$\frac{\pi}{2}$	α_6
d_1	0	0	d_4	0	d_6	a_1	a_2	a_3	a_4	a_5	a_6	$\frac{\pi}{2}$	0	0	$\frac{\pi}{2}$	0	α_6
d_1	0	0	d_4	0	d_6	a_1	a_2	a_3	a_4	a_5	a_6	0	$\frac{\pi}{2}$	$\frac{\pi}{2}$	0	0	α_6
d_1	0	0	d_4	0	d_6	a_1	a_2	a_3	a_4	a_5	a_6	0	$\frac{\pi}{2}$	0	0	$\frac{\pi}{2}$	α_6
d_1	0	0	d_4	0	d_6	a_1	a_2	a_3	a_4	a_5	a_6	0	0	$\frac{\pi}{2}$	$\frac{\pi}{2}$	$\frac{\pi}{2}$	α_6
d_1	0	0	d_4	0	d_6	a_1	a_2	a_3	a_4	a_5	a_6	0	0	$\frac{\pi}{2}$	$\frac{\pi}{2}$	0	α_6
d_1	0	0	d_4	0	d_6	a_1	a_2	a_3	a_4	a_5	a_6	0	0	$\frac{\pi}{2}$	0	$\frac{\pi}{2}$	α_6
d_1	0	0	d_4	0	d_6	a_1	a_2	a_3	a_4	0	a_6	$\frac{\pi}{2}$	$\frac{\pi}{2}$	0	0	$\frac{\pi}{2}$	α_6
d_1	0	0	d_4	0	d_6	a_1	a_2	a_3	a_4	0	a_6	$\frac{\pi}{2}$	0	0	$\frac{\pi}{2}$	$\frac{\pi}{2}$	α_6
d_1	0	0	d_4	0	d_6	a_1	a_2	a_3	a_4	0	a_6	0	$\frac{\pi}{2}$	0	0	$\frac{\pi}{2}$	α_6
d_1	0	0	d_4	0	d_6	a_1	a_2	a_3	a_4	0	a_6	0	0	$\frac{\pi}{2}$	$\frac{\pi}{2}$	$\frac{\pi}{2}$	α_6
d_1	0	0	d_4	0	d_6	a_1	a_2	a_3	a_4	0	a_6	0	0	$\frac{\pi}{2}$	0	$\frac{\pi}{2}$	α_6
d_1	0	0	d_4	0	d_6	a_1	a_2	a_3	0	a_5	a_6	$\frac{\pi}{2}$	0	0	$\frac{\pi}{2}$	$\frac{\pi}{2}$	α_6
d_1	0	0	d_4	0	d_6	a_1	a_2	a_3	0	a_5	a_6	$\frac{\pi}{2}$	0	0	$\frac{\pi}{2}$	0	α_6
d_1	0	0	d_4	0	d_6	a_1	a_2	a_3	0	a_5	a_6	0	0	$\frac{\pi}{2}$	$\frac{\pi}{2}$	$\frac{\pi}{2}$	α_6
d_1	0	0	d_4	0	d_6	a_1	a_2	a_3	0	a_5	a_6	0	0	$\frac{\pi}{2}$	$\frac{\pi}{2}$	0	α_6

Table A.18 – The D-H parameter values of robots whose det($\mathbf{J}$) factors into three components.

d_1	d_2	d_3	d_4	d_5	d_6	a_1	a_2	a_3	a_4	a_5	a_6	α_1	α_2	α_3	α_4	α_5	α_6
d_1	0	0	d_4	0	d_6	a_1	a_2	a_3	0	0	a_6	0	$\frac{\pi}{2}$	0	$\frac{\pi}{2}$	$\frac{\pi}{2}$	α_6
d_1	0	0	d_4	0	d_6	a_1	a_2	0	a_4	a_5	a_6	$\frac{\pi}{2}$	$\frac{\pi}{2}$	$\frac{\pi}{2}$	0	0	α_6
d_1	0	0	d_4	0	d_6	a_1	a_2	0	a_4	a_5	a_6	$\frac{\pi}{2}$	0	$\frac{\pi}{2}$	0	0	α_6
d_1	0	0	d_4	0	d_6	a_1	a_2	0	a_4	a_5	a_6	0	$\frac{\pi}{2}$	$\frac{\pi}{2}$	0	0	α_6
d_1	0	0	d_4	0	d_6	a_1	a_2	0	a_4	a_5	a_6	0	0	$\frac{\pi}{2}$	$\frac{\pi}{2}$	$\frac{\pi}{2}$	α_6
d_1	0	0	d_4	0	d_6	a_1	a_2	0	a_4	a_5	a_6	0	0	$\frac{\pi}{2}$	$\frac{\pi}{2}$	0	α_6
d_1	0	0	d_4	0	d_6	a_1	a_2	0	a_4	a_5	a_6	0	0	$\frac{\pi}{2}$	0	$\frac{\pi}{2}$	α_6
d_1	0	0	d_4	0	d_6	a_1	a_2	0	a_4	0	a_6	0	0	$\frac{\pi}{2}$	$\frac{\pi}{2}$	$\frac{\pi}{2}$	α_6
d_1	0	0	d_4	0	d_6	a_1	a_2	0	a_4	0	a_6	0	0	$\frac{\pi}{2}$	0	$\frac{\pi}{2}$	α_6
d_1	0	0	d_4	0	d_6	a_1	a_2	0	0	a_5	a_6	$\frac{\pi}{2}$	$\frac{\pi}{2}$	$\frac{\pi}{2}$	$\frac{\pi}{2}$	$\frac{\pi}{2}$	α_6
d_1	0	0	d_4	0	d_6	a_1	a_2	0	0	a_5	a_6	$\frac{\pi}{2}$	0	$\frac{\pi}{2}$	$\frac{\pi}{2}$	$\frac{\pi}{2}$	α_6
d_1	0	0	d_4	0	d_6	a_1	a_2	0	0	a_5	a_6	0	$\frac{\pi}{2}$	$\frac{\pi}{2}$	$\frac{\pi}{2}$	$\frac{\pi}{2}$	α_6
d_1	0	0	d_4	0	d_6	a_1	a_2	0	0	a_5	a_6	0	0	$\frac{\pi}{2}$	$\frac{\pi}{2}$	$\frac{\pi}{2}$	α_6
d_1	0	0	d_4	0	d_6	a_1	a_2	0	0	a_5	a_6	0	0	$\frac{\pi}{2}$	$\frac{\pi}{2}$	0	α_6
d_1	0	0	d_4	0	d_6	a_1	a_2	0	0	0	a_6	$\frac{\pi}{2}$	$\frac{\pi}{2}$	$\frac{\pi}{2}$	$\frac{\pi}{2}$	$\frac{\pi}{2}$	α_6
d_1	0	0	d_4	0	d_6	a_1	a_2	0	0	0	a_6	$\frac{\pi}{2}$	0	$\frac{\pi}{2}$	$\frac{\pi}{2}$	$\frac{\pi}{2}$	α_6
d_1	0	0	d_4	0	d_6	a_1	a_2	0	0	0	a_6	0	$\frac{\pi}{2}$	$\frac{\pi}{2}$	$\frac{\pi}{2}$	$\frac{\pi}{2}$	α_6
d_1	0	0	d_4	0	d_6	a_1	0	a_3	a_4	a_5	a_6	$\frac{\pi}{2}$	$\frac{\pi}{2}$	$\frac{\pi}{2}$	0	0	α_6
d_1	0	0	d_4	0	d_6	a_1	0	a_3	a_4	a_5	a_6	$\frac{\pi}{2}$	$\frac{\pi}{2}$	0	0	$\frac{\pi}{2}$	α_6
d_1	0	0	d_4	0	d_6	a_1	0	a_3	a_4	a_5	a_6	0	$\frac{\pi}{2}$	$\frac{\pi}{2}$	0	0	α_6
d_1	0	0	d_4	0	d_6	a_1	0	a_3	a_4	a_5	a_6	0	$\frac{\pi}{2}$	0	0	$\frac{\pi}{2}$	α_6
d_1	0	0	d_4	0	d_6	a_1	0	a_3	a_4	0	a_6	$\frac{\pi}{2}$	$\frac{\pi}{2}$	0	0	$\frac{\pi}{2}$	α_6
d_1	0	0	d_4	0	d_6	a_1	0	a_3	a_4	0	a_6	0	$\frac{\pi}{2}$	0	0	$\frac{\pi}{2}$	α_6
d_1	0	0	d_4	0	d_6	a_1	0	a_3	0	0	a_6	$\frac{\pi}{2}$	$\frac{\pi}{2}$	0	$\frac{\pi}{2}$	$\frac{\pi}{2}$	α_6
d_1	0	0	d_4	0	d_6	a_1	0	a_3	0	0	a_6	0	$\frac{\pi}{2}$	$\frac{\pi}{2}$	$\frac{\pi}{2}$	$\frac{\pi}{2}$	α_6
d_1	0	0	d_4	0	d_6	a_1	0	a_3	0	0	a_6	0	$\frac{\pi}{2}$	0	$\frac{\pi}{2}$	$\frac{\pi}{2}$	α_6
d_1	0	0	d_4	0	d_6	a_1	0	0	a_4	a_5	a_6	$\frac{\pi}{2}$	$\frac{\pi}{2}$	$\frac{\pi}{2}$	$\frac{\pi}{2}$	$\frac{\pi}{2}$	α_6
d_1	0	0	d_4	0	d_6	a_1	0	0	a_4	a_5	a_6	$\frac{\pi}{2}$	$\frac{\pi}{2}$	$\frac{\pi}{2}$	$\frac{\pi}{2}$	0	α_6
d_1	0	0	d_4	0	d_6	a_1	0	0	a_4	a_5	a_6	$\frac{\pi}{2}$	$\frac{\pi}{2}$	$\frac{\pi}{2}$	0	0	α_6
d_1	0	0	d_4	0	d_6	a_1	0	0	a_4	a_5	a_6	0	$\frac{\pi}{2}$	$\frac{\pi}{2}$	$\frac{\pi}{2}$	$\frac{\pi}{2}$	α_6
d_1	0	0	d_4	0	d_6	a_1	0	0	a_4	0	a_6	$\frac{\pi}{2}$	$\frac{\pi}{2}$	$\frac{\pi}{2}$	$\frac{\pi}{2}$	$\frac{\pi}{2}$	α_6
d_1	0	0	d_4	0	d_6	a_1	0	0	a_4	0	a_6	$\frac{\pi}{2}$	$\frac{\pi}{2}$	$\frac{\pi}{2}$	0	$\frac{\pi}{2}$	α_6
d_1	0	0	d_4	0	d_6	a_1	0	0	a_4	0	a_6	0	$\frac{\pi}{2}$	$\frac{\pi}{2}$	$\frac{\pi}{2}$	$\frac{\pi}{2}$	α_6
d_1	0	0	d_4	0	d_6	a_1	0	0	a_4	0	a_6	0	$\frac{\pi}{2}$	$\frac{\pi}{2}$	0	$\frac{\pi}{2}$	α_6
d_1	0	0	d_4	0	d_6	a_1	0	0	0	a_5	a_6	$\frac{\pi}{2}$	$\frac{\pi}{2}$	$\frac{\pi}{2}$	$\frac{\pi}{2}$	$\frac{\pi}{2}$	α_6
d_1	0	0	d_4	0	d_6	a_1	0	0	0	a_5	a_6	$\frac{\pi}{2}$	$\frac{\pi}{2}$	$\frac{\pi}{2}$	$\frac{\pi}{2}$	0	α_6
d_1	0	0	d_4	0	d_6	a_1	0	0	0	a_5	a_6	0	$\frac{\pi}{2}$	$\frac{\pi}{2}$	$\frac{\pi}{2}$	$\frac{\pi}{2}$	α_6

Table A.19 – The D-H parameter values of robots whose det(**J**) factors into three components.

d_1	d_2	d_3	d_4	d_5	d_6	a_1	a_2	a_3	a_4	a_5	a_6	α_1	α_2	α_3	α_4	α_5	α_6
d_1	0	0	0	d_5	d_6	a_1	a_2	a_3	a_4	a_5	a_6	$\frac{\pi}{2}$	$\frac{\pi}{2}$	0	0	$\frac{\pi}{2}$	α_6
d_1	0	0	0	d_5	d_6	a_1	a_2	a_3	a_4	a_5	a_6	$\frac{\pi}{2}$	0	$\frac{\pi}{2}$	0	0	α_6
d_1	0	0	0	d_5	d_6	a_1	a_2	a_3	a_4	a_5	a_6	$\frac{\pi}{2}$	0	0	$\frac{\pi}{2}$	$\frac{\pi}{2}$	α_6
d_1	0	0	0	d_5	d_6	a_1	a_2	a_3	a_4	a_5	a_6	$\frac{\pi}{2}$	0	0	$\frac{\pi}{2}$	0	α_6
d_1	0	0	0	d_5	d_6	a_1	a_2	a_3	a_4	a_5	a_6	0	$\frac{\pi}{2}$	$\frac{\pi}{2}$	0	0	α_6
d_1	0	0	0	d_5	d_6	a_1	a_2	a_3	a_4	a_5	a_6	0	$\frac{\pi}{2}$	0	0	$\frac{\pi}{2}$	α_6
d_1	0	0	0	d_5	d_6	a_1	a_2	a_3	a_4	a_5	a_6	0	0	$\frac{\pi}{2}$	$\frac{\pi}{2}$	$\frac{\pi}{2}$	α_6
d_1	0	0	0	d_5	d_6	a_1	a_2	a_3	a_4	a_5	a_6	0	0	$\frac{\pi}{2}$	$\frac{\pi}{2}$	0	α_6
d_1	0	0	0	d_5	d_6	a_1	a_2	a_3	a_4	a_5	a_6	0	0	$\frac{\pi}{2}$	0	$\frac{\pi}{2}$	α_6
d_1	0	0	0	d_5	d_6	a_1	a_2	a_3	a_4	0	a_6	$\frac{\pi}{2}$	$\frac{\pi}{2}$	0	0	$\frac{\pi}{2}$	α_6
d_1	0	0	0	d_5	d_6	a_1	a_2	a_3	a_4	0	a_6	$\frac{\pi}{2}$	0	0	$\frac{\pi}{2}$	$\frac{\pi}{2}$	α_6
d_1	0	0	0	d_5	d_6	a_1	a_2	a_3	a_4	0	a_6	0	$\frac{\pi}{2}$	0	0	$\frac{\pi}{2}$	α_6
d_1	0	0	0	d_5	d_6	a_1	a_2	a_3	a_4	0	a_6	0	0	$\frac{\pi}{2}$	$\frac{\pi}{2}$	$\frac{\pi}{2}$	α_6
d_1	0	0	0	d_5	d_6	a_1	a_2	a_3	a_4	0	a_6	0	0	$\frac{\pi}{2}$	0	$\frac{\pi}{2}$	α_6
d_1	0	0	0	d_5	d_6	a_1	a_2	a_3	0	a_5	a_6	$\frac{\pi}{2}$	0	0	$\frac{\pi}{2}$	$\frac{\pi}{2}$	α_6
d_1	0	0	0	d_5	d_6	a_1	a_2	a_3	0	a_5	a_6	$\frac{\pi}{2}$	0	0	$\frac{\pi}{2}$	0	α_6
d_1	0	0	0	d_5	d_6	a_1	a_2	a_3	0	a_5	a_6	0	0	$\frac{\pi}{2}$	$\frac{\pi}{2}$	$\frac{\pi}{2}$	α_6
d_1	0	0	0	d_5	d_6	a_1	a_2	a_3	0	a_5	a_6	0	0	$\frac{\pi}{2}$	$\frac{\pi}{2}$	0	α_6
d_1	0	0	0	d_5	d_6	a_1	a_2	a_3	0	0	a_6	$\frac{\pi}{2}$	0	0	$\frac{\pi}{2}$	$\frac{\pi}{2}$	α_6
d_1	0	0	0	d_5	d_6	a_1	a_2	a_3	0	0	a_6	0	0	$\frac{\pi}{2}$	$\frac{\pi}{2}$	$\frac{\pi}{2}$	α_6
d_1	0	0	0	d_5	d_6	a_1	a_2	0	a_4	a_5	a_6	$\frac{\pi}{2}$	$\frac{\pi}{2}$	$\frac{\pi}{2}$	0	0	α_6
d_1	0	0	0	d_5	d_6	a_1	a_2	0	a_4	a_5	a_6	$\frac{\pi}{2}$	0	$\frac{\pi}{2}$	0	0	α_6
d_1	0	0	0	d_5	d_6	a_1	a_2	0	a_4	a_5	a_6	0	$\frac{\pi}{2}$	$\frac{\pi}{2}$	0	0	α_6
d_1	0	0	0	d_5	d_6	a_1	a_2	0	a_4	a_5	a_6	0	0	$\frac{\pi}{2}$	$\frac{\pi}{2}$	$\frac{\pi}{2}$	α_6
d_1	0	0	0	d_5	d_6	a_1	a_2	0	a_4	a_5	a_6	0	0	$\frac{\pi}{2}$	$\frac{\pi}{2}$	0	α_6
d_1	0	0	0	d_5	d_6	a_1	a_2	0	a_4	a_5	a_6	0	0	$\frac{\pi}{2}$	0	$\frac{\pi}{2}$	α_6
d_1	0	0	0	d_5	d_6	a_1	a_2	0	a_4	0	a_6	0	0	$\frac{\pi}{2}$	$\frac{\pi}{2}$	$\frac{\pi}{2}$	α_6
d_1	0	0	0	d_5	d_6	a_1	a_2	0	a_4	0	a_6	0	0	$\frac{\pi}{2}$	$\frac{\pi}{2}$	0	α_6
d_1	0	0	0	d_5	d_6	a_1	a_2	0	0	a_5	a_6	$\frac{\pi}{2}$	$\frac{\pi}{2}$	$\frac{\pi}{2}$	$\frac{\pi}{2}$	$\frac{\pi}{2}$	α_6
d_1	0	0	0	d_5	d_6	a_1	a_2	0	0	a_5	a_6	$\frac{\pi}{2}$	$\frac{\pi}{2}$	$\frac{\pi}{2}$	$\frac{\pi}{2}$	0	α_6
d_1	0	0	0	d_5	d_6	a_1	a_2	0	0	a_5	a_6	$\frac{\pi}{2}$	0	$\frac{\pi}{2}$	$\frac{\pi}{2}$	$\frac{\pi}{2}$	α_6
d_1	0	0	0	d_5	d_6	a_1	a_2	0	0	a_5	a_6	0	$\frac{\pi}{2}$	$\frac{\pi}{2}$	$\frac{\pi}{2}$	$\frac{\pi}{2}$	α_6
d_1	0	0	0	d_5	d_6	a_1	a_2	0	0	a_5	a_6	0	$\frac{\pi}{2}$	$\frac{\pi}{2}$	$\frac{\pi}{2}$	0	α_6
d_1	0	0	0	d_5	d_6	a_1	a_2	0	0	a_5	a_6	0	0	$\frac{\pi}{2}$	$\frac{\pi}{2}$	$\frac{\pi}{2}$	α_6
d_1	0	0	0	d_5	d_6	a_1	a_2	0	0	a_5	a_6	0	0	$\frac{\pi}{2}$	$\frac{\pi}{2}$	0	α_6
d_1	0	0	0	d_5	d_6	a_1	a_2	0	0	0	a_6	$\frac{\pi}{2}$	$\frac{\pi}{2}$	$\frac{\pi}{2}$	$\frac{\pi}{2}$	$\frac{\pi}{2}$	α_6
d_1	0	0	0	d_5	d_6	a_1	a_2	0	0	0	a_6	$\frac{\pi}{2}$	0	$\frac{\pi}{2}$	$\frac{\pi}{2}$	$\frac{\pi}{2}$	α_6
d_1	0	0	0	d_5	d_6	a_1	a_2	0	0	0	a_6	0	$\frac{\pi}{2}$	$\frac{\pi}{2}$	$\frac{\pi}{2}$	$\frac{\pi}{2}$	α_6

Table A.20 – The D-H parameter values of robots whose det($\mathbf{J}$) factors into three components.

d_1	d_2	d_3	d_4	d_5	d_6	a_1	a_2	a_3	a_4	a_5	a_6	α_1	α_2	α_3	α_4	α_5	α_6
d_1	0	0	0	d_5	d_6	a_1	a_2	0	0	0	a_6	0	0	$\frac{\pi}{2}$	$\frac{\pi}{2}$	$\frac{\pi}{2}$	α_6
d_1	0	0	0	d_5	d_6	a_1	0	a_3	a_4	a_5	a_6	$\frac{\pi}{2}$	$\frac{\pi}{2}$	$\frac{\pi}{2}$	0	0	α_6
d_1	0	0	0	d_5	d_6	a_1	0	a_3	a_4	a_5	a_6	$\frac{\pi}{2}$	$\frac{\pi}{2}$	0	0	$\frac{\pi}{2}$	α_6
d_1	0	0	0	d_5	d_6	a_1	0	a_3	a_4	a_5	a_6	0	$\frac{\pi}{2}$	$\frac{\pi}{2}$	0	0	α_6
d_1	0	0	0	d_5	d_6	a_1	0	a_3	a_4	a_5	a_6	0	$\frac{\pi}{2}$	0	0	$\frac{\pi}{2}$	α_6
d_1	0	0	0	d_5	d_6	a_1	0	a_3	a_4	0	a_6	$\frac{\pi}{2}$	$\frac{\pi}{2}$	0	0	$\frac{\pi}{2}$	α_6
d_1	0	0	0	d_5	d_6	a_1	0	a_3	a_4	0	a_6	0	$\frac{\pi}{2}$	0	0	$\frac{\pi}{2}$	α_6
d_1	0	0	0	d_5	d_6	a_1	0	0	a_4	a_5	a_6	$\frac{\pi}{2}$	$\frac{\pi}{2}$	$\frac{\pi}{2}$	$\frac{\pi}{2}$	0	α_6
d_1	0	0	0	d_5	d_6	a_1	0	0	a_4	a_5	a_6	$\frac{\pi}{2}$	$\frac{\pi}{2}$	$\frac{\pi}{2}$	0	0	α_6
d_1	0	0	0	d_5	d_6	a_1	0	0	a_4	a_5	a_6	0	$\frac{\pi}{2}$	$\frac{\pi}{2}$	$\frac{\pi}{2}$	0	α_6
d_1	0	0	0	d_5	d_6	a_1	0	0	a_4	a_5	a_6	0	$\frac{\pi}{2}$	$\frac{\pi}{2}$	0	0	α_6
d_1	0	0	0	d_5	d_6	a_1	0	0	a_4	0	a_6	$\frac{\pi}{2}$	$\frac{\pi}{2}$	$\frac{\pi}{2}$	$\frac{\pi}{2}$	$\frac{\pi}{2}$	α_6
d_1	0	0	0	d_5	d_6	a_1	0	0	a_4	0	a_6	$\frac{\pi}{2}$	$\frac{\pi}{2}$	$\frac{\pi}{2}$	0	$\frac{\pi}{2}$	α_6
d_1	0	0	0	d_5	d_6	a_1	0	0	a_4	0	a_6	0	$\frac{\pi}{2}$	$\frac{\pi}{2}$	$\frac{\pi}{2}$	$\frac{\pi}{2}$	α_6
d_1	0	0	0	d_5	d_6	a_1	0	0	a_4	0	a_6	0	$\frac{\pi}{2}$	$\frac{\pi}{2}$	0	$\frac{\pi}{2}$	α_6
d_1	0	0	0	0	d_6	a_1	a_2	a_3	a_4	a_5	a_6	$\frac{\pi}{2}$	$\frac{\pi}{2}$	$\frac{\pi}{2}$	0	0	α_6
d_1	0	0	0	0	d_6	a_1	a_2	a_3	a_4	a_5	a_6	$\frac{\pi}{2}$	$\frac{\pi}{2}$	0	0	$\frac{\pi}{2}$	α_6
d_1	0	0	0	0	d_6	a_1	a_2	a_3	a_4	a_5	a_6	$\frac{\pi}{2}$	0	$\frac{\pi}{2}$	0	0	α_6
d_1	0	0	0	0	d_6	a_1	a_2	a_3	a_4	a_5	a_6	$\frac{\pi}{2}$	0	0	$\frac{\pi}{2}$	$\frac{\pi}{2}$	α_6
d_1	0	0	0	0	d_6	a_1	a_2	a_3	a_4	a_5	a_6	$\frac{\pi}{2}$	0	0	$\frac{\pi}{2}$	0	α_6
d_1	0	0	0	0	d_6	a_1	a_2	a_3	a_4	a_5	a_6	0	$\frac{\pi}{2}$	$\frac{\pi}{2}$	0	0	α_6
d_1	0	0	0	0	d_6	a_1	a_2	a_3	a_4	a_5	a_6	0	$\frac{\pi}{2}$	0	0	$\frac{\pi}{2}$	α_6
d_1	0	0	0	0	d_6	a_1	a_2	a_3	a_4	a_5	a_6	0	0	$\frac{\pi}{2}$	$\frac{\pi}{2}$	$\frac{\pi}{2}$	α_6
d_1	0	0	0	0	d_6	a_1	a_2	a_3	a_4	a_5	a_6	0	0	$\frac{\pi}{2}$	0	$\frac{\pi}{2}$	α_6
d_1	0	0	0	0	d_6	a_1	a_2	a_3	a_4	0	a_6	$\frac{\pi}{2}$	$\frac{\pi}{2}$	0	0	$\frac{\pi}{2}$	α_6
d_1	0	0	0	0	d_6	a_1	a_2	a_3	a_4	0	a_6	$\frac{\pi}{2}$	0	0	$\frac{\pi}{2}$	$\frac{\pi}{2}$	α_6
d_1	0	0	0	0	d_6	a_1	a_2	a_3	a_4	0	a_6	0	$\frac{\pi}{2}$	0	0	$\frac{\pi}{2}$	α_6
d_1	0	0	0	0	d_6	a_1	a_2	a_3	a_4	0	a_6	0	0	$\frac{\pi}{2}$	$\frac{\pi}{2}$	$\frac{\pi}{2}$	α_6
d_1	0	0	0	0	d_6	a_1	a_2	a_3	a_4	0	a_6	0	0	$\frac{\pi}{2}$	0	$\frac{\pi}{2}$	α_6
d_1	0	0	0	0	d_6	a_1	a_2	a_3	0	a_5	a_6	$\frac{\pi}{2}$	0	0	$\frac{\pi}{2}$	$\frac{\pi}{2}$	α_6
d_1	0	0	0	0	d_6	a_1	a_2	a_3	0	a_5	a_6	$\frac{\pi}{2}$	0	0	$\frac{\pi}{2}$	0	α_6
d_1	0	0	0	0	d_6	a_1	a_2	a_3	0	a_5	a_6	0	0	$\frac{\pi}{2}$	$\frac{\pi}{2}$	$\frac{\pi}{2}$	α_6
d_1	0	0	0	0	d_6	a_1	a_2	a_3	0	a_5	a_6	0	0	$\frac{\pi}{2}$	$\frac{\pi}{2}$	0	α_6
d_1	0	0	0	0	d_6	a_1	a_2	a_3	0	0	a_6	$\frac{\pi}{2}$	$\frac{\pi}{2}$	$\frac{\pi}{2}$	$\frac{\pi}{2}$	$\frac{\pi}{2}$	α_6
d_1	0	0	0	0	d_6	a_1	a_2	a_3	0	0	a_6	$\frac{\pi}{2}$	$\frac{\pi}{2}$	0	$\frac{\pi}{2}$	$\frac{\pi}{2}$	α_6
d_1	0	0	0	0	d_6	a_1	a_2	a_3	0	0	a_6	$\frac{\pi}{2}$	0	$\frac{\pi}{2}$	$\frac{\pi}{2}$	$\frac{\pi}{2}$	α_6
d_1	0	0	0	0	d_6	a_1	a_2	a_3	0	0	a_6	$\frac{\pi}{2}$	0	0	$\frac{\pi}{2}$	$\frac{\pi}{2}$	α_6
d_1	0	0	0	0	d_6	a_1	a_2	a_3	0	0	a_6	0	$\frac{\pi}{2}$	$\frac{\pi}{2}$	$\frac{\pi}{2}$	$\frac{\pi}{2}$	α_6

Table A.21 – The D-H parameter values of robots whose det(**J**) factors into three components.

d_1	d_2	d_3	d_4	d_5	d_6	a_1	a_2	a_3	a_4	a_5	a_6	α_1	α_2	α_3	α_4	α_5	α_6
d_1	0	0	0	0	d_6	a_1	a_2	a_3	0	0	a_6	0	$\frac{\pi}{2}$	0	$\frac{\pi}{2}$	$\frac{\pi}{2}$	α_6
d_1	0	0	0	0	d_6	a_1	a_2	0	a_4	a_5	a_6	$\frac{\pi}{2}$	$\frac{\pi}{2}$	$\frac{\pi}{2}$	0	0	α_6
d_1	0	0	0	0	d_6	a_1	a_2	0	a_4	a_5	a_6	$\frac{\pi}{2}$	0	$\frac{\pi}{2}$	0	0	α_6
d_1	0	0	0	0	d_6	a_1	a_2	0	a_4	a_5	a_6	0	$\frac{\pi}{2}$	$\frac{\pi}{2}$	0	0	α_6
d_1	0	0	0	0	d_6	a_1	a_2	0	a_4	a_5	a_6	0	0	$\frac{\pi}{2}$	$\frac{\pi}{2}$	$\frac{\pi}{2}$	α_6
d_1	0	0	0	0	d_6	a_1	a_2	0	a_4	a_5	a_6	0	0	$\frac{\pi}{2}$	$\frac{\pi}{2}$	0	α_6
d_1	0	0	0	0	d_6	a_1	a_2	0	a_4	a_5	a_6	0	0	$\frac{\pi}{2}$	0	$\frac{\pi}{2}$	α_6
d_1	0	0	0	0	d_6	a_1	a_2	0	a_4	0	a_6	0	0	$\frac{\pi}{2}$	$\frac{\pi}{2}$	$\frac{\pi}{2}$	α_6
d_1	0	0	0	0	d_6	a_1	a_2	0	a_4	0	a_6	0	0	$\frac{\pi}{2}$	0	$\frac{\pi}{2}$	α_6
d_1	0	0	0	0	d_6	a_1	a_2	0	0	a_5	a_6	$\frac{\pi}{2}$	$\frac{\pi}{2}$	$\frac{\pi}{2}$	$\frac{\pi}{2}$	$\frac{\pi}{2}$	α_6
d_1	0	0	0	0	d_6	a_1	a_2	0	0	a_5	a_6	$\frac{\pi}{2}$	$\frac{\pi}{2}$	$\frac{\pi}{2}$	$\frac{\pi}{2}$	0	α_6
d_1	0	0	0	0	d_6	a_1	a_2	0	0	a_5	a_6	$\frac{\pi}{2}$	0	$\frac{\pi}{2}$	$\frac{\pi}{2}$	$\frac{\pi}{2}$	α_6
d_1	0	0	0	0	d_6	a_1	a_2	0	0	a_5	a_6	$\frac{\pi}{2}$	0	$\frac{\pi}{2}$	$\frac{\pi}{2}$	0	α_6
d_1	0	0	0	0	d_6	a_1	a_2	0	0	a_5	a_6	0	$\frac{\pi}{2}$	$\frac{\pi}{2}$	$\frac{\pi}{2}$	$\frac{\pi}{2}$	α_6
d_1	0	0	0	0	d_6	a_1	a_2	0	0	a_5	a_6	0	$\frac{\pi}{2}$	$\frac{\pi}{2}$	$\frac{\pi}{2}$	0	α_6
d_1	0	0	0	0	d_6	a_1	a_2	0	0	a_5	a_6	0	0	$\frac{\pi}{2}$	$\frac{\pi}{2}$	$\frac{\pi}{2}$	α_6
d_1	0	0	0	0	d_6	a_1	a_2	0	0	a_5	a_6	0	0	$\frac{\pi}{2}$	$\frac{\pi}{2}$	0	α_6
d_1	0	0	0	0	d_6	a_1	0	a_3	a_4	a_5	a_6	$\frac{\pi}{2}$	$\frac{\pi}{2}$	$\frac{\pi}{2}$	0	0	α_6
d_1	0	0	0	0	d_6	a_1	0	a_3	a_4	a_5	a_6	$\frac{\pi}{2}$	$\frac{\pi}{2}$	0	0	$\frac{\pi}{2}$	α_6
d_1	0	0	0	0	d_6	a_1	0	a_3	a_4	a_5	a_6	0	$\frac{\pi}{2}$	$\frac{\pi}{2}$	0	0	α_6
d_1	0	0	0	0	d_6	a_1	0	a_3	a_4	a_5	a_6	0	$\frac{\pi}{2}$	0	0	$\frac{\pi}{2}$	α_6
d_1	0	0	0	0	d_6	a_1	0	a_3	a_4	0	a_6	$\frac{\pi}{2}$	$\frac{\pi}{2}$	0	0	$\frac{\pi}{2}$	α_6
d_1	0	0	0	0	d_6	a_1	0	a_3	a_4	0	a_6	0	$\frac{\pi}{2}$	0	0	$\frac{\pi}{2}$	α_6
d_1	0	0	0	0	d_6	a_1	0	a_3	0	0	a_6	$\frac{\pi}{2}$	$\frac{\pi}{2}$	$\frac{\pi}{2}$	$\frac{\pi}{2}$	$\frac{\pi}{2}$	α_6
d_1	0	0	0	0	d_6	a_1	0	a_3	0	0	a_6	$\frac{\pi}{2}$	$\frac{\pi}{2}$	0	$\frac{\pi}{2}$	$\frac{\pi}{2}$	α_6
d_1	0	0	0	0	d_6	a_1	0	a_3	0	0	a_6	0	$\frac{\pi}{2}$	$\frac{\pi}{2}$	$\frac{\pi}{2}$	$\frac{\pi}{2}$	α_6
d_1	0	0	0	0	d_6	a_1	0	a_3	0	0	a_6	0	$\frac{\pi}{2}$	0	$\frac{\pi}{2}$	$\frac{\pi}{2}$	α_6
d_1	0	0	0	0	d_6	a_1	0	0	a_4	a_5	a_6	$\frac{\pi}{2}$	$\frac{\pi}{2}$	$\frac{\pi}{2}$	$\frac{\pi}{2}$	$\frac{\pi}{2}$	α_6
d_1	0	0	0	0	d_6	a_1	0	0	a_4	a_5	a_6	$\frac{\pi}{2}$	$\frac{\pi}{2}$	$\frac{\pi}{2}$	$\frac{\pi}{2}$	0	α_6
d_1	0	0	0	0	d_6	a_1	0	0	a_4	a_5	a_6	$\frac{\pi}{2}$	$\frac{\pi}{2}$	$\frac{\pi}{2}$	0	$\frac{\pi}{2}$	α_6
d_1	0	0	0	0	d_6	a_1	0	0	a_4	a_5	a_6	$\frac{\pi}{2}$	$\frac{\pi}{2}$	$\frac{\pi}{2}$	0	0	α_6
d_1	0	0	0	0	d_6	a_1	0	0	a_4	a_5	a_6	0	$\frac{\pi}{2}$	$\frac{\pi}{2}$	$\frac{\pi}{2}$	$\frac{\pi}{2}$	α_6
d_1	0	0	0	0	d_6	a_1	0	0	a_4	a_5	a_6	0	$\frac{\pi}{2}$	$\frac{\pi}{2}$	$\frac{\pi}{2}$	0	α_6
d_1	0	0	0	0	d_6	a_1	0	0	a_4	a_5	a_6	0	$\frac{\pi}{2}$	$\frac{\pi}{2}$	$\frac{\pi}{2}$	$\frac{\pi}{2}$	α_6
d_1	0	0	0	0	d_6	a_1	0	0	a_4	0	a_6	$\frac{\pi}{2}$	$\frac{\pi}{2}$	$\frac{\pi}{2}$	$\frac{\pi}{2}$	$\frac{\pi}{2}$	α_6
d_1	0	0	0	0	d_6	a_1	0	0	a_4	0	a_6	$\frac{\pi}{2}$	$\frac{\pi}{2}$	$\frac{\pi}{2}$	0	$\frac{\pi}{2}$	α_6
d_1	0	0	0	0	d_6	a_1	0	0	a_4	0	a_6	0	$\frac{\pi}{2}$	$\frac{\pi}{2}$	$\frac{\pi}{2}$	$\frac{\pi}{2}$	α_6
d_1	0	0	0	0	d_6	a_1	0	0	a_4	0	a_6	0	$\frac{\pi}{2}$	$\frac{\pi}{2}$	0	$\frac{\pi}{2}$	α_6

Table A.22 – The D-H parameter values of robots whose det($\mathbf{J}$) factors into three components.

BIBLIOGRAPHY

[And+19] Joel A E Andersson et al. « CasADi – A software framework for nonlinear optimization and optimal control ». In: *Mathematical Programming Computation* (2019).

[Ang85] Jorge Angeles. « On the Numerical Solution of the Inverse Kinematic Problem ». In: *The International Journal of Robotics Research* 4.2 (1985), pp. 21–37. DOI: 10.1177/027836498500400203. URL: https://doi.org/10.1177/027836498500400203.

[Ben17] Romain Benoit. « Qualitative analysis of robots ». French. PhD thesis. Angers: University of Angers, Nov. 2017.

[Ben91] Fouad Bennis. « Contribution a la modelisation geometrique et dynamique des robots a structure simple et complexe ». PhD thesis. Ecole Centrale de Nantes, 1991, 252 p. URL: http://www.theses.fr/1991NANT2008.

[BL86] Paul Borrel and Alain Liegeois. « A study of multiple manipulator inverse kinematic solutions with applications to trajectory planning and workspace determination ». In: *Proceedings. 1986 IEEE International Conference on Robotics and Automation*. Vol. 3. San Francisco, CA, USA: Institute of Electrical and Electronics Engineers, 1986, pp. 1180–1185.

[BP84] H.G. Bock and K.J. Plitt. « A Multiple Shooting Algorithm for Direct Solution of Optimal Control Problems* ». In: *IFAC Proceedings Volumes* (1984).

[Bra16] Mathias Brandstötter. « Adaptable Serial Manipulators in Modular Design ». PhD thesis. University of Innsbruck, Nov. 2016. DOI: 10.13140/RG.2.2.16537.62565.

[Bur89] Joel W Burdick. « On the Inverse Kinematics of Redundant Manipulators: Characterization of the Self-Motion Manifolds ». en. In: *1989 International Conference on Advanced Robotics*. Vol. 4. Ohio, 1989, p. 10.

[BWC04] Maher Baili, Philippe Wenger, and Damien Chablat. « A classification of 3R orthogonal manipulators by the topology of their workspace ». en. In: *IEEE International Conference on Robotics and Automation, 2004. Proceedings. ICRA '04. 2004.* New Orleans, LA, USA: IEEE, 2004, 1933–1938 Vol.2. (Visited on June 2, 2020).

[Cha+22] Damien Chablat et al. « Deciding Cuspidality of Manipulators through Computer Algebra and Algorithms in Real Algebraic Geometry ». In: *Proceedings of the 2022 International Symposium on Symbolic and Algebraic Computation.* ISSAC '22. Villeneuve-d'Ascq, France: Association for Computing Machinery, 2022, 439–448. ISBN: 9781450386883. DOI: 10.1145/3476446.3535477.

[CM19] Jose Capco and Saraleen Mae Manongsong. « Implementing HuPf Algorithm for the Inverse Kinematics of General 6R/P Manipulators ». In: *Computer Algebra in Scientific Computing.* Ed. by Matthew England et al. Cham: Springer International Publishing, 2019, pp. 78–90. ISBN: 978-3-030-26831-2.

[Cor05] Solen Corvez. « Study of polynomial system: contribution to the classification of a family of manipulators and calculating the intersection of A-spline curve ». fr. PhD thesis. Rennes, France: University of Rennes, May 2005.

[Cor+09] Thomas H Cormen et al. *Introduction to algorithms.* Third. MIT press, 2009.

[CR04] Solen Corvez and Fabrice Rouillier. « Using Computer Algebra Tools to Classify Serial Manipulators ». en. In: *Automated Deduction in Geometry.* Ed. by Gerhard Goos et al. Vol. 2930. Series Title: Lecture Notes in Computer Science. Berlin, Heidelberg: Springer Berlin Heidelberg, 2004, pp. 31–43. ISBN: 978-3-540-20927-0 978-3-540-24616-9. DOI: 10.1007/978-3-540-24616-9_3. (Visited on Jan. 28, 2021).

[CSEDS20] Jose Capco, Mohab Safey El Din, and Josef Schicho. « Robots, computer algebra and eight connected components ». In: *ISSAC '20: International Symposium on Symbolic and Algebraic Computation.* ISSAC'20: Proceedings of the 45th International Symposium on Symbolic and Algebraic Computation. Kalamata / Virtual, Greece: ACM, July 2020, pp. 62–69.

[DH55] Jacques Denavit and Richard Scheunemann Hartenberg. « A Kinematic Notation for Lower-Pair Mechanisms Based on Matrices ». In: *Journal of Applied Mechanics* 22.2 (June 1955), pp. 215–221. ISSN: 0021-8936. DOI: 10.1115/1.4011045. URL: https://doi.org/10.1115/1.4011045.

[Dot+95] Keith L Doty et al. « Robot manipulability ». In: *IEEE Transactions on Robotics and Automation* (1995).

[EOW95] Jouad El Omri and Philippe Wenger. « How to recognize simply a nonsingular posture changing 3-DOF manipulator ». In: *Proc. 7th Int. Conf. on Advanced Robotics*. 1995, pp. 215–222.

[Fre73] Ferdinand Freudenstein. « Kinematics: Past, present and future ». In: *Mechanism and Machine Theory* 8.2 (1973), pp. 151–160. ISSN: 0094-114X. DOI: https://doi.org/10.1016/0094-114X(73)90049-9. URL: https://www.sciencedirect.com/science/article/pii/0094114X73900499.

[GL14] *Polynomial Inverse Kinematic Solution of the Jaco Robot*. Vol. Volume 5B: 38th Mechanisms and Robotics Conference. International Design Engineering Technical Conferences and Computers and Information in Engineering Conference. Aug. 2014, V05BT08A055. DOI: 10.1115/DETC2014-34152. URL: https://doi.org/10.1115/DETC2014-34152.

[HOC08] Manfred Husty, Erika Ottaviano, and Marco Ceccarelli. « A Geometrical Characterization of Workspace Singularities in 3R Manipulators ». In: *Advances in Robot Kinematics: Analysis and Design*. Ed. by Jadran Lenarčič and Philippe Wenger. Dordrecht: Springer Netherlands, 2008, pp. 411–418.

[HPS07] Manfred L. Husty, Martin Pfurner, and Hans-Peter Schröcker. « A new and efficient algorithm for the inverse kinematics of a general serial 6R manipulator ». en. In: *Mechanism and Machine Theory* 42.1 (Jan. 2007), pp. 66–81. ISSN: 0094114X. DOI: 10.1016/j.mechmachtheory.2006.02.001. URL: https://linkinghub.elsevier.com/retrieve/pii/S0094114X06000310 (visited on Dec. 19, 2019).

[IPC98] Carlo Innocenti and Vincenzo Parenti-Castelli. « Singularity-free evolution from one configuration to another in serial and fully-parallel manipulators ». In: *ASME J. Mechanical Design* 120 (1998), pp. 73–99.

[Jel99] Zbigniew Jelonek. « Testing sets for properness of polynomial mappings ». In: *Mathematische Annalen* 315.1 (1999), pp. 1–35.

[KD04] Wissama Khalil and Etienne Dombre. *Modeling, Identification and Control of Robots*. New York: Springer, 2004. DOI: https://doi.org/10.1016/B978-1-903996-66-9.X5000-3.

[Kin] URL: http://kinovarobotics.com.

[KPMA19] C. K. Koukos-Papagiannis, V. C. Moulianitis, and N. A. Aspragathos. « Cuspidality Investigation of a Metamorphic Serial Manipulator. » en. In: *Advances in Mechanism and Machine Science*. Ed. by Tadeusz Uhl. Vol. 73. Series Title: Mechanisms and Machine Science. Cham: Springer International Publishing, 2019, pp. 2491–2500. ISBN: 978-3-030-20130-2 978-3-030-20131-9. DOI: 10.1007/978-3-030-20131-9_246. (Visited on July 21, 2023).

[KS85] Dilip Kohli and J. Spanos. « Workspace Analysis of Mechanical Manipulators Using Polynomial Discriminants ». en. In: *Journal of Mechanisms, Transmissions, and Automation in Design* 107.2 (June 1985), pp. 209–215. ISSN: 0738-0666. DOI: 10.1115/1.3258710. (Visited on Nov. 4, 2020).

[Mar+23] Tobias Marauli et al. « Optimal Motion Planning for Cuspidal Manipulators: Application to Commercial Robots ». In: *2023 IEEE/RSJ International Conference on Intelligent Robots and Systems, Detroit, USA*. 2023.

[MD99] P. R. McAree and R. W. Daniel. « An Explanation of Never-Special Assembly Changing Motions for 3–3 Parallel Manipulators ». In: *The International Journal of Robotics Research* 18.6 (1999), pp. 556–574. DOI: 10.1177/0278364992206639 4. URL: https://doi.org/10.1177/02783649922066394.

[NBW12] Dinh Quan Nguyen, Sebastien Briot, and Philippe Wenger. « Analysis of the Dynamic Performance of Serial 3R Orthogonal Manipulators ». In: vol. Volume 3: Advanced Composite Materials and Processing; Robotics; Information Management and PLM; Design Engineering. Engineering Systems Design and Analysis. July 2012, pp. 175–184. DOI: 10.1115/ESDA2012-82208.

[NM65] J. A. Nelder and R. Mead. « A Simplex Method for Function Minimization ». In: *The Computer Journal* 7.4 (Jan. 1965), pp. 308–313.

[OCH07] Erika Ottaviano, Marco Ceccarelli, and Manfred Husty. « Workspace Topologies of Industrial 3R Manipulators ». en. In: *International Journal of Advanced Robotic Systems* 4.3 (Sept. 2007), p. 38. ISSN: 1729-8814, 1729-8814. DOI: 10.5772/5679. URL: http://journals.sagepub.com/doi/10.5772/5679 (visited on July 21, 2023).

[OHC06] Erika Ottaviano, Manfred L. Husty, and Marco Ceccarelli. « Level-set method for workspace analysis of serial manipulators ». In: *Advances in Robot Kinematics*. 2006.

[Pag08] Davide Paganelli. « Topological Analysis of Singularity Loci for Serial and Parallel Manipulators ». en. PhD thesis. Bologna, Italy: Universita di Bologna, 2008.

[PCI88] Vincenzo Parenti-Castelli and Carlo Innocenti. « Position analysis of robot manipulators: Regions and subregions ». en. In: *Proceedings of 1988 conference on Advances in Robot Kinematics*. Ljubljana, Sept. 1988, pp. 151–158.

[Pie68] Donald Lee Pieper. « The Kinematics of Manipulators Under Computer Control ». en. PhD thesis. USA: Stanford University, Oct. 1968.

[PL92] Dinesh K. Pai and Ming C. Leu. « Genericity and singularities of robot manipulators ». In: *IEEE Transactions on Robotics and Automation* 8.5 (Oct. 1992), pp. 545–559. (Visited on Apr. 19, 2021).

[Pri86] Eric John Fyfe Primrose. « On the input-output equation of the general 7R-mechanism ». In: *Mechanism and Machine Theory* 21.6 (1986), pp. 509–510. ISSN: 0094-114X. DOI: https://doi.org/10.1016/0094-114X(86)90134-5.

[Rag+90] Madhusudan Raghavan et al. « A General Solution for the Inverse Kinematics of all Series Chains, 8th Symposium on theory and practice of robots and manipulators ». In: *RoManSy 8, ROMANSY -CONFERENCE-, 8th Symposium on theory and practice of robots and manipulators, RoManSy 8*. 8. Warsaw University of Technology; 1990, pp. 24–31. ISBN: 8390050129. URL: https://www.tib.eu/de/suchen/id/BLCP%3ACN004610702.

[Rou99] Fabrice Rouillier. « Solving Zero-Dimensional Systems Through the Rational Univariate Representation ». In: *Journal of Applicable Algebra in Engineering, Communication and Computing* 9 (May 1999), pp. 433–461.

[RR93] M. Raghavan and B. Roth. « Inverse Kinematics of the General 6R Manipulator and Related Linkages ». In: *ASME Journal of Mechanical Design* 115.3 (Sept. 1993), pp. 502–508. DOI: 10.1115/1.2919218.

[Sal+22a] Durgesh Salunkhe et al. « Geometry Based Analysis of 3R Serial Robots ». In: *Advances in Robot Kinematics 2022*. Ed. by Oscar Altuzarra and Andrés Kecskeméthy. Cham: Springer International Publishing, 2022, pp. 65–72. ISBN: 978-3-031-08140-8.

[Sal+22b] Durgesh Haribhau Salunkhe et al. « Necessary and sufficient condition for a generic 3R serial manipulator to be cuspidal ». In: *Mechanism and Machine Theory* 171 (Jan. 2022), p. 104729. ISSN: 0094-114X.

[SCW23] Durgesh Haribhau Salunkhe, Damien Chablat, and Philippe Wenger. « Trajectory planning issues in cuspidal commercial robots ». In: *2023 IEEE International Conference on Robotics and Automation (ICRA)*. 2023, pp. 7426–7432. DOI: 10.1109/ICRA48891.2023.10161444.

[SEDS17] Mohab Safey El Din and Éric Schost. « A nearly optimal algorithm for deciding connectivity queries in smooth and bounded real algebraic sets ». In: *Journal of the ACM (JACM)* 63.6 (2017), pp. 1–37.

[SL90] David Rowland. Smith and Harvey Lipkin. « Analysis of fourth order manipulator kinematics using conic sections ». en. In: *Proceedings., IEEE International Conference on Robotics and Automation*. Cincinnati, OH, USA: IEEE Comput. Soc. Press, 1990, pp. 274–278. ISBN: 978-0-8186-9061-7. DOI: 10.1109/ROBOT.1990.125986. (Visited on Apr. 28, 2021).

[SL93] David Rowland. Smith and Harvey Lipkin. « Higher order singularities of regional manipulators ». In: *[1993] Proceedings IEEE International Conference on Robotics and Automation*. 1993, 194–199 vol.1. DOI: 10.1109/ROBOT.1993.291982.

[Tho15] Federico Thomas. « A Distance Geometry Approach to the Singularity Analysis of 3R Robots ». In: *Journal of Mechanisms and Robotics* 8.1 (Aug. 2015),

p. 011001. ISSN: 1942-4302. DOI: 10.1115/1.4029500. URL: https://doi.org/10.1115/1.4029500.

[TKA93] Kao-Yueh Tsai, Dilip Kohli, and J. Arnold. « Trajectory Planning in Joint Space for Mechanical Manipulators ». In: *Journal of Mechanical Design* 115.4 (Dec. 1993), pp. 909–914. ISSN: 1050-0472. DOI: 10.1115/1.2919286. URL: https://doi.org/10.1115/1.2919286.

[Tri+15] *A Geometrical Approach to the Inverse Kinematics of 6R Serial Robots With Offset Wrists*. Vol. Volume 5C: 39th Mechanisms and Robotics Conference. International Design Engineering Technical Conferences and Computers and Information in Engineering Conference. Aug. 2015, V05CT08A016.

[TW11] Federico Thomas and Philippe Wenger. « On the topological characterization of robot singularity loci. a catastrophe-theoretic approach ». en. In: *2011 IEEE International Conference on Robotics and Automation*. Shanghai, China: IEEE, May 2011, pp. 3940–3945. ISBN: 978-1-61284-386-5. DOI: 10.1109/ICRA.2011.5979573. URL: http://ieeexplore.ieee.org/document/5979573/ (visited on July 21, 2023).

[Ver21] Achille Verheye. *Why hasn't anyone heard of cuspidal robots?, http://achille0.medium.co has-no-one-heard-of-cuspidal-robots-fa2fa60ffe9b*. 2021. URL: http://achille0.medium.com/why-has-no-one-heard-of-cuspidal-robots-fa2fa60ffe9b (visited on Sept. 10, 2022).

[WB06] Andreas Wächter and Lorenz T Biegler. « On the implementation of an interior-point filter line-search algorithm for large-scale nonlinear programming ». In: *Mathematical programming* (2006).

[WC22] Philippe Wenger and Damien Chablat. « A Review of Cuspidal Serial and Parallel Manipulators ». In: *Journal of Mechanisms and Robotics* 15.4 (Nov. 2022), p. 040801. ISSN: 1942-4302. DOI: 10.1115/1.4055677. URL: https://doi.org/10.1115/1.4055677.

[WCB05] Philippe Wenger, Damien Chablat, and Maher Baili. « A DH-parameter based condition for 3R orthogonal manipulators to have 4 distinct inverse kinematic solutions ». en. In: *Journal of Mechanical Design* 127 (2005), pp. 150–155.

[WE97] Phillippe Wenger and Jouad El Omri. « Comments on “A classification of 3R regional manipulator geometries and singularities” ». In: *Mechanism and Machine Theory* 32.4 (1997), pp. 529–532. ISSN: 0094-114X. DOI: https://doi.org/10.1016/S0094-114X(96)00061-4. URL: https://www.sciencedirect.com/science/article/pii/S0094114X96000614.

[Wen04] Philippe Wenger. « Uniqueness Domains and Regions of Feasible Paths for Cuspidal Manipulators ». en. In: *IEEE Transactions on Robotics* 20.4 (Aug. 2004), pp. 745–750. (Visited on June 2, 2020).

[Wen19] Philippe Wenger. « Cuspidal Robots ». In: *Singular Configurations of Mechanisms and Manipulators*. Ed. by Andreas Müller and Dimiter Zlatanov. Cham: Springer, 2019, pp. 67–99.

[Wen92] Philippe Wenger. « A New General Formalism for the Kinematic Analysis of All Non-redundant Manipulators ». en. In: *Proceedings of the 1992 IEEE International Conference on Robotics and Automation*. Nice, France, May 1992, pp. 442–447.

[Wen98] Philippe Wenger. « Classification of 3R Positioning Manipulators ». en. In: *Journal of Mechanical Design* 120.2 (June 1998), pp. 327–332. ISSN: 1050-0472, 1528-9001. DOI: 10.1115/1.2826976. URL: https://asmedigitalcollection.asme.org/mechanicaldesign/article/120/2/327/429674/Classification-of-3R-Positioning-Manipulators (visited on July 21, 2023).

[WEO96] Philippe Wenger and Jouad El Omri. « Changing posture for cuspidal robot manipulators ». en. In: *Proceedings of IEEE International Conference on Robotics and Automation*. Vol. 4. Minneapolis, MN, USA: IEEE, 1996, pp. 3173–3178. (Visited on Oct. 30, 2020).

[Whi55] Hassler Whitney. « On Singularities of Mappings of Euclidean Spaces. I. Mappings of the Plane into the Plane ». In: *Annals of Mathematics* 62.3 (Nov. 1955).

[ZBSO21] Hamed Montazer Zohour, Bruno Belzile, and David St-Onge. « Kinova Gen3-Lite manipulator inverse kinematics: optimal polynomial solution ». In: *ArXiv* abs/2102.01217 (2021).

[ZWC06] Mazen Zein, Philippe Wenger, and Damien Chablat. « An exhaustive study of the workspace topologies of all 3R orthogonal manipulators with geometric simplifications ». en. In: *Mechanism and Machine Theory* 41.8 (Aug. 2006), pp. 971–986. ISSN: 0094114X. DOI: 10.1016/j.mechmachtheory.2006.03.013. URL: https://linkinghub.elsevier.com/retrieve/pii/S0094114X06000711 (visited on Feb. 4, 2021).

COLLEGE SCIENCES
DOCTORAL DE L'INGENIERIE
PAYS DE LA LOIRE ET DES SYSTEMES

CENTRALE NANTES

Titre : Robots cuspidaux : étude théorique, classification et application aux robots commerciaux

Mot clés : cinématique, design, planification de trajectoire, robots cuspidaux, optimisation.

Résumé : Les robots cuspidaux sont des robots qui possèdent au moins une région connectée avec de multiples solutions cinématiques inverses. Cela permet aux robots cuspidaux de changer de solutions sans traverser de singularités.
Cette thèse doctorale présente une étude théorique sur l'analyse cuspidale des robots sériels à 3 articulations rotatives (3R). La thèse présente également des algorithmes d'identification pour déterminer la cuspidalité des robots génériques à 6R. Ensuite, l'application de la cuspidalité est présentée en abordant les problèmes et en développant un cadre de planification de trajectoire pour les robots commerciaux cuspidaux. Une conclusion est apportée à la conjecture sur les robots cuspidaux à 3R à la suite du travail présenté, et la question du nombre d'aspects dans un robot générique à 3R est éclaircie. Une preuve de l'existence d'aspects réduits pour un robot générique à 3R est également présentée. La preuve présentée sur la cuspidalité des robots à 6R est réexaminée, et la nécessité de prêter attention au sujet de la cuspidalité dans la planification de trajectoire est d'autant plus motivée. Les problèmes critiques existant dans les robots commerciaux à 6R, largement ignorés, sont exposés, et un cadre de planification de trajectoire pour leur atténuation est présenté.

Title: Cuspidal robots: theoretical study, classification, and application to commercial robots.

Keywords: kinematics, design, path planning, cuspidal robots, optimisation.

Abstract: Cuspidal robots are robots that have at least one connected region with multiple inverse kinematic solutions. This allows cuspidal robots to change solutions without crossing singularites.
This doctoral thesis presents theoretical study on the cuspidal analysis of 3 revolute jointed (3R) serial robots. The thesis also presents identification algorithms to decide cuspidality of generic 6R robots. Later, the application of cuspidality is presented by discussing issues and developing a trajectory planning framework of cuspidal commercial robots. A closure to the conjecture in 3R cuspidal robots is provided as a result of the presented work, and the question on number of aspects in generic 3R robot is concluded. A proof for the existence of reduced aspects for a generic 3R robot is presented too. A presented proof on cuspidality in 6R robots is reinvestigated, and the need of attention to the topic of cuspidality in path planning is further motivated. The critical issues existing in commercial 6R robots that are largely ignored are shown, and a path planning framework for their mitigation is presented.